Electrical characterization of process induced defects in germanium

by

Sergio Manuel Martins Coelho

Submitted in partial fulfilment of the requirements for the degree
Philosophiae Doctor
in the Faculty of Natural and Agricultural Sciences (Department of Physics)
University of Pretoria, Pretoria

July 2014

DECLARATION OF ORIGINALITY

I, Sergio Manuel Martins Coelho, declare that the thesis which I hereby submit for the degree Philosophiae Doctor in Physics at the University of Pretoria is my own work and has not previously been submitted by me for a degree at this or any other tertiary institution.

SIGNATURE:

DATE:

Publication data:

Sergio Manuel Martins Coelho. Electrical characterization of process induced defects in germanium. Doctoral thesis, Department of Physics, University of Pretoria, Pretoria, South Africa, July 2014.

Electrical characterization of process induced defects in germanium

by

Sergio Manuel Martins Coelho
E-mail: sergio@up.ac.za

Abstract

The origins and identity of process induced defects in semiconductors has proven to be a particularly difficult problem to solve. Germanium, a semiconductor once again at the forefront of device technology, has played a leading role in advancing semiconductor physics and now, through the use of readily available ultra-pure germanium, allows us to interrogate a crystal structure electrically with a sensitivity that is unsurpassed. This thesis presents a number of recently discovered process induced electron and hole traps, the most noteworthy of which is $E_{0.31}$. This point defect with an energy level of 0.31 eV below the conduction band modified the properties of germanium rendering it immune to the introduction of electron beam deposition (EBD) induced defects. $E_{0.31}$ was introduced during etching with a subthreshold energy argon plasma, was annealed to a level below 10^{11} cm^{-3}, the detection limit of our system, but could then not be reintroduced in the sample. This result suggests that plasma etching modified an existing defect that did not have a deep level in the bandgap.

Investigations into the conditions experienced by substrates during EBD before the deposition, termed electron beam exposure (EBE) herein, introduced defects not seen after EBD with only the E-center common to both processes. The substantial differences in defect type and concentration noted between these processes has not been explained as the role of the growing metal film remains unclear in EBD defect introduction. Inserting mechanical shields to block energetic particles created in the electron-beam path from

colliding with samples resulted in Schottky barrier diodes being manufactured with EBD defect concentrations that were too low to measure using deep level transient spectroscopy. This observation confirms that energetic particles created in collisions with 10 keV electrons were responsible for EBD defects and not high energy electrons, as previously reported.

Keywords: Germanium, deposition, defects, Deep level transient spectroscopy.

Supervisors : Professor F. D. Auret
Doctor J. M. Nel
Department : Department of Physics
Degree : Philosophiae Doctor

For my wife, Alice

"The greatest obstacle to your success is probably you."

Frank Tyger

"All you need in this life is ignorance and confidence; then success is sure."

Mark Twain

Acknowledgements

My sincere thanks go to the following persons for contributing to this study:

- My promoter, Professor F. Danie Auret for his tireless support throughout this study;
- My co-promoter, Doctor Jackie M. Nel that always found time to guide me;
- Professor Michael Hayes who started this journey with me;
- Professor Gerrit Myburg for demonstrating the value of determination;
- Doctor Nick van der Berg that was always willing to assist me;
- Gerrit Pretorius, Nico van Vuuren and Danie Joubert for building the required equipment and then insisting that I complete this study;
- Jaco Smith for his efforts in repairing our electrical apparatus;
- All my colleagues that had to endure my endless questions;
- The staff of the University of Pretoria for all their assistance;
- The National Research Foundation for funding this work;
- My family and friends that always found new ways to support my research;
- My wife, Alice, for encouraging me when the way forward was obscured;
- My parents and my grand mother, Dilia, for starting me on this path and encouraging me to stay on it.

Contents

List of Figures

List of Tables

Glossary

amphoteric A species, either molecule or ion, capable of reacting as a base or as an acid

eutectic alloy with a melting point lower than that of any other combination of the same components

flux the rate of flow of a property per unit area

germanide a binary compound of germanium and a more electropositive element

ideality measure of how closely a diode follows the ideal diode equation

irradiation the process by which an object is exposed to radiation

Acronyms

A Ampére

AMU atomic mass unit

BC bond-centered

C-V capacitance-voltage

CMOS complementary metal-oxide-semiconductor

CVD chemical vapour deposition

DB dangling bond

DC direct current

DLTS deep level transient spectroscopy

e-gun electron gun

EB electron beam

EBD electron beam deposition

EBE electron beam exposure

EOR end-of-range

FA furnace annealing

fRTP flash-assist rapid thermal processing

GOI germanium-on-insulator

HP high purity

I-T current-temperature

I-V current-voltage

IC integrated circuit

ICP inductively coupled plasma

IR infra-red

L-DLTS Laplace-DLTS

MBE molecular beam epitaxy

MOSFET metal-oxide-semiconductor field effect transistor

PLD pulsed laser deposition

PTIS photo-thermal ionization spectroscopy

PV photovoltaic

PVD physical vapour deposition

RBS Rutherford backscattering spectroscopy

RE resistive evaporation

RF radio frequency

RG recombination/generation

RTA rapid thermal annealing

S/N ratio signal-to-noise ratio

SBD Schottky barrier diode

scr space-charge region

SD sputter deposition

VdG Van de Graaff

Chapter 1

Introduction

Germanium is once again at the forefront of the semiconductor revolution as it holds the promise of even faster devices for the not too distant future. However, from a materials point of view, it is the ideal material to study extremely small changes both on its surface and in its bulk due to the availability of ultra-pure germanium.

Element 32, Ge, was used during the pioneering years of semiconductor research to formulate theories and demonstrate physical principles that are still applicable today. The McWhorter theory for 1/f noise, plasticity in a diamond lattice semiconductor and Frank-Read dislocation sources were first studied in Ge (Claeys and Simoen 2007). The discovery of the transistor at Bell Labs in 1948 on a Ge slab was the starting point for the Microelectronics Industry with a market estimated to exceed US $304 billion in 2013 (report of the World Semiconductor Trade Statistics organization). This enterprise is the largest worldwide and is predicted to continue growing for the immediate future but it faces unique challenges. With the ever increasing need for faster and smaller devices the limit in miniaturization is approaching for Si integrated circuits(ICs). Ge, strained SiGe and strained Si with their high mobility charge carriers are now seen as good candidates for devices operating at increased speeds. The instability of the GeO_2 layer that was always a major disadvantage has been annulled by the need for high-κ dielectrics on

Si at the 65 nm complementary metal-oxide-semiconductor (CMOS) technology node and beyond. These fundamentals are very encouraging but many challenges remain as Ge has never been subjected to the level of investigation that Si has experienced. Material availability may be the biggest drawback against the widespread use of Ge in microelectronics which highlights the importance of using only a thin layer in schemes like germanium-on-insulator (GOI).

Defects studies shed light on the most interesting properties of semiconductors. Point defects and impurities influence the local resistivity, doping type and doping concentration. Devices in the future, as a consequence of miniaturization, will have extremely shallow junctions with high conductivity, where the role of defects that enhance diffusion of the implanted dopant species will have to be better understood (Law et al. 2008). Not all defects are electrically active which further complicates analysis. The most obvious example of such a defect is one that has been passivated using hydrogen, a common practice during material growth and device fabrication. The ability of defects to influence the carrier lifetime can be used constructively but must be carefully controlled as they can also become efficient carrier lifetime killers (Simoen, Claeys et al. 2007). Defect studies on Ge are of particular interest as very little has been done when compared to similar research on Si considering that Ge could be utilized in technologically superior devices if its potential is actualized.

1.1 Motivation

A summarized yet remarkably complete history of Ge, from a semiconductor perspective, was written by Haller 2006. It emphasizes the important results that were achieved and mentions the niche applications that this interesting material is used for. The future use of Ge for microelectronics applications looks promising but many challenges remain. The property of Ge that has rekindled interest in this material is that when compared to bulk Si, it exhibits electron and hole mobilities that are higher by factors of ~2 and 4, respectively. Promising results in the development of Ge metal-oxide-semiconductor field effect transistors(MOSFETs) have been obtained but major obstacles

remain (Simoen and Claeys 2007). The way forward is further complicated by industry's need to translate existing Si device manufacturing technology across when considering novel devices. Possible future directions for the semiconductor industry and the role that Ge can play is discussed in Claeys and Simoen 2007. Additional information on the successes and the challenges of using Ge as a mainstream semiconductor is covered in a number of chapters of this excellent resource. While the semiconductor properties of Ge are of great importance, one should not lose sight of the possibility to use these same properties to shed light on fundamental physics problems.

This study is primarily concerned with the introduction of point defects in Ge during processing and the impact that these have on the electrical properties of Ge. The term defect will always refer to an electrically active point defect unless specified differently. The creation of extended defects was not investigated, although possible to measure electrically, as our focus on creating devices with exceptional rectifying characteristics would be lost. To advance our current electronic technology it will be necessary to not only build faster devices but these will have to be smaller too. Only by understanding how the electrical and physical properties of semiconductors relate to each other can we hope to further develop the manufacturing and spectroscopic techniques that will result in better devices. Defects in semiconductors may influence device performance adversely but have also been shown to improve the switching speed of select devices thus ensuring the relevance of defect studies.

Deep level transient spectroscopy (DLTS), based on work started more than forty years ago (Lang 1974), was chosen as the most suitable tool to investigate defects in Ge. A number of studies in the early years of DLTS reported on defects in Ge but as the technique was still in its infancy, many of the values obtained varied significantly from measurements taken later (Fage-Pedersen et al. 2000). A vast quantitative improvement to conventional DLTS arrived with the idea to use the Laplace transform method to analyse the decay transient (Dobaczewski et al. 1994). Not only was the resolution of DLTS improved by more than an order of magnitude, but for the first time fine structure could be discerned from broad peaks that were obtained conventionally. This technique, known as Laplace-DLTS (L-DLTS), has had a profound effect on the spectroscopy of

electrical defects (Peaker, Markevich, Hawkins et al. 2012) but requires a dedicated experimentalist to analyse the data. Many defects have been observed in Ge and a small number of these have been identified (E-center, A-center and V_2-H, as examples). From a survey of the available literature it is clear that the majority of the research is decades old and that a great deal of it needs to be revisited (Vanhellemont, Simoen et al. 2007). Process-induced defects is an area that has received very little attention. Not only are the majority of these defects unidentified at present but also the defect causing mechanisms are, in many cases, not well understood. These mechanisms are manifestations of physical phenomena that play a role in many systems and deserve detailed examination, both experimentally and theoretically.

The future device that will form the backbone of the semiconductor industry is undecided presently. The Schottky barrier diode (SBD) is a candidate worth considering and efforts to improve this devices' properties yield results applicable to other rectifying junctions while providing the ideal window through which to observe defects in the Ge bulk.

1.2 Objectives

This work set out to investigate the effect that certain critical fabrication processes had on device performance and to attempt to improve these processes if they were found to influence device performance adversely. Excellent devices are required to obtain accurate measurements and we aimed to make this the foundation of our experimental investigations. Defects, if any, introduced during fabrication processes like deposition and etching may influence device performance thus characterizing these defects is central to this study. Our main objectives were the following:

- To produce diodes with ideality close to one by first investigating both wet and dry surface cleaning methods and then optimizing the metal deposition process.
- The characterization of defects introduced during device manufacture as well as damage by irradiation from various sources.

- Optimize essential fabrication processes to control defect introduction.
- Identifying the agents responsible for defect introduction during critical process steps like metal deposition and plasma etching, if possible.

1.3 Contributions

The application of known chemical cleaning recipes with careful manipulation of vacuum conditions during film deposition resulted in SBDs being produced with excellent rectifying properties. Novel experiments were constructed to shed light on which agents were responsible for introducing the defects that were observed after device manufacture as well as to establish the mechanisms by which defects came to be where they were observed in the crystal bulk. More specifically, the following contributions were made to this field:

- This study resulted in germanium SBDs being produced that had an ideality of 1.02 where 1 would represent the ideal diode. This result was repeated with silicon SBDs.
- There were a number of novel defects discovered that were introduced during device fabrication. $E_{0.31}$, an electron trap, introduced during inductively coupled plasma (ICP) is an example of one such defect.
- Defects that had previously been observed could be identified but the novel defects that were introduced during processing could only be characterised electrically without any certainty as to their physical form.
- Modifying the electron beam deposition (EBD) system in combination with improved vacuum conditions resulted in SBDs being produced that had defect concentrations too low to be measured with DLTS.
- Energetic ions were identified as the agents that cause the damage observed during EBD and not subthreshold electrons as previously reported.

- Results from this thesis have contributed towards twenty three publications in peer reviewed journals.

1.4 Thesis Outline

This thesis is arranged in the following order:

- **Chapter 2** focusses on the theoretical aspects that are important to understand the research that was undertaken. The theory includes descriptions of the relevant deposition techniques used, defect creation and the measurement of device properties and defects.
- **Chapter 3** covers the experimental techniques that were applied during the fabrication of devices and their subsequent measurement. Special considerations and modifications to these techniques is also discussed.
- **Chapter 4** deals with the results that were obtained. This takes the form of a brief introduction followed by the complete published article. Pertinent results from select articles are listed that focus on the primary objectives of this study.
- **Chapter 5** emphasises the more important conclusions that were made in the articles in Chapter 4 and additional conclusions that were drawn by considering the results of linked studies. No research study is ever complete thus possible work for the future is also listed.

Appendices have been provided after the bibliography to address areas that are not central to the study objectives but still merit inclusion:

- **Appendix A** lists the defects that were studied during the course of this research. Where these have been identified or if they are similar to defects from other research findings, a reference is provided.

- **Appendix B** lists the publications that were contributed to during the course of this study.
- **Appendix C** consist of an article where electron beam exposure (EBE) on Si was reported. This illustrates that some results obtained for Ge may be applicable to other semiconductors.

Chapter 2

Theoretical Overview

The theoretical aspects of this study cover a broad range of topics that will be dealt with in detail if specifically relevant to the research that was undertaken. Historically, most of the techniques discussed have been available to scientists and engineers for many decades and thus information is easily accessed in the excellent reference material. The following will be discussed:

- Physical vapour deposition with emphasis on the energy transferred to substrates during deposition.
- Defect creation that results in point defects with energy levels “deep" within the bandgap.
- Electrical characterization and how it relates to the devices that were measured.
- Annealing as a strategy to remove or convert defects.

2.1 Physical Vapour Deposition

Deposition technology can be regarded as the most important aspect of semiconductor device fabrication and together with the advancement of spectroscopic techniques has been responsible for the rapid growth of this industry (Seshan 2001). Physical vapour deposition (PVD) that also includes chemical vapour deposition (CVD) encompasses many techniques that aim to coat a sample with a thin layer of an evaporated species. This layer may be a few nanometres to several micrometres thick and could be deposited using techniques that are purely physical, chemical or a combination of the two. The introduction by Graper (1996c, in *Handbook of Thin Film Process Technology*) covers the basics in some detail beginning with the importance of the vacuum environment for PVD and the vacuum pressure expressed in terms of mean free path. Increasing the source to substrate distance will necessitate a corresponding drop in vacuum pressure, thus maintaining the ratio of mean free path to source-sample distance at 10:1 or greater. This ensures that the evaporant has few interactions with the residual gas in the chamber.

A survey and classification of thin-film deposition technologies is to be found in Table 1 of Kern et al. 2001 or in the text edited by Martin (2010, Table 1.1). Only those techniques that were used to manufacture the ohmic and Schottky contacts that are described in Chapter 4 will be discussed. Physical vapour deposition describes these techniques, all falling within two categories: Evaporative methods and Glow-discharge processes. Three basic steps are required for physical vapour deposition processes to proceed:

- The creation of a vapour-phase species. Conversion to vapour can be due to evaporation, sputtering or by chemical means.
- Transport of the vapour from the source to the receiving surface, i.e. the substrate. This may occur in the molecular or viscous flow regime.
- Condensation of the vapour on the substrate to form a solid film. Film nucleation and growth on the substrate involves a number of processes.

Deposition techniques may appear simple but the successful practitioner will require

an understanding of vacuum and material science, thermodynamics, surface mobility, condensation and more. For semiconductor depositions it is vitally important that exposure of the substrates to energetic particles be kept to a minimum. The evaporant gives up energy to the substrate upon condensation and this is the principal source of substrate heating. The evaporant velocity can be deduced from the evaporation temperature as this determines the evaporants' median kinetic energy (1000 °C = 0.2 eV and 2000 °C = 0.4 eV) (Graper 1996c). The pressure dependent point at which evaporation occurs is typically 0.1 to 1 mBar during thin film evaporation, this being the pressure just above the evaporants' surface. The deposition rate dependent evaporation temperature can be calculated but is best determined empirically. By consulting vapour pressure tables or graphs (Honig 1962) the temperature can be estimated. Table 2.1 lists the metals that were used for SBD devices herein with their approximate evaporation temperatures, that then provide an indication of the energy, per collision, that the substrate was subjected to during deposition.

Table 2.1: Material Deposition*

Material	Symbol	MP (°C)	g/cm^3	0.1 mBar†	1 mBar†	Techniques used
Aluminium	Al	660	2.7	1350	1550	RE, EBD
Gold	Au	1064	19.32	1550	1750	EBD, RE, SD
Irridium	Ir	2410	22.42	2720	3020	EBD
Nickel	Ni	1453	8.9	1650	1900	EBD, RE
Palladium	Pd	1554	12.02	1600	1850	EBD, RE
Platinum	Pt	1772	21.45	2300	2550	EBD
Titanium	Ti	1660	4.5	1900	2150	EBD
Tungsten	W	3410	19.35	3500	3900	EBD

MP	Melting point
†	Temperature (°C) for the given vapour pressure
*	data from Honig and Kramer 1969

When considering only evaporation then the thermal energy determines the kinetic energy of the evaporant but in processes like sputter deposition (SD) particles may become ionised and undergo further acceleration in the electric field used to generate the plasma. This additional energy may have a dramatic impact on the growing film, improving adhesion and film density but also raising the substrate temperature to an unacceptable level as well as introducing defects in the substrate (Grusell et al. 1980; Leclerc et al. 1996).

Deposition of alloys is not easily accomplished if the aim is to transfer the alloy to the substrate in the same ratio of constituents. This will only occur in the rare instances when the alloys' constituent elements evaporate at exactly the same temperature. In practical evaporations, one of the elements, say element A, will evaporate faster leaving behind a source depleted of A. As the evaporation proceeds the film will initially have a high concentration of element A but this will diminish resulting in a graduated film rather than one with an invariant distribution. SD is a technique capable of transferring alloys or dielectrics to a substrate with the resultant thin film having the same element proportions as the target. Such precision was not required for the deposition of the Au-Sb films used as ohmic contacts.

For large area evaporations it is vital that the substrate gets coated uniformly. This is often difficult to achieve as thermal evaporation is a ballistic process where the evaporant usually originates from a point source. Applying strategies like sample rotation or backfilling the chamber with inert gas to scatter the evaporant can be very effective, but ultimately unnecessary when samples are relatively small and only produced in a limited number as is common for research into defects.

The decision of when to replenish or replace the evaporant charge must be considered carefully. Replacing a crucible with a small amount of a precious metal in it can be costly and often unnecessary as older sources are usually very well outgassed and produce purer films. The film qualities that are most desired by the user are the best arbiter of how often sources should be replenished or discarded. For semiconductor contacts where a film is desired with few defects, it is preferable to replenish sources less frequently.

The requirement by engineers for ever purer films drives this technology to greater heights with an accompanying improvement of in situ measurement of film properties.

2.1.1 Resistive Evaporation

The first practical thin film deposition using an evaporation source consisting of a resistance heated element was reported in 1912 (Graper 1996b), but already in 1857 Faraday prepared thin films in a vacuum using an exploding wire (Deshpandey et al. 1991). Only after the second world war did this technology find widespread use with the arrival of improved vacuum systems. Resistive evaporation (RE) systems comprise a vacuum chamber, source, substrate holder, shutter and thickness monitor. The relative simplicity and economy of these systems ensures that they continue to find favour in industry and research institutions although technologically, electron beam evaporated sources and sputtering offer many advantages. For semiconductor research and specifically for the study of defects, RE is not known to introduce electrically active defects and is an indispensable tool for preparing reference samples.

A resistance heated source made of a refractory metal is both the container and heater of the evaporant. This is the heart of the system and the most likely cause of failure thus careful source selection is particularly important. Catalogues from companies like R.D. Mathis offer a large selection of boats, coils, rods and special box designs in molybdenum, tantalum and tungsten but very little advice on evaporant compatibility considering that many elements alloy with refractory metals once heated. Sources are chosen to meet the requirements of evaporant compatibility, available power and capacity. The references in Graper 1996b, provide data on making these choices but there is no substitute for field experience as compromises are often required. For example, Al is used to provide electrical contact with various semiconductors but is challenging to evaporate. Small amounts can be evaporated using low-cost tungsten coils but these sources coat in all directions and this is wasteful in coat-up applications typical of semiconductor work. As Al alloys easily with tungsten, the lifetime of the coil decreases dramatically and the resultant film will contain traces of tungsten. Using thicker boats may increase the

lifetime of the source but is costly and difficult to manufacture. Boats coated with an inert material, usually alumina (Al_2O_3), may solve this alloying issue but require a higher operating temperature due to the introduction of an insulator between evaporant and heater subsequently lowering the boat lifetime. For this research conical alumina coated sources, of the smallest practical size, were most often used as they were compatible with most metals, exposed the substrates to less heat than larger sources and directed the metal vapour thus lowering waste of costly metals.

The design of a successful RE system begins with defining its primary area of application. Research and industrial systems will both benefit from well designed vacuum pumping stages that provide oil-free vacuum. Design criteria for industrial systems is mostly concerned with robustness where sources must function without failure through many heating and cooling cycles with their accompanying expansion and contraction. For research, flexibility is usually more important where systems may include a number of sources that are easily rotated into position to allow for multilayer coatings. The power supply will be required to provide 1-20 V and up to 5 kW of power to control the source temperature and thereby the deposition rate. Typically a step-down transformer matches the source load to the power supply and this should be matched so that neither the transformer's primary voltage nor its amperage exceed 100% of its rating. Care should be exercised so as not to partially short coils or boats as this shorting increases the current required to maintain the evaporation and heats the boat contacts excessively. This is best accomplished by only partially filling boats.

For efficient thin film production there are a number of parameters that may be optimized. System layout, that is the relative position of source and substrate, as well as the shield placement is critically important (see Figure A1.1.1 in Graper 1996b). Flexible bus bars will minimize boat distortion while well placed heat shields near the source will assist in keeping the chamber heat down and lowering the power required by the source. Film thickness may vary by up to 30% for relatively large films but this can be lowered to below 5% if the substrate is rotated. It was unnecessary to apply sample rotation or to introduce additional source shields as all samples were relatively small and most depositions were completed swiftly so that chamber heating was low.

2.1.2 Electron Beam Deposition

An electron beam heated source relies on energy transfer from incident electrons, typically accelerated to 10 keV, to thermally evaporate one of a large variety of solid targets. The modern electron gun (e-gun) that was introduced in the early 1960s, remaining virtually unchanged since then, has found application in metallization on semiconductors, optics (Graper 1996a) and in industrial processes like the deposition of corrosion protective coatings on strip metal (Reinhold et al. 2011). This is a mature technology that has been largely replaced in the semiconductor industry by planar magnetron sputtering sources that proved to be easier to automate. A detailed description of the EBD source and the power supplies that control it is available in Graper 1996a, and will not be repeated herein, however a brief description will follow with additional information due to new developments.

The EBD source consists of three components: the electron emitter, magnetic lens and water-cooled cavity or hearth. The emitter is strategically located out of line-of-sight of the evaporant and the electron beam follows a circular path curved by the magnetic lens through 270° so as to impinge on the centre of the hearth. This protects the emitter from becoming coated by the evaporant, thus lowering the risk of short circuits and also conveniently shields the substrate from energetic particles that may be accelerated by the high potential of the emitter. Three power supplies are required to first heat the filament (tungsten coil) thus providing a source of electrons, secondly to accelerate these electrons and finally to power the electro-magnets of the lens to control the electron beam (EB). 10 kV is the most common accelerating voltage at a current of up to 1.5 Ampére (A), however, higher power e-guns are available with accelerating voltages of 60 kV with nominal power output of several hundred kW. In modern systems most tetrode based high voltage power supplies have been replaced with solid state equivalents that are well protected from short circuits due to arcing. For safety in operation, today's e-gun has a magnetic lens that consists of a permanent magnet to direct the EB towards the hearth centre, as well as electro-magnets to focus and raster the beam. Modern magnet power supplies no longer defocus the beam to cover a larger area of the evaporant but rather maintain a focused beam that is scanned over the target surface in a complex pattern

at a frequency not exceeding 200 Hz. This arrangement ensures that the target material is evenly heated thus better utilised and should the magnet supply fail then the EB remains focused on the centre of the hearth. High voltage supplies are considered to be extremely dangerous in operation thus e-guns must be properly earthed and interlocks included to shut down power in the event of a malfunction.

Advantages of EBD over RE are primarily that energy transfer to the evaporant is virtually limitless and that contamination from the hearth is almost non-existent as for most evaporants no reaction occurs with the water-cooled hearth. Different liners are available to address issues where materials are not compatible with the copper hearth or to introduce a means of limiting the heat lost through conduction. This is the case with evaporating aluminium, an excellent conductor of heat. Liners are produced in many materials including BN, C, Cu, Mo, Al_2O_3 and W. Perhaps the greatest advance in liner technology has been the introduction of relatively inexpensive glassy carbon and Fabmate® liners. These liners are compatible with many evaporants and have the added advantage of outgassing at a much lower rate than conventional carbon liners thus speeding up the conditioning process that is always needed when a new target is being prepared. In almost all cases targets have to be prepared from lump, shot or compressed pellets as powders or granules heat up locally without adequate conduction to the rest of the hearth load rendering conditioning impossible. Powders also have too large a surface area that encourages absorption of water vapour and other contaminants resulting in spitting as the target is heated. Patience is required while conditioning most materials while some targets will need to be rotated to ensure adequate conditioning. Before an evaporation is performed even targets that are pre-conditioned should be heated again to ensure that outgassing during deposition is minimized. During operation efficient water cooling is of paramount importance if the hearth is to remain inert. Coolant failure may result in the destruction of the e-gun or damage to the magnet assembly.

The disadvantage of EBD is that it introduces defects in sensitive semiconductors (Auret and Mooney 1984; Kleinhenz et al. 1985; Klose et al. 1993). This damage has previously been attributed to an emission of soft x-rays or energetic electrons that are most probably reflected from the target (Graper 1996a). The magnetic field of the e-

gun will cause the majority of reflected electrons to be captured by the shield placed over the permanent magnet and is a significant part of the design as approximately 30% of the beam energy is reflected. A small portion of the evaporant flux is ionised as it passes through the incident electron beam further complicating matters. Another source of energetic particles that has previously been neglected is those ions that are created in the electron beam path by collisions between electrons and residual gas atoms or molecules. Even for fast moving atoms like hydrogen the probability of collision while traversing a typical 10 kV, 0.1 A electron beam is above one. Furthermore, as an evaporation proceeds the vacuum pressure tends to increase with increasing outgassing due to heating of the vacuum chamber and the components in the chamber, resulting in the number of available particles that may undergo collisions increasing proportionately with an increase in pressure.

To account for subthreshold electron damage a two-step process was suggested (Naber et al. 1958) where an intermediate light impurity atom, such as hydrogen, could produce a displacement of a germanium atom. This process requires the electron to first strike the light atom that then strikes the germanium atom transferring almost three times more energy than a direct collision. The electron threshold energy for such a displacement was found to be 90 keV, assuming that 15 eV is required to displace a germanium atom from the lattice (Chen et al. 1968). While this threshold is much higher than the typical available electron energy, defects observed in gold and copper were postulated to be due to ever present impurity atoms (Bauer et al. 1964). Similarly, in germanium, light-atom impurities are the most probable subthreshold mechanism agent. Naber and James may only have considered atoms present in the crystal lattice, but using light atoms that are present in the vacuum to transfer energy to lattice atoms yields the same result. From conservation of momentum and energy, if we consider two particles denoted by the subscripts 1 and 2 then let m_1 and m_2 be the masses, u_1 and u_2 be the velocities before collision and v_1 and v_2 be the velocities after collision:

$$m_1u_1 + m_2u_2 = m_1v_1 + m_2v_2, \tag{2.1}$$

and

$$\frac{1}{2}m_1u_1^2 + \frac{1}{2}m_2u_2^2 = \frac{1}{2}m_1v_1^2 + \frac{1}{2}m_2v_2^2. \tag{2.2}$$

For the simplest case where $u_2 = 0$ the maximum energy transferred to particle 2 is given by

$$T_{max} = \frac{1}{2}m_2v_2^2 = \frac{1}{2}m_1u_1^2\frac{4m_1m_2}{(m_1+m_2)^2} = E_i\frac{4m_1m_2}{(m_1+m_2)^2} \ , \tag{2.3}$$

assuming a one dimensional case of an elastic collision where E_i is the initial energy of particle 1. This energy transfer between a 10 keV electron and particles of atomic mass from 1 to 75 atomic mass units(AMUs) is illustrated in Graph 2.1 (black solid plot). The red bars denote the energy variation if the velocity of the second particle in vacuum (assuming an ideal gas at room temperature) is taken into account and including this consideration then the maximum energy transferred to a H atom is approximately 24 eV. Plotting the example of collisions between a 24 eV H atom and particles of atomic mass 1 to 75 AMUs illustrates that this knock-on process is capable of transferring the same (when AMU = 1) or more energy than a direct collision with an electron. To evaluate this process for the specific case of Ge, Graph 2.2 plots the knock-on energy transfer between particles of various masses that were initially accelerated in a 10 keV electron collision and then collide with a stationary Ge atom. Collisions of the lightest particles with Ge result in the highest energy transfer, that is, at most, 1.3 eV. The direct energy transfer from 10 keV electron to Ge will transfer a maximum of 0.34 eV. The knock-on energy transfer process may result in more energy being transferred but this is still not sufficient to displace a Ge atom from the lattice, however Chen et al. (1968), noted that defects were only produced in Ge grown in a hydrogen atmosphere thus it is likely that hydrogen in the crystal lattice played a role. This will be discussed in more detail in section 2.2.1.

The latest developments in EBD technology are of tremendous value to industry but have not found widespread application in the semiconductor industry. The production of silicon solar cells has benefited by combining two processes, EBD and SD, in an inline coater to deposit a thick layer of Al followed by a much thinner Au or Cu layer as a back-contact in one 50 s cycle (reference 8 in Reinhold et al. 2011). The most significant

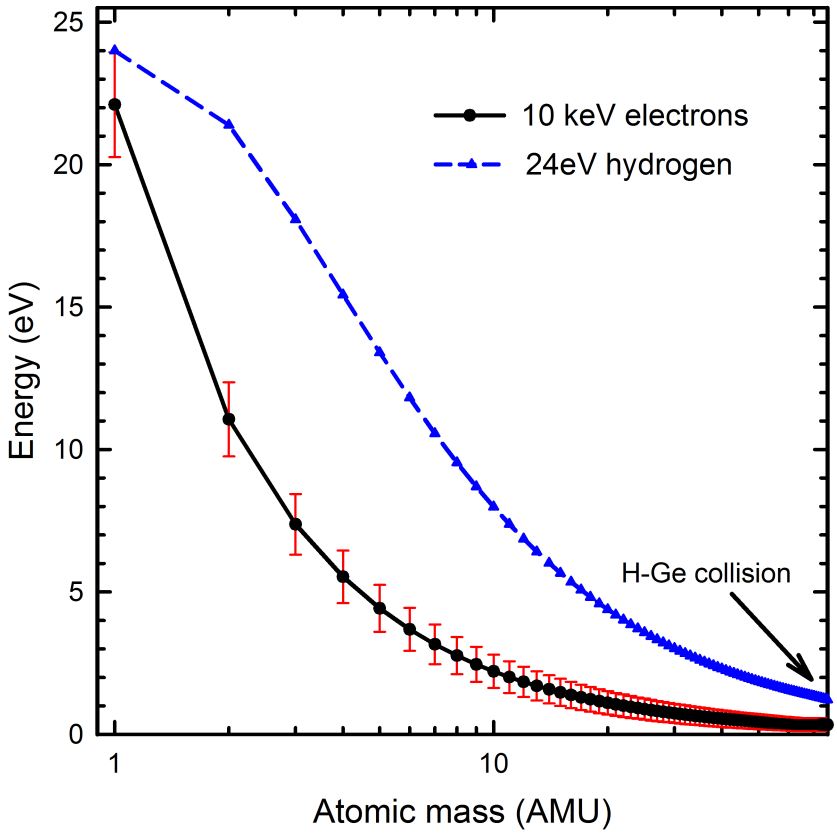

Figure 2.1: Theoretical maximum energy transfer in an elastic collision of a 10 keV electron (black solid plot) or between a 24 eV hydrogen atom (blue dash plot) and particles of mass 1 to 75 AMU. Bars denote the energy variation dependent on the velocity of the second particle in a vacuum, assuming an ideal gas at room temperature, parallel to the direction of the impinging particle. Calculations were performed relativistically for electron collisions but relativistic considerations only accounted for a 0.9% increase in energy transfer at this velocity.

technological breakthrough in recent times was achieved by varying the distance between cathode and anode of the e-gun resulting in greater control of the e-beam power over long production runs. Unlike traditional e-guns where the filament current or accelerating voltage is varied, the vario-cathode principal e-guns do not have the disadvantage of the electron beam moving with changing power. Accelerating voltages up to 60 kV are now attainable in production campaigns that exceed 100 hours (Reinhold et al. 2011).

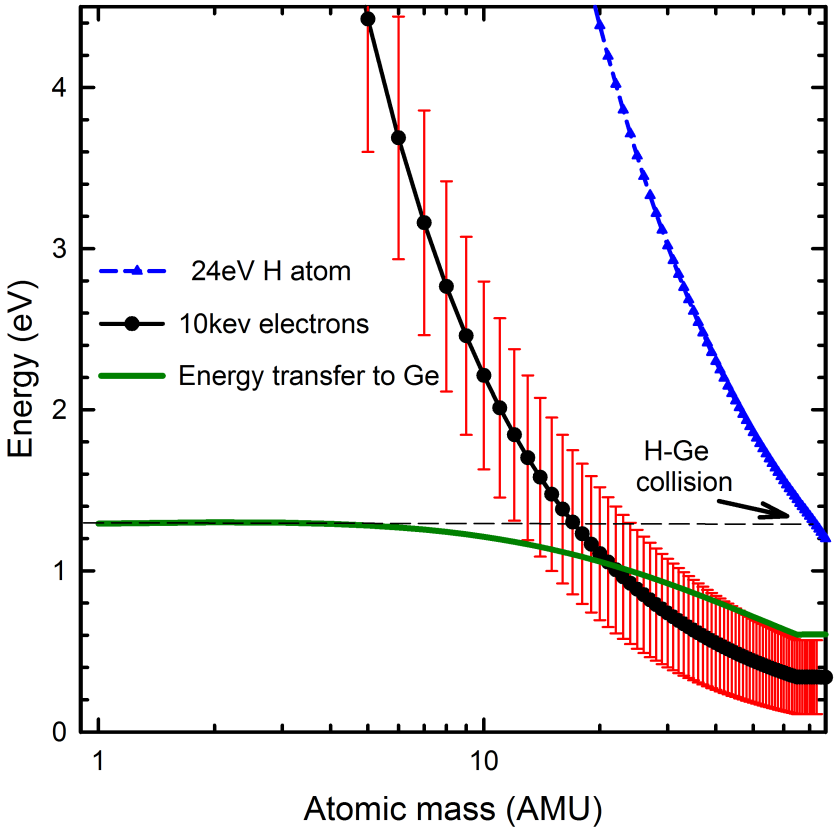

Figure 2.2: This figure considers the case where a 10 keV electron collides with a particle of mass 1 to 75 AMU (intermediate particle) that then collides with a stationary Ge lattice atom. The green plot represents the maximum energy transferred to a Ge atom as a function of the mass of the intermediate particle. The maximum energy transferred was found to be 1.3 eV that coincides with an AMU of 2, indicated by the black dashed line. The black solid plot and blue dashed plot are the same as in Figure 2.1

2.1.3 Sputter Deposition (SD)

This is, without reservation, the most important and most widely used deposition technology in use in the semiconductor industry. A large volume of work already exists describing SD (Vossen et al. 1991; Seshan 2001; Rossnagel et al. 1990; Martin 2010, to mention just a few sources) yet still much remains to be studied. By comparing the

number of publications published and patents registered for magnetron sputtering and other sputter techniques with deposition techniques like pulsed laser deposition (PLD), RE, EBD and molecular beam epitaxy (MBE), it is apparent that in industry sputtering remains the most popular technique (data up until 2005). In academia magnetron sputtering is as popular a research field as PLD which confirms the importance of these investigations (Depla et al. 2010). In the last decade rapid advances in this field has led to the development of so many variations of sputtering and hybrid techniques that discussing the use and influence of plasmas in semiconductor processing is a good subject to start with.

Plasmas are an abundant state of matter in the universe, yet on earth they occur infrequently and are not true plasmas. By definition a plasma consists of an equal number of negatively and positively charge particles but this is impossible to achieve in a laboratory as the faster moving electrons are constantly lost to the surrounding environment at a faster rate when compared to the positive ions. Due to their versatility, gas plasmas have found applications in many fields and come in a few forms but we will discuss only the most common types which are discharge plasmas that are generated when an electric field is applied to a volume of gas.

Applying an electric field on an ionised gas results in a faster energy transfer to the electrons than to the ions leading to an energy transfer between electrons and ions, atoms and molecules via elastic collisions. As the mass ratio between electrons and ions is large, only a small portion of the electron's energy is transferred in a collision that has a high probability of exciting, ionizing or dissociating gas atoms or molecules in low-pressure plasmas. These energetic particles can, in turn, interact with surfaces and films in the chamber, modifying their physical and chemical properties, which is why low-pressure plasmas have become so popular for materials processing (Walton et al. 2010; Shah 1996). Whether the aim is to etch a surface or to deposit a thin film, there is a plasma system available that can treat areas of many square meters or deposit material at a rate comparable to other deposition techniques, as is now the normal requirement in, for example, the photovoltaic (PV) industry.

An introduction to plasma chemistry as it relates to deposition was recently pub-

lished (Walton et al. 2010) that exceeds what is required for semiconductor processing as it takes into account the complex nature of plasmas at gas pressures from 10^{-3} to 10^{4} Torr. Only low pressure plasmas are applicable for etching or deposition in the semiconductor industry which simplifies matters somewhat. At a pressure of 10^{-3} Torr that is approximately 10^{-3} mBar the electron temperature T_e far exceeds the gas temperature T_g which is an important consideration as a plasma can be seen as a system where energy is transferred between particles in the plasma and also to the boundaries, which in this case are our chamber walls, target, substrate and growing film. First, electrical energy is transferred to a gas (more rapidly to the electrons) via the applied electric field. Then energy is transferred in collisions between energetic particles in the gas. These interaction probabilities are often described in terms of their cross-sections or the mean path between collisions that not only sustain the plasma but ultimately determine the rate at which reactive species interact with the substrate, establishing the fundamental importance of understanding these interactions. For low pressure plasmas, electron-electron interactions are less likely and for a gas at room temperature, the energy of the gas atoms can be neglected when considering electron-atom interactions. Electrons accumulate sufficient energy to excite, ionize or dissociate heavier atoms or molecules in inelastic collisions.

Measurement of plasma conditions has been performed by various means for which a large body of literature exists (Hershkowitz 1996; Schwabedissen et al. 1997). Interpretation of results is challenging, especially when dealing with multi-component plasmas. For low discharge currents, Langmuir probes inserted into a plasma measured electron energies ranging from 2 - 10 eV and densities of 10^{10} to 10^{11} cm^{-3}. Taking many measurements at higher currents was impractical due to thermal damage to the probes. Electron temperature was found to decrease and electron density increased with increasing pressure (Rossnagel et al. 1990).

Magnetron Sputtering

A brief description of direct current (DC) and radio frequency (RF) glow discharges is crucial to understanding more complex sputter techniques and was first described by

Penning in 1936 (Penfold 1996). Sputter systems comprise two electrodes, a cathode and an anode, placed in a vacuum chamber separated by a space, typically of a few centimetres. If a DC electric field is applied between cathode and anode, initially a small current flows that increases with increasing target voltage as more charge carriers arise from impact ionization and secondary electrons being emitted from the cathode (target). Only when ions impacting on the target generate enough electrons so that the production of ions and electrons in the plasma are approximately equal has the discharge reached a steady state, known as the “normal glow" state. A sharp rise in the current and drop in voltage shifts the plasma into the “abnormal glow" state which is the regime where sputtering occurs.

An increase in the current will lead to an increase in the sputtering rate and can be accomplished in two ways, increasing the target voltage or the plasma gas pressure. Unfortunately the interaction cross-section decreases once the electron energy exceeds 100 eV and increasing the sputtering pressure eventually lowers the sputter rate as ions collide more frequently with gas atoms. This can be represented as a curve known as the Paschen curve (Vossen et al. 1991, p. 26) that illustrates the optimal conditions necessary for sputtering.

A major drawback of DC sputtering is the inability to sputter non-conducting targets. Substituting the DC power supply with a high frequency RF supply removes this restriction as it can be coupled through any kind of impedance. For frequencies above 50 kHz the ions are essentially stationary while the electrons, due to their lower mass and higher velocities, cycle between electrodes eliminating the need for secondary electron emission to sustain the plasma. At the 13.56 MHz frequency that is mandated by law the stationary ions would remain between the target and substrate for a balanced system and no sputtering would occur. In reality, sputter systems are rarely balanced as the target electrode surface area is usually much smaller than the substrate that is typically earthed together with the chamber walls, ensuring that most of the voltage drop occurs at the target. Alternatively coupling the target through a capacitor in series with the RF generator ensures that more current flows in one half of the cycle than in the other half resulting in ions experiencing a nett force in the direction of the target. The cycling

of electrons and the limited loss of secondary electrons ensures that RF discharges are maintained at lower pressures.

The introduction of a magnetic field with lines parallel to the target is a popular and low-cost strategy to optimize the ionization efficiency of sputtering systems. Electrons moving near the target experience a force perpendicular to their direction of travel that results in electrons following a spiral path around field lines. This effectively traps electrons near the target from which they were emitted and greatly enhances ionization of the plasma gas (Shah 1996).

In an RF magnetron sputter system it is a simple matter to alternate between sputtering and deposition. For wafers placed on the capacitively coupled electrode, sputter etching of the wafer surface will take place. Careful or minimal application of a magnetic field is required to avoid uneven etching of the wafer. During deposition, the target is ablated by the plasma ions and the ejected target atoms or clusters, mostly neutrals although some atoms will be ionised, travel outwards from the target in random directions. Evaporant atoms arriving at the sample will have energies ranging from 10 - 40 eV (Shah 1996) that is sufficient to generate defects in Ge and also in other semiconductors. Sputter etching is carried out for accelerating voltages ranging from 0.5 to 5 kV, subjecting substrates to collisions with particles that not only have the energy to generate vacancies, but extended defects as well. The rate at which material is sputtered is influenced by a number of parameters including, pressure, power, process gas species and substrate temperature. The sputter rate will influence the defect introduction rate, especially for purely physical sputtering processes involving an inert gas.

Inductively Coupled Plasma (ICP)

ICP sources have a number of distinct advantages over capacitively coupled plasma sources. They typically consist of a cylindrical inductor wound around the vacuum chamber that is energised by a suitable RF power supply. Planar coils have also been investigated, (Schwabedissen et al. 1997) and share the same advantage of locating the inductor coil outside the chamber thus minimizing contamination. ICP sources have

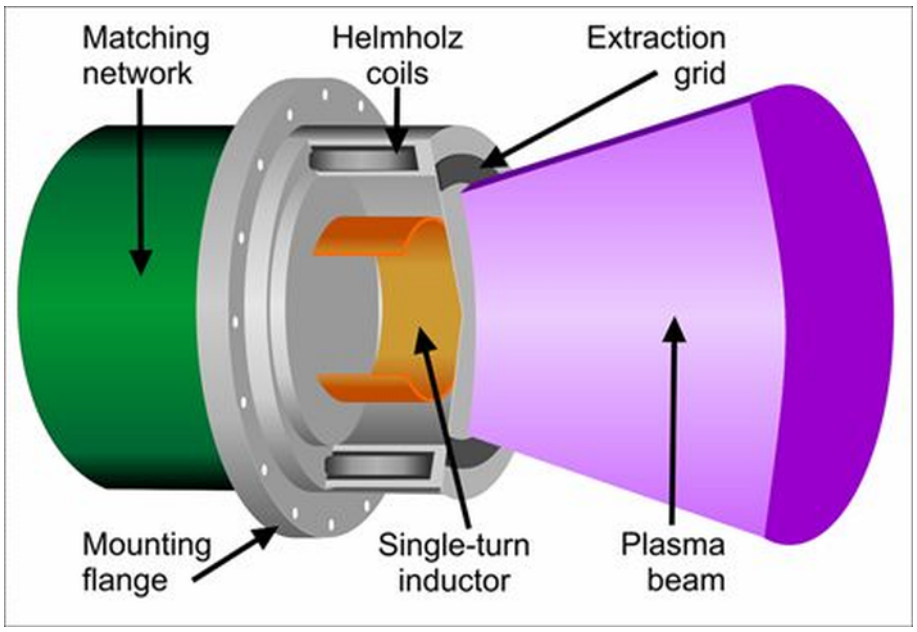

Figure 2.3: Inductively coupled plasma source (CCR Technology information brochure).

undergone rapid development recently as there is a need in the semiconductor industry for a source that operates at low pressures and at high plasma densities. Low pressure ensures that less collisions occur in the accelerating sheath thus enhancing anisotropic etching and high density results in greater throughput (references in Schwabedissen et al. 1997).

The essential phenomena that determine how inductively-coupled plasmas operate are no different to inductive heating of metals and this has been known for more than a century. An inductor, usually placed outside the plasma chamber, energised at an optimal frequency and power induces an electric field inside the chamber that when it interacts with the plasma gas sustains a stable discharge. In 1961 Reed demonstrated that such a discharge could be maintained in an open tube while gas streamed through it (Boulos 1985). Figure 2.3 is a simplified diagram of the Copra source manufactured by CCR Technology where the plasma discharge chamber and processing chamber are separate. The single-turn inductor that is placed around the plasma chamber is connected to a 13.56 MHz RF power supply through a matching network. The plasma presents a load to the power supply and matching is required to maintain the reflected power

as low as possible so that maximum energy (forward power) can be transferred to the plasma. In cylindrical ICP chambers the plasma is toroidal in shape with the plasma concentrated in a thin region, the width of which is known as the skin depth, dependent on the load conductivity and oscillator frequency. A magnetic field, generated by the Helmholtz coils connected to a low voltage DC source, enhances the magnetic coupling thus improving the density and uniformity of the plasma (Meziani et al. 2001).

Due to the difference in velocities between electrons and ions in an RF electric field, the plasma loses electrons faster in collisions with the chamber walls. This gives rise to a time averaged positive potential in the plasma, that is described in detail in Rossnagel et al. (1990). While many ICP sources rely on diffusion, this source extracts the ions from the source by utilising the potential that exists between the plasma and the earthed extraction grid. Samples to be etched are placed in the processing chamber in the zone labelled "Plasma beam" of Figure 2.3 where they experience collisions with incident ions and neutrals. The ion energy is determined by the plasma potential but is best measured using a Faraday cup placed at the same position that samples will occupy.

Modern ICP sources have a number of distinct advantages over their capacitively coupled counterparts. These sources are both capacitively (high energy regime) and inductively (low energy regime) coupled that gives rise to two peaks in their ion energy spectrum. The ion energy is inversely proportional to the process gas pressure and as the energy decreases, so does the capacitive coupling. At ion energies below 18 eV when the source is predominantly inductively coupled, single narrow energy peaks were measured with a full width at half maximum of 3 eV (Chevolleau et al. 2000). Ion energies that are pressure, power and distance dependent rarely exceed 250 eV but ICP density could be as high as 10^{11} cm $^{-3}$ as ionisation efficiency is excellent at $\approx 5\%$. For diatomic process gasses dissociation can be as high as 90% which improves chemical reactivity at the substrate surface. Plasma etching generates defects in semiconductors, not only at the surface but also deeper into the bulk, and any technique that delivers low energy particles in high enough numbers is of immense value as junctions are continually decreasing in width.

2.2 Creation of Defects in Germanium

Point defects and impurities have a profound influence on the electrical properties of all semiconductors. Interesting changes in the doping density, local resistivity and carrier lifetime are just a few of the effects that have been observed but then too, device yield, performance and long-term reliability will be impacted on. First we need to understand the mechanisms by which defects are introduced so that when observed, there is a probability that these defects can be identified and not only characterised. References 9 to 13 in Cardona (2007) describe a few properties of semiconductors that are influenced by defects.

Defects in crystalline materials can be found in many forms. Vacancies, interstitials, impurities and in the case of a Frenkel pair, a combination of a vacancy with an interstitial are examples of the most fundamental point defects. By adding defects together extended defects and clusters can be created. In all solids an equilibrium concentration of defects exists due to random vibration of the crystal lattice at temperatures above 0 K. As almost all devices will be stored at approximately 300 K and have to operate up to a temperature of 400 to 500 K, it is important to be mindful of this. For defect studies Ge is readily available with low enough equilibrium defect concentrations so that they either cannot be measured or if at a higher concentration, are electrically inactive.

Most studies of the material properties of germanium are now decades old and a concerted effort is required to update this data base (Vanhellemont, Simoen et al. 2007). Defect studies are no exception, although recently a number of papers clarified the characteristics of important point defects (Fage-Pedersen et al. 2000; Markevich, Hawkins, Peaker, Litvinov, Murin, Dobaczewski and Lindström 2002; Markevich, Hawkins, Peaker, Litvinov, Murin and Dobaczewski 2004; Mesli et al. 2008; Vanhellemont, Lauwaert et al. 2009; Kolkovsky, Christian Petersen et al. 2010) and metal related defects (Simoen, Opsomer et al. 2008; Lauwaert and Clauws 2010). Process induced defects have also received attention in the last decade (Auret, Meyer, Coelho and Hayes 2006; Lajaunie et al. 2011; Coelho, Auret, Janse van Rensburg et al. 2013) and yet for some primary defects, experimental studies are rare (Carvalho et al. 2007). Hydrogen related defects have also

not received the attention they deserve (Budde, Bech Nielsen, Leary et al. 1998; Coomer et al. 1999) even though this is an important impurity in Ge (Weber, Hiller et al. 2006). Grown-in, process-induced and radiation-induced defects will be discussed as they relate to semiconductors in general with a description of the most relevant defects found in Ge that relate to this study.

2.2.1 Grown-in Defects

Without exception, all samples prepared were cut from wafers grown by the Czochralski (Cz) process at Umicore in Belgium. These high purity (HP) germanium wafers are guaranteed to be dislocation free thus well suited to semiconductor research. An extensive review of grown-in defects in germanium was carried out by Vanhellemont, Simoen et al. (2007) that includes details of both theoretical and experimental contributions to this topic. Every application imposes its own requirements in terms of material purity and dislocation density, the most sensitive applications having the most rigorous requirements. For future devices it will be necessary to investigate the defects introduced during epitaxial growth but at present bulk-grown Ge fulfilled our requirements.

Complications arise in the experimental investigations into intrinsic defects as many of these defects are mobile at temperatures well below room temperature. A great deal of theoretical studies have been carried out on these defects and where experimental data exists, these results compare well with this data. A number of approaches to gather data have been tried that include quenching at high temperatures followed by annealing at lower temperatures, plastic deformation at high temperatures, low temperature irradiation and *ab initio* calculations. Quenching did not yield good results for studying vacancies in Ge, the most prevalent point defect predicted (Vanhellemont, Hens et al. 2005), as diffusion occurs too quickly making vacancy clustering unavoidable. Radiation at low temperatures provided data on defects that were tentatively identified as the Frenkel pair, the self-interstitial, the vacancy (Mesli et al. 2008) and di-vacancy (Kolkovsky, Christian Petersen et al. 2010) in good agreement with theoretical predictions. In Ge vacancy mediated diffusion is the dominant process unlike in Si where interstitials play

a greater role. This is explained in part by the energy required for vacancy formation being less for Ge than for Si (Vanhellemont, Simoen et al. 2007).

Crystal growth starts with the Cz process that has been reviewed by Sinno et al. (2000), in an article that focusses on mathematical modelling of the introduced defects. Numerical simulation of these processes is becoming increasingly important as the material requirements become more stringent. As the seed is slowly extracted from the melt a solid/melt interface is set up where it is assumed there is an equilibrium concentration of vacancies and self-interstitials (Voronkov model). These defects diffuse axially due to thermal diffusion and also as the crystal is moving away from the melt. The velocity that the crystal is extracted with, combined with defect recombination determines the dominant intrinsic defect that is present in the crystal. Sources of extrinsic defects are the crucible and the atmosphere that crystals are grown in. Quartz crucibles tend to introduce more silicon and oxygen into the crystal whereas graphite crucibles are sources of carbon contamination.

The control of dislocation density is important for certain optical applications but for semiconductor grade material only dislocation free Ge is appropriate. Although dislocations are not present in these high quality crystals a number of other defects remain. The dopant is introduced by design and is either antimony (Sb) or phosphorus (P) for n-type Ge and boron (B) or gallium (Ga) for p-type substrates. Carbon incorporation is less of a problem than in Si crystal growth as carbon is not miscible with Ge. At the melt temperature of Ge the equilibrium concentration is estimated to be approximately 10^8 cm^{-3}. Oxygen also has less of an affinity for Ge than it has for Si, tending to stay in the liquid phase of Ge. This leads to an increased oxygen concentration in the tail of the pulled crystal where oxygen's usual lattice position is bond-centered (BC), between two host atoms. Increased oxygen concentrations have been observed when Ge is grown in an oxygen environment. A review of oxygen related defects in Ge was undertaken by Clauws (2007) that discusses interstitial oxygen, oxygen dimers, precipitates and the vacancy-oxygen (VO) defect or A-center in detail. The dimer and VO are the only two oxygen related defects that have been identified experimentally and in the case of VO, three charge states were reported (Markevich, Hawkins, Peaker, Litvinov, Murin,

Dobaczewski and Lindström 2002).

Hydrogen, nitrogen and silicon are impurity atoms that are also found in HP-Ge. The most important impurity found in semiconductors is probably hydrogen with its many possible interactions, both with the host lattice but then also with other impurities. It was long thought to be electrically inactive in semiconductors and in Ge it has been impossible to grow the best single crystal material without growth taking place in an H_2 atmosphere. Recently, theory predicted that VH, VH_2 and VH_3, a vacancy populated with one, two or three H's respectively, have acceptor levels in the bandgap (Coomer et al. 1999). VH_2, VH_4 and V_2H_6 together with H_2^* and IH_2 have been observed in proton and deuteron implanted Ge using infra-red (IR) spectroscopy (Budde, Bech Nielsen, Keay et al. 1999). Ge device quality has trailed that of silicon devices, possibly due to vacancies and dangling bonds(DBs) that do not respond to hydrogen passivation. This has been reported to be as a consequence of interstitial hydrogen in Ge being stable exclusively in the negative charge state (Weber, Janotti et al. 2007), unlike in Si where hydrogen exhibits amphoteric behaviour and passivation of defects is well established.

Nitrogen is also an important grown-in impurity as Ge crystals are often grown in an N_2 atmosphere. As nitrogen has low solubility in Ge and the dominant nitrogen species is the N pair (Ge-N split interstitials) as opposed to substitutional N, it manifests as a weak donor. Additionally a number of N-related shallow acceptors were identified using photo-thermal ionization spectroscopy (PTIS).

Silicon inclusion must also be expected when molten Ge is in contact with a quartz crucible. This often takes the form of SiO_x precipitates after high temperature anneals as Si has a greater affinity to oxygen than to Ge. SiO_2 is believed to be responsible for smooth pits that have been observed and that exhibited no changes after annealing, testament to the high stability of these defect clusters.

2.2.2 Process-induced Defects

Process-induced defects in semiconductors can be defined as any defect, including point and extended defects, that were introduced during operations such as epitaxial film growth, dopant diffusion, implantation and metallization. These defects have been reported on extensively in the literature (Claeys and Vanhellemont 1993; Queisser et al. 1998; Cerva et al. 2001) and a recent publication was dedicated to dealing with this subject for Ge (Claeys and Simoen 2009). Once defects have been introduced then one must either use, passivate or remove these defects, however, in all scenarios a thorough identification of the defects as well as their source is essential.

With the move of shallower junctions as a consequence of device miniaturization, diffusion of dopants has been largely replaced with implantation where the depth is controlled by the incident ion energy and concentration is dose dependent. Other treatments that expose substrates to harsh conditions during device manufacture are high temperature oxidation, sputter deposition, plasma etching and even wet chemical treatments that are known to introduce hydrogen into the crystal. Process-induced defects have been separated from grown-in defects but to some extent there is correlation between these defect types when we consider defect generation and nucleation. There is substantial interest in process-induced defects as they are often detrimental to the performance of semiconductor devices.

For Ge device processing the most important form of damage occurs during ion implantation. For Si a large body of research exists that still fails, theoretically and experimentally, to explain the structure of these damaged regions. Annealing has been shown to form better defined defects in Si but these, although point like, were different to defects observed after electron irradiation. Recently there has been renewed interest in investigating ion implantation damage in Ge (Peaker, Markevich, Murin et al. 2005; Markevich 2006a; Impellizzeri et al. 2010) but as in the Si case, there is no guarantee that a rigorous understanding of these defects is at hand. Ge being far more dependent on vacancy mediation than Si makes it likely that vacancy clusters will be of greater technological significance going forward.

During RF sputter etching substrate degradation was found to be proportional to bias voltage as higher voltage leads to particles with more kinetic energy impinging on the surface. The defects introduced during sputter etching (Nyamhere, Das, Auret, Chawanda et al. 2009) and sputter deposition (Auret, Coelho, Meyer et al. 2007) have been characterized using DLTS but many of these defects remain physically unidentified and what the damage causing agents were is unclear. Similar problem persist for other processes and at present it suffices that damage minimizing strategies are applied that limit the defects introduced during processing to ensure device reliability.

2.2.3 Radiation-induced Defects

An overview discussing radiation and particle damage in Ge was undertaken by Markevich, Peaker and Larsen (2007) that covers the identification of defects produced, their annealing characteristics and impact on device performance. There is also a large overlap between radiation-induced defects and those produced during processing. In sputter deposition, for example, substrates are exposed to high energy electrons, heavy particle bombardment, x-ray and ultraviolet radiation. Most of the investigations into radiation damage concentrate on interactions that result in the displacement or displacements of a native atom from the lattice resulting in a vacancy and interstitial forming, or creating a Frenkel pair as this is also known as. This is the simplest case and such displacements may be accomplished by interactions with energetic electrons, gamma rays, neutrons and ions of any species. Fundamental differences between radiation that creates isolated Frenkel pairs and radiation by heavier particles that may create clusters is discussed whereas ionizing radiation that results in the generation of electron-hole pairs will be omitted.

The interaction of a high energy particle with a lattice atom to create a Frenkel pair was dealt with in section 2.1.2 as was the concept of threshold energy, but incident particles with sufficient energy may also cause multiple particle displacements when the recoil atom has enough energy to displace atoms. Due to the high mobility at room temperature of the created vacancies and interstitials it is now possible that they migrate

to the surface, recombine as a vacancy-interstitial or interstitials can accumulate in the end of range region to form stacking faults. Another option that is often more common is that interstitials and vacancies are trapped by impurity atoms that are then detected as stable defects or defect clusters. The E-center, a combination of a vacancy with a dopant atom and the A-center, a vacancy and an oxygen atom, are well studied examples of this. For ion-solid interactions the usual treatment is to describe these in terms of collision cascade theory (Claeys and Simoen 2009). Part if the ion energy goes into a series of atomic displacement and the larger fraction is taken up interacting with valence electrons of the crystal atoms leading to ionization reactions. Atoms along the ion track are displaced, these knock-on atoms with sufficient energy may then displace additional atoms and finally near the end of the ion track damage events are spaced closer together resulting in the most change occurring at the end-of-range (EOR).

The threshold energy required for displacements, often quoted as 15 eV for Ge, is an important parameter that software packages like SRIM make use of to predict the amount of vacancies and interstitials generated as well as the approximate EOR for a non-crystalline solid. Generally it has been shown that higher energy results in greater displacements and that the magnitude and type of displacements are crystal orientation dependent. The NIEL hypothesis ("Non Ionizing Energy Loss") has been very successful in estimating the total damage from the sum of the elastic and inelastic contributions of different radiation sources but neglects recombination of vacancies and interstitials and furthermore provides no information on the types of damage produced. The NIEL calculations are given by

$$\text{NIEL} = \frac{N}{A} \times [\sigma_e T_e + \sigma_i T_i], \tag{2.4}$$

where N is Avogadro's number, A is the gram atomic weight of the target material, σ_e and σ_i refer to the total cross sections and T_e and T_i are the effective average recoil energies corrected for ionization loss where the subscripts e and i refer to the elastic and inelastic contributions, respectively.

High energy electrons and MeV α-particles were the principle forms of radiation considered herein. The defects introduced by high energy electron irradiation have been reported on in a number of articles (Fukuoka et al. 1974; Poulin et al. 1980; Mooney

et al. 1983; Peaker, Markevich, Murin et al. 2005) as have the α-particle induced defects (Markevich, Peaker, Markevich et al. 2006; Kolkovsky, Petersen et al. 2007; Roro et al. 2009). For more information on the specific defects that have been observed after electron irradiations the mini-review by Fage-Pedersen et al. (2000) is recommended and also deals with proton irradiation. High energy particles should, in principle, transfer above threshold energy to lattice atoms in elastic collisions but in practice, electron and α-particle damage share few similarities. Damage from high energy electrons is well spaced so that there is a smaller probability of these isolated sites interacting with one another. This typically results in single vacancies that then migrate and form stable complexes when paired with impurity atoms, that is, point defect formation is more likely. In comparison, heavier particles like protons, neutrons, α-particles and ions generate displacements and an increased probability of damage cascades with closely spaced defects as the energy of these particles increases. Depending on the energy and the target material the region where most damage occurs, the EOR, may be in the active region of the semiconductor device. Closely spaced defects, be they vacancies or interstitials, are more likely to interact with each other to form di-vacancies, multi-vacancies or clusters, especially near the EOR.

Protons, although of comparable mass to neutrons, interact with the target atoms on an electronic level during irradiation and once they come to rest remain highly reactive. The positively charged hydrogen atom is known to passivate donors and also radiation induced defects. Some controversy exists in Ge if we consider experimental evidence of hydrogen passivation of defects (Pearton et al. 1983; Lauwaert, Van Gheluwe et al. 2008) whereas theory predicts that hydrogen passivation of DBs is unlikely (Weber, Janotti et al. 2007). This matter will not be cleared up easily but what is certain is that unlike Si, hydrogen passivation of defects in Ge is not a foregone conclusion.

The defects observed after irradiation are discussed in chapter 4 but one final point to consider is that MeV electron and α-particle irradiation induced defects that were similar and yet DLTS results confirm that in some cases defects observed were not found after both processes. This has led to speculation that electron irradiation defects are point defects whereas some defects observed after irradiation by heavier particles are

point-like.

2.3 Electrical Characterization

Techniques for the characterization of semiconductors have developed at an incredible pace and play a leading role in the success story of this industry. Physical and electrical characterization have been indispensable tools in the laboratory and now also on the factory floor. This section is only concerned with the electrical characterization tools that were used for the investigations included in chapter 4 and some techniques used today are introduced in Grundmann (2010) whereas more advanced spectroscopic techniques are described in detail in the text by Schroder (2006).

2.3.1 C-V, I-V and I-T Measurements

Capacitance

At the heart of the capacitance-voltage (C-V) technique lies the semiconductor property that for a rectifying junction, the width of a reverse-biased space-charge region (scr) depends on the applied voltage.

The capacitance per unit area A of a SBD to a n-type substrate is given by

$$\frac{C}{A} = \left[\frac{qN_{\mathrm{D}}\epsilon_{\mathrm{s}}}{2(V_{\mathrm{bi}} - V - \frac{kT}{q})}\right]^{1/2}, \tag{2.5}$$

that can be written as

$$\frac{1}{C^2} = \frac{2(V_{\mathrm{bi}} - V - \frac{kT}{q})}{A^2 q N_{\mathrm{D}} \epsilon_{\mathrm{s}}}, \tag{2.6}$$

where V_{bi}, V, k, T, q, N_{D}, and ϵ_{s} are the built-in voltage, applied voltage, Boltzmann constant, temperature in K, charge of an electron, majority carrier concentration and the static dielectric constant of a semiconductor, respectively. This assumes that $N_{\mathrm{D}} > N_{\mathrm{A}}$

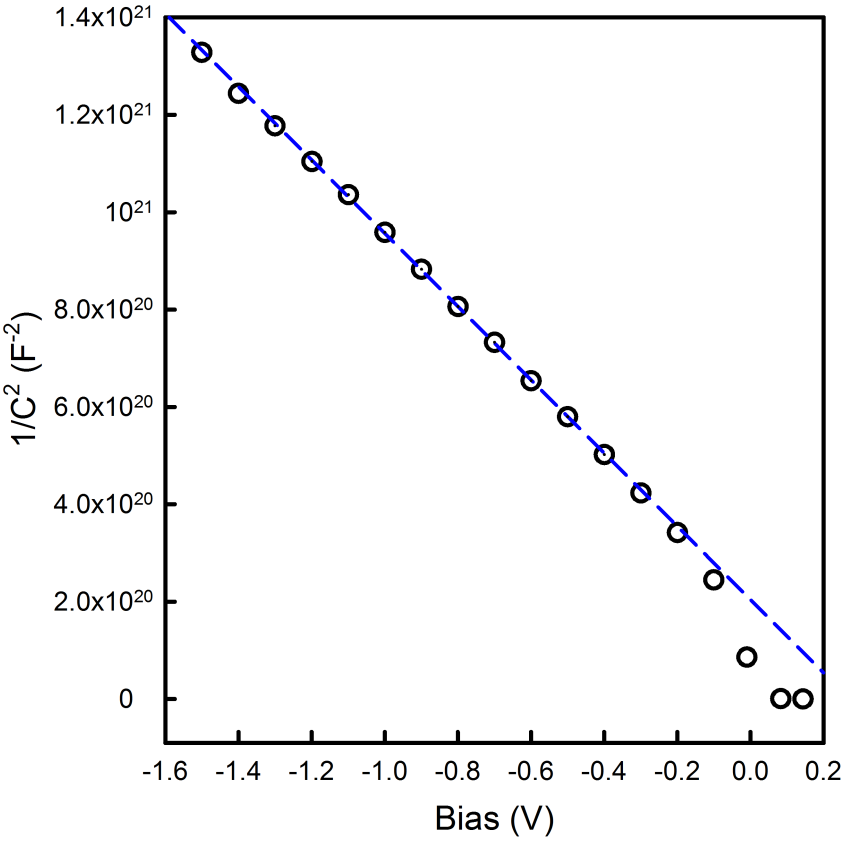

Figure 2.4: $1/C^2$ versus bias voltage (black circles) dependence for a Pt Schottky diode ($A = 2.8 \times 10^{-3}$ cm^2) deposited on n-Ge by EBD. A linear fit (blue dashes) is shown for $V < -0.4$ V. By extrapolating this fit to $1/C^2 = 0$, $V_\mathrm{b} = 0.232\ V$ is obtained. From the slope N_D was calculated to be 1.4×10^{15} cm^{-3}.

and care must be exercised in measuring the diode area as it scales by a factor squared (Schroder 2006). For $1/C^2$ measured as a function of bias, this plot is linear if the doping is homogeneous. Doping and free carrier concentrations are assumed to be equal and is obtained from the slope by the following procedure. The built-in potential is related to the barrier height by

$$\phi_\mathrm{B} = V_\mathrm{bi} + V_0. \tag{2.7}$$

Here $V_0 = (kT/q)\ln(N_\mathrm{c}/N_\mathrm{D})$ where N_c is the effective density of states in the conduction band. Plotting $1/(C/A)^2$ versus V yields a curve with the slope $2/[-qK_\mathrm{s}\epsilon_0 N_\mathrm{D}]$ where

K_s is the semiconductor dielectric constant. This curve has an intercept on the V-axis, $V_i = -V_{bi} + kT/q$. The barrier height, ϕ_B, is then determined from V_i

$$\phi_B = -V_i + V_0 + kT/q. \tag{2.8}$$

Current-Voltage

Here we deal only with thermionic emission with the proviso that the effect of drift and diffusion in the depletion region are assumed to be negligible (Rhoderick et al. 1988). For a SBD with a thin interfacial insulator layer and low series resistance, the current, I, across the diode can be described by

$$I = I_s \left[\exp\left(\frac{qV}{nkT}\right) - 1\right], \tag{2.9}$$

where I_s, the reverse saturation current, is defined as

$$I_s = AA^*T^2 \exp\left(-\frac{q\phi_B}{kT}\right), \tag{2.10}$$

and $A^* = 4\pi qk^2m^*/h^3$, n, m^* and h are the Richardson's constant, ideality factor, effective electron mass and Planck's constant, respectively. The ideality factor that is 1 for the ideal diode and $n > 1$ for non-ideal diodes, combines all those factors that make a diode non-ideal.

A semilog I versus V plot of data according to equation 2.9 is linear for $V \gg kT/q$, as shown in Figure 2.5. I_s can be calculated from 2.9 by extrapolating this linear fit to $V = 0$. Using this value for I_s one can calculate ϕ_B from

$$\phi_B = \frac{kT}{q} \ln\left(\frac{AA^*T^2}{I_s}\right) \tag{2.11}$$

This determination of ϕ_B is only as accurate as your knowledge of A^*. An alternative plot using equation 2.9 is $\log[I/(1 - \exp(-qV/kT))]$ versus V that generates data that is linear all the way to $V = 0$ is useful to extend the linear fit region.

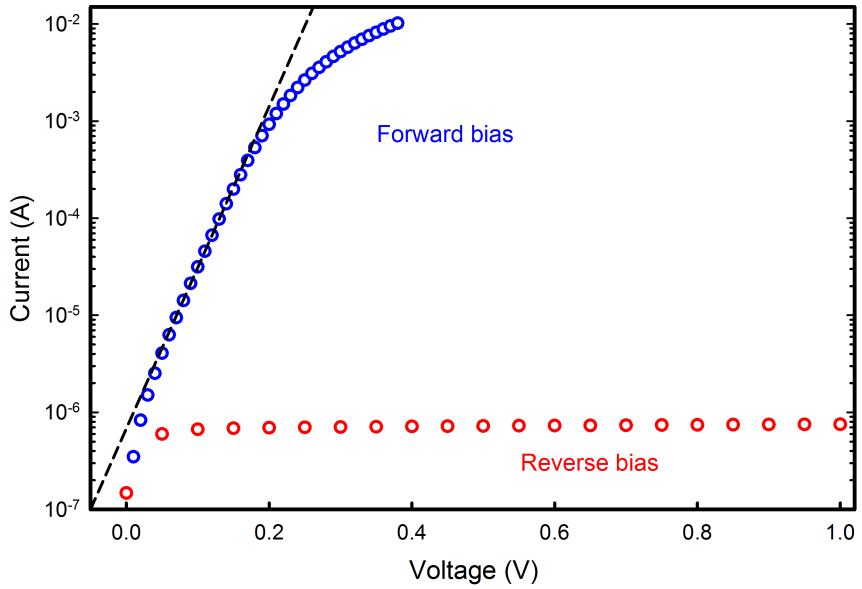

Figure 2.5: Current (A) versus voltage (V) (blue circles - forward bias and red circles - reverse bias) for a Pt Schottky diode ($A = 2.8 \times 10^{-3}$ cm^2) deposited by EBD on n-Ge. A linear fit (dashes) is indicated for $V \geq 3kT/q$ thus avoiding the region $V > 0.18$ V where series resistance becomes significant. The ideality, n, was calculated to be 1.02 at 297 K.

Current-Temperature

Plotting $\ln(I/T^2)$ versus $1/T$ at a constant forward bias, also known as a Richardson plot, can be used to calculate the Richardson constant, A^*. The ideality, n, will have to be determined independently and the extraction of A^* can be prone to large variation. In these studies I versus T plots were used to demonstrate ideal diode behaviour and the effects of recombination/generation (Coelho, Auret, Myburg et al. 2009).

2.3.2 Deep Level Transient Spectroscopy

Conventional DLTS

This is based on the work of Lang (1974) and although DLTS can be performed using decaying waveforms from capacitance, charge or current waveforms, we will discuss capacitance DLTS only. The first single-shot I-t and C-t methods were developed by Sah et al. (1970), but it was only later with Lang's introduction of the rate window concept that a signal could be extracted from the noise thus realising the potential of this technique.

To fully comprehend the purpose of these measurements a researcher must be familiar with semiconductor fundamentals. The space-charge region below a rectifying contact is a feature of semiconductors with a width, W, that according to the abrupt junction approximation is given by

$$W = \left[\frac{2\epsilon_{\mathrm{s}}(V_{\mathrm{bi}} - V - \frac{kT}{q})}{qN_{\mathrm{D}}}\right]^{1/2}. \tag{2.12}$$

The width of the depletion region is affected by the applied bias, V, where W is decreased if $V > 0$ and increased when $V < 0$. The capacitance across this region is discussed in section 2.3.1. In the simplest terms, when the thermal equilibrium of this region is disturbed the system will strive to return to an equilibrium position and this may involve the emission and capture of electrons and holes from defects that have energy levels within the bandgap. With DLTS it is possible to obtain quantitative data about these defects and typically the activation energy or enthalpy, capture cross-section and concentration of a specific defect is extracted.

If we consider the $C-t$ curve of a transient capacitance measurement, it decays exponentially. Obtaining a DLTS spectrum is described in Schroder (2006) as processing a $C-t$ curve so that when "a selected decay produces a maximum output, then a signal whose decay time changes monotonically with time reaches a peak when the rate passes through the rate window of a boxcar averager or the frequency of a lock-in amplifier." Observing these repetitive transients while varying the sample temperature if a defect

emission rate changes, then a peak appears in the capacitance versus temperature plot. This plot is the DLTS spectrum.

The data extraction process involved is probably best understood by considering Boxcar DLTS: Sampling $C-t$ waveforms at a time $t = t_1$ and $t = t_2$ so that the capacitance at t_2 is subtracted from that at t_1, that is, $\delta C = C(t_2) - C(t_1)$. The difference in capacitance is small at low or high temperatures as this corresponds to very slow or very fast transients, respectively. Scanning in temperatures between these extremes generates a difference signal when the time constant is in the order of the gate separation, $t_2 - t_1$. When the capacitance difference passes through a maximum as a function of temperature, the DLTS peak is obtained that, when using weighting function $w(t) = \delta(t - t_1) - \delta(t - t_2)$ is described by

$$\delta C = C(t_1) - C(t_2) = \frac{n_T(0)}{2N_d} C_0 \left(\exp\left(-\frac{t_2}{\tau_e}\right) - \exp\left(-\frac{t_1}{\tau_e}\right) \right) , \tag{2.13}$$

where the period is $T = (t_1 - t_2)$ and τ_e has temperature dependence

$$\tau_e = \frac{\exp(E_c - E_T)/kT}{\gamma_n \sigma_n T^2}, \tag{2.14}$$

with $n_T(0)$, C_0, E_c, E_T, γ_n and σ_n are the deep level trap density (cm^{-3}), capacitance with bias applied, conductance band edge (eV), trap energy (eV), voltage acceleration factor (V^{-1}) and electron capture cross section (cm^2), respectively. When δC exhibits a maximum at temperature $T = T_1$, differentiating equation 2.13 with respect to τ_e and setting the result equal to zero yields $\tau_{e,max}$ at δC_{max}:

$$\tau_{e,max} = \frac{t_2 - t_1}{\ln(t_2/t_1)}. \tag{2.15}$$

This equation is independent of the magnitude of capacitance and by generating a number of plots where t_2/t_1 is fixed but t_1 and t_2 are varied a number of data points are generated for a plot of $\ln(\tau_e/T^2)$ versus $1/T$. The slope of this generated Arrhenius plot is used to calculate the trap energy, E_T and from the intercept of this plot with the τ_e/T^2-axis, the apparent capture cross section is calculated.

Recently, with the personal computer becoming available cheaply, computer DLTS has become more popular and refers to the digitizing of capacitance waveforms so that

these may be managed later. In this way a number of spectra for different rate windows may be collected with a single temperature sweep and the transient may be observed throughout to establish if it is exponential in nature. More averaging from taking a number of transients leads to better signal-to-noise ratios(S/N ratios) that in turn results in more precise measurements.

Laplace DLTS

The possibility of digitizing transients and fitting complex curves to these transients for defect analysis was described two decades ago by Dobaczewski et al. (1994). Where conventional DLTS scans in temperature while taking repetitive measurements, L-DLTS is performed at a fixed temperature and so doing greatly improve the time constant resolution of conventional DLTS. Due to instrumental effects even a perfect defect produces broad peaks in a conventional spectrum that are too course to study fine structure in the emission process whereas L-DLTS outputs a spectrum of delta-like peaks from the digitized output of the capacitance meter, repeated many times and averaged to reduce the noise level. To deal with nonexponentiality observed in capacitance transients it can be assumed that they are characterized by a spectrum of emission rates,

$$f(t) = \int_0^\infty F(s)e^{-st}ds \tag{2.16}$$

where $f(t)$ and $F(s)$ is the recorded transient and the spectral density function, respectively. If this spectrum is represented by a Gaussian overlaying the logarithmic emission rate scale then it is possible to describe the non-exponential transient in terms of broadening of the emission activation energy. The capacitance transient given by the equation above are mathematically represented by the Laplace transform of the true spectral density function, $F(s)$.

A mathematical algorithm that performs an inverse Laplace transform on the function $f(t)$ yields a real spectrum of the emission rates present in the spectrum. This results in either a spectrum of peaks for monoexponential and multiexponential transients or a broad spectrum with no fine structure if the distribution is continuous. Decays must be exponential in the same direction and no other *a priori* assumptions need be made

about the functional shape of the spectrum.

An intensity output as a function of emission rate where the area under each peak is directly related to the trap concentration is the end product of L-DLTS. Several thousand transients are captured at a fixed temperature and averaged. If enough transients are captured to get a good S/N ratio then L-DLTS provides an order of magnitude better energy resolution than conventional DLTS. Practically, this limits the technique to use on samples where the defect density is 5×10^{-4} to 5×10^{-2} of the shallow donor or acceptor density with the proviso that all electrical noise in the system has been reduced as much as possible.

In the past there has been much confusion about the identity of certain defects when analysing broad peaks so using L-DLTS to analyse defects with similar emission rates is the most obvious application of this technique. L-DLTS has been used successfully to investigate fine structure in the thermal emission process of a number of semiconductors and more recently also on Ge (Markevich 2006b; Larsen et al. 2007; Capan et al. 2010).

2.4 Annealing of Defects

Annealing is defined as subjecting a system to a physical treatment, usually heating, that causes a modification or annihilation of defects and dislocations. Different defects anneal out of a semiconductor at different temperatures and when this is coupled with DLTS measurements a defect can be identified with greater certainty. Much of the success in dealing with process induced defects has been due to the advances made in developing novel annealing strategies. Annealing not only removes defects but also increases the mobility of carriers and fully activates the dopant (Fleetwood et al. 2008).

In industry today, furnace annealing (FA) has mostly been replaced with rapid thermal annealing (RTA) as shallow junctions require careful control of the thermal budget of these anneals to remove defects while avoiding excessive diffusion of the dopant (Claeys and Simoen 2009). In this work isochronal annealing in an argon environment was the only strategy applied to investigate the annealing characteristics of point defects

introduced during processing and by irradiation. This involves a number of anneals, for a specific time, while increasing the temperature per anneal by a set amount. This may also provide information about defect evolution.

A promising technique that has been used on Si to investigate damage created by Ge implants is known in industry as flash-assist rapid thermal processing (fRTP). This process has the advantage over conventional RTA in that the high quality optical light sources deliver more power with a faster response time and deliver this power as short wavelength radiation that is more effective at heating. The typical energy burst is in the order of 1 µs whereas 20 to 30 µs is required for heat to dissipate in a Si substrate. The bulk of the wafer, acting as a heat sink, provides for efficient cooling of the hot zone leading to an anneal with a fast ramp up and cool down with no dwell time at the maximum temperature. Interstitial decay rates for fRTP between 1000 °C and 1300 °C were reported to be three orders of magnitude greater than what has been reported before (references in Fleetwood et al. 2008, p.15).

2.5 Summary

Various aspects of manufacturing devices, defect introduction and the electrical characterization of semiconductors have been covered in this chapter. Only the parts of this theory with direct relevance to this work have been included with occasional mention of a technique that holds promise for the future. Where more in-depth understanding is desired the interested reader should make use of the excellent references provided. In the following chapter the experimental aspects will be discussed with emphasis on the practical application of the techniques listed so far.

Chapter 3

Experimental Techniques

3.1 Introduction

A number of experimental techniques were utilised during the course of this study and will be described briefly in the following chapter. A more detailed explanation will be presented when the technique that was used differed substantially from what is widely applied in research or manufacturing.

3.2 Device Fabrication

All samples were prepared on bulk-grown Ge that was acquired from Umicore. It was thus only necessary to manufacture two device types, ohmic contacts and Schottky barrier diodes (SBDs). Substrates were first chemically cleaned (Mattox 1996) before further processing could be applied. A number of recipes were attempted (Camp 1955) and subsequently discarded in favour of the cleaning procedure outlined in the following section. Recipes that included hydrofluoric acid were also later abandoned due to safety concerns.

3.2.1 Ohmic Contacts

Cleaning recipes typically include two parts. The first stage involves degreasing the substrate and this is followed by an etch stage that removes the oxide top layer, if such a layer exists. Etching as a third stage of sample cleaning then removes a few atomic layers from the substrate exposing clean material below, free of any surface contaminants. All chemical treatment of samples was performed in glassware that had been cleaned in a solution of NH_3 (30%) : H_2O_2 (31%) (1 : 1 ratio) for 24 hours. The following degreasing procedure was used:

- Trichloroethylene dip in an ultrasonic bath for 5 minutes.
- Isopropanol dip in an ultrasonic bath for 5 minutes.
- Methanol dip in an ultrasonic bath for 5 minutes.

The following etch procedure was applied:

- A 1 minute dip in a solution of H_2O_2 (30%) : H_2O in a ratio of 5 : 1.

To lower the probability of surface oxides forming on the clean substrates, samples were loaded into a vacuum chamber as quickly as practically possible. Once the vacuum chamber had been pumped down to a pressure of 10^{-6} mbar, AuSb (0.6% Sb) was deposited on the back surface using resistive evaporation (RE). Annealing of the samples at 350 °C in an Ar ambient for 10 minutes lowered the contact resistance rendering the contact ohmic. Dry etching using inert or reactive species in a plasma could also have been used for sample cleaning but were not evaluated in this role.

3.2.2 Schottky Barrier Diodes

The same cleaning procedure was followed, as outlined above, prior to SBD fabrication. Once cleaned, samples were loaded into one of a number of vacuum chambers where

metal was deposited through a metal contact mask onto the sample front surface. This deposition by RE, electron beam deposition (EBD) or sputter deposition (SD) typically resulted in 8 diodes with a diameter of 0.6 mm being deposited.

3.3 Defect Introduction

A number of sources were used to introduce defects in the studied samples. In the case of process-induced defects, it was not always possible to isolate a specific defect causing agent. When known sources of energetic particles are used then the outcome is often more predictable as the fluence and the energy range are known. A description of the damage causing mechanisms employed follows with special considerations, when appropriate.

3.3.1 Electron Beam Deposition

All the samples prepared by EBD were exposed to a 10 keV electron source. Up until 2010 this source was powered by a tetrode based power supply that was replaced by an updated solid-state power supply. The main advantage of using a solid-state power supply was that the beam current was better controlled and maintained within 1 to 2 mA of the setpoint. Samples loaded into the vacuum chamber were shielded from the source until such time as the evaporation had stabilized and deposition onto the sample could proceed. Once the required metal thickness had been deposited, as measured by an in situ quartz microbalance, the sample was once again shielded from the evaporant source. Additional shielding was applied during deposition for select samples and this is shown in Figure 3.1.

Depositions were started when the vacuum pressure was approximately 10^{-6} mbar in the chamber but the pressure during device fabrication changed dependent on the metal used, beam current and deposition duration. Chamber bakeout prior to deposition and careful conditioning of the evaporant sources ensured that the vacuum pressure remained

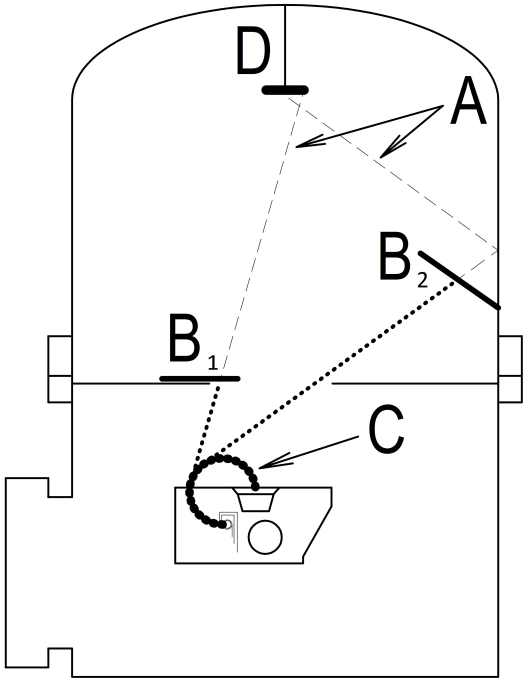

Figure 3.1: Layout of the EBD system chamber showing possible paths taken by energetic particles (A), shields (B_1 and B_2), electron beam path (C) and the sample positioned near the top of the chamber (D).

below 10^{-4} mbar during depositions of metals with high melting points.

3.3.2 Plasma Processing

Substrates placed in a plasma will be subjected to a bombardment by a variety of energetic particles, some of which will have enough energy to displace native atoms from the substrate, not only on the surface but deeper in the substrate too. Heating of samples may also occur, especially if no cooling is applied and plasma treatment is allowed to continue for any length of time exceeding a few minutes.

RF sputtering

Sputter deposition of SBDs was carried out using a Leybold Z400 system. A 5 kV radio frequency (RF) power supply that was capacitively coupled to the target provided the energy to maintain the plasma. Only Ar was used as the plasma species thus no chemical reactions were expected with the process gas during deposition or etching. With a sample to target distance of approximately 30 mm and no shutter for shielding resulted in samples being exposed to the plasma from the moment that the plasma ignited. Initial pressure in the chamber was 3×10^{-6} mbar, raised to an Ar partial pressure of 6×10^{-2} mbar during deposition. Samples were placed on a water-cooled stainless steel surface in the chamber but localized heating of the substrate may have occurred during etching and deposition. Typically, 1 to 5 kV accelerating voltage was used during deposition and 1 kV or less was applied during etching of the Ge samples.

Inductively Coupled Plasma

Plasma etching of Ge was carried out using either a Copra DN160 or DN200 manufactured by CCR Technology. These inductively coupled plasma (ICP) sources were primarily designed for research and development work but all results obtained can be scaled up with ease for production purposes. After sample loading, via a load-lock chamber, the main vacuum chamber was pumped down to 10^{-6} mbar with the sample rotated away from the plasma source. A pressure burst of the process gas, Ar, was used to ignite the plasma. By throttling the vacuum pumps and controlling the gas flow into the chamber the Ar partial pressure was maintained at a pressure that was typically between 10^{-2} and 10^{-3} mbar. Once the plasma conditions were stable the sample was rotated into position facing the source at a distance of 10 cm from the extraction grid (Figure 2.3). Plasma etching of the degreased Ge samples was carried out for set times varied between 1 and 10 minutes, after which samples were either rotated towards an EBD source for deposition or removed from the chamber for SBD evaporation elsewhere.

3.3.3 Radionuclide Sources

Two radionuclide sources were used to create defects in Ge for comparison with process induced defects: americium-241 (Am-241) and strontium-90 (Sr-90). These sources are convenient to use due to their portability and long life-span.

Am-241 with a half-life of 430 years for the α decay mode emits α particles with an energy of ~5.5 MeV. This source was assumed to be monoenergetic and has been described in Auret, Goodman et al. (1993). When last measured, in 1991, this Am-241 foil was found to have a flux of 7.1×10^6 $cm^{-2}s^{-1}$. Due to the long halflife of this isotope, the flux of this source is not expected to have changed significantly since it was last measured. Samples exposed to this source were placed in contact with this foil for irradiation treatments that rarely exceeded 2 hours. This was found to be the maximum dose permissible as the measured defect concentration was then measured at 10% of the dopant concentration, the maximum allowed for reliable deep level transient spectroscopy (DLTS) measurements. The end of range for 5 MeV α particles implanted in Ge was predicted by a SRIM simulation to be 30 µm, well beyond the measurement range of our DLTS setup but resulting in a constant defect concentration within the measurement range.

The Sr-90 source used in this study has also been described in Auret, Goodman et al. (1993). This source emits electrons with energies ranging from approximately 100 to 2000 keV in a continuous spectrum and was last measured in 2009 when it was found to have a flux of 1.1×10^9 $cm^{-2}s^{-1}$. With a half-life of 28.5 years for the decay to yttrium, this source too was not expected to have changed appreciably during this study. Contact between source and sample did not occur as this disk shaped source is housed in a holder so that when samples were irradiated a gap of approximately 1 mm remains between sample and source. Typical irradiation time was 24 hours that resulted in sufficient damage to ensure a signal-to-noise ratio (S/N ratio) for DLTS measurements. Care should be exercised when handling these sources and protocols for the safe use of radioactive materials must be followed.

3.3.4 Van de Graaff Accelerator

A 2.5 MV Van de Graaff (VdG) belt-type electrostatic generator was used to accelerate positive ions, namely protons and α-particles, for Rutherford backscattering spectroscopy (RBS) (McGuire 1988; Bunshah 1994) and defect creation. A detailed description and explanation of the working principle of a VdG can be found in Choppin et al. (2013).

Particles with an atomic mass above one, when accelerated to energies above an MeV are capable of creating Frenkel pairs in the bulk of a semiconductor crystal with such collisions typically resulting in numerous displacements of the native crystal atoms. The rate at which defects are created in small samples is also relatively high thus short exposure times are mandatory and irradiations are usually performed after SBD fabrication, that is, through the metal contact. This strategy protects the semiconductor surface from some damage but for repeatable results and ease of use it was preferable to expose samples to radionuclide sources.

Au films evaporated onto Ge were analysed using RBS (Hayes et al. 2008; Nel et al. 2009) but as these investigations were not central to the theme of this work RBS will not be discussed further.

3.4 Device Measurement

The systems used for the electrical measurement of devices will be described briefly with emphasis on aspects of these systems that differ from what is commonly used in research or industry. These systems were assembled in-house from components that are readily available in the marketplace. Physical constants used in the calculations and especially those constants describing the properties of Ge were obtained from the second edition of Sze et al. (1981).

3.4.1 I-V and C-V Measurements

The current-voltage (I-V) and capacitance-voltage (C-V) measurement system consists of a probe station, HP 4140 pA meter/DC Voltage Source and HP 4192A LF Impedance Analyzer. Devices to be analysed, either ohmic contacts of SBDs, were placed on the probe station that in turn was housed in a dark box. Measurements were performed in the absence of light to minimise the photo generation of carriers. All the instruments were controlled by a Labview program especially developed for our group. The Labview I-V/C-V program not only performs repetitive measurement routines unassisted but then automatically generates plots and calculates a diode's ideality factor, n, Schottky barrier height, ϕ_{iv} and the device series resistance, R_{s} for I-V measurements. For C-V measurements the program calculates the carrier concentration, N_{D}, Schottky barrier height, ϕ_{cv}, built in voltage, V_{bi} as well as plotting a depth profile of the carrier concentration.

3.4.2 DLTS Measurements

The DLTS system is comprised of a closed cycle helium cryostat, Boonton 7200 Capacitance Meter, Agilent 33220A Function / Arbitrary Waveform Generator, oscilloscope and computer control system. The computer system in turn includes a National Instruments GPIB interface card and runs software routines to collect and analyse data. The GPIB interface not only provides the interface with the instruments used but can also bias and pulse the device under test. The Trapview software package that was used for DLTS and Laplace-DLTS (L-DLTS) measurements was provided by A. R. Peaker (Centre for Electronic Materials Devices and Nanostructures, University of Manchester) and L. Dobaczewski (Institute of Physics, Polish Academy of Sciences). For sensitive measurements when defect concentrations were low, the GPIB card was used to trigger the Agilent waveform generator and this instrument then provided the bias voltage and pulse for our measurements. It was found that this measure alone improved the S/N ratio by up to a factor of 10.

Samples were placed on a sapphire disk on the cold tip of the cryostat. This arrangement ensured that samples were electrically insulated from earth and a thin indium foil

between sapphire and sample provided thermal contact while maintaining electrical contact with the sample back surface. Probes on the indium foil and on a diode on the front surface completed the circuit. Once the bias and pulse conditions had been programmed into the waveform generator and then applied, the waveform could be observed on the oscilloscope. This proved to be an invaluable tool as the leading and trailing edges of the pulse were then iteratively optimised to lower the overshoot of the pulse. Typically, a 30 μs sloped leading and trailing edge was sufficient to remove most of the overshoot ensuring that the bias conditions were accurately applied. After a quick ramp down in temperature under zero bias conditions, a conventional DLTS scan could proceed while ramping up at a rate that did not exceed 0.1 K s^{-1}. For multi-rate window scans the rate of temperature ramping was considerably slower. During all measurements the samples were kept in the dark and vacuum was maintained by a rotary vane pump.

A similar procedure was applied for L-DLTS measurements. Samples were cooled to a pre-set temperature. The temperature was allowed to stabilize so that fluctuations were less than 0.1 K before L-DLTS measurements were taken. For low defect concentrations these measurements had to be repeated many times to raise the S/N ratio so that meaningful results were obtained.

3.5 Annealing of Defects

Most of the annealing of defects was carried out in a borosilicate tube three-zone furnace. An inert atmosphere was created by flowing Ar gas through the tube throughout the annealing process. Samples were loaded on a movable tray inside the tube that was then only shifted into the hot zone once the tube was flooded with Ar. A thermocouple with its tip placed near the sample was used to monitor the temperature and regulation was accomplished by either moving the sample further into or out of the hot zone. Once the annealing was complete, the sample was moved out of the hot zone and allowed to cool in an Ar atmosphere. The same apparatus was used for ohmic contact fabrication.

3.6 Summary

Many of the experimental procedures outlined in this chapter involved the use of high vacuum. It suffices to mention that sound vacuum practices were applied as explained in Harris (1989). The importance of good vacuum practices cannot be emphasized enough if ones goal is to produce repeatable results. In every experiment performed a combination of the techniques outlined above was used, starting with device preparation and then proceeding to the measurements. Techniques like scanning electron microscopy, Auger electron spectroscopy, atomic force microscopy and others that were attempted but did not contribute significantly to this study were not included. In the following chapter the results of this thesis will be presented as a series of published articles.

Chapter 4

Results

4.1 Introduction

Results are presented as a series of articles that have been published from 2006 to 2013. In many cases an article is relevant to two or more sections of this chapter and in such cases has been placed in the the last section of this chapter that it applies to. While some repetition is inevitable, this is mostly the case in the article introduction sections. Where research on Ge has been contributed to but is not central to this thesis, such articles have been included in title and abstract form only. References appearing in articles are not listed in the main reference list unless cited elsewhere as well.

4.2 Material Characterization

The research carried out in Coelho, Auret, Janse Van Rensberg et al. 2008, was undertaken after considerable time had already been dedicated to optimizing the deposition processes used so that the Schottky barrier diodes (SBDs) required were of a high quality. This article also serves as an introduction to the effects of electron beam deposition (EBD) and sputter deposition (SD) on n-Ge diode properties by comparing current-

voltage (I-V) and capacitance-voltage (C-V) measurements of these diodes with those of diodes manufactured using resistive evaporation (RE).

Current-temperature (I-T) measurements are reported on in Coelho, Auret, Myburg et al. 2009 that has been included in section 4.5. While the I-T scans discovered recombination/generation (RG) of carriers in the measured diodes, it was the low temperature I-V measurements that revealed the excellent rectifying properties of inductively coupled plasma (ICP) treated diodes.

I-V and C-V measurements were performed by Chawanda et al. 2012, on iridium SBDs and has been included in section 4.7. Annealing may be the primary focus of this contribution but it also aims to demonstrate that near ideal diodes are attainable when a high melting point metal like iridium is deposited by EBD and that the rectifying behaviour is not lost when the Ge-Ir system is annealed beyond an eutectic point. Auret, Coelho, Hayes et al. 2008, and Auret, Coelho, Janse van Rensburg et al. 2008, discuss I-V measurements on Ge and are included in sections 4.3.1 and 4.7 respectively. The former article investigates the correlation between the vacuum pressure during EBD of various metals and the number of defects introduced as a high defect concentration will impact negatively on diode performance. The latter article also examines the effect of EBD on the rectifying qualities of our devices and compares these results to those of diodes manufactured using SD, establishing SD as the more damaging process.

Hayes et al. 2008, is primarily concerned with characterizing the interface between Ge and an Au metal layer. Here I-V measurements were also reported on to demonstrate the effect of annealing on diode properties. With the annealing of the samples above 361 °C a Pd-Au eutectic forms thus transforming the Au diode into a germanide. The effects of germanide formation on the SBD properties were thus investigated. Coelho, Auret, Janse van Rensburg et al. 2013, aims to show that the rectifying qualities of SBDs manufactured by EBD can be improved even further and has been included in section 4.3.2.

As Nel et al. 2009, deals mostly with characterization of the material surface using scanning electron microscopy and Rutherford backscattering, only the title and abstract are included.

phys. stat. sol. (c) **5**, No. 2, 626–629 (2008) / **DOI** 10.1002/pssc.200776815

physica status solidi c
www.pss-c.com
current topics in solid state physics

IV and CV measurements of Schottky diodes deposited on Ge by electron beam and sputter deposition

S. M. M. Coelho, F. D. Auret*, P. J. Janse van Rensberg, C. Nyamhere, J. M. Nel, and M. Hayes

Physics Department, University of Pretoria, Pretoria 0002, South Africa

Received 2 May 2007, accepted 5 September 2007
Published online 10 December 2007

PACS 61.82.Fk, 73.30.+y, 73.40.Ei

* Corresponding author: e-mail fauret@postino.up.ac.za

Various Schottky metal contacts were deposited on bulk grown (111) Sb-doped n-type Germanium. The Schottky contacts were deposited by resistive evaporation, electron beam deposition and RF sputter deposition. Current–voltage (IV) and capacitance–voltage (CV) measurements revealed differences in the diode performance that suggested damage caused to the germanium semiconductor crystal by the more energetic deposition methods of electron beam deposition and sputter deposition. Subsequent annealing improved the diode performance thus succeeding in removing some of the defects introduced, but not all. Sputter deposition produced the poorest diodes highlighting this as the most damaging process.

1 Introduction In the manufacture of semiconductor devices, metal contacts have always played a pivotal role, especially in MOSFET and CMOS devices. Understanding the effect of different metallization techniques on the electrical properties of a semiconductor is of critical importance as we advance into the age of ultra-fast devices. Germanium is now receiving renewed attention as its high mobility carriers (holes and electrons) make it an ideal medium to build the next-generation ultra fast switching devices with. In addition, there are several important niche applications for germanium such as high-resolution gamma-ray detectors, far IR detectors and low temperature thermistors (see [1] and references therein).

In-depth investigations regarding the defects introduced in Ge during critical processing steps, like etching and metallization, are still in progress. Metallization procedures, such as sputtering and electron beam deposition, are known to introduce defects at and close to the metal-semiconductor junction. Defect introduction influences the barrier heights of the contacts and alters device performance [2–7]. These defects are dependant on interacting, energetic species reaching the semiconductor surface and subsequently influencing the device in a positive or negative manner.

2 Experimental procedure A bulk-grown (111) *n*-type Ge wafer doped with Sb to a level of 2.5×10^{15} cm^{-3} was cut into manageable pieces and degreased in successive trichloroethylene, acetone and methanol ultrasonic baths. After a de-ionized water rinse, samples were etched in a mixture of H_2O_2 (30%) : H_2O (1:5) for one minute and inserted into a vacuum chamber where AuSb (0.6% Sb) was deposited on their back surfaces. A ten minute anneal at 350 °C in Ar lowers the barrier height and the contact becomes ohmic. Phase two involves the same cleaning and etching procedure as above followed by metal deposition onto the front of the samples. These Schottky metal contacts are deposited through a mechanical contact mask's 0.6 mm diameter holes in a resistive evaporation, electron beam or RF sputter deposition system. Initial vacuum was better than 10^{-5} mbar for all depositions regardless of the metal or the system used. Where possible, a 200 nm thick metal layer was deposited onto the germanium to form the Schottky barrier diodes (SBDs) considered herein. In situ monitoring of the film thickness growth was achieved in the resistive and electron beam system via an Inficon crystal growth monitor. The first 10 nm of metal was deposited at a rate of 0.1 nm/s to minimise damage to the germanium substrate, with subsequent ramping up to 0.3 nm/s for the remainder of the deposition. A 10 kV electron gun, the

filament of which was mechanically shielded from the samples, generated the electron beam in the electron beam deposition system. The beam current was approximately 0.1 ampere during most of the depositions, however, the deposition rates were lower during the Pt and Ru depositions. RF sputter deposition was carried out in a vacuum chamber that was backfilled with argon and kept at a partial pressure of 6×10^{-2} mbar. The power supply voltage that ignited the plasma was set at 700 V (0.15 A) and so Au was sputter deposited onto the germanium substrate at a predetermined deposition rate.

The electrical measurements were performed in two systems, a room temperature and a closed-cycle helium cryostat IV system, respectively. In the room temperature IV station measurements were taken under normal atmospheric conditions, without the sample being exposed to light. In the cryostat the sample is kept in a vacuum wherein the temperature can be varied from 20 K up until room temperature. Metal probes are used to establish electrical contact with the Schottky diode that is being measured, and all instruments were controlled by a proprietary Labview routine that also records the data being gathered.

3 Results and discussion Electron beam (EB) and sputter deposition (SD) systems have the advantage of being able to deposit high melting point metals, however depositing Au, a metal with a relatively low melting point, affords us the opportunity to compare results obtained by using resistive evaporation as well. EB and SD have the added advantage that, being higher energy processes, good adhesion between sample and deposited species is far more likely. A disadvantage is that energetic species that are generated during the electron beam deposition [6] and the sputter deposition [3] processes have been shown to damage the substrate that is being deposited onto. Pd, Pt and Ru diodes were also prepared by EB deposition for the purpose of comparison.

Ideality factors were calculated from a linear fit of the forward bias log[I/(1-exp(-qV/kT))] versus V plot [8] that also yielded the IV barrier heights. For comparison the CV barrier height was obtained from a linear fit of the $1/C^2$ versus V plot and is displayed in Table 1. Idealities below 1.1 are considered good [9] with the proviso that an accurate linear fit is obtained from the forward bias region. Although the resistively evaporated Pd diode achieved the ideality factor closest to unity, it is more significant that the Au and Ru EB deposited diodes demonstrate that manufacturing quality diodes by this energetic process is possible.

Reverse bias current at -1 V (as displayed in Table 1) is another indication of diode quality. Lower leakage current is preferable and values below 10^{-5} A (diode area dependent) represent high quality Schottky barrier diodes on germanium [10]. Comparing the three deposition methods for Au deposition it is clear (and expected) that resistive evaporation yields the best IV and CV characteristics. Sputter deposition produced Au diodes that were electrically measurable but with bad capacitance–voltage response hence the questionable Au CV barrier height. All IV barrier heights were of similar magnitude, regardless of metal or deposition technique used, indicating Fermi level pinning. The work functions of the metals chosen were not similar enough to warrant this high degree of correlation. Sputter deposition was the only technique that produced a diode with an appreciably lower IV barrier height, indicative of damage to the surface due to high energy impingement on the semiconductor. IV and CV characteristics of Pd and Au deposited resistively outperformed all the other Schottky diodes that were considered in this study.

Thermionic emission is the dominant current mechanism describing IV behaviour of ideal Schottky diodes at room temperature given by $J \cong J_s(e^{qV/kT} - 1)$ where $J_s \sim e^{q\Phi/kT}$ is the saturation current density and Φ, the barrier height. As the temperature is lowered then so too is the current density. In Fig. 1, the measurement performed on an Au diode at 120 K had a lower reverse and forward bias current than the room temperature measurement at the same voltage, regardless of the deposition method used. Under reverse bias conditions $J \sim -J_s \sim -e^{q\Phi/kT}$, explaining the lowering of the reverse bias current of the diodes that are measured at lower temperatures. At room temperature, resistive, electron beam and sputter deposition produced better to worse diodes respectively. This is even more apparent when the same measurements were taken at 120 K where a difference of three orders of magnitude between the -1V reverse bias of the electron beam and sputter deposition diodes was measured. Electron beam [6] and sputter deposition [4] introduced defects at and below the semi-

Table 1 Schottky diodes manufactured by different deposition methods, measured at 298 K.

Metal	Deposition type	Current (A) at -1 V bias	Ideality factor	IV Barrier height (eV)	CV Barrier height (eV)
Au	Resistive	2×10^{-6}	1.07	0.56	0.43
Au	Electron beam	1.8×10^{-5}	1.08	0.55	0.46
Au	Sputter deposition	5.9×10^{-5}	2.05	0.44	~0.25
Pd	Resistive	2.3×10^{-6}	1.06	0.55	0.43
Pd	Electron beam	3.9×10^{-5}	1.29	0.52	0.44
Pt	Electron beam	3.5×10^{-6}	1.13	0.56	0.48
Ru	Electron beam	3×10^{-6}	1.07	0.57	0.53

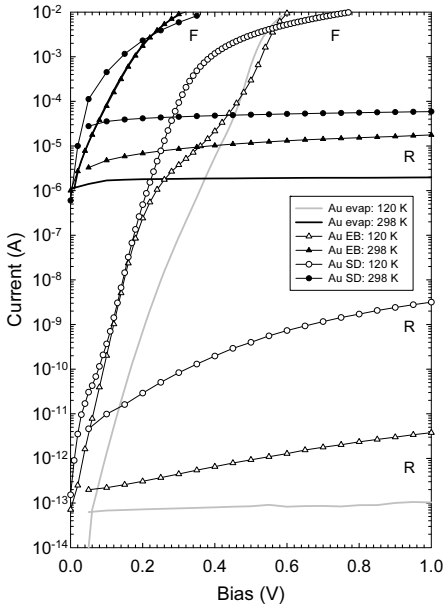

Figure 1 Current-voltage measurements under forward (F) and reverse (R) bias conditions for a Au Schottky diode recorded at 120 K and 298 K respectively.

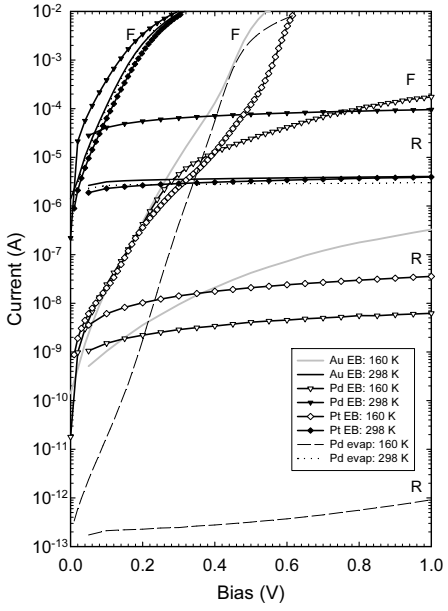

Figure 2 Comparative IV responses of different electron beam deposited Schottky diodes at room temperature and 160 K respectively.

tion [4] introduced defects at and below the semiconductor surface as evidenced by the higher reverse bias current compared to the measured reverse bias current of the resistively deposited diodes; resistive evaporation being a method known not to introduce defects [7].

The characteristics of Au and Pt diodes produced by electron beam deposition were found to be remarkably similar to those of the Pd diodes (control) prepared by resistive evaporation when measured at room temperature, as shown in Fig. 2. The reverse leakage current of the electron beam deposited Pd diode is more than an order of magnitude worse than those of Au and Pt diodes measured at 298 K, yet performs better than both the Au and Pt electron beam diodes when measured at 160 K (reverse bias comparison). It is not clear why the EB Pd diode performed so poorly at room temperature, warranting further investigation. The Au and Pt EB diodes demonstrated non-ideal behaviour in the forward bias region above ~0.3 V when measured at 120 K and 160 K respectively. This can be attributed to recombination and generation currents given by $I_{RG} \approx I_0 e^{qV/2kT}$ for energy levels close to the centre of the bandgap. In addition, differences in the forward bias IVs of the Au EB and SD diodes measured below 200 K suggests that the defects introduced during these depositions may also be different. The origin of these defects might be due to energetic particles that interact with the substrate during the deposition process. These high energy particles collide with the surface and form, among others, vacancies that diffuse into Ge and combine with Sb to form the V-Sb complex [7].

4 Conclusions Resistive evaporation consistently produced the highest quality Schottky barrier diodes with the lowest leakage currents and ideality factors closest to unity. More significant is that high quality diodes were also produced by electron beam deposition.

Sputter deposited Au Schottky barrier diodes exhibited much poorer characteristics than the electron beam deposited diodes suggesting that the germanium was damaged to a greater degree in the sputter system. Differences in the 120 K forward bias plots of the Au diodes manufactured by these high energy deposition processes are not only indicative of defect introduction but further suggest that these defects are dissimilar and may have different origins.

Acknowledgements The authors gratefully acknowledge the financial support of the South African National Research Foundation.

References

[1] E. E. Haller, Mater. Sci. Semicond. Process. **9**, 408-422 (2006).
[2] F. D. Auret, O. Paz, and N. A. Bojarczuk, J. Appl. Phys. **55**(6), 1581-1589 (1984).
[3] M. Mamor, F. D. Auret, M. Willander, S. A. Goodman, G. Myburg, and F. Meyer, Semicond. Sci. Technol. **14**, 611-614 (1999).

[4] F. D. Auret, S. A. Goodman, F. K. Koschnik, J.-M. Spaeth, B. Beaumont, and P. Gibart, Appl. Phys. Lett. **74**(15), 2173-2175 (1999).
[5] G. Myburg and F. D. Auret, J. Appl. Phys. **71**, 6172-6176 (1992).
[6] C. Christensen, J. W. Petersen, and A. Nylandsted Larsen, Appl. Phys. Lett. **61**, 1426-1428 (1992).
[7] F. D. Auret, W. E. Meyer, S. Coelho, and M. Hayes, Appl. Phys. Lett. **88**, 242110 (2006).
[8] J. D. Waldrop, Appl. Phys. Lett. **44**, 1002-1004 (1984).
[9] E. H. Rhoderick and R. H. Williams, Metal-Semiconductor Contacts (Clarendon Press, Oxford, 1988).
[10] A. Thanailakis and D. C. Northrop, Solid-State Electron. **16**, 1383-1389 (1973).

IVC-17/ICSS-13 and ICN+T2007 IOP Publishing
Journal of Physics: Conference Series **100** (2008) 042005 doi:10.1088/1742-6596/100/4/042005

RBS investigation of annealed thin gold layers on crystalline germanium

M. Hayes[1], F. Schrempel[2], S.M.M. Coelho[1], F.D. Auret[1], J.M. Nel[1] and W. Wesch[2].

[1]*Department of Physics, University of Pretoria, Pretoria, South Africa*
[2]*Institut für Festkörperphysik, Friedrich-Schiller-Universität, Jena, Germany*
mhayes@postino.up.ac.za

Abstract. In this work we report firstly on the behaviour of Schottky barrier diodes (SBD's) when subjected to thermal treatment after metallization. To better understand this, a systematic study of the interaction between thin gold films and crystalline germanium substrates was undertaken. Gold metal films having thicknesses of 30 and 100 nm have been prepared by means of thermal evaporation on bulk-grown (111) *n*-type germanium doped with Sb to a level of 2.5×10^{15} cm^{-3}. Before metallization the samples were first degreased and then etched in a mixture of H_2O_2:H_2O (1:5) for one minute. Subsequently the samples have been thermally treated in Ar-atmosphere for 10 minutes and at temperatures ranging from 300 to 600°C. Rutherford backscattering spectrometry (RBS) has been performed to estimate the composition of the as-deposited and thermally treated films. It was found, that the composition of the as-deposited film remains unchanged under thermal treatment up to 340°C. Between 340°C and 360°C a gold-rich layer containing a very small amount of germanium is formed. At 361°C this layer suddenly converts to a germanium-rich layer with a small amount of gold. This transition is accompanied by the formation of agglomerates on the surface of the substrate.

1. Introduction

Germanium has been the preferred host for most of the early studies on defects in semiconductors. The research was driven by the search for sensitive detectors for gamma radiation [1]. Defects and defect formation in Ge, being in the shade over the last two decades, have recently generated new interest because of their potential applications. The low effective mass of holes in Ge has opened up the possibility of using Ge in ultrafast complimentary metal-oxide-semiconductor devices [2]. This, in turn, has sparked renewed interest in the properties of defects in Ge because defects ultimately determine the performance of devices. Germanium-on-insulator (GeOI), which combines high mobility of charge carriers with the advantage of a silicon-on-insulator (SOI) structure, is an attractive integration platform for the future integrated circuit technology. Also, due to its low lattice mismatch with GaAs, III-V compound transistors as well as opto-electronic functions can be integrated on GeOI [3].

To exploit the advantages of germanium an appropriate contact technology will have to be developed. Analogous to the silicon-based technology, where metal silicides are used to obtain low-resistance contacts, contacts made of metal germanides could exhibit low sheet and contact resistance, good stability after heat treatment and could be formed by means of simple technological processes like thermal evaporation at low temperatures. Data concerning the behaviour of metal thin films on germanium upon thermal treatment is relatively scarce. The thin film reactions of 20 transition metals,

IVC-17/ICSS-13 and ICN+T2007 IOP Publishing
Journal of Physics: Conference Series **100** (2008) 042005 doi:10.1088/1742-6596/100/4/042005

excluding gold, with germanium substrates have been reported [4]. It was found that among the investigated materials Ni and Pd were the most promising candidates because the formation of NiGe and PdGe at low temperatures lead to contacts with low resistivity, limited film roughness, sufficient thermal stability and limited sensitivity to oxidation. The formation of particularly NiGe contacts has been investigated in some detail [5].

2. Experimental

A bulk-grown (111) 2-inch Ge wafer doped *n*-type with Sb to a level of 2.5×10^{15} cm^{-3} was cut into manageable pieces (3 mm × 5 mm) and degreased in successive trichloroethylene, acetone and methanol ultrasonic baths. After a de-ionized water rinse, the samples are etched in a mixture of H_2O_2 (30%) : H_2O (1:5) for one minute, rinsed again in de-ionized water, and inserted into a vacuum chamber where 100 nm thick AuSb (0.6 % Sb) was resistively deposited on their back surfaces as ohmic contacts. A ten minute anneal at 350 °C in Ar lowers the barrier height and the contact becomes ohmic. Phase two involves the same cleaning and etching procedure as above followed by metal deposition onto the front of the samples. These 0.6 mm diameter Schottky metal contacts are resistively evaporated through a mechanical contact mask to a thickness of 200 nm, thus forming a Schottky barrier diode (SBD). For the topography and RBS measurements, the Ge samples were degreased and etched as described above and 30 nm and 100 nm thick layers were resistively evaporated onto the same side where the Schottky contacts would have been deposited normally. In situ monitoring of the film thickness growth was achieved via an Inficon crystal growth monitor. The first 10 nm of metal was deposited at a rate of 0.1 nm/s to minimise damage to the germanium substrate, with subsequent ramping up to 0.3 nm/s for the remainder of the deposition.

The electrical measurements were performed using a current-voltage (IV) station where measurements are taken under normal atmospheric conditions, at room temperature without the sample being exposed to light. Metal probes are used to make electrical contact with the Schottky diode that is being measured. Composition and structural analyses was performed by utilizing 1.4 MeV He^+ ions from a 2.5 MV Van de Graaff accelerator at room temperature performing Rutherford Backscattering (RBS) in both the random and channeled orientations.

3. Results

Some metallization procedures are known to introduce defects at and close to the metal-semiconductor junction. Defect introduction influences the barrier heights of the contacts and alters device performance [6-9]. These defects are dependant on interacting, energetic species reaching the semiconductor surface and subsequently influencing the device in a positive or negative manner. In order to remove some of these defects, the SBD's were subjected to thermal treatment up to 600 °C. The quality of the SBD's was tested by measuring the reverse and forward bias I-V characteristics and the results are depicted in figure 1.

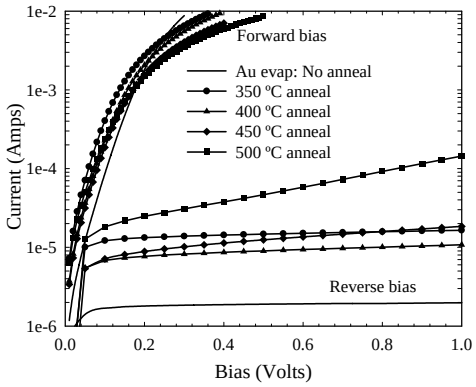

Figure 1. Current-voltage measurements under forward and reverse bias of Au Schottky diodes recorded at 300 K before and after 10 minute annealing in Ar-atmosphere. The Au Schottky contact was 200 nm thick and the AuSb ohmic contact was 100 nm thick.

From this figure we observed only a negligible change in the forward bias characteristics, but an increase in the reverse leakage current with increasing temperature up to 350 °C. Thereafter, there is a

IVC-17/ICSS-13 and ICN+T2007 IOP Publishing
Journal of Physics: Conference Series **100** (2008) 042005 doi:10.1088/1742-6596/100/4/042005

decrease in reverse leakage current up to 400 ºC. After 400 ºC, an increase in the slope of the reverse leakage current is observed up to 450 ºC, where after an increase in both slope of and reverse leakage current is observed.

Along with the change in I-V properties, there was a visible change in the morphology of the contact when viewed at low magnifications under an optical microscope. The cause of this phenomenom was investigated by performing RBS on 100 nm and 30 nm thick Au layers evaporated resistively onto the same side of the Ge as is used for Schottky contact deposition. The RBS spectra 30 nm thick layers are depicted in figure 2.

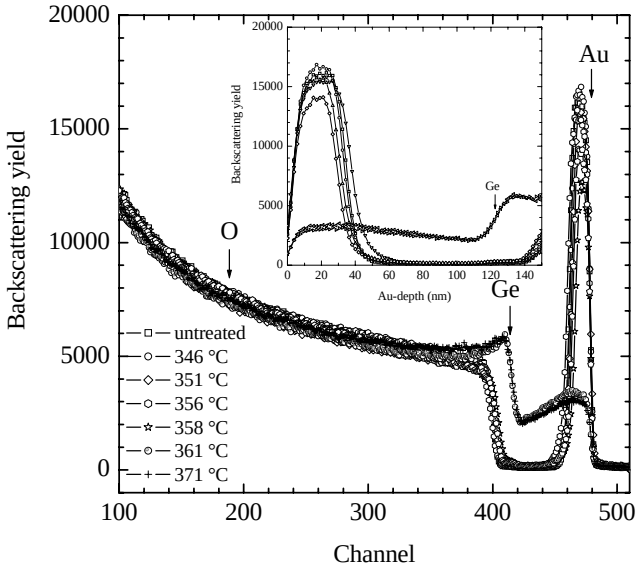

Figure 2. Energy spectra of 1.4 MeV He ions backscattered on 30 nm thick Au-layers deposited on <111>Ge and thermally treated at different temperatures. The inset shows the energy to depth conversion with respect to the Au-surface.

It is clear from figure 2 that between 358°C and 361°C, the distribution of gold on the germanium substrate changes. This is also seen in figure 3, where the atomic percentage of Au and Ge near the surface is plotted as a function of temperature. In this temperature range a eutectic point exists in the Au-Ge system (361 °C and 28 % Ge) [10]. The solid solubility of Ge in Au is 3.1 %, but that of Au in Ge is very low, $<10^{-5}$ % [11]. From figure 3 it can be seen that at temperatures between 350 ºC and 360 ºC, there is an slight increase in the concentration of Ge on the surface, and it is expected that this is due to diffusion of Ge through the gold thin film to the surface, in a similar manner to previously reported polycrystalline thin films of Au and Ge [12, 13]. A sharp increase in Ge content occurs between 360°C and 361°C, which coincides with the eutectic temperature, but the Ge concentration is much higher than expected at the eutectic point. The dramatic change in the distribution of gold and germanium at the eutectic temperature can thus be attributed to the Au-Ge liquid phase which would form at 361°C. From SEM micrographs, not shown here, eutectic Au-Ge island growth is observed with holes around that which lead all that way down to the Ge substrate and the higher than expected Ge signal observed by RBS thus most probably comes from the Ge substrate. However, this still needs to be investigated in more detail. No oxygen content, thus no GeO, was detected using RBS. This is currently being investigated using TOF-SIMS profiles on these films.

Although diffusion is commonly reported for Au/Ge bi-layer systems, where both the Au and Ge layers are polycrystalline, to the authors' knowledge, the diffusion of Ge from the crystalline substrate through the polycrystalline Au layers has not been reported yet. It is also interesting to note that from channeling measurements (not shown here), the polycrystalline Au layers, to a certain extent, align to the crystal structure of the crystalline Ge substrate and it was possible to observe a reduction of more

IVC-17/ICSS-13 and ICN+T2007 IOP Publishing
Journal of Physics: Conference Series **100** (2008) 042005 doi:10.1088/1742-6596/100/4/042005

than 30% in the Au peak of the channeled RBS spectra when compared to that in the randomly orientated RBS spectra.

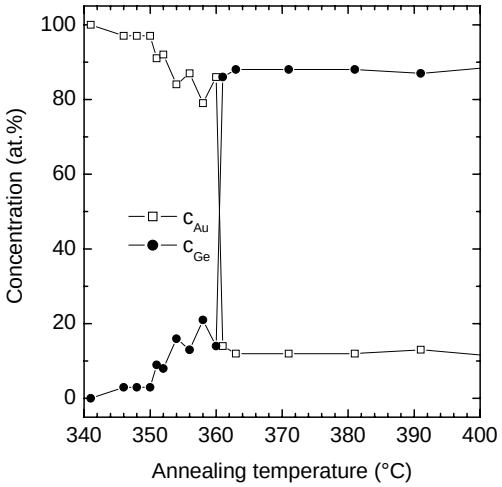

Figure 3. Atomic percentage of Au and Ge near the surface versus annealing temperature for 30 nm thick Au-layers deposited on <111> Ge and thermally treated in a Ar-atmosphere. The concentration was calculated using the WinDF program described in [14].

4. Conclusion

The visible change in the morphology of the Au contacts upon annealing, can be attributed to the segregation of Ge that diffused from the crystalline substrates through the polycrystalline Au layers for temperatures between 350 ºC and 360 ºC. . The dramatic change in the distribution of gold and germanium at the eutectic temperature can be attributed to the Au-Ge liquid phase which would form at 361°C. The higher than expected concentration of Ge might be due to the formation of holes around eutectic Au-Ge islands leading all the way to the Ge substrate.

References

[1] J. Weber, M. Hiller and E.V. Lavrov, Materials Science in Semiconductor Processing **9**, 564 (2006).
[2] *Germanium Silicon: Physics and Materials*, Semiconductors and Semimetals Vol. 56, edited by R. Hull and J. C. Bean, Academic Press, San Diego (1999).
[3] T. Akatsu, C. Deguet, L. Sanchez, F. Allibert, D. Rouchon, T. Signamarcheix, C. Richtarch, A. Boussagol, V. Loup, F. Mazen, J-M. Hartmann, Y. Vampidelli, L. Clavelier, F. Letertre, N. Kernevez and C. Mazure, Materials Science in Semiconductor Processing **9**, 444 (2006).
[4] S. Gaudet, C. Detavernier, A.J. Kellock, P. Desjardins, C. Lavoie, J. Vac. Sci. Technol. **A 24(3)**, 474 (2006).
[5] Q. Zhang, N. Wu, Th. Osipowicz, L.K. Bera, C. Zhu, Jap. J. Appl. Phys. **44** (45), 1389 (2005).
[6] F. D. Auret, O. Paz and N. A. Bojarczuk, J. Appl. Phys. **55** (6), 1581 (1984).
[7] M. Mamor, F. D. Auret, M. Willander, S. A. Goodman, G. Myburg, and F. Meyer, Semiconductor Science and technology **14**, 611 - 614 (1999).
[8] F. D. Auret, S. A. Goodman, F. K. Koschnik, J.-M. Spaeth, B. Beaumont and P. Gibart, Appl. Phys. Lett. **74** (15), 2173-2175 (1999).
[9] G. Myburg and F. D. Auret, J. Appl. Phys. **71**, 6172 (1992).
[10] P-Y Chevalier, Thermochimica Acta **141,** 217 (1989).
[11] G. V. Samsonov and V. N. Bondarev, *Germanides*, Published by consultants Bureau, New York, 52 (1969).
[12] S. Zhang, St. J. Dixon-Warren, S. R. Das, J. Appl. Phys. **95,** 3521 (2004).
[13] S. Ingrey and B. MacLaurin, J. Vac. Sci. Technol. **A 2**, 358 (1984).
[14] N.P. Barradas, C. Jeynes, R.P. Webb, Appl. Phys. Lett. **71,** 291(1997).

J.M Nel, A. Chawanda, F.D Auret, W. Jordaan, R.Q. Odendaal, M. Hayes and S. Coelho. 'Microstructural and surface characterization of thin gold films on n-Ge (1 1 1)'. *Physica B: Condensed Matter* **404**.22 (2009), pp. 4493–4495. DOI: 10.1016/j.physb.2009.09.035, **Abstract**: Thin gold films were fabricated by vacuum resistive deposition on the n-Ge (1 1 1) wafers. The films were annealed between 300 and 600 °C. These resulting thin films were then characterised using scanning electron microscopy (field emission and back-scattering modes), Rutherford back scattering spectroscopy and time of flight secondary ion mass spectroscopy (TOF-SIMS). For temperatures below the eutectic temperature the distribution of both the gold and the germanium on the surface are uniform. Above the eutectic temperature, the formation of gold rich islands on the surface of the Germanium were observed. These changes in the microstructure were found to correspond to changes in the electrical characteristics of the diodes.

4.3 Electron Beam Deposition

EBD is the area of primary interest of this thesis and seven articles are mentioned in this section. EBD induced defects as well as defects introduced when a sample is exposed to EBD conditions *without metal deposition*, termed electron beam exposure (EBE) herein, were investigated.

4.3.1 EBD Induced Defects

The articles by Auret, Meyer, Coelho, Hayes and Nel 2006, Auret, Coelho, Janse van Rensburg et al. 2008, and Auret et al. 2010, have been included in sections 4.7, 4.7 and 4.5 respectively. The articles by Auret, Meyer, Coelho and Hayes 2006, and Auret, Coelho, Hayes et al. 2008, deal primarily with the defects introduced during EBD of Au, Ir, Pd, Pt, Ru and Ti on Ge. While the results were found to be qualitatively similar for different metals, quantitative differences exist in the defect concentrations observed. The following are the aims of the EBD work presented in this section's contributions:

- To investigate the effect if EBD on the I-V and C-V characteristics of diodes manufactured by this process and to then compare these results with those from diodes deposited by less damaging processes.
- The characterization by deep level transient spectroscopy (DLTS) of defects introduced by EBD, a process that exposes semiconductors to subthreshold radiation. EBD introduced defect distribution will be measured and compared to defect distributions obtained after MeV electron and alpha particle irradiation.
- The manipulation of EBD conditions (vacuum pressure and EBD current) to determine the effect of this on the number and type of defects introduced while monitoring if there are significant changes to the rectifying qualities of the diodes produced.
- Au, Ir, Pd, Pt, Ru, and Ti SBDs were produced using EBD with the aim of comparing the obtained results.
- The defects observed can be compared to those introduced by MeV electron irradiation, sputter deposition and alpha particle irradiation to assist with their identification, but more importantly, to establish differences between the concentration and types of defects observed.
- To introduce mechanical shields in the EBD chamber with the aim of lowering defect concentration and observing the impact on diode performance.

Ir SBDs were produced by Chawanda et al. 2012 (section 4.7). A summary of EBD results can be found in Coelho, Auret, Janse van Rensburg et al. 2013 (section 4.3.1)

Lajaunie et al[1] reported on EBD of Co on n-Ge.

[1] L. Lajaunie et al. 'Physical properties of Co/n-Ge Schottky contacts'. *Journal of Physics D: Applied Physics* **44**.12 (2011), p. 125103. DOI: 10.1088/0022-3727/44/12/125103.

APPLIED PHYSICS LETTERS **88**, 242110 (2006)

Electrical characterization of defects introduced during electron beam deposition of Pd Schottky contacts on *n*-type Ge

F. D. Auret,[a] W. E. Meyer, S. Coelho, and M. Hayes
Physics Department, University of Pretoria, Pretoria 0002, South Africa

(Received 12 April 2006; accepted 2 May 2006; published online 14 June 2006)

We have investigated by deep level transient spectroscopy the hole and electron trap defects introduced in *n*-type Ge during electron beam deposition (EBD) of Pd Schottky contacts. We have also compared the properties of these defects with those introduced in the same material during high-energy electron irradiation. Our results show that EBD introduces several electron and hole traps at and near the surface of Ge. The main defect introduced during EBD has electronic properties similar to those of the V–Sb complex, or *E* center, introduced during high-energy particle irradiation of Ge. This defect has two levels $E_{0.38}$ and $H_{0.30}$ that correspond to its $(--,-)$ and $(-,0)$ charge states. © *2006 American Institute of Physics*. [DOI: 10.1063/1.2213203]

The low effective mass of holes in Ge has opened up the possibility of using Ge in ultrafast complementary metal-oxide-semiconductor devices.[1] This, in turn, has sparked renewed interest in the properties of defects in Ge because defects ultimately determine the performance of devices. In a detailed study of proton and electron irradiated Ge a comparison was made to previously observed radiation induced defects and level assignments of the *E* center (V–Sb), *A* center (V–O), and divacancy (V–V) were proposed.[2] Several other O- and Sb-related defects were characterized in O-doped and Sb-doped Ge, respectively. More recently it was convincingly demonstrated that the *E* center in Sb-doped Ge can be present in three charge states and the level positions associated with these level states were determined.[3] The properties of *E* centers due to P, As, and Bi,[4] as well as the *A* center (V–O),[5] have been determined and compared.

Although the most prominent high-energy radiation induced defects in Ge have been characterized, no in-depth investigations regarding the defects introduced in Ge during critical processing steps, e.g., metallization, have been reported. These investigations are important because it is well known that metallization procedures, e.g., sputtering and electron beam deposition, introduce defects at and close to the metal-semiconductor junction. These defects influence device performance and alter the barrier heights of the contacts.[6–9] The defects responsible for these barrier adjustments are formed when energetic particles reach the semiconductor surface and interact with the semiconductor. Depending on the application, these defects may either be beneficial or detrimental for optimum device functioning. For Si it has been shown that the defects introduced during high-energy electron and proton irradiation increase the switching speed of devices.[10]

In this study we report the electronic properties of defects introduced in *n*-type Ge during electron beam deposition (EBD) of Pd Schottky contacts. We show that EBD introduces one prominent electron and hole trap and several other electron and hole traps. The two prominent EBD induced trap levels were found to belong to the V–Sb center that was also introduced during high-energy electron irradiation of the same material.

[a]Electronic mail: danie.auret@up.ac.za

For deep level transient spectroscopy (DLTS) of the defects introduced in Ge during EBD of Schottky barrier contacts on it, we have used bulk-grown (111) *n*-type material doped with Sb to a level of 2.5×10^{15} cm^{-3}. Before metallization the samples were first degreased and then etched in a mixture of H_2O_2:H_2O (1:5) for 1 min. Directly after cleaning they were inserted into a vacuum chamber where AuSb (0.6% Sb) was deposited on their back surfaces as ohmic contacts. The samples were then annealed at 350 °C in Ar for 10 min to minimize the contact resistivity of the Ohmic contacts. Before Schottky contact deposition, the samples were again chemically cleaned as described above. Pd contacts, 0.63 mm in diameter and 200 nm thick, were deposited in an EBD system through a mechanical mask. A Varian 10 kW electron gun (model 989-1118) vacuum evaporation system was used for this process. In this system the samples are positioned about 40 cm above the electron gun. "Control" Pd Schottky contacts were deposited on identical samples by resistive evaporation—a process known not to introduce defects in semiconductors. Following contact fabrication, current-voltage (*I-V*) and capacitance-voltage (*C-V*) measurements were performed to assess the quality of the diodes and to determine the free carrier density of the Ge, respectively. Thereafter both conventional and high-resolution Laplace DLTS (Refs. 11 and 12) were used to study the defects introduced in the Ge during the EBD process. Because minority carrier injection can easily be achieved in Schottky contacts to Ge,[3,5] electron as well as hole traps could be studied. In order to identify the defects introduced by EBD, they were compared to defects introduced in identical samples by high-energy (MeV) electron irradiation from a Sr^{90} source.

I-V measurements indicated that the rectification quality of the control and EBD Schottky contacts was sufficient for DLTS measurements with reverse bias (2 V) leakage currents of 10^{-5}–10^{-6} A at room temperature (295 K) and 10^{-12}–10^{-14} A at 100 K. The series resistances of the diodes remained in the 10–20 Ω in the entire temperature regime investigated, indicating that the AuSb back contacts retained their ohmic character, even down to 16 K, the lowest temperature achievable in our cryostat. *C-V* measurements yielded the free carrier density of the Ge as $(2.5\pm0.5)\times10^{15}$ cm^{-3}.

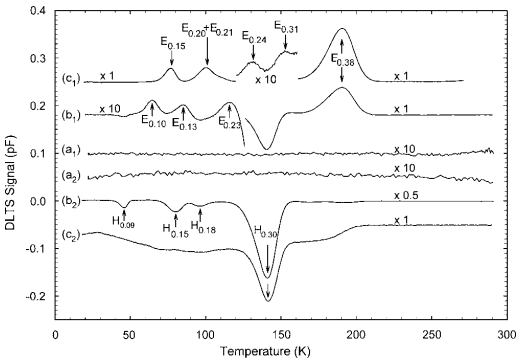

FIG. 1. DLTS spectra of the resistively deposited (control) Pd Schottky contacts to *n*-Ge reveal that these samples contain no electron or hole traps [curves (a_1) and (a_2), respectively] within the detection limit of our DLTS system. Curves (b_1) and (b_2) are the DLTS electron and hole trap spectra, respectively, of Pd Schottky contacts deposited by EBD, recorded using a rate window of 80 s^{-1} at a quiescent reverse bias of −1 V. For the electron-trap spectra the pulse V_p was 0.15 V into forward bias. Hole trap spectra were obtained by applying an injection pulse of V_p=3 V into forward bias. Curves (c_1) and (c_2) are the spectra for electron irradiated resistively deposited Pd Schottky contacts to *n*-Ge, recorded under the same conditions as curves (b_1) and (b_2), respectively.

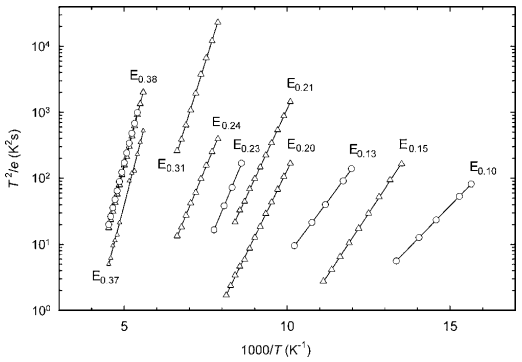

FIG. 2. Arrhenius plots for EBD (circles) and electron irradiation induced (triangles) electron traps in Ge. All data were acquired using the bias and pulsing conditions defined in the caption of Fig. 1.

In Fig. 1 we depict the DLTS spectra for control and EBD Pd contacts. Curves (a_1) and (a_2) are the electron and hole spectra for the control diodes and they clearly indicate that this material does not contain electron or hole traps in measurable concentrations. In the nomenclature used here to name the curves, the subscripts "1" and "2" indicate that the spectra are for electron and hole traps, respectively. The traps introduced in the Ge during EBD of Pd contacts are shown by curves (b_1) and (b_2) for electron and hole traps, respectively. Even though we attempted to detect majority carriers only in curve (b_1) by not using injection conditions, a prominent hole trap $H_{0.30}$ was still present and prevented the possible detection of electron traps with peaks in its vicinity. The difficulty here is that the EBD induced defects reside very close to the interface and therefore, ideally, forward bias filling pulses should be applied to maximize the signals of these defects. However, forward bias leads to hole injection, and hence to the problem above. The most significant electron trap in curve (b_1) is $E_{0.38}$. Three defects in lower concentrations, $E_{0.10}$, $E_{0.13}$, and $E_{0.24}$, were also characterized.

In Fig. 1 we also compare the electron trap spectrum of control diodes that were irradiated with high-energy electrons at a dose of 2×10^{14} cm^{-2} [curve (c_1)] to that of the EBD diodes discussed above. We have used Laplace DLTS to separate the signals of the $E_{0.20}$ and $E_{0.21}$ of electron irradiated samples [curve (c_1)]. From this comparison it seems that only the $E_{0.38}$ electron trap is introduced by both EBD and high-energy electron irradiation. The minor electron

TABLE I. Electronic properties of defects introduced in *n*-type Ge during electron beam deposition (EBD) and MeV electron irradiation of Pd Schottky contacts.

Process	Defect	E_T (eV)	σ_a (cm^2)	T_{peak}[a] (K)	Similar defects/defect ID
EBD	$E_{0.10}$	$E_C-0.10$	3.7×10^{-16}	65	
	$E_{0.13}$	$E_C-0.13$	1.9×10^{-16}	85	
	$E_{0.23}$	$E_C-0.23$	3.4×10^{-14}	116	
	$E_{0.38}$	$E_C-0.38$	1.0×10^{-14}	191	$E_{0.377}$,[b] $E_{0.37}$,[c] V–Sb(--/-)[b,c]
	$H_{0.09}$	$E_V+0.09$	2.1×10^{-13}	47	
	$H_{0.15}$	$E_V+0.15$	7.1×10^{-14}	82	
	$H_{0.18}$	$E_V+0.18$	3.5×10^{-14}	97	
	$H_{0.27}$	$E_V+0.27$	2.4×10^{-13}	133	
	$H_{0.30}$	$E_V+0.30$	6.2×10^{-13}	141	$H_{0.307}$,[b] $H_{0.30}$,[c] V–Sb (-/0)[b]
MeV electron irradiation	$E_{0.15}$	$E_C-0.15$	5.0×10^{-14}	77	
	$E_{0.20}$	$E_C-0.20$	1.4×10^{-14}	100	$E_{0.19}$,[c] Sb and *I* related?[c]
	$E_{0.21}$	$E_C-0.21$	3.6×10^{-14}	109	$E_{0.21}$,[c] Sb related?[c]
	$E_{0.24}$	$E_C-0.24$	2.5×10^{-15}	131	$E_{0.23}$,[c] Sb and *I* related?[c]
	$E_{0.31}$	$E_C-0.31$	5.0×10^{-14}	151	$E_{0.30}$,[c] *I* and impurity related?[c]
	$E_{0.37}$	$E_C-0.37$	2.9×10^{-14}	181	
	$E_{0.38}$	$E_C-0.38$	1.1×10^{-14}	191	$E_{0.377}$,[b] $E_{0.37}$,[c] V–Sb (--/-)[b,c]
	$H_{0.30}$	$E_V+0.30$	3.66×10^{-13}	142	$H_{0.307}$,[b] $H_{0.30}$,[c] V–S (-/0)[b]

[a]Peak temperature at a rate window of 80 s^{-1}.
[b]See Ref. 3.

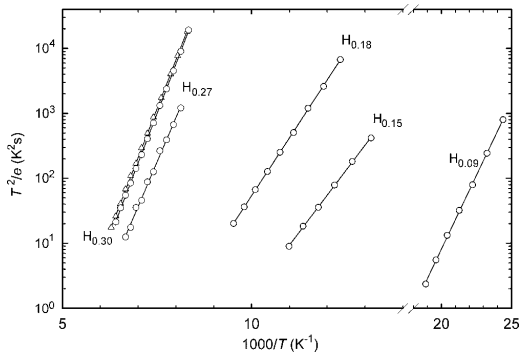

FIG. 3. Arrhenius plots for EBD (circles) and electron irradiation induced (triangles) hole traps in Ge. All data were acquired using the bias and pulsing conditions defined in the caption of Fig. 1.

traps introduced by EBD ($E_{0.10}$, $E_{0.13}$, and $E_{0.24}$) seem to be quite different from those introduced by electron irradiation ($E_{0.15}$, $E_{0.20}$, and $E_{0.21}$).

The activation energies E_T and apparent capture cross sections for electrons σ_{na} and holes σ_{pa} (i.e., the DLTS "signatures") of the particle induced electron traps were determined from the Arrhenius plots in Fig. 2 and are summarized in Table I. Note that we have not corrected these energy values to take into account the temperature dependence of the capture cross section, that has been shown to significantly change the activation energy of the E center.[3] The most prominent radiation induced electron trap that we have detected, $E_{0.38}$, has been shown to be the $(--/-)$ charge state of the E center (V–Sb) in Sb-doped Ge.[2,3] It is clear from the Arrhenius plot and Table I that the $E_{0.38}$ introduced by EBD and the $E_{0.38}$ introduced by electron irradiation have, within the experimental error, the same DLTS signature, and are therefore most probably the same defect—the V–Sb center.

Next, consider the hole traps introduced by EBD and electron irradiation. Curve (b_2) in Fig. 1 was recorded under minority carrier injection conditions (3 V pulse into forward bias). It shows that EBD introduced four hole traps, $H_{0.09}$, $H_{0.15}$, $H_{0.18}$, and $H_{0.30}$. Again we compare this spectrum to those of hole traps produced during electron irradiation [curve (c_2) in Fig. 1]. From these spectra and the Arrhenius plots in Fig. 3 it is clear that the prominent defect, $H_{0.30}$, is introduced by both processes. The three hole traps in smaller concentrations, $H_{0.09}$, $H_{0.15}$, and $H_{0.18}$, are not present in electron irradiated Ge (Fig. 1). This suggests that they are physically different from the simple point defects introduced by high-energy irradiation. The signature of the $H_{0.30}$ defect corresponds closely to that reported for the H_{307}, speculated to be the single acceptor level $(-/0)$ of the Sb–V center in Ge, created during electron irradiation.[2,3] Since both levels of the E center were observed in depletion layers of EBD Au contacts on Ge, we conclude that the EBD process introduces vacancies in the Ge, at and close to the junction, that migrate and combine with, among others, Sb atoms to form Sb–V pairs (E centers). These vacancies have been proposed to be the result of energetic particles that originate in the region of the filament and then impinge on the semiconductor.[13]

As in previous studies on other semiconductors,[6–9] we have found that the defects introduced during EBD of contacts on Ge are located close to the metal-semiconductor interface. In the present study it was, however, difficult to obtain quantitatively accurate depth profiles. The main reason for this is the sharp increase in minority carrier injection with increasing forward pulse voltage that leads to nondetection of the prominent trap $E_{0.38}$ [curve (b_2) in Fig. 1].

In summary, we have investigated, using conventional as well as high-resolution Laplace DLTS, the defects introduced during electron beam deposition (EBD) of Pd contacts on n-type Ge. We have also compared these defects with those introduced in the same material during high-energy electron irradiation. Our results revealed that the main defect introduced during EBD has the same electronic properties as that of the V–Sb complex, or E center, introduced during high-energy electron irradiation of Ge. This defect has two levels $E_{0.38}$ and $H_{0.30}$ that correspond to its $(--,-)$ and $(-,0)$ charge states.[3] EBD also introduced several defects that are not introduced by electron irradiation. Since EBD defects are introduced by heavy metal or gas ions,[13] these defects could possibly be higher order vacancy clusters and complexes thereof with impurities. The role of these electron beam deposition and radiation induced defects in optimizing device performance for specific applications will have to be carefully examined in order to ensure optimum device performance.

The authors gratefully acknowledge financial support of the South African National Research Foundation. The Laplace DLTS software and hardware used in the research were kindly provided by A. R. Peaker (Centre for Electronic Materials Devices and Nanostructures, University of Manchester) and L. Dobaczewski (Institute of Physics, Polish Academy of Sciences).

[1] *Germanium Silicon: Physics and Materials*, Semiconductors and Semimetals Vol. 56, edited by R. Hull and J. C. Bean (Academic, San Diego, 1999).
[2] J. Fage-Pedersen, A. Nylandsted Larsen, and A. Mesli, Phys. Rev. B **62**, 10116 (2000).
[3] V. P. Markevich, A. R. Peaker, V. V. Litvinov, V. V. Emstev, and L. I. Murin, J. Appl. Phys. **95**, 4078 (2004).
[4] V. P. Markevich, I. D. Hawkins, A. R. Peaker, K. V. Emstev, V. V. Emstev, V. V. Litvinov, and L. Dobaczewski, Phys. Rev. B **70**, 235213 (2004).
[5] V. P. Markevich, I. D. Hawkins, A. R. Peaker, V. V. Litvinov, L. Dobaczewski, and J. L. Lindström, Appl. Phys. Lett. **81**, 1821 (2002).
[6] F. D. Auret, O. Paz, and N. A. Bojarczuk, J. Appl. Phys. **55**, 1581 (1984).
[7] M. Mamor, F. D. Auret, M. Willander, S. A. Goodman, G. Myburg, and F. Meyer, Semicond. Sci. Technol. **14**, 611 (1999).
[8] F. D. Auret, S. A. Goodman, F. K. Koschnik, J.-M. Spaeth, B. Beaumont, and P. Gibart, Appl. Phys. Lett. **74**, 2173 (1999).
[9] G. Myburg and F. D. Auret, J. Appl. Phys. **71**, 6172 (1992).
[10] D. C. Sawko and J. Bartko, IEEE Trans. Nucl. Sci. **30**, 1756 (1983).
[11] L. Dobaczewski, P. Kaczor, I. D. Hawkins, and A. R. Peaker, J. Appl. Phys. **76**, 194 (1994).
[12] L. Dobaczewski, A. R. Peaker, and K. Bonde Nielsen, J. Appl. Phys. **96**, 4689 (2004).
[13] C. Christensen, J. W. Petersen, and A. Nylandsted Larsen, Appl. Phys. Lett. **61**, 1426 (1992).

phys. stat. sol. (a) **205**, No. 1, 159–161 (2008) / **DOI** 10.1002/pssa.200776814

physica status solidi a
www.pss-a.com
applications and materials science

Electrical characterization of defects introduced in Ge during electron beam deposition of different metals

F. D. Auret*, S. M. M. Coelho, M. Hayes, W. E. Meyer, and J. M. Nel

Department of Physics, University of Pretoria, Pretoria 0002, South Africa

Received 2 May 2007, accepted 22 October 2007
Published online 15 January 2008

PACS 71.55.Cn, 73.20.Hb, 73.40.Ns

* Corresponding author: e-mail fauret@postino.up.ac.za

We have used deep level transient spectroscopy to characterize the defects introduced in n-type, Sb-doped, Ge during electron beam deposition of different metals for Schottky contact formation. We have found that the relative concentration of the electron beam induced defects depended on the metal used: metals that required a higher beam intensity to evaporate, e.g. Ru, resulted in larger defect concentrations than metals that required a lower beam intensity, e.g. Pd. The nature of some of these defects could be established by comparing their properties to those of well-known defects introduced by electron irradiation of the same material. The most prominent defect thus identified was the E-center, i.e. the Sb-V center. This defect forms when vacancies, that are introduced during the interaction of energetic metal and other particles with the Ge surface, diffuse into the Ge where they bond to Sb dopant atoms.

1 Introduction The low effective mass of holes in Ge has opened up the possibility of using Ge in ultrafast complimentary metal–oxide–semiconductor (CMOS) devices [1]. A Ge channel MOSFET has attractions as a performance booster for future scaled CMOS circuits, because it offers higher mobility for electrons and holes than in a Si MOSFET [2, and references therein]. Thus, Metal Source/Drain MOSFETs (MSD-MOSFETs) with ultra-thin Ge-on-Insulator (GeOI) channels have been proposed and realised [2]. This interest in Ge devices, in turn, has sparked renewed interest in the properties of defects in Ge because defects ultimately determine the performance of devices. In recent studies the properties of the defects introduced during high-energy gamma-, electron- and proton irradiation [3–6], as well as indium-ion implantation [7], of Ge were reported. The defects introduced in Ge during electron beam deposition of Pt Schottky contacts have also been characterised [8]. The investigations of metallization-induced defects are important because it is well known that metallization procedures, e.g. sputtering and electron beam deposition, introduce defects at and close to the metal–semiconductor junction. These defects influence device performance and alter the barrier heights of the contacts [9, 10]. The defects responsible for these barrier adjustments are formed when energetic particles reach the semiconductor surface and interact with it, resulting in lattice damage. Depending on the application, these defects may either be beneficial or detrimental for optimum device functioning. For example, for Si it has been shown that the defects introduced during high-energy electron and proton irradiation increase the switching speed of devices [11].

Electron beam is a popular method for depositing metals because of its ability to deposit at a highly controllable rate and because of its ability to deposit high melting point metals. However, as pointed out above, it is also known that this deposition method introduces defects at and below the semiconductor surface [8, 10]. In this study we compare the concentrations of defects introduced in n-type Ge during electron beam deposition (EBD) of different metals used as Schottky contacts. We show that the concentrations of the electron beam induced defects depend on the metallization conditions, e.g. the filament current and deposition rate, and the vacuum during metal deposition.

Table 1 Deposition parameters and conditions for different metals as well as the reverse leakage current at –1 V, $I_{R\,(-1V)}$, of the Schottky diodes.

metal	work function (eV)	melting point (°C)	thickness (nm)	deposition rate (nm/s)	EB emission current (mA)	starting vacuum (mbar)	$I_{R\,(-1V)}$ (A)
Au	5.30	1064	200	0.5	60	5×10^{-5}	3×10^{-6}
Pd	5.12	1552	200	0.4	60	2×10^{-4}	5×10^{-6}
Ti	4.33	1660	100	0.4	75	2×10^{-6}	1×10^{-5}
Pt	5.70	1720	100	0.22	125	1×10^{-4}	4×10^{-6}
Ru	5.02	2250	50	0.02	70	6×10^{-5}	3×10^{-6}

2 Experimental procedure For deep level transient spectroscopy (DLTS) of the defects introduced in Ge during EBD of Schottky barrier contacts on it, we have used bulk-grown (111) n-type material doped with Sb to a level of 2.5×10^{15} cm^{-3}. Before metallization the samples were first degreased and then etched in a mixture of H_2O_2:H_2O (1:5) for one minute. Directly after cleaning they were inserted into a vacuum chamber where AuSb (0.6% Sb) was deposited on their back surfaces as ohmic contacts. The samples were then annealed at 350 °C in Ar for 10 minutes to minimise the contact resistivity of the ohmic contacts. Before Schottky contact deposition, the samples were again chemically cleaned as described above. Directly after cleaning the samples were inserted into the vacuum system that was pumped down overnight to a vacuum of better than 10^{-6} mbar. Schottky contacts of different metals (Table 1), 0.63 mm in diameter and of various thicknesses, were deposited in an EBD system through a mechanical mask. A Varian 10 kW electron gun (Model 989-1118) vacuum evaporation system was used for this process. In this system the samples are positioned about 40 cm above the electron gun. During heating of the metals by the electron beam and evaporation thereafter, the vacuum increased to levels that depended on the metal being evaporated (Table 1). "Control" Pd Schottky contacts were deposited on identical samples by resistive evaporation – a process known not to introduce defects in semiconductors.

Following contact fabrication, current–voltage (I–V) and capacitance–voltage (C–V) measurements were performed to assess the quality of the diodes and to determine the free carrier density of the Ge, respectively. Thereafter conventional DLTS was used to study the defects introduced in the Ge during the EBD process. Because minority carrier injection can easily be achieved in Schottky contacts to Ge [4, 6], electron as well as hole traps could be studied. In order to identify the defects introduced by EBD, they were compared to defects introduced in identical samples by high energy (MeV) electron irradiation from a Sr^{90} source [8].

3 Results and discussion From Table 1 we see that I–V measurements indicated that the rectification quality of the control and EBD Schottky contacts was sufficient for DLTS measurements with reverse bias (–1 V) leakage currents of 10^{-5}–10^{-6} A at room temperature (298 K). The slightly higher reverse leakage current of the Ti diode is due to the fact that its work function (Table 1) is significantly lower than that of the other metals investigated here. C–V measurements yielded the free carrier density of the Ge as $(2.5 \pm 0.05) \times 10^{15}$ cm^{-3}.

No defects could be detected in the control SBDs fabricated by resistive deposition. This indicates that the Ge is of high quality and contains no defects in measurable concentrations. In Fig. 1 we depict the DLTS results recorded using SBDs of three different metals, namely Ti, Pd and Ru. The results for Au and Pt are almost identical to those of Pd and therefore only the Pd spectra are shown. The top three curves ((a), (b) and (c)) are for electron traps but hole injection could not totally be eliminated and therefore they still show some hole trap activity. The lower three curves ((d), (e) and (f)) are for hole traps and were obtained after using intentional hole injection under conditions outlined in the Fig. caption. The most significant electron trap in curves (a)–(c) is $E_{0.38}$. Curve (b) also shows the presence of a defect $E_{0.13}$ in a lower concentration. In the nomenclature used here "E" means electron trap and the number following it is the activation energy of electron emission to the conduction band. A similar nomenclature is used for hole traps but there the number is the activation energy of hole emission to the valence band. The characteristics of these defects have been presented previously [8]. The most prominent electron beam induced electron trap that we have detected, $E_{0.38}$, has been shown to be the (–/–/–) charge state of the E-center (V-Sb) in Sb-doped Ge [4, 6]. Curves (d)–(f) in Fig. 1 show that $H_{0.30}$ is the prominent hole defect. Several smaller hole peaks can also be observed. The signature of the $H_{0.30}$ defect corresponds closely to that reported for the H_{307}, assigned as the single acceptor level (–/0) of the Sb-V center in Ge, created during electron irradiation [4, 6]. In the case of EBD this defect forms when energetic particles create Ge vacancies at and close to the Ge surface. These vacancies are mobile at room temperature and migrate into the Ge where they combine with Sb dopant atoms to form the V-Sb defect.

From Fig. 1 it is evident that, as far as the main electron and hole traps are concerned ($E_{0.38}$ and $H_{0.30}$, respectively) the peak size (defect concentration) increases from Ti to Pd to Ru. In order to explain this trend, it should be borne in mind that the defects introduced by EBD are caused by particles that are accelerated from the region near the fila-

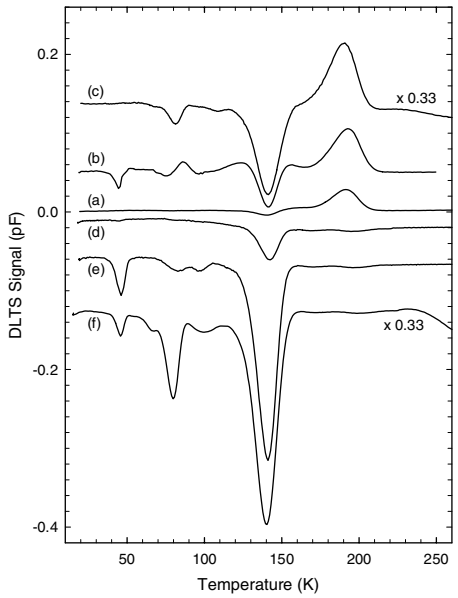

Figure 1 Curves (a)–(c) are the DLTS electron-trap spectra of Ti, Pd and Ru Schottky contacts respectively, deposited by EBD, whereas curves (d), (e) and (f) are the hole trap spectra for Ti, Pd and Ru Schottky contacts, respectively. All spectra were recorded using a rate window of 80 s^{-1} and a quiescent reverse bias of –1 V. For electron trap spectra the pulse, V_p, was 0.15 V into forward bias. The hole trap spectra were recorded by applying an injection pulse of $V_p = 3$ V into forward bias. The spectra of Au and Pt were almost identical to those of Pd and are therefore not shown here. Note that the spectra for Ru have been reduced by a factor of 3.

ment [12]. These are ionized particles comprising the residual gas atoms in the vacuum. The concentration of these ionised particles will increase with increasing residual gas pressure as well as with increasing emission current. In the case of Ti evaporation the starting vacuum was at least an order of magnitude lower than for any of the other metals (Table 1). This means that a lower flux of particles reaches the sample surface during evaporation, which in turn implies a lower level of damage, as observed in Fig. 1.

When comparing the conditions for Pd and Ru it can be seen from Table 1 that the vacuum during Pd deposition was significantly poorer than for Ru deposition and the filament current for Pd was about the same as for Ru. This may suggest that more damage should be present in Pd than in Ru SBDs due to the poorer vacuum. Clearly, from Fig. 1, this is not the case. However, if we consider the deposition rates then we notice that, due to its high melting point, the deposition rate of Ru is about one twentieth of that of Pd. This implies that it takes 20 times longer to deposit the same thickness of Ru as Pd. This in turn means that the Ge surface is exposed to energetic particles for a much longer time during Ru deposition than during Pd deposition, leading to the high concentrations of defects for Ru.

4 Conclusions The main electron and hole traps introduced in Ge during EBD is $E_{0.38}$ and $H_{0.30}$, respectively. We have found that when depositing different metals on Ge by EBD, then these main electron and hole traps are introduced in different relative conditions. The reason for this is two-fold. Firstly, some metals, e.g. Ru, have high melting points and are therefore deposited at a lower rate as metals with lower melting points, e.g. Au and Pd. This means that the Ge surface is bombarded for a longer time during metallization of Ru and therefore more defects are formed. Secondly, the vacuum is different for different the metals. The poorer the vacuum, the more ionised particles are accelerated from the filament region to the Ge where they cause an increased defect formation rate. It should be noted that Ti evaporation actually improves the vacuum because of its sublimation pumping action and consequently results in a lower defect introduction rate.

Acknowledgements The authors gratefully acknowledge financial support of the South African National Research Foundation.

References

[1] R. Hull and J. C. Bean (eds.), Germanium Silicon: Physics and Materials, Semiconductors and Semimetals, Vol. 56 (Academic Press, San Diego, 1999).
[2] K. Ikeda, T. Maeda, and S. Takagi, Thin Solid Films **508**, 359 (2006).
[3] J. Fage-Pedersen, A. Nylandsted Larsen, and A. Mesli, Phys. Rev. B **62**, 10116 (2000).
[4] V. P. Markevich, A. R. Peaker, V. V. Litvinov, V. V. Emstev, and L. I. Murin, J. Appl. Phys. **95**, 4078 (2004).
[5] V. P. Markevich, I. D. Hawkins, A. R. Peaker, K. V. Emstev, V. V. Emstev, V. V. Litvinov and L. Dobaczewski, Phys. Rev. B **70**, 235213 (2004).
[6] V. P. Markevich, I. D. Hawkins, A. R. Peaker, V. V. Litvinov, L. Dobaczewski, and J. L. Lindström, Appl. Phys. Lett. **81**, 1821 (2002).
[7] F. D. Auret, S. Coelho, M. Hayes, J. M. Nel, and W. E. Meyer, Appl. Phys. Lett. **89**, 152123 (2006).
[8] F. D. Auret, S. Coelho, M. Hayes, and W. E. Meyer, Appl. Phys. Lett. **88**, 242110 (2006).
[9] F. D. Auret, S. A. Goodman, F. K. Koschnik, J.-M. Spaeth, B. Beaumont, and P. Gibart, Appl. Phys. Lett. **74**(15), 2173–2175 (1999).
[10] G. Myburg and F. D. Auret, J. Appl. Phys. **71**, 6172 (1992).
[11] D. C. Sawko and J. Bartko, IEEE Nucl. Sci. **30**, 1756 (1983).
[12] C. Christensen, J. W. Petersen, and A. Nylandsted Larsen, Appl. Phys. Lett. **61**, 1426 (1992).

4.3.2 EBE Defects

The conditions that a sample is exposed to while in an EBD chamber but before metal deposition starts, termed EBE herein, were investigated and yielded surprising results. These results were reported on in Coelho, Auret, Janse van Rensburg et al. 2013, that also includes a mini-review of the defects induced in germanium during EBD, SD, MeV electron irradiation and alpha particle irradiation.

The main aim of developing the EBE technique was to see if EBD induced defects can be introduced in a controlled way. Excessive exposure (time and beam current) would reduce the usefulness of diodes for further study thus putting a limit on how much damage could be introduced. Energetic particles that cause EBD damage are present during EBE but interact directly with the semiconductor whereas during EBD this interaction mostly occurs via the metal used as a contact. This study aims to investigate the differences between these techniques with regards to the defects introduced and their concentrations. All defects introduced were characterized using DLTS and then compared to those observed after EBD. The manipulation of the background gas during EBE was aimed at establishing a link between specific defects and the introduced gas species. This part of the study remains to be completed with only isolated results to date.

An article by Auret et al[2] reports on EBE induced defects in silicon and has been included as an appendix. This study on silicon was undertaken using the same methodology as the EBE study of Ge and while the results are similar, differences were also observed. A detailed comparison of these two studies is however beyond the scope of this thesis.

[2]F.D. Auret, S.M.M. Coelho, J.M. Nel et al. 'Electrical characterization of defects introduced in n-Si during electron beam deposition of Pt'. *Physica Status Solidi (a)* **209**.10 (2012), pp. 1926–1933. DOI: 10.1002/pssa.201200578.

JOURNAL OF APPLIED PHYSICS **114**, 173708 (2013)

Electrical characterization of defects introduced in n-Ge during electron beam deposition or exposure

S. M. M. Coelho, F. D. Auret, P. J. Janse van Rensburg, and J. M. Nel
Department of Physics, University of Pretoria, Private Bag X20, Hatfield, 0028, South Africa

(Received 14 September 2013; accepted 18 October 2013; published online 6 November 2013)

Schottky barrier diodes prepared by electron beam deposition (EBD) on Sb-doped n-type Ge were characterized using deep level transient spectroscopy (DLTS). Pt EBD diodes manufactured with forming gas in the chamber had two defects, $E_{0.28}$ and $E_{0.31}$, which were not previously observed after EBD. By shielding the samples mechanically during EBD, superior diodes were produced with no measureable deep levels, establishing that energetic ions created in the electron beam path were responsible for the majority of defects observed in the unshielded sample. Ge samples that were first exposed to the conditions of EBD, *without metal deposition* (called electron beam exposure herein), introduced a number of new defects not seen after EBD with only the E-center being common to both processes. Substantial differences were noted when these DLTS spectra were compared to those obtained using diodes irradiated by MeV electrons or alpha particles indicating that very different defect creation mechanisms are at play when too little energy is available to form Frenkel pairs. These observations suggest that when EBD ions and energetic particles collide with the sample surface, inducing intrinsic non-localised lattice excitations, they modify defects deeper in the semiconductor thus rendering them observable. © *2013 AIP Publishing LLC*. [http://dx.doi.org/10.1063/1.4828999]

I. INTRODUCTION

In the microelectronics and photovoltaic industries, metallization is a necessary process. Deposition of high melting point metals and the ability to accurately control the deposition rate make electron beam deposition (EBD) an ideal choice that is widely accepted in industry.[1] Metallization processes, including EBD, introduce defects at and close to the metal-semiconductor junction that influence device performance[2] and alter a contact's barrier height.[3] The defects that are responsible for this device modification are introduced when energetic particles impinge on the semiconductor surface causing lattice damage such as vacancies or interstitials.[4]

Here, we report on the defects introduced in bulk-grown, antimony doped, n-type germanium during EBD of Pt while mechanically shielding the sample from the direct path of energetic particles that originate in the electron beam (EB). The availability of ultra-pure germanium made it an ideal candidate for this study.[5] The effect of vacuum quality on defect introduction is also noted. Furthermore, exposing samples to EB conditions, *without metal deposition* [termed EB exposure (EBE) herein] prior to metal deposition by resistive evaporation (RE) was used to illustrate fundamental differences between the defects introduced. These diodes exhibited defects not seen after EBD, RF sputter deposition, or MeV electron irradiation.

II. EXPERIMENTAL PROCEDURE

Umicore bulk grown Ge doped with Sb to a level of $1 \times 10^{15}\,cm^{-3}$ was degreased in successive 5 min ultrasonic baths of trichloroethylene, isopropanol, and methanol and then etched in a solution of 5:1, H_2O:H_2O_2 (30%) for 1 min. Au/Sb (0.6%) alloy was evaporated resistively onto the back surface and subsequently annealed at 350 °C for 10 min, lowering the contact resistance, thus forming an ohmic contact. This cleaning procedure was repeated before samples were again loaded into a vacuum chamber and pumped to a pressure below 10^{-6} mbar, where metal was deposited onto the front surface through a metal contact mask, typically yielding eight Schottky barrier diodes with a diameter of 0.6 mm. All samples were cut from the same wafer.

Vacuum pumping was carried out by a dry pump in series with a turbomolecular pump and to lower the H_2 concentration. Ti and Pd were evaporated in the chamber with the sample rotated away from the evaporation source. While the pre-deposition vacuum was typically 5×10^{-7} mbar, this soon went up to approximately 3×10^{-6} mbar during the evaporation. As the vacuum conditions vary greatly during EBD, forming gas H15 with a composition of N_2:H_2 of 85%:15% by volume was also used to raise the pressure in the vacuum chamber to 10^{-4} mbar and kept constant during processing of select samples. EBE of samples and EBD of contacts were accomplished using a 10 kV source (MDC model e-Vap 10CVS) with the samples positioned 50 cm above the crucible. EBD samples were turned away from the target until such time as the evaporation rate had stabilised and then deposition could proceed. Shielding of samples from energetic particles originating in the EB path was carried out using 1 mm thick stainless steel plates, shield 1 shielding from particles on a direct trajectory from the electron beam path to the sample, and shield 2 placed to shield from energetic particles reflected off the chamber wall, shown diagrammatically in Ref. 6. A beam current of 100 mA was required to evaporate Pt at a rate of $0.02\,nm{\cdot}s^{-1}$ resulting in 50 nm thick Schottky barrier diodes in an evaporation of approximately 40 min. During EBE, *without metal deposition*, the samples were exposed for 50 min; while the beam heated a tungsten source using a beam current of

100 mA, this current being insufficient to evaporate W, thus exposing the samples to EB conditions comparable to those experienced during deposition. Platinum with its high work function was chosen as a moderately high beam current was required to evaporate it and the same beam current was sufficient to introduce defects during the EBE process, albeit in low concentrations. Palladium diodes were used for all the other samples prepared for this study as it can be evaporated resistively, a process that is known to not introduce defects in concentrations measurable by deep level transient spectroscopy (DLTS).

After contact fabrication, current-voltage (IV) and capacitance-voltage (CV) measurements were performed to determine diode quality and the free carrier concentration of the Ge samples, found to be 1.3×10^{15} cm^{-3}. Conventional DLTS and Laplace DLTS (L-DLTS)[7] were then used to study the defects introduced by EBD and EBE. Comparing these defects to those introduced by high energy electron irradiation from a strontium-90 (Sr-90) source,[8] α-particle irradiation from an americium 241 (Am-241) radio-nuclide, low energy RF sputter etching, and both capacitively and inductively coupled plasma (ICP) etching, allowed us to identify defects that were only observed after the 10 kV EBD or the EBE process. This Sr-90 source has an effective fluence rate of electrons with energies above 200 keV of 10^9 electrons cm^{-2} s^{-1}, and the Am-241 foil has an effective fluence for α-particles of 7×10^6 α-particles cm^{-2} s^{-1} with energies of 5.4 MeV. Samples were exposed to these sources for 20 h and 3 h, respectively. DLTS spectra obtained for these samples were then compared to those obtained from 100 nm thick Pd diodes prepared by EBD. Furthermore, L-DLTS was used to split DLTS signals of defects with energies that were too closely spaced for conventional DLTS to resolve. DLTS peak amplitudes can be converted to deep level concentration, N_T, as $\frac{N_T}{N_D} \approx \frac{2\Delta C}{C}$, where N_D is the concentration of shallow impurities, ΔC is the DLTS peak height, and C is the junction capacitance. The samples prepared for this study had similar measured capacitances at room temperature that were reduced by, at most, 5 pF as the samples were cooled to 25 K making it easy to compare relative defect concentrations by comparing peak heights of DLTS spectra directly.

III. RESULTS AND DISCUSSIONS

A. High energy particle irradiation

A mini review of the literature with regards to the defects observed after 2 MeV proton irradiation is available,[9] but as the defects introduced during EBD of Schottky barrier diodes will be compared with those observed after high energy (MeV) electron irradiation and α-particle irradiation, it is instructive to first discuss the possible mechanisms by which defects are introduced in single crystal germanium. Grown-in electrically active defects were not present in measurable quantities in these samples, that is, with concentrations above 10^{11} cm^{-3} (control, Figure 1), and thus only defects resulting from collisions of energetic particles with the crystal will be considered. The first type of defect is created when an incident particle imparts enough energy E_d to a lattice atom to displace it forming a stable vacancy-interstitial defect known as a

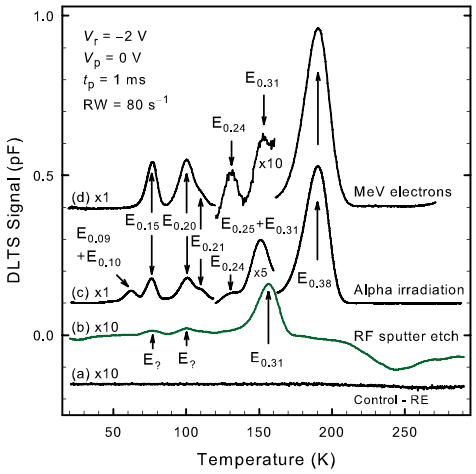

FIG. 1. DLTS spectra of n-Ge resistively evaporated Pd diodes that were (a) not irradiated (control), (b) RF sputter cleaned in a plasma with 300 eV Ar ions, (c) irradiated with α-particles from an Am-123 source, and (d) MeV electron-irradiated by a Sr-90 source. All spectra were recorded with a rate window of 80 s^{-1}, pulse width of 1 ms, quiescent reverse bias of −2 V, and a filling pulse amplitude 2 V. Plots have been offset along the y-axis for clarity.

Frenkel pair. Divacancies, trivacancies, and vacancy clusters can form when vacancies combine. In germanium, experimentally obtained values for E_d vary from 15 to 30 eV and Holmstrom *et al.* concluded that their calculated value of 11.5 eV as a global minimum is in fair agreement with experiment.[10] For the specific case of electron irradiation, applying conservation of momentum while neglecting relativity, an incident electron is required to have a threshold energy E_d of 380 keV to transfer the 11.5 eV required to displace a Ge atom from its lattice position assuming a perfect elastic collision. A two-step process has been suggested involving a light impurity atom, like hydrogen, as a more efficient energy transfer mechanism, and this was discussed in some detail by Chen and MacKay.[4] At that time, they concluded that the defects they observed could only have been generated by sub-threshold energy electrons in germanium crystals grown in hydrogen as they observed damage after 40 keV irradiations, establishing this as the minimum required to generate defects. Using an intermediate light atom would have raised the energy transferred by a small fraction, but this alone would not be enough to account for their observations. Much later, Mooney and Bourgoin concluded that intrinsic point defects are not created by sub-threshold irradiation[11] as previous evidence of point defect creation failed to take into account defects caused by impurities or the effect of surface states on measurements. They reported that MeV electron irradiation introduced vacancy and divacancy defects in Ge, but their conclusions with regard to sub-threshold electron irradiation are in contradiction to subsequent reports of the E-center, for example, the vacancy-Sb complex in Sb doped Ge, being introduced by EBD in Ge (Ref. 12) and Si.[6] When considered in context, the observations of Mooney and Bourgoin support the theory, and the conclusions drawn from their observations

are valid as their DLTS measurement parameters would not have observed defects that are only found close to the metal-semiconductor interface, in small concentrations.

Impurity atoms may be present in the semiconductor or they can also be introduced during processing, intentionally (implantation), or unintentionally, when accelerated particles penetrate the semiconductor occasionally moving deeper into the crystal aided by diffusion processes. These impurity atoms may distort the crystal lattice but are also known to attach themselves to dangling bonds, thus passivating shallow donors, shallow acceptors, as well as defects with levels deep in the bandgap.[13,14] The complexes formed by hydrogen with germanium fall within this class of defect, and while this has been studied extensively in silicon,[13] very few similar studies have been undertaken in germanium.[15] The properties of hydrogen in germanium were not expected to differ vastly from silicon and yet some as yet unexplained differences have been observed.[16] Hydrogen is readily incorporated into Ge in concentrations of 10^{14} to $10^{15}\,cm^{-3}$ during growth,[17] but attempts to passivate defects by H implantation have been unsuccessful.[16] Using density functional theory calculations, VH_n ($n = 1, 2, 3,$ or 4) in Ge was predicted to have energy levels in the bandgap[18] for $n = 1$ and $n = 3$. If the hydrogen is removed, then the vacancy that results is mobile at room temperature and can form a complex with other impurities, the most likely one of which is the E-center. The Ge-Ge and Ge-H bond strengths are 1.93 and 3.59 eV, respectively,[19,20] but as only one bond is being broken at a time in the Ge-H case and as H is much lighter than Ge, a 10 keV electron can transfer as much as 24 eV to a H atom, more than enough to break the Ge-H bond. Calculating the maximum energy in which an incident electron is able to transfer in an elastic collision yields the surprising result that it is required to have energy as much as 300 times lower to displace H compared to the 380 keV required to displace Ge from the lattice. This argument also holds for H in the Si lattice although the energy difference ratio will be lower.

In Figure 1, DLTS spectra from MeV electron irradiated,[12] alpha particle irradiated,[21] and 300 eV RF sputter etched Ge are plotted for comparison purposes. A control sample prepared by RE demonstrates that no defects were present in the Ge samples in measurable quantities before irradiation, i.e., above $10^{10}\,cm^{-3}$. The MeV electron and alpha irradiated samples are very similar except that the alpha irradiated Ge had three additional defects, $E_{0.09}$, $E_{0.10}$, and $E_{0.25}$, where E refers to an electron trap and the subscript 0.10 refers to an energy level that is 0.10 eV below the conduction band. A similar convention will apply for hole traps except that $H_{0.31}$ will indicate a hole trap with an energy 0.31 eV above the valence band. The RF sputter etched sample was exposed to energetic argon ions with a maximum energy of 300 eV for 10 min, and this treatment yielded a spectrum that only had one defect $E_{0.31}$ with a concentration high enough to be measured using L-DLTS. From the Arrhenius plot in Figure 3, we deduce that this defect is different to a defect of similar energy introduced by MeV electron and alpha irradiation but that this defect was previously observed after ICP etching with argon[22] and H-passivation.[23] ICP etching was carried out using argon ions with energies less than 100 eV and did not introduce the defects that RF plasma etching introduced at the positions of the $E_{0.15}$ and $E_{0.20}$ defects, although these were present in very low concentrations. A more appropriate comparison between RF sputtering and ICP sputtering was not possible as 300 V was the lowest accelerating voltage that could sustain a plasma in the Leybold Z400 sputter system. Nyamere *et al.* reported on the defects introduced by 3 keV Ar sputtering of Ge after which $E_{0.38}$ and an additional seven hole traps were observed, some of these defects only being observed after annealing.[24] The defects observed after 300 eV RF sputtering or ICP etching were not observed by Nyamere *et al.* suggesting that $E_{0.31}$ is introduced when the Ar ion accelerating voltage is low and not necessarily dependant on the plasma being capacitively or inductively coupled. ICP etching with 4 eV Ar ions still introduces $E_{0.31}$ but as ions with lower energy were not attempted, 4 eV was not established as the lowest energy that is required to introduce this defect. Hydrogen,[23] neon, and oxygen plasmas also introduced the same defect, without additional defects being observed.

B. Electron beam deposition

EBD introduces a number of defects in Ge that have been reported before and are summarized in Table I.[12,25,26] Comparing DLTS spectra in the literature, it is evident that while similarities exist between EBD spectra of different metals evaporated onto Ge, there are also differences, both in the defects observed and the relative heights of these peaks. When EBD diodes are compared to MeV electron and alpha particle irradiated diodes, then only the E-center, $E_{0.38}$, is common to all three processes. $H_{0.30}$ (V-Sb related) is introduced by EBD and MeV electron irradiation. The $E_{0.10}$ defect introduced during α-particle irradiation has the same energy as a defect introduced during EBD, but it is unlikely that this defect is common to these two processes as there is a small difference in the Arrhenius plots of these defects. Also, the absence of this defect after MeV electron irradiation, a process using energetic particles with energy between EBD and α-particle irradiation, suggests that $E_{0.10}$ (α) and $E_{0.10}$ (EBD) are different defects. It is possible that $E_{0.10}$ (EBD) and $E_{0.09}$ (α) are the same defect, but in the absence of annealing data, we cannot be certain. Not all α-particle irradiation defects were reported on previously, and thus $E_{0.09}$, $E_{0.24}$, $E_{0.25}$, $E_{0.31}$, and $H_{0.31}$ have been included here for completeness.

During the coating process, samples in EBD chambers are bombarded by both negatively and positively charged particles as verified by measuring the current flowing through the sample holder during deposition. A 10 kV potential was applied to accelerate electrons emitted by the EB filament, and modern EBD systems are carefully designed to shield this filament from the samples being coated. The filament is positioned below the crucible, requiring that the electron beam be manipulated by a magnetic field to follow a circular path towards the crucible through an angle of 270°. The magnetic field will focus electrons onto the target, but positive ions generated near the filament will follow a path away from the crucible with a much larger radius due to their larger mass. This arrangement makes it highly improbable

TABLE I. Defects observed in Ge after various processing or irradiation techniques. "*" shows experimental data in this report.

Process	Defect label	E_T (eV)	σ_a ($\times 10^{-15}$ cm^2)	T_{80}[a] (K)	Similar defects/defect ID/Ref.
EBD	$E_{0.10}$	$E_C-0.10$	0.37	65	$E_{0.10}$ (Ref. 12)
	$E_{0.13}$	$E_C-0.13$	0.19	85	$E_{0.13}$ (Ref. 12)
	$E_{0.23}$	$E_C-0.23$	34	116	$E_{0.13}$ (Ref. 12)
	$E_{0.38}$	$E_C-0.38$	10	191	$E_{0.37}$,[9] E_{377},[30] $E_{0.38}$,[12,25] V-Sb (–/-) (Refs. 9 and 30)
	$H_{0.09}$	$E_V+0.09$	210	47	$H_{0.09}$,[12] V-Sb (0/+) (Ref. 31)
	$H_{0.15}$	$E_V+0.15$	71	82	$H_{0.15}$ (Ref. 12)
	$H_{0.18}$	$E_V+0.18$	35	97	$H_{0.18}$ (Ref. 12)
	$H_{0.27}$	$E_V+0.27$	240	133	$H_{0.27}$,[12] H_{270} (Ref. 30)
	$H_{0.30}$	$E_V+0.30$	620	141	H_{307},[30] $H_{0.30}$,[9] V-Sb (-/0) (Ref. 30)
	$H_{0.29}$	$E_V+0.29$	1.3	176	$H_{0.29}$ (Ref. 25)
EBD (f/gas)	$E_{0.28}$	$E_C-0.28$	11	153	*
	$E_{0.31}$	$E_C-0.31$	9.0	163	*
EBE	$E_{0.16}$	$E_C-0.16$	320	77	*
	$E_{0.22}$	$E_C-0.22$	515	101	*
	$E'_{0.22}$	$E_C-0.22$	69	108	*
	$E_{0.33}$	$E_C-0.33$	246	152	*
	$E_{0.37}$	$E_C-0.37$	35.4	182	*, $E_{0.37}$ (Ref. 12)
	$E_{0.38}$	$E_C-0.38$	13.8	192	*, E_{377},[30] $E_{0.38}$,[12,25] V-Sb (–/-) (Ref. 30)
	$H'_{0.15}$	$E_V+0.15$	65	86	*
	$H_{0.22}$	$E_V+0.22$	1960	106	*
	$H_{0.26}$	$E_V+0.26$	89	139	*
	$H_{0.34}$	$E_V+0.34$	172	171	*
ICP	$E_{0.31}$	$E_C-0.31$	10	157	$E_{0.31}$,[22] $E(0.30)$ (Ref. 23)
Sputter etch	$E_{0.31}$	$E_C-0.31$	10	157	* (~300 eV Ar), $E_{0.31}$ (Refs. 22 and 23)
Sputter	$ES_{0.14}$	$E_C-0.14$	5.5	78	$ES_{0.14}$,[32] $E_{0.13}$, Sb and *I* related[9]
deposition	$ES_{0.20}$	$E_C-0.20$	37	100	$ES_{0.20}$,[32] $E_{0.19}$, Sb and *I* related[9]
	$ES_{0.21}$	$E_C-0.21$	20	109	$ES_{0.21}$,[32] $E_{0.21}$ (Ref. 9)
	$ES_{0.24}$	$E_C-0.24$	3.3	131	$ES_{0.24}$,[32] $E_{0.23}$ (Ref. 9)
	$ES_{0.31}$	$E_C-0.31$	15	151	$ES_{0.31}$,[32] $E_{0.29}$,[9] Divacancy?[9]
MeV	$E_{0.15}$	$E_C-0.15$	50	77	$E_{0.15}$ (Ref. 12)
electron	$E_{0.20}$	$E_C-0.20$	14	100	$E_{0.20}$,[12] $E_{0.19}$, Sb and *I* related[9]
irradiation	$E_{0.21}$	$E_C-0.21$	36	109	$E_{0.21}$,[12] $E_{0.21}$, Sb related?[9]
	$E_{0.24}$	$E_C-0.24$	2.5	131	$E_{0.24}$,[12] E(0.23) (Ref. 33)
	$E_{0.31}$	$E_C-0.31$	50	151	$E_{0.31}$ (Ref. 12)
	$E_{0.37}$	$E_C-0.37$	29	181	$E_{0.37}$ (Ref. 12)
	$E_{0.38}$	$E_C-0.38$	11	191	E_{377},[30] $E_{0.37}$,[9] V-Sb (–/-) (Ref. 30)
	$H_{0.30}$	$E_V+0.30$	366	142	H_{307},[30] $H_{0.30}$,[9] V-Sb (-/0) (Ref. 30)
Alpha	$E_{0.09}$	$E_C-0.09$	0.66	63	*, $E_{0.10}$?[12]
irradiation	$E_{0.10}$	$E_C-0.10$	9.2	59	$E_{0.10}$ (Ref. 21)
	$E_{0.15}$	$E_C-0.15$	62	76	$E_{0.15}$ (Ref. 21)
	$E_{0.20}$	$E_C-0.20$	78	99	$E_{0.20}$,[21] $E_{0.19}$, Sb and *I* related[9]
	$E_{0.21}$	$E_C-0.21$	29	109	$E_{0.21}$,[21] $E_{0.21}$, Sb related?[9]
	$E_{0.24}$	$E_C-0.24$	14.5	130	*, $E_{0.23}$ (Ref. 9)
	$E_{0.25}$	$E_C-0.25$	0.37	149	*
	$E_{0.31}$	$E_C-0.31$	98	151	*, $E_{0.30}$ (Ref. 9)
	$E_{0.38}$	$E_C-0.38$	13	190	$E_{0.38}$,[21] V-Sb (–/-) (Ref. 30)
	$H_{0.31}$	$E_v+0.31$	1000	142	*, $H_{0.31}$,[21] $H_{0.30}$,[9] H_{307}, V-Sb (-/0) (Ref. 30)

[a]Peak temperature at a rate window of 80 s^{-1}.

that 10 keV ions originated near the filament will arrive at the sample in sufficient numbers to cause measurable defects. The same cannot be said for ions that are generated in the electron beam path when 10 keV electrons collide with residual gas atoms in the vacuum. Slow moving, heavy atoms in the beam path have a greater probability of colliding with energetic electrons, but even for a fast moving atom like hydrogen, the probability of a collision is above one if it travels across a typical electron beam required to melt Pt.

The number of energetic particles that collide with a sample is dependent on many parameters, including the EB current, vacuum pressure, residual gas composition, beam diameter, sample distance, and deposition time, and most parameters that are not readily controlled. Shielding the sample during deposition is easily implemented, and the spectra in Figure 2 illustrate that mechanical shielding of the sample can have an impact on the number of defects introduced during EBD. All the diodes were prepared in the same vacuum system

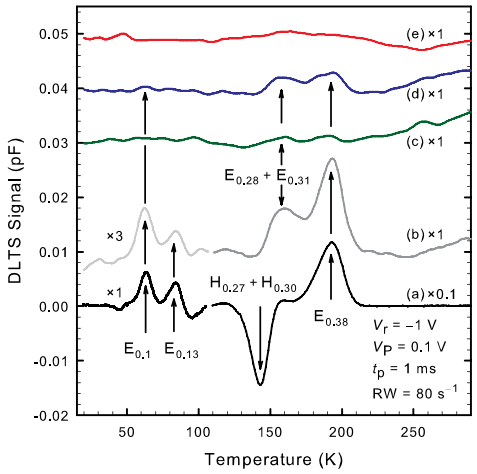

FIG. 2. DLTS spectra of EBD Pt SBDs (Schottky barrier diodes) to demonstrate the effects of shielding on defect concentration: (a) no shielding and standard vacuum conditions. For curves (b)–(d), the chamber was backfilled with forming gas to 10^{-4} mbar where (b) no shielding was applied, (c) one shield applied to shield from direct particles, and (d) two shields to additionally shield from particles reflected off the chamber wall. Curve (e) diode was deposited in a superior vacuum with two shields in place.

that was initially pumped down to 10^{-6} mbar. An oil-filled rotary vane pump was used only when depositing Pt for the diode of plot (a), whereas all other diodes were prepared after the chamber was evacuated using a dry pump. Dry pumping minimizes the potential for hydrocarbons to contaminate the deposition chamber. As the chamber heats up during EBD, it is often a problem that the pressure increases sharply

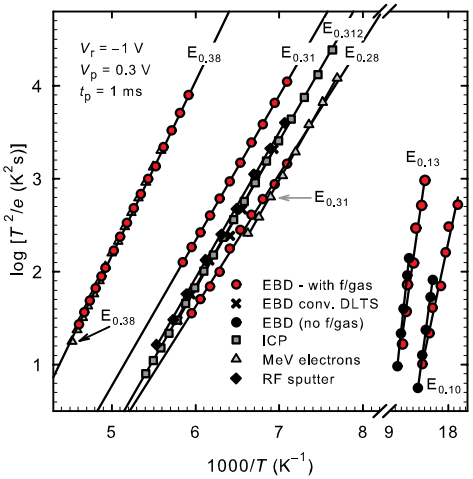

FIG. 3. L-DLTS Arrhenius plots of electron trap defects observed after Pt EBD in forming gas (filled circles). Where these defects have also been observed after MeV electron irradiation, argon RF sputter etching, and argon ICP, these plots have also been included. The defect peak plot (crosses) obtained by conventional DLTS was then split using L-DLTS into $E_{0.28}$ and $E_{0.31}$.

during deposition. During the deposition of diode (a), the vacuum pressure increased to approximately 10^{-4} mbar, whereas during the EBD of diode (e), the pressure only increased to 3×10^{-6} mbar. All other diodes were prepared at a pressure of 10^{-4} mbar that was kept constant by adjusting the flow of forming gas into the chamber.

Seven defects were introduced during EBD of Pt when there were neither shields used nor forming gas introduced in the chamber (Figure 2, plot (a)). The hole traps, $H_{0.27}$, $H_{0.29}$, and $H_{0.30}$, were only observed in this sample. Once forming gas was introduced into the chamber, two electron traps, $E_{0.28}$ and $E_{0.31}$, were introduced that were not previously seen after EBD. The E-center ($E_{0.38}$) was common to all samples except the sample prepared in a superior vacuum with two shields in place as this sample did not have any defects with a concentration high enough to measure. As the DLTS graph peak heights are proportional to the defect concentrations, the smaller peak heights in Figure 2 of the shielded samples demonstrate the effectiveness of shielding in lowering defect concentration. All the defects observed after EBD in forming gas have been plotted in the Arrhenius plot of Figure 3, and the defects that are similar to defects observed after ICP, MeV electron irradiation, and RF sputtering have also been included. The defect concentrations of the $E_{0.10}$ and $E_{0.13}$ defects were too small to provide an accurate energy level determination, and the energies displayed were calculated using data from the EBD sample deposited without using forming gas (Figure 2, plot (a)). Using conventional DLTS, the $E_{0.31}$ defect (crosses in Figure 3) seemed identical to a defect observed after ICP etching, and this ICP defect is labelled $E_{0.312}$ for clarity. L-DLTS of this peak splits this single peak into two peaks with energies $E_{0.28}$ and $E_{0.31}$ that were only observed once forming gas was introduced. Three electron traps, all with enthalpy of approximately 0.31 eV, have been plotted in Figure 3. The Arrhenius plots of these defects, although similar, do not line up indicating that they are different defects. At present, the best evidence that these are unique defects observed after different processing techniques is found by comparing the respective peak temperatures of their 80 s^{-1} rate window DLTS spectra (Table I). Multiple scans that took approximately 20 h were performed at each temperature to improve the signal to noise ratio thus making it possible to extract useful data. This serves as a good example of the value of L-DLTS, both in resolving very small signals and in splitting a peak consisting of two closely spaced energy levels.

A summary of the IV and CV data collected for these diodes appears in Table II. All EBD diodes manufactured with shields in place had superior characteristics as their ideality was less than 1.06 and the reverse bias current measured with 1 V applied was below 8×10^{-4} A cm^{-2}. Diodes manufactured with a good vacuum and two shields had ideality closest to one (below 1.02 in some instances) and the lowest reverse bias current of all diodes that have been fabricated to date by this group. IV plots in Figure 4 compare such a diode (crosses) with diodes manufactured without shielding. By comparing the best seven out of eight diodes manufactured for each EBD scheme, the diodes evaporated in a superior vacuum with two shields in place had the

TABLE II. EBD Pt diodes fabricated under different vacuum and system configuration conditions. F/gas refers to forming gas with a ratio of 85%:15%, nitrogen: hydrogen.

Pt diodes	Ideality—best diode	I at 1 V reverse bias ($A \cdot cm^{-2}$)	I average of 7 diodes (Std. deviation) ($A \cdot cm^{-2}$) at −1 V	Schottky barrier height—IV (eV)	Schottky barrier height—CV (eV)
Unshielded	1.12	1.24×10^{-3}	1.42×10^{-3} (8.58×10^{-4})	0.56 ± 0.04	0.50 ± 0.03
Unshielded and f/gas	1.05	7.78×10^{-4}	6.65×10^{-3} (5.76×10^{-3})	0.55 ± 0.04	0.51 ± 0.03
Shield 1 and f/gas	1.04	2.90×10^{-4}	6.20×10^{-3} (7.30×10^{-3})	0.58 ± 0.04	0.50 ± 0.03
Shield 1 and 2, f/gas	1.03	3.47×10^{-4}	2.03×10^{-2} (2.88×10^{-2})	0.58 ± 0.04	0.51 ± 0.03
Shield 1 and 2	1.02	2.48×10^{-4}	3.47×10^{-4} (2.05×10^{-4})	0.59 ± 0.04	0.51 ± 0.03

lowest reverse bias current at 1 V coinciding with the lowest standard deviation.

The most significant observation from this series of EBD samples is that the DLTS peak heights consistently decreased in height with the application of mechanical shields (Figure 2, plots (c) and (d)) with a further reduction in concentrations to below the measurement threshold when the vacuum improved (Figure 2, plot (e)). The small fluctuations in plot (e) of Figure 2 are indicative of surface states that may be damage caused by a small number of light ions deflected by the EB system magnetic field to follow a curved trajectory around shield 1. The shields were positioned to minimize the number of energetic ions that reached the samples and were unable to eliminate bombardment from electrons being reflected off the metal target. This was confirmed by measuring the current at the sample position with a Faraday cup, such negative current is increased by an order of magnitude as the target surface melted. While 10 keV electrons have enough energy to damage our Ge samples, they were not the primary cause of the defects observed. Rather the energetic ions that are always present during EBD, colliding with the semiconductor or the metal surface, introduced the observed defects. As the semiconductor surface is rapidly coated with metal, most of the EBD-induced damage must be introduced by collisions of low energy ions, atoms, or molecules with the metal layer, while this metal layer grows in thickness.

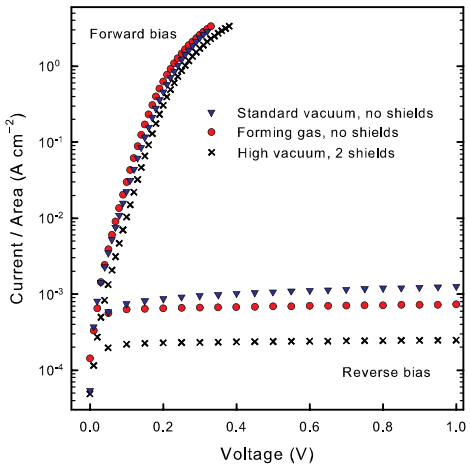

FIG. 4. Current vs voltage plots of Pt SBDs prepared by EBD in a vacuum that varies between 10^{-6} and 10^{-4} mbar without shielding (blue triangles); in forming gas at a pressure of 10^{-4} mbar (red circles) and with two shields at 10^{-6} mbar vacuum (crosses). Forward and reverse bias plots are displayed on the same positive x-axis.

C. Electron beam exposure, without deposition

In experimental setups, it is standard practice to mechanically shield samples until the evaporation has reached a stable state and the deposition is ready to proceed. This is not always practical in industrial systems where large areas have to be coated. An investigation of the effect of this practice was carried out by exposing samples to the conditions of EBD without deposition, termed EBE in this article. A beam with a current of 100 mA was rastered over a tungsten target as this did not produce evaporant from the target while still creating the conditions prevalent in the chamber during deposition of a lower melting point metal such as platinum.

Samples were exposed for 2, 10, or 50 min periods prior to RE of Pd Schottky barrier diodes onto the exposed surfaces. Subsequent DLTS scans revealed the presence of deep level defects in all samples in very low concentrations, and thus, only the 50 min EBE sample had defects in a high enough concentration to facilitate subsequent analysis (Figure 5). Pulse voltages applied were intentionally small to lower the effect that the electric field has on measurements. EBE followed by Pd RE was found to introduce an electron trap, $E_{0.16}$, as well as four hole traps, $H'_{0.15}$, $H_{0.22}$, $H_{0.26}$, and $H_{0.34}$. Characterization of these defects was performed using L-DLTS and is summarized in Table I. All these defects were found to be different from the EBD defects that were previously reported, as illustrated in the Arrhenius plot (Figure 6). While the Arrhenius plot of $H_{0.26}$ overlaps with the known $H_{0.30}$ defect with activation energy for hole emission from E(−/0) determined as 0.307 eV by Markevich *et al.*,[26] it is not likely to be the same defect as their apparent capture cross sections are different by a factor of 2. An annealing study will have to be performed in future as the final arbiter. By evaporating Au onto the EB exposed Ge surface, it was possible to obtain DLTS spectra where the electron-traps were dominant (DLTS—Figure 7 and Arrhenius plots—Figure 8). In plot (e) of Figure 7, five defects are visible: $E_{0.16}$, $E_{0.22}$, $H_{0.26}$, $E_{0.33}$, and $E_{0.38}$. L-DLTS further splits two of these peaks yielding the additional defects $E'_{0.22}$ and $E_{0.37}$. Only $E_{0.38}$ (E-center) and $E_{0.37}$ have been observed before. To the best of our knowledge, none of the other EBE-induced defects have been reported before. Defects $E_{0.16}$, $E_{0.22}$, and $E'_{0.22}$ annealed out within five days at room temperature, but the rest of the defects

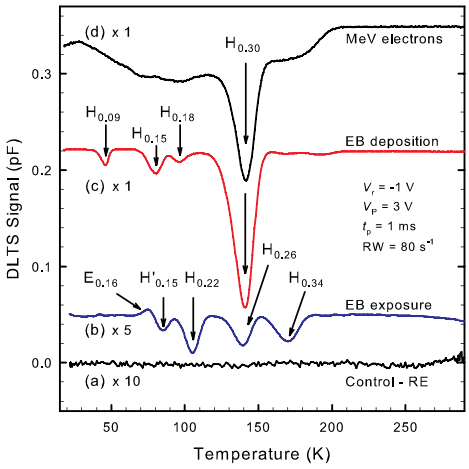

FIG. 5. An 80 s^{-1} rate window DLTS spectra recorded under hole-injection conditions for resistively evaporated Pd diodes where (a) is a RE control spectrum, (b) RE diode pre-exposed to EB conditions for 50 min, (c) EB deposited diode, and (d) a diode exposed to MeV electrons from a Sr-90 source.

remained almost unchanged. No further annealing studies have been undertaken.

By the end of a 50 min EBE treatment, the sample temperature had increased to approximately 365 K. Performing EBE in 10 min treatments with 50 min slots in between for cooling ensured that the sample temperature remained below 335 K. The effect of this strategy on defect concentration can be observed by comparing plots (c) and (d) of Figure 7. Peak heights were at least three times higher for all defects introduced by EBE in the cooler sample. Similar defect concentration changes were observed for the Au diodes.

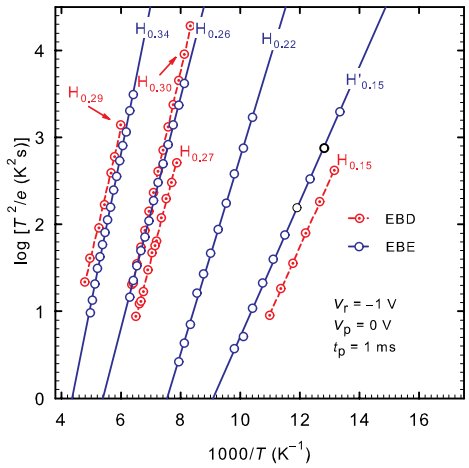

FIG. 6. Arrhenius plots of defects observed after EBD (red circles) and EBE followed by Pd evaporation (blue circles). Only empty circles that denote hole traps are shown as they dominate the Pd EBE spectrum. $E_{0.16}$ is plotted in Figure 8.

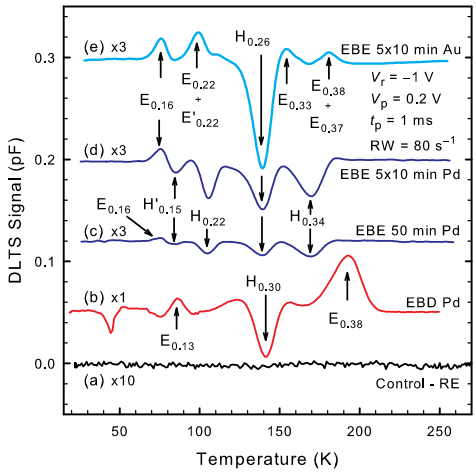

FIG. 7. 80 s^{-1} rate window DLTS spectra recorded at a reverse bias of 1 V, V_p of 0.2 V and pulse width of 1 ms for resistively evaporated diodes [(a), (c), (d), and (e)], where (a) is an Au control spectrum, (b) Pd EB deposited diode, (c) RE diode pre-exposed to EB conditions for 50 min, (d) a Pd RE diode RE pre-exposed to EB conditions for 5×10 minutes, and (e) a gold RE diode pre-exposed to EB conditions for 5×10 min.

IV. DISCUSSION

The significant differences between the DLTS spectra of the EBD and EBE diodes were surprising and not easily explained, especially as most of these defects have not yet been identified. With regards to the energy of impinging particles, the EBD samples were exposed to the lowest energy followed by EBE and 4 eV Ar ICP in order of increasing energy. In all these cases, particles with sub-threshold energy induced the observed defects, the difference being that in the EBD case energy was transferred to the sample through the metal contact,

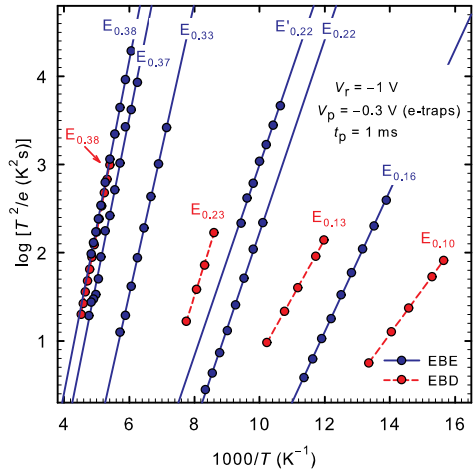

FIG. 8. Arrhenius plots of electron-trap defects observed after EBD (red circles) and EBE (blue circles). EBE defects were measured using Au diodes. Only EBD defects with similar energies to EBE defects are shown and the measurement parameters are noted in the figure.

whereas in the EBE case, these energetic particles interact directly with the semiconductor surface. While it is unlikely that EBD-induced defects are the result of implantation, it is possible that some of the EBE-induced defects were caused by particles that were implanted during the EBE process and diffused deeper into the Ge. The presence of the E-center in EBD and EBE samples demonstrates that at least one defect is not implantation related. There was not enough energy available to generate Frenkel pairs in either of these processes, thus a mechanism to transfer energy deep into the Ge crystal was required to generate E-centers. Such a mechanism, known as discrete breathers (DBs), has been described theoretically and with experimental observations as well.[27] These stationary or moving non-linear localized lattice excitations, having energies in molecular dynamics (MD) from a few eV to 10 eV with long lifetimes, have been shown to exist in some metals.[28] Stationary breathers have been found in germanium[29] and work to demonstrate that moving breathers can also exist in this semiconductor, with a detailed analysis of the energy transfer from ion to crystal lattice will be published in a follow-up paper.

Phonon activity in the 50 min EBE sample disrupted defect introduction as the concentrations of all defects were lower than in the cooler sample. While it may be argued that defects in the sample exposed to a higher temperature annealed out, thus accounting for the lower concentrations observed, this small increase in temperature is highly unlikely to have affected all defects equally. EBE followed by Au RE yielded additional defects which is not observed in the Pd diodes, but a discussion of these differences is beyond the scope of this report.

V. CONCLUSIONS

Varying the conditions during EBD introduced two new defects, $E_{0.28}$ and $E_{0.31}$, which were not previously observed in Ge. The introduction of shields not only lowered defect concentrations but also ensured that superior diodes were produced. EBE that exposed the sample to very similar conditions as those of EBD was responsible for introducing ten defects. We can only speculate why the E-center and $E_{0.37}$ were the only defects that have previously been observed. To determine how sub-threshold particles cause damage in Ge, it was necessary to identify the energetic ions, atoms, or molecules generated in the electron beam path as the energy carriers, then consider the interaction of these energetic particles with light atoms in the crystal lattice, and subsequently identify a mechanism whereby energy can be transferred deep into the crystal without the need for an ion-solid interaction. As the shielded EBD samples continued to be bombarded by energetic electrons without significant damage being observed, it can be concluded that sub-threshold electrons are not responsible for the EBD-induced defects. The disruption of defect introduction by phonon activity in EBE diodes is further evidence that discrete breathers are the most likely energy transfer mechanism responsible for EBE as well as EBD-induced defects. As damage has been observed after EBD on Si and other semiconducting materials, it is safe to conclude that this damage causing mechanism is applicable to other semiconductors as well.

ACKNOWLEDGMENTS

The authors gratefully acknowledge financial support of the South African National Research Foundation. The Laplace DLTS software and hardware used in the research was kindly provided by A. R. Peaker (Centre for Electronic Materials Devices and Nanostructures, University of Manchester) and L. Dobaczewski (Institute of Physics, Polish Academy of Sciences). Special thanks to J. F. R. Archilla and D. I. Tetelbaum.

[1]E. Reinhold and J. Faber, Surf. Coat. Technol. **206**, 1653 (2011).
[2]S. Z. Karazhanov, J. Appl. Phys. **89**, 332 (2001).
[3]G. Myburg and F. D. Auret, J. Appl. Phys. **71**, 6172 (1992).
[4]Y. Chen and J. W. MacKay, Phys. Rev. **167**, 745 (1968).
[5]E. E. Haller, Mater. Sci. Semicond. Process. **9**, 408 (2006).
[6]F. D. Auret, S. M. M. Coelho, J. M. Nel, and W. E. Meyer, Phys. Status Solidi A **209**, 1926 (2012).
[7]L. Dobaczewski, P. Kaczor, I. D. Hawkins, and A. R. Peaker, J. Appl. Phys. **76**, 194 (1994).
[8]J. A. Lauber, S. Gascon-Shotkin, R. G. Kellogg, and G. R. Martinez, Nucl. Instrum. Methods Phys. Res. A **396**, 165 (1997).
[9]J. Fage-Pedersen, A. Nylandsted Larsen, and A. Mesli, Phys. Rev. B **62**, 10116 (2000).
[10]E. Holmstrom, K. Nordlund, and A. Kuronen, Phys. Scr. **81**, 035601(4 pages) (2010).
[11]P. M. Mooney and J. C. Bourgoin, Phys. Rev. B **29**, 1962 (1984).
[12]F. D. Auret, W. E. Meyer, S. Coelho, and M. Hayes, Appl. Phys. Lett. **88**, 242110 (2006).
[13]A. R. Peaker, V. P. Markevich, and L. Dobaczewski, *Defects in Microelectronic Materials and Devices* (CRC, New York, 2009), pp. 27–55.
[14]R. Jones, B. J. Coomer, J. P. Goss, B. Hourahine, and A. Resende, Solid State Phenom. **71**, 173 (2000).
[15]M. Budde, B. Bech Nielsen, P. Leary, J. Goss, R. Jones, P. Briddon, S. Öberg, and S. Breuer, Phys. Rev. B **57**, 4397 (1998).
[16]J. R. Weber, A. Janotti, P. Rinke, and C. G. Van de Walle, Appl. Phys. Lett. **91**, 142101 (2007).
[17]J. Weber, M. Hiller, and E. V. Lavrov, Mater. Sci. Semicond. Process. **9**, 564 (2006).
[18]B. J. F. Coomer, *A First Principles Study of Radiation Defects in Semiconductors* (University of Exeter, 2000).
[19]C. Kittel, *Introduction to Solid State Physics*, 6th ed. (Wiley, New York, 1986).
[20]*CRC Handbook of Chemistry and Physics*, 73rd ed., edited by David R. Lide (CRC Press, Boca Raton, FL, 1992).
[21]K. T. Roro, P. J. Janse van Rensburg, F. D. Auret, and S. Coelho, Physica B **404**, 4496 (2009).
[22]F. D. Auret, S. M. M. Coelho, G. Myburg, P. J. Janse van Rensburg, and W. E. Meyer, Physica B **404**, 4376 (2009).
[23]C. Nyamhere, A. Venter, D. M. Murape, F. D. Auret, S. M. M. Coelho, and J. R. Botha, Physica B **407**, 2935 (2012).
[24]C. Nyamhere, A. G. M. Das, F. D. Auret, A. Chawanda, W. Mtangi, Q. Odendaal, and A. Carr, Physica B **404**, 4379 (2009).
[25]F. D. Auret, W. E. Meyer, S. Coelho, M. Hayes, and J. M. Nel, Mater. Sci. Semicond. Process. **9**, 576 (2006).
[26]V. P. Markevich, I. D. Hawkins, A. R. Peaker, K. V. Emtsev, V. V. Emtsev, V. V. Litvinov, L. I. Murin, and L. Dobaczewski, Phys. Rev. B **70**, 235213 (2004).
[27]S. Flach and A. V. Gorbach, Phys. Rep. **467**, 1 (2008).
[28]V. Hizhnyakov, M. Haas, A. Pishtshev, A. Shelkan, and M. Klopov, Nuclear Instrum. Methods Phys. Res. B **303**, 91 (2013).
[29]N. K. Voulgarakis, G. Hadjisavvas, P. C. Kelires, and G. P. Tsironis, Phys. Rev. B **69**, 113201 (2004).
[30]V. P. Markevich, A. R. Peaker, V. V. Litvinov, V. V. Emtsev, and L. I. Murin, J. Appl. Phys. **95**, 4078 (2004).
[31]V. P. Markevich, Mater. Sci. Semicond. Process. **9**, 589 (2006).
[32]F. D. Auret, S. Coelho, W. E. Meyer, C. Nyamhere, M. Hayes, and J. M. Nel, J. Electron. Mater. **36**, 1604 (2007).
[33]C. Nyamhere, M. Das, F. D. Auret, and A. Chawanda, Phys. Status Solidi (C) **5**, 623 (2008).

4.4 Sputter Deposition Defects

Defects introduced during SD are characterized in Auret, Coelho, Meyer et al. 2007. A comparison is made with MeV electron irradiation defects. Auret, Coelho, Janse van Rensburg et al. 2008, has been included in section 4.7 as the annealing of defects is also reported on therein.

SD is an important technique for the fabrication of devices in the semiconductor industry that, as such, deserves study with the aim to characterize the defects introduced during SD and their impact on the quality of devices produced. Defects introduced during SD were compared with MeV electron irradiation induced defects and to those introduced during EBD. These comparisons are crucial to the understanding of the differences between above and below threshold irradiation reactions in germanium. As Au was used in this work as the SBD metal, it was then possible to compare the results obtained with depositions of the same metal by other techniques. Such comparisons are often not possible as high melting point metals that are readily sputter deposited cannot be evaporated resistively. Magnetic materials, like Ni and Fe, are easily evaporated but are challenging to deposit using magnetron SD thus eliminating them from being considered. Another aspect of this technique that was investigated was sputter etching of the germanium surface prior to metal evaporation. This was only performed at very low energy in an argon plasma so that the devices produced were still acceptable for DLTS measurements and so that a comparison could be made with ICP etching (section 4.3.2).

Journal of ELECTRONIC MATERIALS, Vol. 36, No. 12, 2007 *Regular Issue Paper*
DOI: 10.1007/s11664-007-0245-y

Electrical Characterization of Defects Introduced During Sputter Deposition of Schottky Contacts on *n*-type Ge

F.D. AURET,[1,2] S. COELHO,[1] W.E. MEYER,[1] C. NYAMHERE,[1] M. HAYES,[1] and J.M. NEL[1]

1.—Physics Department, University of Pretoria, Pretoria 0002, South Africa. 2.—e-mail: danie.auret@up.ac.za

The authors have investigated by deep level transient spectroscopy the electron traps introduced in *n*-type Ge during sputter deposition of Au Schottky contacts. They have compared the properties of these defects with those introduced in the same material during high-energy electron irradiation. They found that sputter deposition introduces several electrically active defects near the surface of Ge. All these defects have also been observed after high-energy electron irradiation. However, the main defect introduced by electron irradiation, the V-Sb center, was not observed after sputter deposition. Annealing at 250°C in Ar removed the defects introduced during sputter deposition.

Key words: Germanium, sputter deposition, Schottky contacts, defects, deep level transient spectroscopy (DLTS)

INTRODUCTION

The low effective mass of holes in Ge has opened up the possibility of using Ge in ultrafast complimentary metal-oxide-semiconductor (CMOS) devices.[1] A Ge channel MOSFET has benefits as a performance booster for future scaled CMOS circuits, because it offers higher mobility for electrons and holes than in a Si MOSFET.[2] Thus, Metal Source/Drain MOSFETs (MSD-MOSFETs) with ultra-thin Ge-on-Insulator (GOI) channels have been proposed and realized.[2] This interest in Ge devices, in turn, has sparked renewed interest in the properties of defects in Ge because defects ultimately determine the performance of devices. In recent studies the properties of the defects introduced during high-energy gamma-, electron- and proton irradiation,[3–6] as well as indium-ion implantation,[7] of Ge were reported. The defects introduced during electron beam deposition of Pt Schottky contacts have also been characterized.[8] The investigations of metallization-induced defects are important because it is well known that metallization procedures, e.g. sputtering and electron beam deposition, introduce defects at and close to the metal-semiconductor junction. These defects influence device performance and alter the barrier heights of the contacts.[9,10] The defects responsible for these barrier adjustments are formed when energetic particles reach the semiconductor surface and interact with it, resulting in lattice damage. Depending on the application, these defects may either be beneficial or detrimental for optimum device functioning. For example, for Si it has been shown that the defects introduced during high-energy electron and proton irradiation increase the switching speed of devices.[11]

In this study we report the electronic properties of defects introduced in *n*-type Ge during sputter deposition of Au Schottky contacts. We show that sputter deposition introduces several electron traps and that the electronic properties of these defects are the same as some of the defects introduced during MeV electron irradiation of the same material.

(Received February 22, 2007; accepted March 20, 2007; published online September 21, 2007)

EXPERIMENTAL PROCEDURE

For this experiment we used bulk-grown (111) *n*-type Ge doped with Sb to a level of 2.5×10^{15} cm^{-3}.

Before metallization the samples were first degreased and then etched in a mixture of H_2O_2 (30%): H_2O (1:5) for 1 min. Directly after cleaning they were inserted into a vacuum chamber where AuSb (0.6% Sb) was deposited on their back surfaces as ohmic contacts. The samples were then annealed at 350°C in Ar for 10 min. Before Schottky contact deposition, the samples were again chemically cleaned as described above. Au contacts, 0.63 mm in diameter, were sputter-deposited through a mechanical mask. For sputter deposition Ar was leaked into the system to a pressure of 6×10^{-2} mbar to create the plasma. The accelerating sputter voltage was 700 V and the power was 100 W. The sputter-deposited contacts were deposited at a rate of about 2 nm s^{-1} and were 400 nm thick. "Control" Au Schottky contacts were deposited on identical samples by resistive evaporation—a process known not to introduce defects in semiconductors. Both conventional and high-resolution Laplace DLTS[12,13] were used to study the defects introduced in the Ge during the sputter deposition process.

RESULTS AND DISCUSSION

Room temperature capacitance–voltage (*C–V*) measurements revealed that the barrier heights of control (resistively deposited) contacts and sputter deposited contacts were 0.44 ± 0.01 eV and 0.45 ± 0.01 eV, respectively. This is the same for all practical purposes and shows that sputter deposition does not introduce defects in a sufficiently high concentration to alter the built-in voltage of the Au-Ge interface. Room temperature current–voltage (*I–V*) measurements, however, showed that the reverse leakage current of the sputter deposited contact (at −1 V bias) was about an order of magnitude higher (5×10^{-5} A) than that of the resistively deposited contact (2×10^{-6} A). This is illustrated in Fig. 1. This, together with the fact that the *C–V* Schottky barrier height was not decreased during sputter deposition, suggests that the increase in reverse current is caused by sputter deposition introduced defects that act as recombination-generation centers. We have also measured the reverse current (at −1 V bias) as a function of temperature. Upon cooling, the reverse current of the control diode (at −1 V bias) decreased from 2×10^{-6} A at room temperature to 1×10^{-13} A at 100 K (Fig. 1). The lower current limit of our current (*I*) measurement system is about 2×10^{-14} A. The reverse current (at −1 V bias) of the sputtered diode, on the other hand, slowly decreased from 5×10^{-5} A at room temperature to 3×10^{-9} A at 100 K, where the reverse current was almost four orders of magnitude higher than that of the control diode (Fig. 1). The fact that the reverse current of the sputtered diode was so much higher than that of the control diode emphasizes the importance of sputter deposition introduced defects as recombination centers, especially at low temperatures.

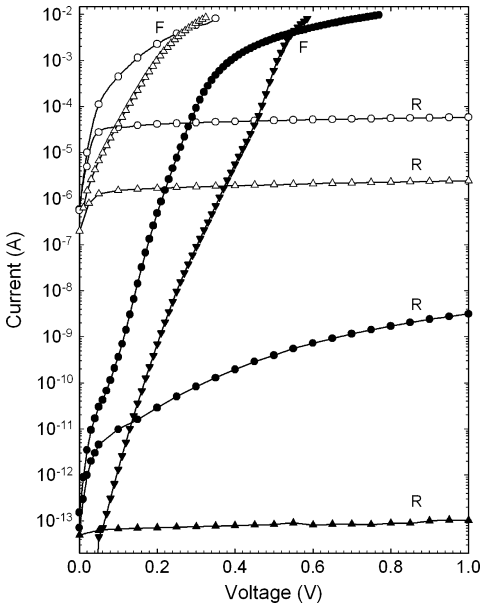

Fig. 1. *I–V* curves of resistively deposited (*triangles*) and sputter deposited (*circles*) Au Schottky contacts to Ge, recorded at room temperature (*open symbols*) as well as at 100 K (*solid symbols*). Note that the forward 'F' and reverse 'R' currents are plotted in the same quadrant.

In Fig. 2 we depict the DLTS spectra for control and sputter-deposited Au contacts. The DLTS spectrum, curve (a), of the control diode does not contain any detectable DLTS peaks. Curve (b) shows that sputter deposition introduced several electron traps: $ES_{0.14}$, $ES_{0.20}$, $ES_{0.21}$, $ES_{0.24}$, and $ES_{0.31}$. In this nomenclature 'ES' means electron trap induced by sputtering, and the subscript is the activation energy determined from the Arrhenius plots in Fig. 3. The electronic properties of these defects are summarised in Table I. The peaks of $ES_{0.20}$ and $ES_{0.21}$ could only be clearly resolved after using high-resolution Laplace DLTS.[12,13] In Fig. 2 we also compare the DLTS spectrum of sputter-induced defects to those of Au Schottky diodes formed by electron beam deposition (EBD) (curve c) and to the spectrum of Ge irradiated with high energy electrons (curve d).[8] This comparison reveals that, except for the V-Sb center, sputter deposition introduces the same defects as high energy electron irradiation. This is also verified in Fig. 3 where the DLTS signatures of these defects are compared. Interestingly, none of the defects introduced by EBD, except the V-Sb complex, correspond to defects introduced by high-energy electron irradiation or sputter deposition. Unlike in previous studies of high-energy electron irradiated Ge and

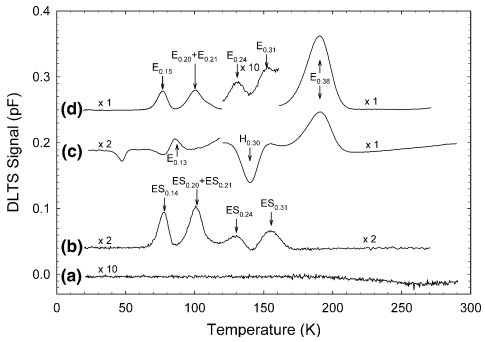

Fig. 2. DLTS spectra of Schottky contacts to *n*-Ge. Curve (a) resistively deposited (control) Au contact; curve (b) sputter deposited Au contact; curve (c) Au contact deposited by electron beam deposition; and curve (d) Pd contact irradiated with MeV electrons.[7] All spectra were recorded using a rate window of 80 s^{-1} at a quiescent reverse bias of −1 V and a pulse, V_p, of 0.15 V into forward bias.

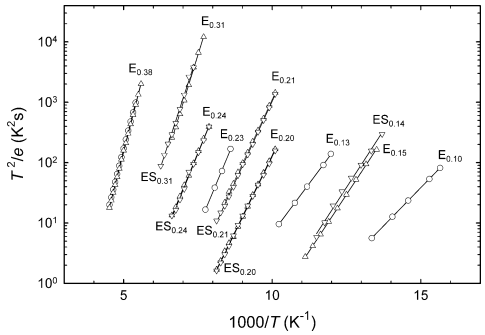

Fig. 3. Arrhenius plots for defects introduced in *n*-type Ge during electron beam deposition (*circles*), sputter deposition (*upside down triangles*) and high-energy electron irradiation induced (*upright triangles*). All data was acquired using the bias and pulsing conditions defined in the caption of Fig. 2.

electron beam deposited (EBD) Schottky diodes,[8] we could not detect any hole traps in the sputter deposited contacts studied here, even when applying a strong forward bias. After irradiating the sputter deposited contacts with MeV electrons the hole traps typical of electron irradiation could be observed. This means that sputter deposition by itself does not introduce any hole traps in detectable concentrations.

The main electron trap introduced by EBD and electron irradiation was the $E_{0.38}$, which was shown to be the (–/–) charge state of the V-Sb center. The fact that this defect is not observed after sputter deposition implies that this process does not introduce a sufficient number of single vacancies at and close to the surface that can diffuse into the Ge and combine with Sb ions to form V-Sb, as in the case of EBD.[8] It should be realised that most of the damage that we observe after sputter deposition is caused by backscattered neutral Ar ions that have a maximum energy of 700 eV. From TRIM[14] modelling we have found that the range and straggle of these ions are 2.1 nm and 1.2 nm, respectively. In the first 3 nm they deposit on average 20 eV/nm to the Ge lattice and produce, on average, 5 vacancies/nm. This implies that defects larger than the single vacancy, e.g. divacancy and vacancy (or interstitial) clusters, can be formed. Whereas vacancy clusters, such as the divacany, are stable at room temperature,[3] interstitial clusters, by nature, are not very stable. It is therefore conceivable that when they break up, interstitials are injected into the Ge during sputter deposition. Based on this we speculate that the defects we observe after sputter deposition are related to interstitial-impurity complexes (e.g. I-Sb), vacancy- or interstitial clusters, or complexes of these clusters with impurities. The signature of $ES_{0.31}$ (similar to that of $E_{0.31}$) is close to that reported for the divacancy ($E_{0.29}$),[3] whereas the signatures of $ES_{0.14}$, $ES_{0.20}$, and $ES_{0.21}$ are close to that of the $E_{0.13}$, $E_{0.19}$, and $E_{0.23}$ proposed to be related to Sb and the Ge interstitial.[3]

As in previous studies on other semiconductors,[8–10] we have found that the defects introduced during sputter deposition of contacts on Ge are located close to the metal-semiconductor interface. A depth profile constructed using the fixed-bias variable-pulse method showed that the concentration of the sputter-induced defects is of the order of 10^{13} cm^{-3} at 100 nm below the interface and decreased exponentially into the Ge. However, it should be pointed out that from TRIM modelling we have found that most of the directly produced sputter damage is located within the first 5 nm below the surface. It is well known that it is not possible to accurately probe defects by DLTS so close to the surface. Therefore, the defects that we observe beyond 100 nm reached that location by diffusion and their concentration is not a fair reflection of that of the defects directly produced by sputter-deposition close to the interface.

We have also investigated the thermal stability of the sputter deposition induced defects by isochronal annealing in argon. After annealing at 150°C for 10 min the $ES_{0.14}$, $ES_{0.20}$, and $ES_{0.24}$ levels could no longer be detected but the concentration of $ES_{0.31}$ increased by about a factor of two. Annealing at 200°C reduced the concentrations of $ES_{0.21}$ and $ES_{0.31}$ by 10% and 30%, respectively, and annealing at 250°C removed them completely, and sputter deposition induced defects could no longer be detected. After annealing at 300°C, no additional defects, i.e. no 'second generation' defects could be observed, indicating that the sputter deposition induced defects did not reconstruct during annealing to form larger defects or different defect complexes. The removal temperature of $ES_{0.31}$ of 250°C is higher than the 180°C reported by Fage-Pedersen et al.[3] for removing the divacancy (with a similar energy level). However,

Table I. Electronic Properties of Prominent Defects Introduced in *n*-Type Ge During Sputter Deposition and MeV Electron Irradiation of Schottky Contacts

Sputter Deposition				MeV Electron Irradiation				
Defect	**E_T (eV)**	**σ_a (cm^2)**	**T^a_{peak} (K)**	**Defect**	**E_T (eV)**	**σ_a (cm^2)**	**T^a_{peak}(K)**	**Similar Defects / Defect ID**
$ES_{0.14}$	E_C–0.14	5.5×10^{-15}	78	$E_{0.15}$	E_C–0.15	2.8×10^{-14}	77	$E^b_{0.13}$, Sb and *I* related[c]
$ES_{0.20}$	E_C–0.20	3.7×10^{-14}	100	$E_{0.20}$	E_C–0.20	1.4×10^{-14}	100	$E^c_{0.19}$, Sb and *I* related[c]
$ES_{0.21}$	E_C–0.21	2.0×10^{-14}	109	$E_{0.21}$	E_C–0.21	3.6×10^{-14}	109	$E^b_{0.21}$, Sb related?[c]
$ES_{0.24}$	E_C–0.24	3.3×10^{-15}	131	$E_{0.24}$	E_C–0.24	2.5×10^{-15}	131	$E^c_{0.23}$, Sb and *I* related?[c]
$ES_{0.31}$	E_C–0.31	1.5×10^{-14}	151	$E_{0.31}$	E_C–0.31	5.0×10^{-14}	150	$E^c_{0.29}$?, V^c_2?
—	—	—	—	$E_{0.38}$	E_C–0.38	1.1×10^{-14}	191	$E^b_{0.377}$, $E^c_{0.37}$, V-Sb (–/–)[b, c]
—	—	—	—	$H_{0.30}$	E_V + 0.30	3.66×10^{-13}	142	$H^b_{0.307}$, $H^c_{0.30}$, V-Sb (–/0)[b]

[a] Peak temperature at a rate window of 80 s^{-1}; [b] See Ref. 4; [c] See Ref. 3.

it should be borne in mind that the annealing reported by Fage-Pedersen et al.[3] was performed under zero bias where most of the defects are filled with electrons. In our case $ES_{0.31}$ is close to the surface and hence above the Fermi level during annealing. It has been reported that reverse bias annealing (E-center above the Fermi level) impedes the annealing of E-centers[2]. Annealing at temperatures of up to 300°C is not expected to give rise to Au-Ge interaction, e.g. germanidation, because the Au-Ge eutectic temperature is 361°C.[15]

Finally, it is interesting to note that sputter deposition also introduced several defects in Si.[15] Unlike the case of Ge above, annealing of sputter-deposited Ti-W Schottky contacts to *n*- and *p*-type Si introduced several second generation defects.[16] It is also important to point out that annealing at 400°C removed some, but not all, of the sputter-induced defects in Si.[16] However, this comparison between sputter-induced defects in Ge and Si may not be very appropriate because the sputter systems and conditions used for the two experiments were different.

SUMMARY

In summary, we have investigated by deep level transient spectroscopy the electron trap defects introduced in *n*-type Ge during sputter deposition of Au Schottky contacts. We have compared the properties of these defects with those introduced in the same material during high-energy electron irradiation and have found that sputter deposition introduces several electrically active defects near the surface of Ge. All these defects have also been observed after high-energy electron irradiation. However, the main defect introduced by high-energy electron irradiation, the V-Sb complex, was not observed after sputter deposition. Annealing at 250°C in Ar removed the defects introduced during sputter deposition but annealing at higher temperatures did not introduce any new defects.

ACKNOWLEDGEMENTS

The authors gratefully acknowledge financial support of the South African National Research Foundation. The Laplace DLTS software and hardware used in the research was kindly provided by A.R. Peaker (Centre for Electronic Materials Devices and Nanostructures, University of Manchester) and L. Dobaczewski (Institute of Physics, Polish Academy of Sciences).

REFERENCES

1. R. Hull and J.C. Bean, eds., *Germanium Silicon: Physics and Materials, Semiconductors and Semimetals*, Vol. 56 (San Diego, CA: Academic, 1999).
2. K. Ikeda, T. Maeda, and S. Takagi, *Thin Solid Films* 508, 359 (2006).
3. J. Fage-Pedersen, A. Nylandsted Larsen, and A. Mesli, *Phys. Rev. B* 62, 10116 (2000).
4. V.P. Markevich, A.R. Peaker, V.V. Litvinov, V.V. Emstev, and L.I. Murin, *J. Appl. Phys.* 95, 4078 (2004).
5. V.P. Markevich, I.D. Hawkins, A.R. Peaker, K.V. Emstev, V.V. Emstev, V.V. Litvinov, and L. Dobaczewski, *Phys. Rev. B* 70, 235213 (2004).
6. V.P. Markevich, I.D. Hawkins, A.R. Peaker, V.V. Litvinov, L. Dobaczewski, and J.L. Lindström, *Appl. Phys. Lett.* 81, 1821 (2002).
7. F.D. Auret, S. Coelho, M. Hayes, J.M. Nel, and W.E. Meyer, *Appl. Phys. Lett.* 89, 152123 (2006).
8. F.D. Auret, S. Coelho, M. Hayes, and W. E. Meyer, *Appl. Phys. Lett.* 88, 242110 (2006).
9. F.D. Auret, S.A. Goodman, F.K. Koschnik, J.-M. Spaeth, B. Beaumont, and P. Gibart, *Appl. Phys. Lett.* 74, 2173 (1999).
10. G. Myburg and F.D. Auret, *J. Appl. Phys.* 71, 6172 (1992).
11. D.C. Sawko and J. Bartko, *IEEE Nucl. Sci.* 30, 1756 (1983).
12. L. Dobaczewski, P. Kaczor, I.D. Hawkins, and A.R. Peaker, *J. Appl. Phys.* 76, 194 (1994).
13. L. Dobaczewski, A.R. Peaker, and K. Bonde Nielsen, *J. Appl. Phys.* 96, 4689 (2004).
14. J.F. Ziegler, J.P. Biersack, and U. Littmark, *The Stopping and Range of Ions in Solids*, Vol. 1, ed. J.F. Ziegler (New York: Pergamon, 1985).
15. G. Le Lay, G. Quentel, J.P. Faurie, and A. Masson, *Thin Solid Films* 35, 289 (1976).
16. F.D. Auret and G.M. Matusiewicz, *Vacuum* 35, 195 (1985).

4.5 ICP Induced Defects

Auret et al. 2009 report on the annealing of the ICP induced defect, $E_{0.31}$, and is thus included in section 4.7. Three additional articles, Coelho, Auret, Myburg et al. 2009, Auret et al. 2010 and Coelho, F.D. et al. 2014, that focus on the defect introduced during ICP etching of germanium appear below. Abstracts from articles by Nyamhere, Venter, Auret et al. 2012 and Nyamhere, Venter, Murape et al. 2012 complete this section.
The aims of studying ICP induced defects were the following:

- To assess the impact of this plasma treatment on device quality.
- To characterize the defects that may be introduced in Ge by ICP.
- The dependence of defects observed after ICP on plasma gas species was also investigated.
- The ion energy is inversely proportional to the gas pressure thus it was possible to study the defects introduced for ion energies ranging between 20 and 80 eV that classifies this technique as one that both uses above and below threshold energy ions.
- By isochronally annealing samples at increasing temperatures we were able to determine at what temperature defects are annealed out of the material and by what mechanism this occurs; defect diffusion or dissociation.

ICP treatment of GaAs was also reported on by Auret et al[3] and Venter et al[4] ,[5] emphasizing the importance of ICP etching for other semiconductors as well.

[3]F.D. Auret, P.J. Janse van Rensburg, W.E. Meyer et al. 'Inductively coupled plasma induced deep levels in epitaxial n-GaAs'. *Physica B: Condensed Matter* **407**.10 (May 2012), pp. 1497–1500. DOI: 10.1016/j.physb.2011.09.070.

[4]A. Venter, C. Nyamhere, J.R. Botha, F.D. Auret, S.M.M. Coelho et al. 'Field dependence of the E1' and M3' electron traps in inductively coupled Ar plasma treated n-Gallium Arsenide'. *Journal of Applied Physics* **111**.9 (2012), p. 093703. DOI: 10.1063/1.4709390.

[5]A. Venter, C. Nyamhere, J.R. Botha, F.D. Auret, P.J. Janse van Rensburg et al. 'Ar plasma induced deep levels in epitaxial n-GaAs'. *Journal of Applied Physics* **111**.1 (2012), p. 013703. DOI: 10.1063/1.3673322.

Physica B 404 (2009) 4389–4392

Contents lists available at ScienceDirect

Physica B

journal homepage: www.elsevier.com/locate/physb

Current–temperature measurements of a SBD evaporated onto inductively coupled plasma cleaned germanium

S.M.M. Coelho *, F.D. Auret, G. Myburg, P.J. Janse van Rensburg, W.E. Meyer

Physics Department, University of Pretoria, Pretoria 0002, South Africa

ARTICLE INFO

PACS:
71.20.Mq
73.40.Ei
61.82.Fk
79.40.+z
73.30.+y

Keywords:
Germanium
Schottky barrier diode
ICP
DLTS
Defects
Dry etch

ABSTRACT

Inductively coupled plasma (ICP) etching has been used primarily on compound semiconductors. There are however compelling reasons to study the effects of ICP etching on Ge. Pd Schottky barrier diodes (SBDs) were resistively evaporated onto Ge (111) that was ICP etched at a rate of 60 Å per minute for three or ten minute intervals. Although plasma cleaning is known to introduce defects that were observed with DLTS, the diodes exhibited excellent current–voltage characteristics when cooled down to 80 K. Current–temperature (*IT*) scans that were recorded from 20 K up to 300 K after cooling under reverse bias showed no effect of recombination/generation (RG). On the other hand, *IT* scans that were recorded after cooling under zero or forward bias clearly exhibited RG effects in the 100–240 K temperature range. This effect was found to be completely reversible. In addition, ICP etching leads to superior devices when compared to devices manufactured by RF sputter deposition.

1. Introduction

In the manufacture of semiconductor devices, metal contacts have always played a pivotal role, especially in MOSFET and CMOS devices. Understanding the effect of different metallization techniques on the electrical properties of a semiconductor is of critical importance as we advance into the age of ultrafast devices. Germanium is now receiving renewed attention as its high mobility carriers, both holes and electrons, make it an ideal material for the next-generation fast switching devices. There are also several important niche applications for germanium such as high-resolution gamma-ray detectors, far IR detectors and low temperature thermistors (see [1] and references therein).

Since the 1970s, the need for higher circuit density has resulted in dry etching processes becoming popular. Their advantage over the cost effective wet etches is that dry etches produce higher resolution pattern transfer. Of the many dry etch processes available today, ICP etching even has advantages over electron cyclotron resonance (ECR) etching as it has no DC magnetic field requirement and large wafers can be accommodated [2]. An ICP system operating under optimal conditions can produce ion currents that are uniform to $\pm 1.5\%$ over a large wafer [3] and this translates into a uniform etch rate across the wafer. It has further been shown that ICP etching produces lower ion damage than traditional plasma etches when applied to compound semiconductors [4–6]. ICP and ECR etches were also found to change the electrical properties of diodes fabricated on compound semiconductors less than conventional reactive ion discharges as RF-induced DC self-biases are much lower in ICP and ECR systems [5].

Device properties will be further influenced by the defects introduced during metallization. High melting point metals cannot be applied onto the semiconductor surface using benign techniques like resistive evaporation, making it necessary to quantify the defects introduced by more energetic deposition processes like electron beam deposition (EBD) and sputter deposition (SD). Defects introduced, unintentionally or intentionally, near the semiconductor—metal interface will alter the barrier heights of contacts influencing device performance [7,8].

2. Experimental procedures

Bulk-grown (111) *n*-type Ge, doped with Sb to a level of $2.5 \times 10^{15}\,cm^{-3}$ was degreased in successive, five minute, trichloroethylene, acetone and methanol ultrasonic baths. After a de-ionized water rinse, samples were etched in a mixture of H_2O_2 (30%) : H_2O (1:5) for one minute, rinsed with de-ionized water and dried with nitrogen gas, then inserted into a vacuum chamber where AuSb (0.6% Sb) was deposited on the wafer back surface by

* Corresponding author. Tel.: +27 12 4205135; fax: +27 12 3625288.
E-mail address: sergio@up.ac.za (S.M.M. Coelho).

0921-4526/$ - see front matter © 2009 Elsevier B.V. All rights reserved.
doi:10.1016/j.physb.2009.09.026

Table 1
Reverse bias current of Pd Schottky diodes manufactured by different deposition methods.

Deposition	Cleaning procedure	Current (A) at −1 V bias (100 K)	Current (A) at −1 V bias (300 K)	Ideality factor/barrier height (eV)
RE	Degrease, H_2O_2 etch	Below 10^{-14}	2.3×10^{-6}	1.06/0.55
RE	Degrease, ICP	$\sim5\times10^{-14}$	2×10^{-5}	1.15/0.53
EB	Degrease only	6×10^{-8}	3×10^{-6}	1.50/0.61
EB	Degrease, H_2O_2 etch	Below 10^{-14}	3.9×10^{-5}	1.30/0.52
EB	Degrease, 3 min ICP	$\sim5\times10^{-14}$	1.5×10^{-5}	1.12/0.59
EB	Degrease, 10 min ICP	$\sim5\times10^{-14}$	1.5×10^{-5}	1.50/0.57
SD–Au	Degrease, H_2O_2 etch	3×10^{-9}	5.9×10^{-5}	2.05/0.44

resistive evaporation (RE). A ten minute anneal in an Ar atmosphere at 350 °C lowered the barrier height resulting in an ohmic contact. Phase two of device fabrication involved cutting the wafer into 3 mm × 5 mm pieces and the same degreasing procedure as above was applied, followed by mounting of a sample on a holder in a vacuum chamber where plasma cleaning and EBD of the front side of the sample took place through a metal contact mask that has 0.6 mm diameter holes in it. ICP and EBD were carried out successively without breaking vacuum. Diodes manufactured by RE, a process known not to introduce measurable defects [9], were plasma etched in one vacuum system, while resistive evaporation was performed in a second vacuum system, exposing the Ge samples to the atmosphere while transferring the sample from one system to another. Initial vacuum was better than 10^{-5} mbar for all processes regardless of the system used. Ten minute and three minute plasma etches were performed by a Copra DN 200 inductively coupled plasma beam source. Radio Frequency (RF) power of 500 W forward (23 W reverse) and an argon pressure of 5×10^{-4} mbar were the conditions used for all plasma treatments followed by a 100 nm thick Pd deposition onto the germanium to form the Schottky barrier diodes (SBDs) considered herein. In situ monitoring of the film thickness growth was achieved in the resistive and EB systems via an Inficon crystal growth monitor. Pd was deposited by RE at a rate of 0.3 nm/s and a similar EB deposition rate was achieved using a 10 kV electron gun with a beam current of approximately 0.1 A.

Current–voltage (*IV*) and deep level transient spectroscopy (DLTS) measurements, except for the room temperature dark *IV* measurements, were performed in vacuum in a closed-cycle helium cryostat.

3. Results and discussion

It was estimated that atomic layer etching of Ge by Ar^+ ions required energy higher than 13 eV [10]. SRIM simulations predicted slightly higher ion energy of 17 eV to dislodge Ge atoms from an amorphous target. ICP etches were carried out with an average Ar^+ ion energy of 80 eV (as measured by Copra) to minimize the damage caused to the Ge crystal lattice while maintaining a reasonable etch rate of 6 nm per minute. Eight diodes were deposited on each sample and room temperature. *IV* measurements were subsequently carried out to ascertain diode quality as well as uniformity across the sample. Ideality factors and the *IV* barrier height was extracted from a linear fit of the forward bias $\log[I/(1-\exp(-qV/kT))]$ versus V plot [11]. Idealities below 1.1 were considered to be "good" provided that an accurate linear fit to the data was obtained [12]. Reverse bias current at −1 V was used as an indication of the diode quality. This current measurement is diode area dependent and for Ge diodes with a diameter of 0.6 mm, values below 10^{-5} A with at least three orders of magnitude between the 1 V forward and reverse bias currents are acceptable.

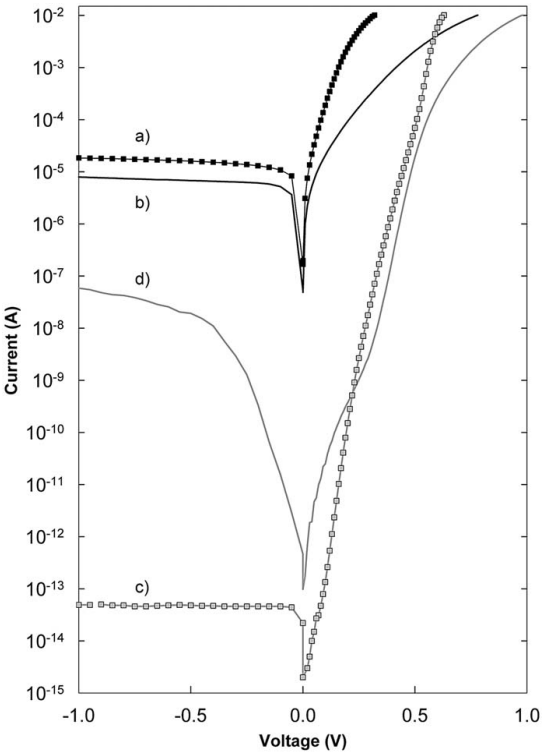

Fig. 1. Current–voltage measurements under forward and reverse bias conditions for Pd Schottky diodes, recorded at 300 and 100 K, respectively: (a) 10 min plasma etched EB deposited diode measured at 300 K, (b) unetched EB deposited diode measured at 300 K, (c) diode (a) measured at 100 K and (d) diode (b) measured at 100 K.

ICP etching and EBD are capable of introducing defects at and below the semiconductor surface as energetic particles are accelerated in both processes and these interacted with the Ge samples. Thus, while it is not surprising that the RE deposited Schottky barrier diode had an ideality closest to one and a low 1 V reverse bias current of 2.3×10^{-6} A as summarized in Table 1, the diode produced by 3 min ICP etching followed by EBD had a slightly worse ideality of 1.12 with a room temperature 1 V reverse bias current that was almost one order of magnitude higher. When these two diodes are compared at 100 K both diodes exhibited 1 V reverse bias currents that were low enough to be at the lower limit measurable by the HP 4140B pA meter. This result was in sharp contrast to the diode produced by EB deposition without ICP that had a 1 V reverse bias current six orders of

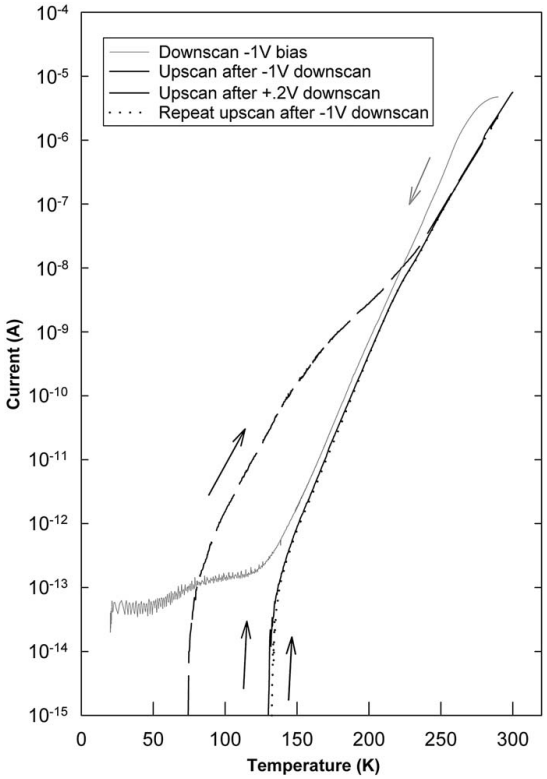

Fig. 2. Cooling under forward and reverse bias and its effect on Current–temperature measurements of ICP etched Ge.

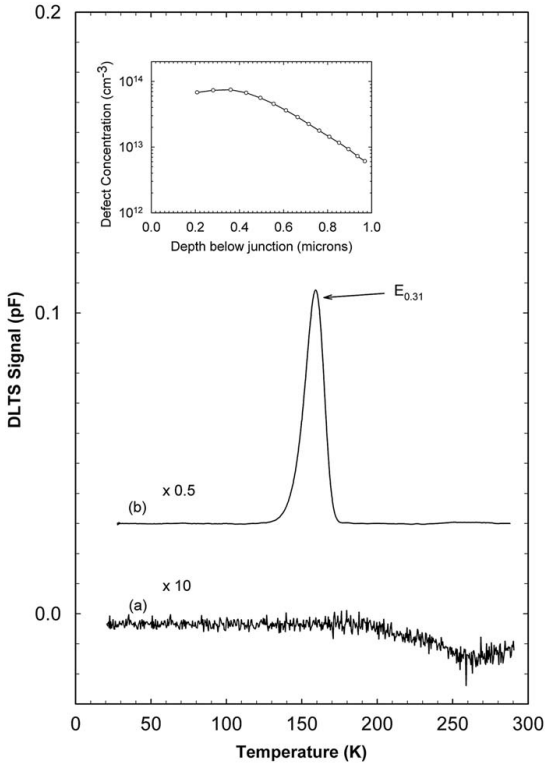

Fig. 3. DLTS electron trap spectra of resistively evaporated Pd SBD's where (a) is the control sample and (b) was ICP cleaned for 10 min. Spectra were recorded using a rate window of 80 s^{-1} and a quiescent reverse bias of 1 V with a superimposed 1.2 V filling pulse, V_p. Inset: Electron defect ($E_{0.31}$) concentration below the junction of the ICP cleaned sample.

magnitude higher at 100 K, yet measured a lower reverse bias current at room temperature than the ICP treated diode. In Fig. 1 an ICP cleaned EB deposited diode was compared to a diode that was degreased but did not undergo ICP cleaning. Room temperature *IV* measurements (Fig. 1(a) and (b)) indicate that the ICP cleaned diode performed slightly worse under reverse bias but then had a steeper and more ideal *IV* curve under forward bias. In Fig. 1(c) and (d), the *IV* measurement was performed at 100 K where a difference of up to six orders of magnitude in the reverse bias characteristics of these diodes can be observed, indicating the superiority of the ICP cleaned diode under reverse and forward bias. Fig. 1(d) also displays evidence of RG effects during forward bias below 0.3 V suggesting the presence of damage-induced electron or hole traps in the unetched EBD sample. Thus, while reverse bias current at room temperature is a good indicator of diode "quality", this measurement cannot be used exclusively for diode selection. Ge etched by ourselves in a RF sputter system at 1 keV was badly damaged and the contacts were ohmic thus not useful as a comparison. The Au SD diode included in Table 1 was not etched directly in the Ar plasma but still sustained damage during the deposition as measured by the high ideality factor.

The linearity of *IT* measurements (Fig. 2) of the 3 min ICP etched EBD diode further illustrates superior diode performance. The 1 V reverse bias plot that was taken while the diode was being cooled from 300 to 20 K (downscan) is not only linear but also very similar to the plot taken while heating the diode from 20 to 300 K (upscan) at a scan rate of 5 K per minute, similar to the downscan rate. The diode was then subjected to another cycle of cooling with a 0.2 V forward bias applied followed by an upscan at −1 V bias. A significant deviation from the previous ideal behaviour was observed and the increase in current from 70 to 240 K is evidence of recombination/generation effects, since empirically the current, J, is proportional to $\exp(-qV/2kT)$ if the recombination current dominates and is proportional to $\exp(-qV/kT)$ if the diffusion current dominates [13]. Cooling under forward bias filled the traps which then released electrons as the sample was heated. Cooling the diode again under reverse bias of 1 V fully restored the device and the upscan that followed was indistinguishable from the initial upscan.

DLTS measurements of this diode confirmed that this defect was indeed an electron trap with energy of 0.31 eV below the conduction band and a distribution of at least 1 μm into the Ge (Fig. 3). No hole traps were observed. SRIM predicted Ar^+ events that were more than three hundred times shallower than the distribution observed and this suggests that this defect may be mobile at room temperature. Defects that have previously been observed by DLTS in EBD Pd SBDs were absent in all ICP treated samples and warrants further investigation.

4. Conclusions

ICP is a suitable cleaning procedure for germanium that introduced defects but had no adverse effect on diode quality. ICP cleaned Ge exhibits excellent low temperature *IV* characteristics with good recovery properties. SRIM simulations suggest that the ICP introduced defect should not be as deep into the material as observed, unless it is mobile at room temperature. The absence of other measurable EBD-induced defects may indicate that ICP etching traps these defects at the Ge surface and bears further investigation.

Acknowledgement

The authors gratefully acknowledge the financial support of the South African National Research Foundation.

References

[1] E.E. Haller, Mater. Sci. Semicond. Process. 9 (2006) 408.
[2] S.J. Pearton, D.P. Norton, Plasma Process. Polym. 2 (2005) 16.
[3] R.W. Boswell, A.J. Perry, M. Emami, J. Vac. Sci. Technol. A 7 (6) (1989) 3345.
[4] R.J. Shul, G.B. McClellan, R.D. Briggs, D.J. Rieger, S.J. Pearton, C.R. Abernathy, J.W. Lee, C. Constantine, C. Barratt, J. Vac. Sci. Technol. A 15 (3) (1997) 633.
[5] J.W. Lee, C.R. Abernathy, S.J. Pearton, F. Ren, W.S. Hobson, C. Constantine, C. Barratt, J. Electrochem. Soc. 144 (4) (1997) 1417.
[6] S.J. Pearton, Appl. Surf. Sci. 117/118 (1997) 597.
[7] F.D. Auret, W.E. Meyer, S. Coelho, M. Hayes, Appl. Phys. Lett. 88 (2006) 242110.
[8] J.D. Waldrop, Appl. Phys. Lett. 44 (1984) 1002.
[9] F.D. Auret, W.E. Meyer, S. Coelho, M. Hayes, Appl. Phys. Lett. 88 (2006) 242110.
[10] T. Sugiyama, T. Matsuura, J. Murota, Appl. Surf. Sci. 112 (1997) 187.
[11] J.D. Waldrop, Appl. Phys. Lett. 44 (1984) 1002.
[12] E.H. Rhoderick, R.H. Williams, Metal-Semiconductor Contacts, Clarendon Press, Oxford, 1988.
[13] S.M. Sze, K.K. Ng, Physics of Semiconductor Devices, Wiley, New York, 2007.

Thin Solid Films 518 (2010) 2485–2488

Contents lists available at ScienceDirect

Thin Solid Films

journal homepage: www.elsevier.com/locate/tsf

Defect introduction in Ge during inductively coupled plasma etching and Schottky barrier diode fabrication processes

F.D. Auret *, S.M.M. Coelho, G. Myburg, P.J. Janse van Rensburg, W.E. Meyer

Department of Physics, University of Pretoria, Lynnwood Road, Pretoria 0002, South Africa

ARTICLE INFO

Available online 13 October 2009

Keywords:
Germanium
Schottky diode fabrication
Defects
DLTS
ICP etching

ABSTRACT

We have etched Sb-doped n-type (111) oriented Ge by inductively coupled plasma (ICP), using argon, and subsequently studied the defects that this process introduced as well as the effect of this etching on Schottky barrier diode quality. Deep level transient spectroscopy (DLTS) revealed that ICP etching introduced only one prominent defect, $EP_{0.31}$, in Ge with a level at 0.31 eV below the conduction band. The properties of this defect are different to those of defects introduced by other particle-related processing steps, e.g. sputter deposition and electron beam deposition, that each introduces a different set of defects. DLTS depth profiling revealed the $EP_{0.31}$ concentration was a maximum (3.6×10^{13} cm^{-3}) close to the Ge surface and then it decreased more or less exponentially into the Ge. Annealing at 250 °C reduced the $EP_{0.31}$ concentration to below the DLTS detection limit. Finally, current–voltage (I–V) measurements as a function of temperature revealed that the quality of Schottky contacts fabricated on the ICP-etched surfaces was excellent at −100 K the reverse leakage current at −1 V was below 10^{13} A (the detection limit of our I–V instrumentation).

1. Introduction

The low effective mass of holes in Ge has opened up the possibility of using Ge in ultra-fast complimentary metal–oxide–semiconductor devices [1]. This, in turn, has sparked renewed interest in the properties of defects in Ge because defects play an important role in the performance of devices. In recent studies the properties of the defects introduced during high-energy gamma-, electron- and proton irradiation of Ge were reported [2–5]. We have reported the properties of defects introduced in Ge during electron beam deposition of various metals [6–8] and sputter deposition of Au [9]. However, no investigation regarding the defects introduced in Ge during surface cleaning processes, e.g. sputter and plasma etching, has been reported yet. These investigations are important because it is well known that the low-energy ions utilized in these processes introduce defects at and close to the metal–semiconductor junction [10]. These defects influence device performance and alter the barrier heights of the contacts [6–9]. The defects responsible for these barrier adjustments are formed when energetic particles strike the semiconductor surface and interact with the semiconductor.

In this study we report the electronic properties of defects introduced in n-type Ge during low-energy (±80 eV) inductively coupled plasma (ICP) etching using Ar. We show that this process introduces only one prominent electron trap with an energy level at $E_C-0.31$ eV. We also show that the properties of this defect are different to those of defects introduced during electron beam deposition and sputter deposition of metals on Ge, and by high-energy electron irradiation of Ge. It is noteworthy that no defects involving single vacancies and interstitials were introduced by ICP etching. We also demonstrate that the quality of Schottky contacts fabricated on Ge etched by ICP is excellent.

2. Experimental procedure

For this experiment, we have used bulk-grown (111) n-type Ge, doped with Sb to a level of 2.5×10^{15} cm^{-3}. For ohmic contact formation the samples were first degreased and then etched in a mixture of H_2O_2:H_2O (1:5, 30% H_2O_2) for 1 min. Directly after cleaning they were inserted into a vacuum chamber where AuSb (0.6 % Sb) was resistively deposited on their back surfaces. The samples were then annealed at 350 °C in Ar for 10 min to obtain low resistivity ohmic contacts. Following this, the samples to be used for fabrication of Schottky barrier diodes by resistive, electron beam and sputter deposition were once again etched and then Schottky contacts were deposited by the various methods. On the first ("control") sample Pd Schottky contacts, 0.60 mm in diameter and 100 nm thick, were deposited by resistive evaporation. It is well known that resistive evaporation does not introduce any defects in semiconductors. The second sample was just degreased, but not chemically etched, before etching it using ICP (Ar) for 10 min. Subsequently, Pd contacts were deposited on it using resistive evaporation. On the third sample Pd Schottky contacts were deposited by electron beam deposition (EBD) [6–8]. On the fourth sample Au Schottky contacts were deposited by

* Corresponding author. Tel.: +27 12 420 2684; fax: +27 12 362 5288.
E-mail address: danie.auret@up.ac.za (F.D. Auret).

0040-6090/$ – see front matter © 2009 Elsevier B.V. All rights reserved.
doi:10.1016/j.tsf.2009.09.130

sputter deposition (SD) [9]. The last sample had resistively deposited Pd Schottky contacts and was irradiated with high-energy electrons from a Sr^{90} radio-nuclide source [6]. Conventional deep level transient spectroscopy (DLTS) and high-resolution (Laplace) DLTS [10,11] were used to study the defects introduced in the Ge during the ICP etch and metallization processes, while current–voltage (I–V) measurements as a function of temperature (I–V–T) were used to evaluate the effect of the defects on the quality of the Schottky contacts.

3. Results and discussion

In Fig. 1 we depict the DLTS spectra of the control sample (curve (a)), for a sample with Pd contacts deposited by resistive evaporation after 10 minute ICP etching (curve (b)), a sample on which Pd contacts were deposited by electron beam deposition (EBD), without ICP, (curve (c)) [8], a sample on which Au contacts were deposited by sputter deposition (curve (d)) [9] and a sample that had been irradiated with high-energy electrons from a Sr^{90} radio-nuclide source (curve (e)) [6]. These results are representative of the results obtained for several identical experiments involving EBD, ICP and sputter deposition.

Curve (a) clearly indicates that this Ge does not contain electron traps in measurable concentrations. From curve (b) we note that ICP etching introduced only one prominent defect, $EP_{0.31}$. Its properties are listed in Table 1. In the nomenclature used here and below "E" and "H" mean electron and hole traps, respectively, "P" means the defect was introduced by the *plasma*, and the subscripts are the activation energies determined from the Arrhenius plots in Fig. 2. DLTS spectra recorded under hole injection conditions revealed that no hole traps were present in the sample that was ICP etched. Furthermore, it is instructive to note that no V–Sb centers (E-centers) or interstitial related defects [2,3] are introduced during the plasma etching of Ge. This may imply that no single vacancies or interstitials were created at and below the Ge surface that could diffuse into the Ge to form the V–Sb center. Alternatively, vacancies or interstitials were introduced at and near the surface but their migration into the Ge was impeded.

Next we discuss the defects introduced by metallization processes and high-energy electron irradiation. The traps introduced in the Ge during EBD of Pd contacts (no ICP etching) are shown by curve (c). The two main traps are an electron trap, $EE_{0.38}$, and a hole trap, $HE_{0.30}$. Here the "E" in $EE_{0.38}$ and $HE_{0.30}$ means the defects were introduced by

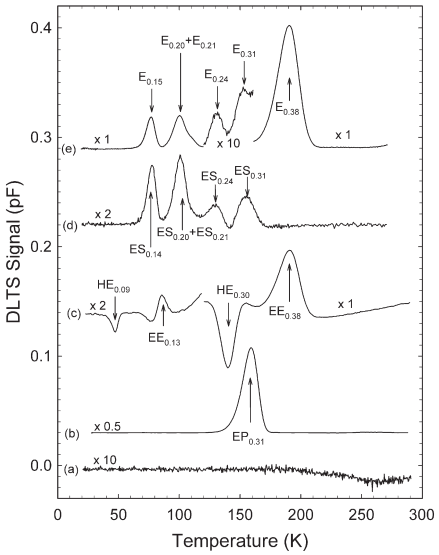

Fig. 1. DLTS spectra of resistively deposited (control) Pd Schottky contacts to n-Ge (curve (a)), resistively deposited Pd Schottky contacts on ICP-etched Ge (curve (b)), Pd Schottky contacts deposited by EBD (curve (c)), sputter-deposited Au contacts on Ge (curve (d)) and high energy electron irradiated Ge with resistively deposited Pd contacts (curve (e)). All spectra were recorded using a rate window of 80 s^{-1} at a quiescent reverse bias of −1 V and a filling pulse, V_p, that was 0.15 V into forward bias and of 1 ms duration.

electron beam deposition. These two levels have been shown to be the (−−/−) and (−/0) charge states, respectively, of the V–Sb in Sb-doped Ge [2,3] and have also previously been observed after EBD of Schottky contacts onto Ge [6–8]. The concentration of the V–Sb introduced by EBD has been shown to depend on the electrical current of the electron beam gun during deposition, which in turn depends on the melting point of the metal being deposited [8]. The higher the melting point, the higher the current and hence the higher the V–Sb concentration. Evidently, the EBD process introduces vacancies in the

Table 1
Electronic properties of prominent defects introduced in n-type Ge during metallization and etching processes, and by MeV electron irradiation.

Sputter deposition				MeV electron irradiation				Similar defects/defect ID
Defect	E_T (eV) (± 0.01)	σ_a (cm^2) (±10%)	T_{peak}[a](K)	Defect	E_T (eV)	σ_a (cm^2)	T_{peak}[a] (K)	
$ES_{0.14}$	$E_C-0.14$	5.5×10^{-15}	78	$E_{0.15}$	$E_C-0.15$	2.8×10^{-14}	77	$E_{0.13}$[b], Sb and I related[c]
$ES_{0.20}$	$E_C-0.20$	3.7×10^{-14}	100	$E_{0.20}$	$E_C-0.20$	1.4×10^{-14}	100	$E_{0.19}$[c], Sb and I related[c]
$ES_{0.21}$	$E_C-0.21$	2.0×10^{-14}	109	$E_{0.21}$	$E_C-0.21$	3.6×10^{-14}	109	$E_{0.21}$[c], Sb related?[c]
$ES_{0.24}$	$E_C-0.24$	3.3×10^{-15}	131	$E_{0.24}$	$E_C-0.24$	2.5×10^{-15}	131	$E_{0.23}$[c], Sb and I related?[c]
$ES_{0.31}$	$E_C-0.31$	1.5×10^{-14}	151	$E_{0.31}$	$E_C-0.31$	5.0×10^{-14}	150	$E_{0.29}$[c]?, V_2[c]?
ICP etching (Ar)								
$EP_{0.31}$	$E_C-0.31$	1.3×10^{-14}	156					
Electron beam deposition								
$EE_{0.10}$	$E_C-0.10$	3.7×10^{-16}	65					
$EE_{0.13}$	$E_C-0.13$	1.9×10^{-16}	85					Ref. [6]
$EE_{0.23}$	$E_C-0.23$	3.4×10^{-14}	116					Ref. [6]
$EE_{0.38}$	$E_C-0.38$	1.0×10^{-14}	191	$E_{0.38}$	$E_C-0.38$	1.1×10^{-14}	191	$E_{0.377}$[b], $E_{0.37}$[c], V–Sb (−−/−)[b,c]
$HE_{0.09}$	$E_V+0.09$	2.1×10^{-13}	47					
$HE_{0.15}$	$E_V+0.15$	7.1×10^{-14}	82					Ref. [6]
$HE_{0.18}$	$E_V+0.18$	3.5×10^{-14}	97					Ref. [6]
$HE_{0.27}$	$E_V+0.27$	2.4×10^{-13}	133					Ref. [6]
$HE_{0.30}$	$E_V+0.30$	6.2×10^{-13}	141	$H_{0.30}$	$E_V+0.30$	3.66×10^{-13}	142	$H_{0.307}$[b], $H_{0.30}$[c], V–Sb (−/0) [b]

The error margins in the value of E_T lie in the third digit after the decimal point whereas that for σ is typically less than 10% of its value.
[a] Peak temperature at a rate window of 80 s^{-1}.
[b] See Ref. [3].
[c] See Ref. [2].

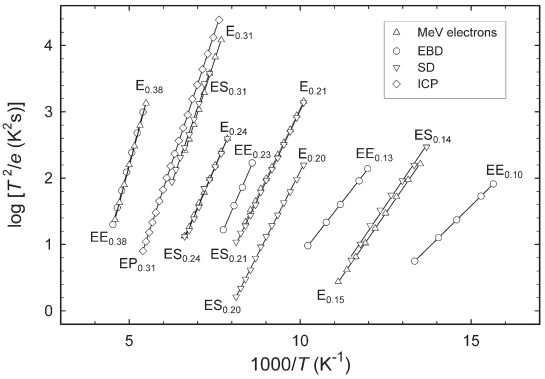

Fig. 2. Arrhenius plots of electron traps introduced in n-type Ge by: plasma etching (diamonds), electron beam deposition (circles), sputter deposition (down triangles), and high energy electron irradiation (up triangles).

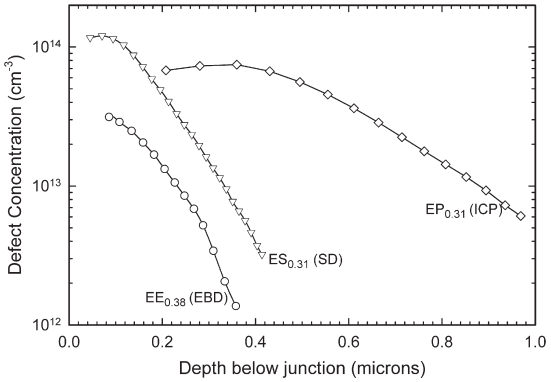

Fig. 3. DLTS depth profiles for the $EP_{0.31}$ defect by plasma etching followed by resistive deposition of Pd (diamonds), E-center ($E_{0.38}$) introduced by electron beam deposition (circles), and the $ES_{0.31}$ defect introduced by sputter deposition of Au contacts on Ge (down triangles).

Ge, at and close to the interface, that migrate and combine with, among others, Sb atoms to form Sb–V pairs. These vacancies have been proposed to be the result of energetic particles that originate in the region of the filament and then impinge on the semiconductor [12]. EBD also introduces the defects $EE_{0.13}$ and $HE_{0.09}$ [8] and sometimes $EE_{0.10}$ [6]. As in the case of the V–Sb defect, the presence and concentration of these minor defects also depend on the EBD conditions and the metal deposited. Whereas the nature of $EE_{0.10}$ and $EE_{0.13}$ is not known, the $HE_{0.09}$ has been shown to be the third charge state (+/0) of the V–Sb center [13].

The DLTS spectrum curve (d) in Fig. 1 shows that rf sputter deposition of Au introduced several electron traps: $ES_{0.14}$, $ES_{0.20}$, $ES_{0.21}$, $ES_{0.24}$ and $ES_{0.31}$ [9]. This sputter deposition did not introduce the V–Sb center. Ideally, this experiment should have been performed by deposition of Pd, but such a target was not available at the time of the experiment. The electronic properties of these defects are summarised in Table 1. The peaks of $ES_{0.20}$ and $ES_{0.21}$ could only be clearly resolved after using high-resolution Laplace DLTS [10,11]. Unlike in the case of high-energy electron irradiated Ge and electron beam deposited (EBD) Schottky diodes [8], we could not detect any hole traps in the sputter-deposited contacts studied here, even when applying a strong forward bias. After irradiating the sputter-deposited contacts with MeV electrons the hole traps typical of electron irradiation (e.g. $H_{0.30}$) could be observed. This means that sputter deposition by itself does not introduce any hole traps in detectable concentrations, nor do the sputter-deposited Schottky contacts impede the detection of hole traps.

In Fig. 1 we also compare the DLTS spectra of process-induced defects discussed above to that of Ge that had been irradiated with high-energy electrons [curve (e)] [8]. This comparison, in conjunction with the Arrhenius plots in Fig. 2, reveals that none of the defects introduced by EBD, except the E-center, is present after high-energy electron irradiation. The $EP_{0.31}$ defect introduced by ICP etching was not observed in samples that had contacts deposited by EBD and SD, neither was it observed after high-energy electron irradiation. Although an $E_{0.31}$ defect was observed after SD and electron irradiation, its capture cross-section is significantly different from that of the $EP_{0.31}$ defect introduced by ICP (Fig. 2 and Table 1). Interestingly, except for the V–Sb center, sputter deposition introduces the same prominent electron traps as high energy electron irradiation (Fig. 2 and Table 1), which have been shown to be related to the presence of Sb or Sb together with the Ge self-interstitial [2].

We have used the fixed-bias variable pulse DLTS method to obtain the spatial distribution of the process-induced defects into the Ge. From Fig. 3 we see that the $EP_{0.31}$ defect introduced by ICP etching is distributed much deeper (at least up to 1 μm) into the Ge than the $ES_{0.31}$ defect introduced by sputter deposition and the $EE_{0.38}$ introduced by EBD. Since these defects are physically different, we propose that these differences in their depth distributions are caused by different diffusivities.

Isochronal annealing (10 min periods, 25 K intervals) was formed to establish the thermal stability of the ICP induced $E_{0.31}$ defect. The DLTS measurements showed that the $EP_{0.31}$ concentration profile remained constant up to 350 K. Upon annealing at higher temperatures its concentration profile broadened with increasing annealing temperature. This indicates that the $EP_{0.31}$ defect anneals by diffusion. After annealing at 450 K the distribution became more or less uniform in the region profiled. Annealing at higher temperatures lowered the concentration until, after annealing at 525 K, it could not be observed anymore. At the moment it is not yet clear if this last step in the annealing is a decomposition of the $EP_{0.31}$ defect, or whether $EP_{0.31}$ simply diffuses out of the sample. By comparison, we have found that the E-center introduced by EBD in the same material annealed out at 500 K [8] and the $ES_{0.31}$ level in sputter-deposited Schottky contacts annealed out at 525 K [9]. For device fabrication it is important to remember that the process-induced defects can be removed by thermal annealing in order to optimise the characteristics of the specific device type.

Finally, we illustrate the effect of process-induced defects on the quality of the Schottky contacts. Fig. 4 depicts the *I–V* characteristics of Schottky contacts at 300 K as well as at 100 K. At 300 K it is difficult to clearly observe the effect of the defects on the *I–V* characteristics. However, at 100 K these differences are amplified and can clearly be seen. Typically, all eight diodes on each sample are evaluated at room temperature. Then the best diode is characterised at low temperatures. From Fig. 4 we see that at 300 K the reverse currents of the SD contacts at −1 V are the highest and that of the resistively deposited contacts is the lowest. At 100 K, however a different picture emerges. The sputter-deposited contacts are still the poorest with reverse currents of above 10^{-9} A. The contacts deposited by EBD are better with reverse currents of just above 10^{-11} A. Surprisingly, the reverse leakage currents of the contacts deposited on Ge that had been ICP etched is slightly lower (below 10^{-13} A) than of those deposited by resistive evaporation (about 10^{-13} A). This is despite the facts that the Ge surface has been damaged during plasma etching and that the ICP-etched Ge contains the deep level defect, $EP_{0.31}$. Note that the fact that we used Au for sputter deposition and Pd for the ICP-etched and resistively deposited

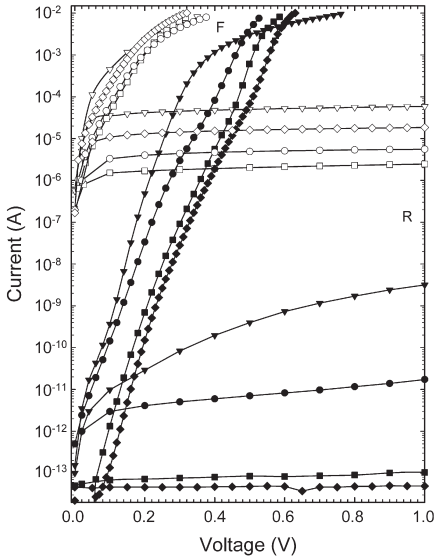

Fig. 4. *I–V* characteristics of Schottky contacts at 300 K (empty symbols) and at 100 K (filled symbols): resistive evaporation of Pd (squares), ICP-etched Ge followed by resistive evaporation of Pd (diamonds), electron beam deposition of Pd (up triangles) and sputter deposition of Au (down triangles). "F" and "R" in the graph indicate the forward and reverse branches if the *I–V* characteristics.

samples will not influence the observation that sputtering results in poorer diodes, i.e. lower barrier heights, than ICP etching or resistive evaporation. The reason for this is that the work function of Au is very similar to that of Pd (both about 5.1 eV).

4. Conclusions

Inductively coupled plasma (ICP) Ar etching of Ge introduced only one prominent defect, the $EP_{0.31}$ electron trap. This defect is different from any other defect that had been introduced in Ge by metallization processes such as electron beam deposition and sputter deposition, and the defects introduced by high-energy electron irradiation. This implies that ICP etching does not introduce any single vacancies or single self-interstitials. SRIM simulations predicted that 80 eV Ar ions will deposit 60 eV/nm/ion. This large amount of energy deposited per unit length makes it possible that an Ar ion may directly form defects like divacancies or di-interstitial during a single damage event. The divacancy has not been observed in particle-irradiated Ge [15]. It usually forms when two migrating single vacancies, formed during irradiation, meet and combine. However, it has been shown theoretically that the single vacancy in Ge is negatively charged [14] and it was also detected by DLTS as V (−−/−) [15]. Single Ge vacancies will therefore not combine with another vacancy to form the divacancy [16]. However, with sufficient energy available, as in the case of ICP etching, defects like the divacancy and di-interstitial can be formed directly. It is therefore conceivable that $EP_{0.31}$ could be the divacancy or di-interstitial, which have not clearly been observed in Ge yet. The activation enthalpy of 0.31 eV is slightly less than what is predicted for the divacancy from an *ab initio* density functional study [16].

It is also instructive to note that sputter deposition of Au and electron beam deposition of Pd each introduce a different set of defects in Ge. None of the defects introduced by sputter deposition has the same DLTS signature as any defect introduced by electron beam deposition, and vice versa. This may be due to the fact that sputter deposition of Au introduces defects due to the collision of heavy Au ions that may inject mainly self-interstitial defects in Ge, as is common for an ion towards the end of its range. During electron beam deposition, on the other hand, defects are created by lighter ions accelerated from the region near the electron beam filament and these particles create vacancies at and near the Ge surface that diffuse into the Ge to form vacancy-related defects, e.g. the V–Sb pair, as observed here.

Finally, and most importantly for device fabrication, ICP etching of Ge does not in any way lead to inferior Schottky diodes as has been reported for sputter deposition and electron beam deposition. In fact, we have shown here that the low temperature (100 K) *I–V* characteristics of ICP-etched Ge with resistively deposited Pd Schottky contacts are slightly better than those of resistively deposited Pd contacts where the Ge had been cleaned by conventional wet chemical etching before Schottky contact deposition.

Acknowledgements

The authors gratefully acknowledge financial support of the South African National Research Foundation. The Laplace DLTS software and hardware used in the research was kindly provided by A. R. Peaker (Centre for Electronic Materials Devices and Nanostructures, University of Manchester) and L. Dobaczewski (Institute of Physics, Polish Academy of Sciences).

References

[1] R. Hull, J.C. Bean (Eds.), Germanium Silicon: Physics and Materials, Semiconductors and Semimetals, vol. 56, Academic Press, San Diego, 1999.
[2] J. Fage-Pedersen, A. Nylandsted Larsen, A. Mesli, Phys. Rev. B 62 (10) (2000) 116.
[3] V.P. Markevich, A.R. Peaker, V.V. Litvinov, V.V. Emstev, L.I. Murin, J. Appl. Phys. 95 (2004) 4078.
[4] V.P. Markevich, I.D. Hawkins, A.R. Peaker, K.V. Emstev, V.V. Emstev, V.V. Litvinov, L. Dobaczewski, Phys. Rev. B 70 (2004) 235213.
[5] V.P. Markevich, I.D. Hawkins, A.R. Peaker, V.V. Litvinov, L. Dobaczewski, J.L. Lindström, Appl. Phys. Lett. 81 (2002) 1821.
[6] F.D. Auret, W.E. Meyer, S. Coelho, M. Hayes, Appl. Phys. Lett. 88 (2006) 242110.
[7] F.D. Auret, W.E. Meyer, S. Coelho, M. Hayes, J.M. Nel, Mater. Sci. Semicond. Process. 9 (2006) 576.
[8] F.D. Auret, S.M.M. Coelho, M. Hayes, W.E. Meyer, J.M. Nel, Phys. Status Solidi, (A) 205 (2008) 159.
[9] F.D. Auret, S. Coelho, W.E. Meyer, C. Nyamhere, M. Hayes, J.M. Nel, J. Electron. Mater. 36 (2007) 1604.
[10] L. Dobaczewski, P. Kaczor, I.D. Hawkins, A.R. Peaker, J. Appl. Phys. 76 (1994) 194.
[11] L. Dobaczewski, A.R. Peaker, K. Bonde Nielsen, J. Appl. Phys. 96 (2004) 4689.
[12] C. Christensen, J.W. Petersen, A. Nylandsted Larsen, Appl. Phys. Lett. 61 (1992) 1426.
[13] C.E. Lindberg, J. Lundsgaard Hansen, P. Bomholt, A. Mesli, K. Bonde Nielsen, A. Nylandsted Larsen, Appl. Phys. Lett. 87 (2005) 172103.
[14] J. Coutinho, R. Jones, V.J.B. Torres, M. Barroso1, S. Öberg, P.R. Briddon, J. Phys.: Condens. Matter 17 (2005) L521.
[15] A. Mesli, L. Dobaczewski, K. Bonde Nielsen, Vl. Kolkovsky, M. Christian Petersen, A. Nylandsted Larsen, Phys. Rev. B 78 (2008) 165202.
[16] J. Coutinho, V.J.B. Torres, S. Öberg, P.R. Briddon, Appl. Phys. Lett. 88 (2006) 091919.

Physica B ■ (■■■■) ■■■–■■■

Contents lists available at ScienceDirect

Physica B

journal homepage: www.elsevier.com/locate/physb

Unexpected properties of the inductively coupled plasma induced defect in germanium

S.M.M. Coelho *, F.D. Auret, P.J. Janse van Rensburg, J.M. Nel

Department of Physics, University of Pretoria, Private Bag X20, Hatfield 0028, South Africa

ARTICLE INFO

Article history:
Received 28 August 2013
Accepted 31 October 2013

Keywords:
Germanium
DLTS
Defect
Anneal
Diffusion

ABSTRACT

Inductively coupled plasma (ICP) etching of germanium introduces a single defect, the $E_{0.31}$ electron trap, for a large range of argon partial pressures from 4×10^{-3} to 6.5×10^{-4} mbar that correspond to ion energies of 8 to 60 eV. Ge of three crystallographic orientations, (1 0 0), (1 1 0) and (1 1 1), treated with 20 and 60 eV ICP had defect concentration profiles that were similar in appearance, with a maximum concentration of 10^{14} cm^{-3} extending more than a μm into the material, approximately three orders of magnitude deeper than what TRIM simulations predicted. All profiles were measured using Laplace deep level transient spectroscopy (L-DLTS), a technique that is sensitive to defect concentrations as low as 10^{11} cm^{-3}. Isochronal annealing of samples showed concentration curves broadening after a 400 K anneal and decreasing to the 10^{13} cm^{-3} level after a 450 K anneal. Unannealed samples measured after a year exhibited similar decreases in defect concentration without broadening of their profiles. A 550 K anneal lowered the defect concentration to levels below the L-DLTS detection limit. Thereafter additional plasma treatment of the surface failed to reintroduce this defect indicating that the structure required for the formation of $E_{0.31}$ was no longer present in the region under observation.

1. Introduction

Germanium was the semiconductor used to demonstrate the first transistor and continues to show promise as a suitable candidate to use in ultra-fast devices. It remains the best material for gamma ray detectors and far infrared detectors [1]. Process induced defects are unfortunately introduced during device manufacture; such defects either improve device performance [2] or, as in the case of photo-voltaics, impair their function [3]. Sputter etching is a key technology in the manufacture of semiconductor devices with RF sputter etching and deposition being the most popular in this industry as large wafers can be processed uniformly [4]. With low energy ions producing low ion damage [4,5], high plasma density and the availability of large area sources, inductively coupled plasma (ICP) etching may in future displace capacitively coupled RF plasma sources as the technology of choice to etch large wafers.

Argon ICP etching introduces only one defect in Ge [6], $E_{0.31}$, with an energy level $E_c-0.31$ eV and an apparent capture cross-section of 3.5×10^{-14} cm^2. This defect has not been observed after MeV electron irradiation [7,8], alpha particle irradiation [9], sputter deposition [10] or electron beam deposition [11] but was observed after dc-hydrogen plasma passivation [12]. Comparing DLTS spectra, the $E_{0.31}$ defect reported on in sputter deposition [10] exhibits a peak at 150 K at a rate window of 80 s^{-1} whereas the ICP induced defect has a peak at 157 K. The Arrhenius plots of these two defects further confirmed that they are different defects. The inertness of argon and the low energy of the ICP Ar ions (measured by the source manufacturer using a Faraday cup) make it unlikely that $E_{0.31}$ would be introduced during high energy processes where conditions are very different. The reproducible introduction of a single defect provides the ideal platform to study the effect of this defect on the properties of a well-known semiconductor. Our focus for this work was to observe the introduction of $E_{0.31}$ in ultra-pure n-type Ge crystals with crystallographic orientations (1 0 0), (1 1 0) and (1 1 1), all bulk grown by Umicore but with differing Sb concentrations of 9×10^{14}, 2.3×10^{14} and 1.3×10^{15} cm^{-3}, respectively. Samples, one of each crystallographic orientation, were processed simultaneously and thereafter Laplace deep level transient spectroscopy (L-DLTS) [13] was used to obtain the defect concentration profiles of $E_{0.31}$ in our samples.

2. Experimental procedure

Electronic grade polished Ge wafers with carbon and oxygen impurity concentrations lower than 10^{16} cm^{-3} (measured using SIMS) of three crystallographic orientations, (1 0 0), (1 1 0) and (1 1 1), were diced into 3×5 mm pieces. These were subsequently

* Corresponding author.
E-mail addresses: sergio@up.ac.za, sercoe@hotmail.com (S.M.M. Coelho).

0921-4526/$ - see front matter © 2013 Elsevier B.V. All rights reserved.
http://dx.doi.org/10.1016/j.physb.2013.10.061

degreased in successive 5 min ultrasonic baths of trichloroethylene, isopropanol and methanol followed by a 1 min etch in 1:5, H_2O_2: H_2O. AuSb (0.6% Sb) was evaporated resistively onto the back surface of all the samples and annealed at 625 K for 10 min in Ar to lower the resistance of these contacts thus making them ohmic. The same wet cleaning procedure was followed prior to loading one sample of each crystallographic orientation into the vacuum chamber for ICP etching using a Copra 160 source from CCR Technology. This source produces an ion energy distribution curve with two narrow peaks with a full width half maximum that is less than 1/3 of the maximum energy. The quoted values herein are for the high energy peaks. The ICP system chamber was pumped down to 1×10^{-6} mbar before being backfilled with Ar up to a partial pressure of 6.5×10^{-4} mbar or 1×10^{-3} mbar for the 3 min or 10 min ICP treatments respectively at 550 W plasma power and 1.5 A coil current. Plasma etching was followed by resistive evaporation (RE) of a 25 nm thick Pd layer through a stainless steel contact mask thus forming eight Schottky barrier diodes 0.6 mm in diameter on the front surface of each sample. RE is known to not introduce defects in quantities measurable by DLTS but diodes prepared by electron beam deposition (EBD) after ICP would also be suitable as no additional defects were observed in such samples.

Current–voltage (*IV*) and capacitance–voltage (*CV*) measurements were performed at room temperature to establish the ideality factor, reverse bias current at 1 V, carrier concentration and built-in voltage V_{bi} of the diodes. Only diodes with an ideality below 1.2 and a reverse bias current below 3×10^2 A cm^{-2} were considered suitable for further investigation. Applying conventional DLTS confirmed that $E_{0.31}$ was introduced and thereafter L-DLTS was used to determine the peak amplitude at a fixed temperature while varying the filling pulse from 0.1 V to 5 V. In Fig. 1 the DLTS peak amplitudes can be converted to concentration of deep levels, N_T, as $(N_T/N_D) \cong (2\Delta C/C)$ where N_D is the

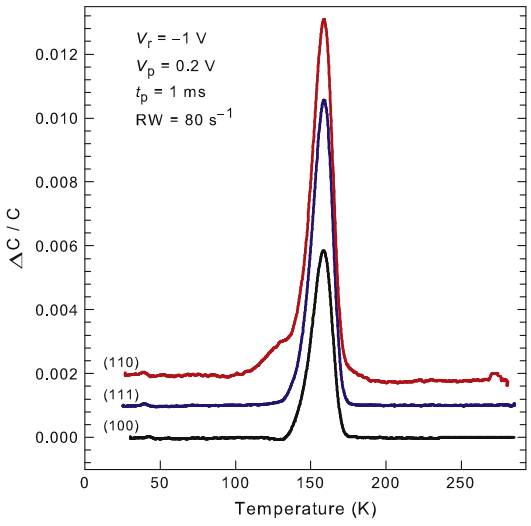

Fig. 1. DLTS spectra of resistively evaporated Pd diodes on ICP etched Ge (1,0,0), (1,1,0) and (1,1,1). The three samples were co-processed and received 3 min of ICP etching. Spectra were recorded at a rate window of 80 s^{-1}, pulse width of 1 ms, quiescent reverse bias of −1 V and a filling pulse with an amplitude of 1.2 V. To distinguish between spectra the (1 1 1) and the (1 1 0) plots have been offset by 0.001 and 0.002 along the *y*-axis, respectively. Some measurements exhibit higher background noise but this did not influence the results.

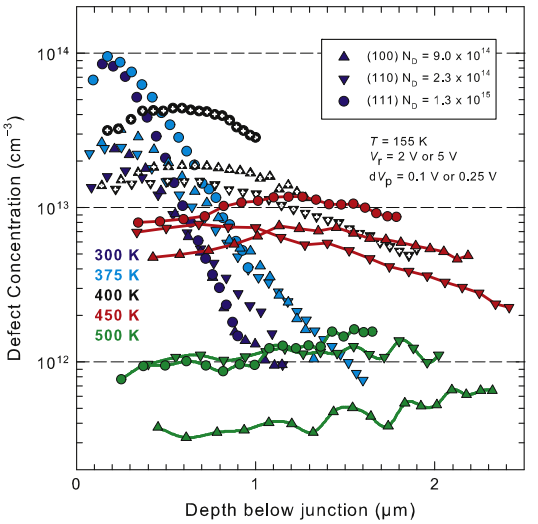

Fig. 2. Depth profiles of the ICP induced $E_{0.31}$ defect in Ge (1,0,0), (1,1,0) and (1,1,1) recorded directly after 3 min ICP etching at an Ar partial pressure of 7×10^{-4} mbar and diode fabrication with subsequent measurements taken after 10 min isochronal annealing at 375 K, 400 K, 450 K and 500 K, respectively. Peak amplitudes for pulses varying from 0.1 V to 2 V or 5 V were determined using L-DLTS.

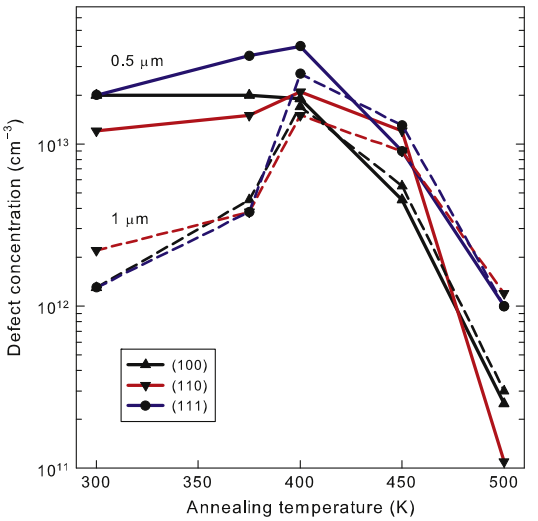

Fig. 3. A summary of Fig. 2, plotting defect concentration versus annealing temperature at 0.5 μm and 1 μm below the metal–semiconductor interface, respectively.

concentration of shallow impurities, ΔC is the DLTS peak height and C is the junction capacitance. To calculate the defect concentrations plotted in Figs. 2–4 the approach of Zohta and Watanabe was used [14].

Samples were isochronally annealed for 10 min at 375 K, 400 K, 450 K, 500 K and 550 K in an Ar ambient and measured (*IV* and *CV*) after each annealing cycle. Long-term study samples were kept at room temperature (RT) between measurements.

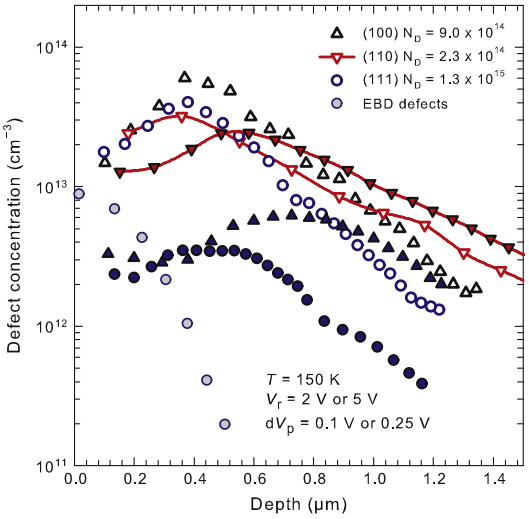

Fig. 4. Depth profiles of the $E_{0.31}$ defect in Ge (1,0,0), (1,1,0) and (1,1,1) recorded directly after a 10 min ICP etch at an Ar partial pressure of 10^{-3} mbar and diode fabrication (hollow symbols). The co-processed samples were kept at room temperature and measured again after one year (solid symbols). Peak amplitudes for pulses varying from 0.1 V to 2 V or 5 V were determined using L-DLTS. The total concentration of EBD induced electron traps recorded immediately after diode deposition is shown for comparison purposes.

3. Results and discussion

ICP etching introduced a single defect in the three crystals under consideration (Fig. 1): the $E_{0.31}$ electron trap. This observation held for ICP treatments at Ar pressures ranging from 4×10^{-3} to 6.5×10^{-4} mbar with corresponding ion energies from 8 to 60 eV. Although the ion current density was fairly constant at low Ar pressures it decreases linearly from 0.35 mA cm^{-2} if the pressure increases above 10^{-3} mbar, leading to a corresponding drop in defect density with rising pressure. The DLTS spectra in Fig. 1 of 60 eV plasma etched diodes were obtained using a reverse bias voltage V_r=1 V, and pulse V_p=1.2 V, these being suitable parameters to probe Ge close to the interface while not activating electron traps that lie deeper in the material. It is significant that near the metal-semiconductor interface the defect concentration in Ge (1 1 1) was substantially higher than that in the (1 0 0) and (1 1 0) samples. TRIM simulations of 60 eV Ar ion bombardment predicted that the majority of ions would come to rest within 3 nm of the surface but did not take channeling or defect motion/diffusion into account. As the (1 1 1) crystal face presents the smallest channels to incident perpendicular ions followed by the (1 0 0) and (1 1 0) faces it is reasonable to expect that more damage occurs nearer to the surface of the (1 1 1) material. This is confirmed by the depth profiles in Fig. 2 up to a depth of 0.5 μm, however, by 0.6 μm depth below the junction the defect concentration was similar for all three samples. At Ar ion energy of 20 eV (Fig. 4, hollow symbols) no significant differences were observed for defect concentrations near the interface.

The 3 min 60 eV plasma treatment introduced $E_{0.31}$ in all three crystals observable up to a depth of almost 2 μm. Beyond a depth of 0.6 μm all samples exhibited a log-linear decrease in concentration with increasing depth below the junction with no clearly discernible differences between crystal orientations. The $E_{0.31}$ concentration may decline slightly more with increasing depth in Ge(1 1 1), however, these differences in Figs. 2 and 4 may also be ascribed to experimental error. A 375 K anneal had a small effect on the defect profiles with the defect profile moving approximately 0.1 μm into the material. A 400 K anneal produced marked changes in the defect profiles with an overall profile broadening and defect concentration lowering as $E_{0.31}$ diffuses deeper into the material, the concentration near the surface reducing by more than 50%. The defect concentration in Ge (1 1 1) remained substantially higher than the concentration in the other crystals in the first μm below the junction and could not be measured deeper into the material due to limitations of the pulse generator. A similar decrease in defect concentration was observed in the measured volume after the 450 K anneal except for the (1 1 1) sample whose defect concentration fell more sharply resulting in it being only slightly higher than the (1 1 0) and (1 0 0) profiles. A further broadening of the defect concentration profile occurred after the 450 K anneal. A 500 K anneal drove the defect concentration down dramatically to the 10^{12} defects cm^{-3} level in the (1 1 1) and (1 1 0) samples and even lower for the (1 0 0) sample. The reason that the defect concentration in the (1 0 0) sample dropped more rapidly is unclear as the samples were always processed together. A 550 K anneal lowered the defect concentration below the measurement threshold of our equipment. The net carrier concentration extracted from CV measurements performed at room temperature did not vary by more than 5% when comparing control diodes to ICP treated diodes and thus did not have a significant impact on the defect depth profiles that were calculated. The depth profiles of the net carrier concentration were constant from a depth of 0.9 μm into the material with a lowering in concentration towards the surface. There were no noticeable changes in the capacitance measured as the samples were annealed at successively higher temperatures.

A summary of Fig. 2 was plotted for the defect concentration at 0.5 μm and 1 μm below the junction (Fig. 3). These depths were chosen as they correspond to readings taken where V_p is large resulting in strong DLTS signals thus improving the measurement accuracy. At both depths below the surface all diodes exhibited the same trends independent of crystal orientation and majority carrier, Sb, concentration. A number of defects in Ge have been shown to be related to Sb, such as the *E*-center, but $E_{0.31}$ shows no dependence on the Sb concentration and is unlikely to be related to the Sb dopant.

Finally, samples ICP etched for 10 min at an Ar partial pressure of 10^{-3} mbar, coinciding with ICP ion energy of 20 eV, were measured and then measured again after a period of a year. The depth profiles are plotted in Fig. 4 together with the cumulative depth profile of the major EBD induced electron traps in Ge. The initial plots (Fig. 4, hollow symbols) are very similar to those plotted for the samples in Fig. 2 before annealing. Measurement of the (1 1 1) sample showed no change after 8 weeks (not plotted) but after one year there is a decrease in concentration of almost an order of magnitude up to a depth of 0.5 μm. Changes in the (1 0 0) and (1 1 0) samples were not as dramatic but all samples exhibited a decrease in concentration and diffusion deeper into the material after a year. In contrast to the samples that were annealed, these samples do not display a broadening of their defect concentration profiles with time even though in the case of the (1 0 0) and (1 1 1) samples the defect concentration fell to levels similar to those observed after the 450 K anneal suggesting that a different process is responsible for these changes, a process that is not dependent on the normal diffusion of this particular defect into the bulk.

The ICP induced defect is also distributed far deeper into the material and in greater concentration than the accumulated defects of a typical 10 keV EBD evaporation and it was previously observed that if the $E_{0.31}$ defect is present then no additional defects are introduced in measurable quantities during EBD [15]. The available defect sites, when occupied by the $E_{0.31}$ defect remain unavailable to EBD induced defects. An attempt to reintroduce the $E_{0.31}$ defect after

a 550 K anneal by ICP etching the sample again and evaporating diodes onto the etched surface was unsuccessful indicating that once the physical system that was required for the ICP defect to be created has been annealed to an undetectable level, no physical systems remain for additional defects to form. This suggests that the same site required for the formation of $E_{0.31}$ is also necessary for the formation of EBD induced defects in ultra-pure Ge. As hydrogen plasma passivation was found to introduce $E_{0.31}$ it was postulated that this defect may be hydrogen related [12], however, as Nyamhere et al. further found that $E_{0.31}$ was also introduced using He plasma, a conclusion was drawn that this defect is not related to H [16] but this is incorrect as there was no determination of whether H was present in the samples prior to treatment or whether the treatment eliminated H from the sample. On the contrary, it has been known for many years that H remains trapped in the crystal in concentrations of 10^{14} to 10^{15} cm^{-3} when it is cooled from the melting point to room temperature (see [17] and reference 4 therein). Hydrogen in germanium has not been as well studied as hydrogen in silicon [18] but it is expected that V_mH_n complexes also form in Ge, wherein VH_2, VH_4 and V_2H_6 were identified using infrared (IR) absorption studies [19]. At present no hydrogen related defects have been identified in Ge using DLTS, however, VH_1 and VH_3 have been predicted to each have a deep level between the valence and conduction bands [20]. IR lines ascribed to VH_2 and VH_4 disappeared after annealing at 400 K and 590 K, respectively [21] and as VH_3 diffuses at a lower temperature than VH in silicon [22] it was expected that annealing the sample to 550 K would diffuse VH_3 into the bulk but not diffuse VH_4 back towards the region under the junction which is one possible explanation of why additional ICP treatment failed to reintroduce this defect. The identification of the $E_{0.31}$ defect as VH_3 is speculative at this time but the lack of other impurities suggests that hydrogen plays a role in the formation of this defect. VH_1 is not a suitable candidate as its annealing temperature would have to be lower than the annealing temperature of VH_2 (400 K). All the processes that introduced $E_{0.31}$ were similar in that the Ge surface was bombarded with ions of energy between 20 eV and 100 eV yet the upper and lower bounds for the introduction of this defect remain to be established.

4. Conclusion

$E_{0.31}$ was introduced by ICP etching up to a maximum concentration of 9×10^{13} cm^{-3} at similar concentrations for all crystal orientations, independent of Sb concentration. It is unlikely that the ICP defect is Sb related and as Ge is known to have low oxygen and carbon impurity levels, these too are unlikely candidates. Hydrogen, or its removal, was found to be the most likely element responsible for the introduction of $E_{0.31}$. Defects were detectable a few microns into the samples, almost 1000 times deeper than predicted by TRIM simulations of Ar implantation into Ge. Defect diffusion and tunneling of Ar ions may play a small role in explaining the unannealed profiles but cannot completely account for these defect distributions considering the depth of defect position and the differences in profile shape between aged samples and annealed samples. ICP was unable to reintroduce $E_{0.31}$ after it had been annealed to undetectable levels. The first plasma treatment proved to be a very efficient process to convert the majority of available sites into $E_{0.31}$ defect sites while the second ICP etch failed to find new sites to convert. The process by which ICP introduces defects deep into the material is not well understood and merits further study.

Acknowledgements

The authors are grateful for the financial support extended to them by the South African National Research Foundation. Special thanks are due to A. R. Peaker (Centre for Electronic Materials Devices and Nanostructures, University Of Manchester) and L. Dobaczewski (Institute of Physics, Polish Academy of Science) for supplying the Laplace software and hardware used in this study.

References

[1] E.E. Haller, Mater. Sci. Semicond. Process. 9 (2006) 408.
[2] D. Sawko, J. Bartko, IEEE Trans. Nucl. Sci. NS-30 (1982) 1756.
[3] S.Z. Karazhanov, J. Appl. Phys. 89 (2001) 332.
[4] T. Chevolleau, W. Fukarek, Plasma Sources Sci. Technol. 9 (2000) 568.
[5] Z. Ren, M. Dineen, L. Deng, A.L. Goodyear, R. Gunn, Mater. Res. Soc. Symp. Proc. 1195 (2010) 115.
[6] F.D. Auret, S.M.M. Coelho, G. Myburg, P.J.J. Van Rensburg, W.E. Meyer, Thin Solid Films 518 (2010) 2485.
[7] N. Fukuoka, H. Saito, Jpn. J. Appl. Phys., Part 1 V 21 (1982) 930.
[8] J. Fage-Pedersen, A. Nylandsted Larsen, A. Mesli, Phys. Rev. B: Condens. Matter 62 (2000) 10116.
[9] Vl. Kolkovsky, M.C. Petersen, A.N. Larsen, Appl. Phys. Lett. 90 (2007) 112110.
[10] F.D. Auret, S. Coelho, W.E. Meyer, C. Nyamhere, M. Hayes, J.M. Nel, J. Electron. Mater. 36 (2007) 1604.
[11] F.D. Auret, S.M.M. Coelho, M. Hayes, W.E. Meyer, J.M. Nel, Phys. Status Solidi A 205 (2008) 159.
[12] C. Nyamhere, A. Venter, D.M. Murape, F.D. Auret, S.M.M. Coelho, J.R. Botha, Physica B 407 (2012) 2935.
[13] L. Dobaczewski, P. Kaczor, J. Appl. Phys. 76 (1994) 194.
[14] Y. Zohta, M.O. Watanabe, J. Appl. Phys. 53 (1982) 1809.
[15] F.D. Auret, S.M.M. Coelho, G. Myburg, P.J. Janse van Rensburg, W.E. Meyer, Physica B 404 (2009) 4376.
[16] C. Nyamhere, A. Venter, F.D. Auret, S.M.M. Coelho, D.M. Murape, J. Appl. Phys. 111 (2012) 044511.
[17] J. Weber, M. Hiller, E.V. Lavrov, Mater. Sci. Semicond. Process. 9 (2006) 564.
[18] A.R. Peaker, V.P. Markevich, L. Dobaczewski, Defects in Microelectronic Materials and Devices, CRC, New York, 2009.
[19] M. Budde, B. Bech Nielsen, J.C. Keay, L.C. Feldman, Physica B 273-274 (1999) 208.
[20] B.J. Coomer, P. Leary, M. Budde, B. Bech Nielsen, R. Jones, S. Öberg, et al., Mater. Sci. Eng., B 58 (1999) 36.
[21] M. Budde, Hydrogen-related Defects in Proton-implanted Silicon and Germanium. An Infrared Absorption Study, Ph.D. Thesis, University of Aarhus, 1998.
[22] S.K. Estreicher, A. Docaj, M.B. Bebek, D.J. Backlund, M. Stavola, Phys. Status Solidi A 209 (2012) 1872.

C. Nyamhere, A. Venter, F.D. Auret, S.M.M. Coelho and D.M. Murape. 'Characterization of the E(0.31) defect introduced in bulk n-Ge by H or He plasma exposure'. *Journal of Applied Physics* **111**.4 (2012), p. 044511. DOI: 10.1063/1.3687426, **Abstract**: Bulk antimony (Sb) doped germanium (n-Ge) samples with doping concentrations ranging between 7.0×10^{14} cm^{-3} and 2.5×10^{15} cm^{-3} were exposed to a dc-hydrogen or helium plasma. Hydrogen exposure resulted in the introduction of a single prominent defect level at E_C −0.31 eV. Exposing similar samples to He plasmas introduced the same electron trap. The trap concentration increased linearly with dopant concentration suggesting that Sb may be a component of this plasma-induced trap. Thermal annealing kinetics studies suggested that this defect anneals out by diffusion.

C. Nyamhere, A. Venter, D.M. Murape, F.D. Auret, S.M.M. Coelho and J.R. Botha. 'dc-Hydrogen plasma induced defects in bulk n-Ge'. *Physica B: Condensed Matter* **407**.15 (2012), pp. 2935–2938. DOI: 10.1016/j.physb.2011.08.047, **Abstract**: Bulk antimony doped germanium (n-Ge) has been exposed to a dc-hydrogen plasma. Capacitance-voltage depth profiles revealed extensive near surface passivation of the shallow donors as evidenced by ∼ 1.5 orders of magnitude reduction in the free carrier concentration up to depth of ∼ 3.2 μm. DLTS and Laplace-DLTS revealed a prominent electron trap 0.30 eV below the conduction (E_C − 0.30 eV). The concentration of this trap increased with plasma exposure time. The depth profile for this defect suggested a uniform distribution up to 1.2 μm. Annealing studies show that this trap, attributed to a hydrogen-related complex, is stable up to 200 °C. Hole traps, or vacancy-antimony centers, common in this material after high energy particle irradiation, were not observed after plasma exposure, an indication that this process does not create Frenkel (V−I) pairs.

4.6 Radiation induced defects

Articles by Auret et al and Roro et al that report on heavy ion implantation damage and alpha-particle irradiation respectively are listed below, appearing with their abstracts.

MeV electron irradiation defects were characterized by Auret et al. 2010 and has been included in section 4.5. The aim of these radiation studies is to characterize the defects introduced by irradiation and how they compare to process induced defects. I-V and C-V data of irradiated devices was also gathered to determine the impact of these irradiations on device performance.

F.D. Auret, P.J. Janse van Rensburg, M. Hayes, J.M. Nel, S. Coelho, W.E. Meyer, S. Decoster, V. Matias, A. Vantomme and D. Smeets. 'Electrical characterization of defects in heavy-ion implanted n-type Ge'. *Nuclear Instruments and Methods in Physics Research Section B: Beam Interactions with Materials and Atoms* **257**.1-2 (Apr. 2007), pp. 169–171. DOI: 10.1016/j.nimb.2007.01.107, **Abstract**: Deep-level transient spectroscopy was used to investigate the electrically active defects introduced in n-type Ge during heavy-ion implantation of 160 keV ions. Various noble heavy-ions were used for implantation and the main defects introduced were found to be electron traps with energy levels at $E_C - 0.09$ eV, $E_C - 0.15$ eV and $E_C - 0.30$ eV. Another defect with a level at $E_C - 0.38$ eV, shown to be the E-center (V−Sb defect), is also present in a very low concentration. The main defects in heavy-ion implanted Ge are different from those introduced by MeV electron irradiation, where the main defect is the E-center. Since electron irradiation introduces mainly point defects, this indicates that heavy-ion implantation introduces defects of a more extended nature, such as vacancy and/or interstitial clusters and their combinations with impurities or foreign species in the Ge. We have also demonstrated that these defects are not species related.

K.T. Roro, P.J. Janse van Rensburg, F.D. Auret and S. Coelho. 'Effect of alpha-particle irradiation on the electrical properties of n-type Ge'. *Physica B: Condensed Matter* **404**.22 (Dec. 2009), pp. 4496–4498. DOI: 10.1016/j.physb.2009.09.033, **Abstract**: Deep-level transient spectroscopy was used to investigate the effect of alpha particle irradiation on the electrical properties of n-type Ge. The samples were irradiated with alpha particles at room temperature using an americium-241 (Am-241) radio nuclide source. The main defects introduced were found to be electron traps with energy

levels at $E_C - 0.38$, $E_C - 0.21$, $E_C - 0.20$, $E_C - 0.15$, and $E_C - 0.10$eV, respectively. The main defects in alpha particle irradiation are similar to those introduced by MeV electron irradiation, where the main defect is the E-center. A quadratic increase in concentration as a function of dose is observed.

4.7 Defect Annealing

Defects that were introduced using the processes reported on in the previous sections were annealed out using isochronal annealing. These annealing studies are included in the following three articles, Auret, Meyer, Coelho and Hayes 2006, Auret, Coelho, Janse van Rensburg et al. 2008, and Auret et al. 2009, as well as the article by Auret, Coelho, Meyer et al. 2007, in section 4.4. A contribution by Chawanda et al. 2012, rounds off this section as it reports on the effect of annealing on the diode properties as well as the changes observed in an iridium SBD as the annealing temperature was increased. The aims of all these annealing studies was to establish the temperatures at which defects annealed out of the material. This information, together with the defect signature obtained with DLTS, confirms the identity of a defect and, by comparison, if it has been observed before. Annealing was also used to ascertain if any defects were activated at higher temperatures as this may be indicative of a defect changing its structure, especially if a corresponding reduction of an existing defect is observed. Heating may also introduce a new defect level when a change occurs in a defect that has an energy level that is too close to the band edges to be observed using DLTS. The mechanism by which the defect concentration changes as a function of annealing was investigated and identified in some cases. Lastly, annealing was used to determine if this heat treatment made a fundamental change in the material that inhibited further defect introduction.

ELSEVIER

Available online at www.sciencedirect.com
ScienceDirect

Materials Science in Semiconductor Processing 9 (2006) 576–579

MATERIALS SCIENCE IN SEMICONDUCTOR PROCESSING

Electrical characterization of defects introduced during electron beam deposition of Schottky contacts on *n*-type Ge

F.D. Auret*, W.E. Meyer, S. Coelho, M. Hayes, J.M. Nel

Physics Department, University of Pretoria, Pretoria 0002, South Africa

Available online 12 September 2006

Abstract

We have investigated by deep level transient spectroscopy the hole and electron trap defects introduced in *n*-type Ge during electron beam deposition (EBD) of Pt Schottky contacts. We have also compared the properties of these defects with those introduced in the same material during high-energy electron irradiation. Our results show EBD introduces several electrically active defects at and near the surface of Ge. The main defect introduced during EBD has electronic properties similar to those of the V–Sb complex, or E-center, introduced during high-energy electron irradiation of Ge. Annealing at 325 °C in Ar removed all the defects introduced during EBD.

Keywords: Germanium; Defects; DLTS; Annealing; Electron beam deposition

1. Introduction

The low effective mass of holes in Ge has opened up the possibility of using Ge in ultrafast complimentary metal–oxide–semiconductor devices [1]. This, in turn, has sparked renewed interest in the properties of defects in Ge because defects ultimately determine the performance of devices. In recent studies the properties of the defects introduced during high-energy gamma-, electron- and proton-irradiation of Ge were reported [2–5]. However, no in-depth investigations regarding the defects introduced in Ge during critical processing steps, e.g. metallization, have been reported. These investigations are important because it is well known that metallization procedures, e.g. sputtering and electron beam deposition (EBD), introduce defects at and close to the metal–semiconductor junction. These defects influence device performance and alter the barrier heights of the contacts [6–9]. The defects responsible for these barrier adjustments are formed when energetic particles strike the semiconductor surface and interact with the semiconductor. Depending on the application, these defects may either be beneficial for or detrimental to optimum device functioning. For example, for Si it has been shown that the defects introduced during high-energy electron and proton irradiation increase the switching speed of devices [10].

In this study we report the electronic properties of defects introduced in *n*-type Ge during EBD of Pt Schottky contacts. We show that EBD introduces one prominent electron- and one prominent hole-trap

*Corresponding author. Tel.: +27 12 420 2684; fax: +27 12 362 5288.
E-mail address: danie.auret@up.ac.za (F.D. Auret).

1369-8001/$ - see front matter © 2006 Elsevier Ltd. All rights reserved.
doi:10.1016/j.mssp.2006.08.008

and several other hole traps. The two prominent EBD induced trap levels were found to belong to the V–Sb center that was also introduced during high-energy electron irradiation of the same material.

2. Experimental procedure

For deep level transient spectroscopy (DLTS) of the defects introduced in Ge during EBD of Schottky barrier contacts, we have used bulk-grown (1 1 1) *n*-type material doped with Sb to a level of $2.5 \times 10^{15}\,cm^{-3}$. Before metallization the samples were first degreased and then etched in a mixture of H_2O_2:H_2O (1:5, 30% H_2O_2) for 1 min. Directly after cleaning they were inserted into a vacuum chamber where AuSb (0.6% Sb) was resistively deposited on their back surfaces as ohmic contacts. The samples were then annealed at 350 °C in Ar for 10 min. Before Schottky contact deposition, the samples were again chemically cleaned as described above. Pt contacts, 0.60 mm in diameter and 200 nm thick, were deposited in an EBD system through a mechanical mask. "Control" Pd Schottky contacts were deposited on identical sample by resistive evaporation—a process known not to introduce defects in semiconductors. Both conventional and high-resolution Laplace DLTS [11,12] were used to study the defects introduced in the Ge during the EBD process.

3. Results and discussion

In Fig. 1 we depict the DLTS spectra for control (Pd) and EBD (Pt) contacts. Curves (1) and (2) are the electron and hole spectra, respectively, for the control diodes and they clearly indicate that this material does not contain electron or hole traps in measurable concentrations. The traps introduced in the Ge during EBD of Pt contacts are shown by curves (3) and (4) for electron and hole traps, respectively. Even though we attempted to detect majority carriers only in curve (3) by not using injection conditions, a prominent hole trap $H_{0.30}$ was still present and prevented the possible detection of electron traps with peaks in its vicinity. In the nomenclature used here "E" and "H" means electron and hole traps, respectively, and the subscript is the activation energy determined from the Arrhenius plots in Fig. 2. The electronic properties of all the defects are summarized in Table 1. We have not corrected the energy values to take into account the temperature dependence of the capture cross-section, that has been shown to significantly change the effective activation energy of the E-center [3]. The most significant electron trap in curve (3) of Fig. 1 is $E_{0.38}$. Curve (4) shows that EBD introduced the hole traps $H_{0.09}$, $H_{0.15}$, $H_{0.18}$, $H_{0.26}$, $H_{0.30}$ and $H_{0.29}$. The signals of $H_{0.26}$ and $H_{0.30}$ could only be separated by using Laplace DLTS

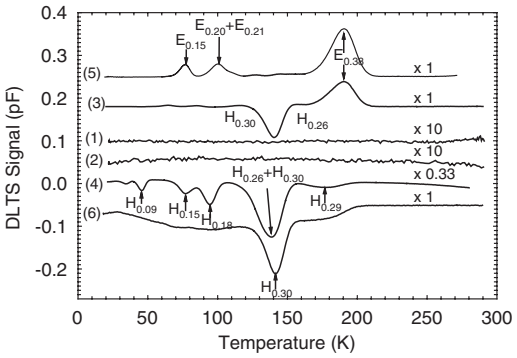

Fig. 1. DLTS spectra of the resistively deposited (control) Pd Schottky contacts to *n*-Ge reveal that these samples contain no electron or hole traps (curves (1) and (2), respectively) within the detection limit of our DLTS system. Curves (3) and (4) are the DLTS electron- and hole-trap spectra, respectively, of Pt Schottky contacts deposited by EBD, recorded using a rate window of $80\,s^{-1}$ at a quiescent reverse bias of −1 V. For the electron-trap spectra the pulse, V_p, was 0.15 V into forward bias. Hole-trap spectra were obtained by applying an injection pulse of $V_p = 3$ V into forward bias. Curves (5) and (6) are the spectra for electron irradiated resistively deposited Pd Schottky contacts to *n*-Ge, recorded under the same conditions as curves (3) and (4), respectively.

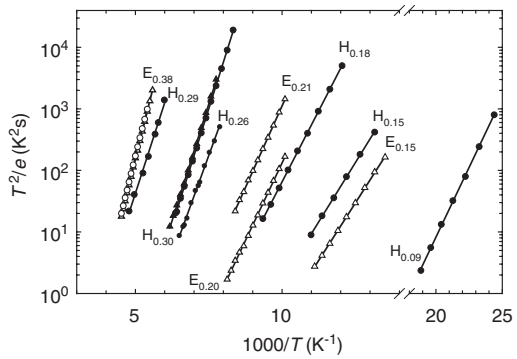

Fig. 2. Arrhenius plots for EBD (circles) and electron irradiation induced (triangles) electron-traps (empty symbols) and hole-traps (solid symbols) in Ge. All data was acquired using the bias and pulsing conditions defined in the caption of Fig. 1.

Table 1
Electronic properties of prominent defects introduced in *n*-type Ge during Pt electron beam deposition and MeV electron irradiation of Schottky contacts

Process	Defect	E_T (eV)	σ_a (cm^2)	T_{peak}[a] (K)	Similar defects/defect ID
EBD	$E_{0.38}$	$E_C-0.38$	1.0×10^{-14}	191	$E_{0.377}$[b], $E_{0.37}$[c], V–Sb (− −/-)[b,c]
	$H_{0.09}$	$E_V+0.09$	2.1×10^{-13}	47	
	$H_{0.15}$	$E_V+0.15$	7.1×10^{-14}	82	
	$H_{0.18}$	$E_V+0.18$	3.5×10^{-14}	97	
	$H_{0.26}$	$E_V+0.26$	4.3×10^{-14}	133	$H_{0.270}$[b]
	$H_{0.30}$	$E_V+0.30$	6.2×10^{-13}	141	$H_{0.307}$[b], $H_{0.30}$[c], V–Sb (-/0)
	$H_{0.29}$	$E_V+0.29$	1.3×10^{-15}	176	
MeV	$E_{0.15}$	$E_C-0.15$	5.0×10^{-14}	77	
Electron irradiation	$E_{0.20}$	$E_C-0.20$	1.4×10^{-14}	100	$E_{0.19}$[c], Sb and *I* related[c]
	$E_{0.21}$	$E_C-0.21$	3.6×10^{-14}	109	$E_{0.21}$[c], Sb related?[c]
	$E_{0.38}$	$E_C-0.38$	1.1×10^{-14}	191	$E_{0.377}$[b], $E_{0.37}$[c], V–Sb (− −/-)[b,c]
	$H_{0.30}$	$E_V+0.30$	3.66×10^{-13}	142	$H_{0.307}$[b], $H_{0.30}$[c], V–Sb (-/0)[b]

[a]Peak temperature at a rate window of 80 s^{-1}.
[b]See Ref. [3].
[c]See Ref. [2].

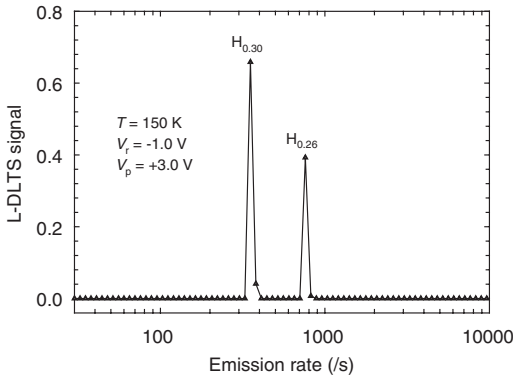

Fig. 3. Laplace DLTS spectrum of the ($H_{0.26}+H_{0.30}$) defect combination. The $H_{0.26}$ and $H_{0.30}$ peaks can clearly be distinguished from each other.

(Fig. 3). Note that the $H_{0.29}$ peak is on the high temperature side of $H_{0.30}$ because its apparent capture cross-section is much lower than that of $H_{0.30}$.

In Fig. 1 we also depict the spectra of "control" Pd diodes that were irradiated with high-energy electrons from a Sr^{90} radionuclide to a dose of 2×10^{14} cm^{-2} (curves (5) and (6)). We have used Laplace DLTS to separate the signals of the $E_{0.20}$ and $E_{0.21}$ of electron irradiated samples shown in curve (5). From Fig. 1 it seems that only $E_{0.38}$ and $H_{0.30}$ are introduced by both EBD and high-energy electron irradiation. The Arrhenius plots in Fig. 2 confirm that the $E_{0.38}$ introduced by EBD and the $E_{0.38}$ introduced by electron irradiation have, within the experimental error, the same DLTS "signature". $E_{0.38}$ has been shown to be the (− −/-) charge state of the E-center (V–Sb) in Sb-doped Ge [2,3]. Similarly, the signatures of the $H_{0.30}$ defects in EBD and electron irradiated Ge are the same and corresponds closely to that reported for the H_{307}, speculated to be the single acceptor level (-/0) of the Sb–V center in Ge [2,3]. Evidently, the EBD process introduces vacancies in Ge, at and close to the junction, that migrate and combine with, among others, Sb atoms to form Sb–V pairs (E-centers). These vacancies have been proposed to be the result of energetic particles that originate in the region of the filament and then impinge on the semiconductor [13].

The hole traps $H_{0.09}$, $H_{0.15}$, $H_{0.18}$, $H_{0.26}$ and $H_{0.29}$ do not correspond to any identified radiation induced defects. They are also not present in the Ge that we irradiated with high-energy electrons. It is well known that high-energy electrons create mainly point defects (vacancies and interstitials) in semiconductors. The particles responsible for the EBD damage are, however, most probably gas or metal ions that deposit more energy per unit length than the electrons. Therefore, they can create defects larger than point defects. We speculate that the hole defects other than $H_{0.30}$ are larger than point defects, probably vacancy- or interstitial-clusters of various sizes.

As in previous studies on other semiconductors [6–9], we have found that the defects introduced

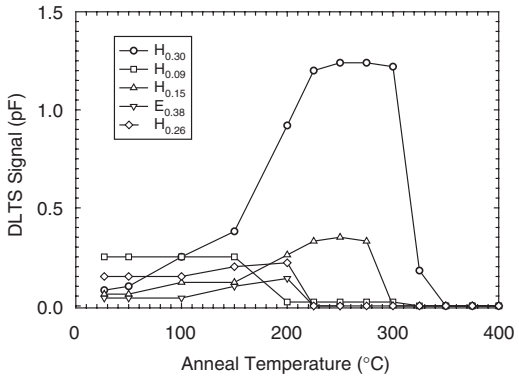

Fig. 4. Isochronal annealing (20 min periods) of the most prominent defects introduced by EBD in *n*-Ge.

during EBD of contacts on Ge are located close to the metal–semiconductor interface. In the present study it was, however, difficult to obtain quantitatively accurate depth profiles. The main reason for this is the sharp increase in minority carrier injection with increasing forward pulse voltage that leads to non-detection of the prominent trap $E_{0.38}$ (curve (4) in Fig. 1).

Finally, we have investigated the thermal stability of the EBD induced defects by isochronal annealing in argon (Fig. 4). Only after annealing at 225 °C could the $E_{0.38}$ and $H_{0.30}$ levels no longer be detected. This is slightly higher than the 175–200 °C reported in Ref. [3] for removing the E-center. However, it should be borne in mind that the annealing in Ref. [3] was under zero bias where most of the E-centers are filled with electrons. In our case, although we annealed at zero bias, the E-centers are very close to the surface and hence the levels of most of them are above the Fermi level. It has been reported that reverse bias annealing (E-center level above the Fermi level) impedes the annealing of E-centers [2]. During annealing the concentration of $H_{0.26}$ increased up to 200–225 °C, rendering it the most prominent defect, and then it annealed out at 325 °C. At this temperature all the defects introduced during EBD were removed.

4. Conclusions

Our results revealed that the main defect introduced during EBD has the same electronic properties as that of the V–Sb complex, or E-center, introduced during high-energy electron irradiation of Ge. This defect has two levels $E_{0.38}$ and $H_{0.30}$ that correspond to its (− −,-) and (-,0) charge states [3]. EBD also introduced several defects that are not introduced by electron irradiation. Since EBD defects are introduced by heavy metal or gas ions [13], these defects could possibly be higher-order vacancy clusters and complexes thereof with impurities. Annealing at 325 °C removed all the defects introduced during EBD of Pt Schottky contacts.

Acknowledgements

The authors gratefully acknowledge financial support of the South African National Research Foundation. The Laplace DLTS software and hardware used in the research was kindly provided by A.R. Peaker (Centre for Electronic Materials Devices and Nanostructures, University of Manchester) and L. Dobaczewski (Institute of Physics, Polish Academy of Sciences).

References

[1] Hull R, Bean JC, editors. Germanium silicon: physics and materials, semiconductors and semimetals, vol. 56. San Diego: Academic Press; 1999.
[2] Fage-Pedersen J, Nylandsted Larsen A, Mesli A. Phys Rev B 2000;62:10116.
[3] Markevich VP, Peaker AR, Litvinov VV, Emstev VV, Murin LI. J Appl Phys 2004;95:4078.
[4] Markevich VP, Hawkins ID, Peaker AR, Emstev KV, Emstev VV, Litvinov VV, et al. Phys Rev B 2004;70:235211–3.
[5] Markevich VP, Hawkins ID, Peaker AR, Litvinov VV, Dobaczewski L, Lindström JL. Appl Phys Lett 2002;81:1821.
[6] Auret FD, Paz O, Bojarczuk NA. J Appl Phys 1984;55(6):1581.
[7] Mamor M, Auret FD, Willander M, Goodman SA, Myburg G, Meyer F. Semicond Sci Technol 1999;14:611.
[8] Auret FD, Goodman SA, Koschnik FK, Spaeth J-M, Beaumont B, Gibart P. Appl Phys Lett 1999;74(15):2173.
[9] Myburg G, Auret FD. J Appl Phys 1992;71:6172.
[10] Sawko DC, Bartko J. IEEE Nucl Sci 1983;30:1756.
[11] Dobaczewski L, Kaczor P, Hawkins ID, Peaker AR. J Appl Phys 1994;76:194.
[12] Dobaczewski L, Peaker AR, Bonde Nielsen K. J Appl Phys 2004;96:4689.
[13] Christensen C, Petersen JW, Nylandsted Larsen A. Appl Phys Lett 1992;61:1426.

Materials Science in Semiconductor Processing 11 (2008) 348–353

Contents lists available at ScienceDirect

Materials Science in Semiconductor Processing

journal homepage: www.elsevier.com/locate/mssp

Electrical characterization of defects introduced during metallization processes in n-type germanium

F.D. Auret *, S.M.M. Coelho, P.J. Janse van Rensburg, C. Nyamhere, W.E. Meyer

Physics Department, University of Pretoria, Pretoria 0002, South Africa

ARTICLE INFO

Available online 21 November 2008

Keywords:
Ge
Metallization
Defects
Deep-level transient spectroscopy
DLTS

ABSTRACT

We have studied the defects introduced in n-type Ge during electron beam deposition (EBD) and sputter deposition (SD) by deep-level transient spectroscopy (DLTS) and evaluated their influence on the rectification quality of Schottky contacts by current–voltage (*I–V*) measurements. *I–V* measurements demonstrated that the quality of sputter-deposited diodes are poorer than those of diodes formed by EBD. The highest quality Schottky diodes were formed by resistive evaporation that introduced no defects in Ge. In the case of EBD of metals the main defect introduced during metallization was the V–Sb complex, also introduced during by electron irradiation. The concentrations of the EBD-induced defects depend on the metal used: metals that required a higher electron beam intensity to evaporate, e.g. Ru, resulted in larger defect concentrations than metals requiring lower electron beam intensity, e.g. Au. All the EBD-induced defects can be removed by annealing at temperatures above 325 °C. Sputter deposition introduces several electrically active defects near the surface of Ge. All these defects have also been observed after high-energy electron irradiation. However, the V–Sb centre introduced by EBD was not observed after sputter deposition. Annealing at 250 °C in Ar removed all the defects introduced during sputter deposition.

1. Introduction

The low effective mass of holes in Ge has opened up the possibility of using Ge in ultrafast complimentary metal-oxide-semiconductor (CMOS) devices [1]. This, in turn, has triggered renewed interest in the properties of defects in Ge because defects ultimately determine the performance of devices. In a detailed study of proton and electron-irradiated Ge a comparison was made to previously observed radiation-induced defects and level assignments of the E-centre (V–Sb), A-centre (V–O) and divacancy (V–V) were proposed [2]. Several other O- and Sb-related defects were characterised in O-doped and Sb-doped Ge, respectively. It was also convincingly demonstrated that the E-centre in Sb-doped Ge can be present in three charge states and the level positions associated with these levels' states were determined [3–5].

Metallization is a critical processing step in the semiconductor industry. Resistive evaporation, electron beam deposition (EBD) and sputter deposition are commonly used metallization methods. It is well known that resistive evaporation does not introduce any detectable defects in the semiconductor. However, it cannot easily deposit high melting point materials e.g. W or Ru. EBD, on the other hand, is useful to deposit high melting point metals at very controllable rates. Sputter deposition can also be used to deposit high melting point metals and is further capable of stoichiometrically depositing alloys from compound targets. Unfortunately, these latter two methods introduce defects in semiconductors. Some investigations regarding the defects introduced in Ge during EBD [6–8] and sputter deposition [9,10] have been reported. The defects introduced during these processes reside in the Ge at and close to the metal–Ge junction;

* Corresponding author. Tel.: +27 12 420 2684; fax: +27 12 362 5288.
E-mail address: danie.auret@up.ac.za (F.D. Auret).

1369-8001/$ - see front matter © 2008 Elsevier Ltd. All rights reserved.
doi:10.1016/j.mssp.2008.09.001

they influence device performance and alter the barrier heights of the contacts [11]. The defects responsible for these barrier adjustments are formed when energetic particles reach the semiconductor surface and interact with the semiconductor. Depending on the application, these defects may either be beneficial or detrimental to optimum device functioning. For Si it has been shown that the defects introduced during high-energy electron and proton irradiation increase the switching speed of devices [12].

In this study, we review the electronic properties of defects introduced in n-type Ge during EBD and sputter deposition of different metal Schottky contacts. We also show that the concentrations of the most prominent EBD-induced defect, the V–Sb centre, depended on the metal deposited by EBD via the melting point of the metal and the influence thereof on the vacuum during metallization. We have found that sputter deposition also introduces several electrically active defects near the surface of Ge, but, contrary to what has been reported elsewhere [9], it did not introduce the V–Sb centre in our experiments. Most of the defects introduced by EBD and sputter deposition have also been observed after high-energy electron irradiation. We also illustrate the effect of these process-induced defects on the current–voltage (I–V) characteristics of the Schottky diodes at different temperatures. Finally, we compare the removal of these metallization-induced defects by thermal annealing.

2. Experimental procedure

The Schottky barrier diodes for this study were fabricated on bulk-grown (111) n-type Ge doped with Sb to a level of $2.5 \times 10^{15}\,cm^{-3}$. Before metallization the samples were first degreased and then etched in a mixture of H_2O_2:H_2O (1:5) for 1 min. Directly after cleaning they were inserted into a vacuum chamber where AuSb (0.6% Sb) was deposited on their back surfaces. The samples were then annealed at 350 °C in Ar for 10 min, yielding ohmic contacts with a low contact resistivity. Before Schottky contact deposition, the samples were again chemically cleaned as described above. Metal (Au, Ti and Ru) contacts, 0.6 mm in diameter and 200 nm thick, were deposited onto the Ge in an EBD system through a mechanical mask. A Varian 10 kV electron gun vacuum evaporation system was used for this process. In this system, the samples are positioned about 0.4 m above the electron gun. In a different system Au Schottky contacts were sputter deposited onto similar Ge samples cut from the same wafer. For sputter deposition Ar was leaked into the system to a pressure of 6×10^{-2} mbar [9]. The sputter-deposited contacts were deposited at a rate of about $2\,nm\,s^{-1}$ and were 400 nm thick. "Control" Au Schottky contacts were deposited on samples cut from the same wafer by resistive evaporation.

Following contact fabrication, current–voltage (I–V) and capacitance–voltage (C–V) measurements were performed to assess the quality of the diodes and to determine the free carrier density of the Ge, respectively. Thereafter both conventional and high-resolution Laplace deep-level transient spectroscopy (DLTS) [13,14] was used to study the defects introduced in the Ge during the EBD and SD processes. The activation energies, E_T, and apparent capture cross sections for electrons, σ_{na}, and holes, σ_{pa}, (i.e. the DLTS "signatures") of the process-induced electron traps were determined from the conventional DLTS Arrhenius plots. In order to identify the defects introduced by the deposition processes, a comparison was made with defects introduced by high-energy (MeV) electron irradiation from a Sr^{90} source in samples cut from the same wafer.

3. Results and discussion

3.1. I–V characteristics of Schottky diodes fabricated by EBD and sputter deposition

I–V measurements were recorded at room temperature as well as at several other lower temperatures. The series resistances of the control diodes remained in the 10–20 Ω range in the entire temperature regime investigated, indicating that the AuSb back contacts retained their ohmic character, even down to 16 K, the lowest temperature attainable in our cryostat. Room temperature C–V measurements yielded the free carrier density of the Ge as $(2.5 \pm 0.05) \times 10^{15}\,cm^{-3}$. In Fig. 1, we compare the forward and reverse I–V characteristics of Au Schottky contacts formed by resistive evaporation, EBD and sputter deposition at room temperature and at 100 K. We chose 100 K as

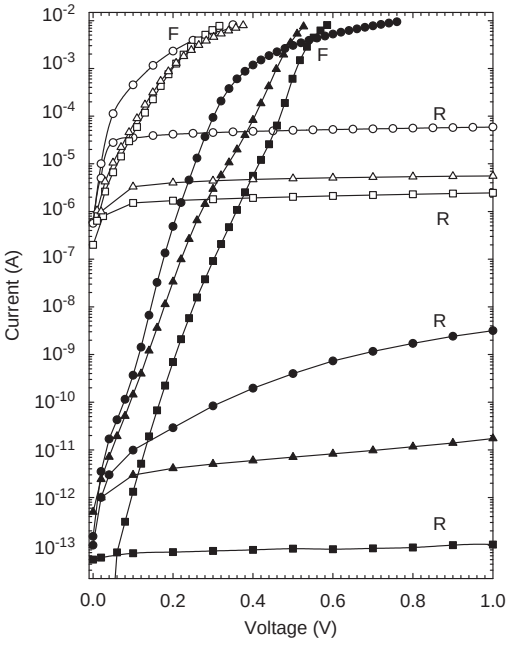

Fig. 1. I–V characteristics of Au Schottky contacts to n-Ge deposited by resistive evaporation (squares), EBD (triangles) and sputter deposition (circles). Open symbols are the data recorded at room temperature while filled symbols represent the data recorded at 100 K.

the lower temperature because at 100 K the reverse leakage current of the best diodes (deposited by resistive evaporation) is between 10^{-13} and 10^{-14} A, which is the lowest current our equipment can accurately measure. At room temperature the *I–V* barrier height of these three contacts were determined as (0.59 ± 0.01), (0.56 ± 0.01) and (0.53 ± 0.01) eV, respectively.

From Fig. 1 we notice several interesting aspects. Firstly, at room temperature, the reverse leakage current of the control diodes are the best whereas that of the sputtered diodes are the poorest, by slightly more than a decade. Secondly, if we compare the characteristics of these diodes at 100 K then we see that the difference between the reverse characteristics of the three diodes has been amplified. The reverse current (at −1 V) of the sputter-deposited diode is more than four orders of magnitude higher than that of the control sample. The forward current characteristic of the sputter-deposited diode is also significantly higher than those of the other two diodes. These higher reverse currents may be the result of process-induced defects that act as generation centres. Another interesting point is that the forward characteristic of the sputter-deposited diode shows a significant increase in series resistance compared to the other diodes. This is especially noticeable for the characteristics recorded at 100 K. This may be due to surface disorder introduced during the sputter deposition process. The control and EBD samples exhibited very similar series resistances, significantly lower than that of the sputter-deposited diode. These *I–V* measurements clearly demonstrate that both EBD and sputter deposition resulted in degraded *I–V* characteristics but that the sputter deposition yields the poorest diodes of the three metallization processes.

3.2. Defects introduced by EBD of different metals

First, we summarise what is already known for the defects introduced during EBD of Pt on Sb-doped Ge [6–8]. Note that no defects could be detected in the control SBDs fabricated by resistive deposition, indicating that the Ge is of high quality. The main defect introduced during EBD of Pt [7] was the E-centre (V–Sb complex) with its prominent associated electron and hole traps $E_{0.38}$, $H_{0.30}$ and $H_{0.09}$, respectively. In the nomenclature used here "E" means electron trap and the number following it is the energy level of this trap below the conduction band. Similarly, "H" means hole trap and the number following it is the energy level of this trap above the valence band. Note that we have not corrected these energy values to take into account the temperature dependence of the capture cross section, which has been shown to significantly change the activation energy of the E-centre [3]. Several other electron traps in lower concentrations were also detected. In the case of EBD the E-centre forms when energetic particles (originating in the region of the filament) impinge on the Ge and create vacancies at and close to the Ge surface [15]. These vacancies are mobile at room temperature and migrate into the Ge where they combine with Sb-dopant atoms to form the E-centre.

In Fig. 2, we compare the DLTS results recorded using SBDs of three different metals, namely Ti, Au and Ru, formed by EBD. The top three curves ((a)–(c)) are for electron traps but clearly hole injection could not be completely eliminated and therefore they still show the $H_{0.30}$ trap. The lower three curves ((d)–(f)) are for hole traps and were obtained after using intentional hole injection. As was the case for Pd and Pt, the most significant defect introduced is the E-centre with the traps $E_{0.38}$, $H_{0.30}$ and $H_{0.09}$ associated with it [3–8]. Curve (b) also shows the presence of a defect $E_{0.13}$ in a lower concentration, whereas curves (e) and (f) reveal the presence of additional hole traps, $H_{0.15}$ and $H_{0.18}$. The DLTS signatures of these defects were extracted from the Arrhenius plot in Fig. 3 and are summarised in Table 1.

From Fig. 2 it is further evident that the concentration of the E-centre increases from Ti to Au to Ru. In order to explain this trend, it should be borne in mind that the defects introduced by EBD are caused by ionised particles that are accelerated from the region near the filament [15] and impinge on the Ge surface. The concentration of these particles in the residual gas in the vacuum will increase with increasing residual gas pressure as well as with increasing emission current (proportional to the filament current). In the case of Ti evaporation, the starting vacuum

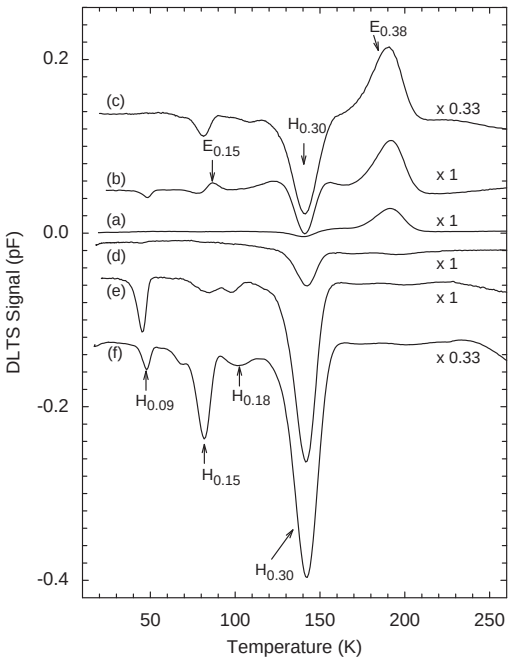

Fig. 2. DLTS spectra of Ti, Au and Ru Schottky contacts deposited by EBD to n-Ge: Curves (a), (b) and (c) are the electron-trap spectra for Ti, Au and Ru, respectively, while curves (d), (e) and (f) are the hole-trap spectra for Ti, Au and Ru, respectively. These spectra were recorded using a rate window of 80 s^{-1} at a quiescent reverse bias of −1 V. For the electron-trap spectra the pulse, V_p, was 0.15 V into forward bias. Hole-trap spectra were obtained by applying an injection pulse of $V_p = 3$ V into forward bias.

was more than an order of magnitude lower than for Au and Ru (Table 2). This means that, although the filament current was slightly higher than for Au deposition, a lower flux of particles reached the sample surface during evaporation, which in turn implies a lower level of damage, as observed in Figs. 1 and 2. When comparing the conditions for Au and Ru it can be seen from Table 2 that the vacuum during Au deposition was about the same as for Ru deposition. The filament current for Au deposition was only slightly lower than for Ru. However, if we consider the deposition rates then we notice that, due to its high melting point, the deposition rate of Ru is about one-twentieth of that of Au. This implies that it takes 20 times longer to deposit the same thickness of Ru as Au. This in turn means that the Ge surface is exposed to energetic particles for a much longer time during Ru deposition than during Au deposition, leading to the high concentration of defects observed for Ru metallization.

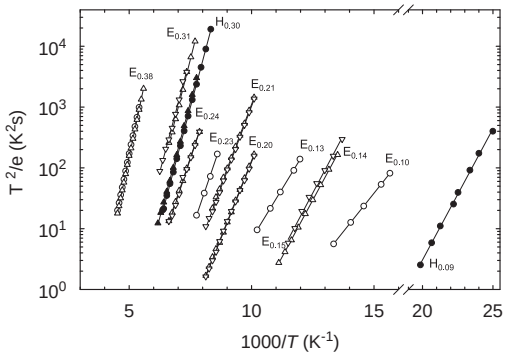

Fig. 3. Arrhenius plots for defects introduced by EBD (circles), MeV electron irradiation induced (triangles up) and sputter deposition (triangles down) in Ge. Filled symbols are for hole traps. All data were acquired using the bias and pulsing conditions defined in the caption of Fig. 2.

3.3. Comparison of defects introduced by EBD and sputter deposition

Curves (b) and (c) in Fig. 4 represent the DLTS spectra for Au Schottky diodes that were deposited by sputter deposition and EBD, respectively. Curve (d) was recorded after irradiating a resistively deposited diode with high-energy electrons at a dose of $2 \times 10^{14}\,cm^{-2}$. We have used Laplace DLTS to separate the signals of the $E_{0.20}$ and $E_{0.21}$

Table 1
Electronic properties of prominent defects introduced in n-type Ge during sputter and electron beam deposition of Schottky contacts, and by MeV electron irradiation

Sputter deposition				MeV electron irradiation				Similar defects/defect ID
Defect	E_T (eV) (±0.01)	σ_a (cm^2) (±10%)	T_{peak}[a] (K)	Defect	E_T (eV)	σ_a (cm^2)	T_{peak}[a] (K)	
$ES_{0.14}$	E_C−0.14	5.5×10^{-15}	78	$E_{0.15}$	E_C−0.15	2.8×10^{-14}	77	$E_{0.13}$[b], Sb and I related[c]
$ES_{0.20}$	E_C−0.20	3.7×10^{-14}	100	$E_{0.20}$	E_C−0.20	1.4×10^{-14}	100	$E_{0.19}$[c], Sb and I related[c]
$ES_{0.21}$	E_C−0.21	2.0×10^{-14}	109	$E_{0.21}$	E_C−0.21	3.6×10^{-14}	109	$E_{0.21}$[c], Sb related?[c]
$ES_{0.24}$	E_C−0.24	3.3×10^{-15}	131	$E_{0.24}$	E_C−0.24	2.5×10^{-15}	131	$E_{0.23}$[c], Sb and I related?[c]
$ES_{0.31}$	E_C−0.31	1.5×10^{-14}	151	$E_{0.31}$	E_C−0.31	5.0×10^{-14}	150	$E_{0.29}$[c]?, V_2[c]?
Electron beam deposition								
$E_{0.10}$	E_C−0.10	3.7×10^{-16}	65					
$E_{0.13}$	E_C−0.13	1.9×10^{-16}	85					
$E_{0.23}$	E_C−0.23	3.4×10^{-14}	116					
$E_{0.38}$	E_C−0.38	1.0×10^{-14}	191	$E_{0.38}$	E_C−0.38	1.1×10^{-14}	191	$E_{0.377}$[b], $E_{0.37}$[c], V–Sb (−/−)[b,c]
$H_{0.09}$	E_V+0.09	2.1×10^{-13}	47					
$H_{0.15}$	E_V+0.15	7.1×10^{-14}	82					
$H_{0.18}$	E_V+0.18	3.5×10^{-14}	97					
$H_{0.27}$	E_V+0.27	2.4×10^{-13}	133					
$H_{0.30}$	E_V+0.30	6.2×10^{-13}	141	$H_{0.30}$	E_V+0.30	3.66×10^{-13}	142	$H_{0.307}$[b], $H_{0.30}$[c], V–Sb (−/0)[b]

The error margins the value of E_T lie in the third digit after the decimal point whereas that for σ is less than 10% of its value.
[a] Peak temperature at a rate window of $80\,s^{-1}$.
[b] See Ref. [3].
[c] See Ref. [2].

Table 2
Electron beam deposition parameters and conditions for different metal Schottky contacts

Metal	Melting point (°C)	Thickness (nm)	Deposition rate (nm/s)	EB filament current (mA)	Starting vacuum (mbar)
Ti	1660	100	0.4	75	2×10^{-6}
Au	1064	200	0.5	60	5×10^{-5}
Ru	2250	50	0.02	70	6×10^{-5}

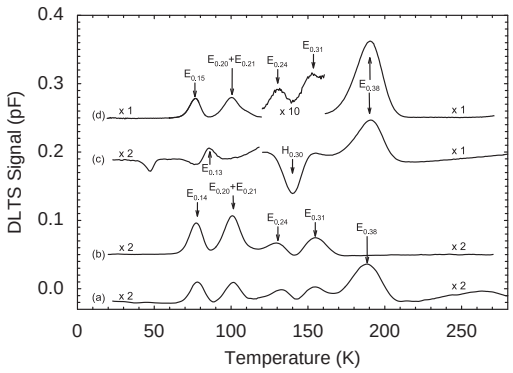

Fig. 4. DLTS spectra of Au Schottky contacts on n-Ge: Curves (a), (b) and (c) are the spectra for a sputter-deposited Au contact, a Au contact deposited by EBD and an electron-irradiated control contact, respectively. These spectra were recorded using a rate window of $80\,s^{-1}$ at a quiescent reverse bias of −1 V. For the electron-trap spectra the pulse, V_p, was 0.15 V into forward bias.

of electron-irradiated samples. As described above, the E-centre is the only defect that is introduced by both EBD and high-energy electron irradiation. Curve (b) shows that sputter deposition introduced several electron traps: $E_{0.14}$, $E_{0.20}$, $E_{0.21}$, $E_{0.24}$ and $E_{0.31}$. However, the main electron trap introduced by EBD and electron irradiation, the E-centre, is not present in sputter-deposited diodes. Also, unlike in previous studies of high-energy electron-irradiated Ge and electron beam-deposited (EBD) Schottky diodes [6,7], we could not detect any hole traps in the sputter-deposited contacts studied here, even when applying a strong forward bias. However, after irradiating the sputter-deposited contacts with MeV electrons the $E_{0.38}$ trap associated with the E-centre could be clearly observed (curve (a) of Fig. 4). This means that sputter deposition by itself, in our sputter equipment and under our deposition conditions, does not introduce the E-centre. It is important to point out that the E-centre has been observed by Simoen et al. [10] after sputter deposition of Pt in a different sputter system.

The fact that the E-centre is not observed after sputter deposition in our system may imply that our sputter process does not introduce a sufficient number of single vacancies at and close to the surface that can diffuse into the Ge and combine with Sb ions to form V–Sb, as in the case of EBD. It should be realised that most of the damage that we observe after sputter deposition is caused by backscattered neutral Ar ions that, for the sputter conditions used here, have a maximum energy of approximately 700 eV of RF power [9]. From TRIM [14] modelling we have found that the range and straggle of these ions are 2.1 and 1.2 nm, respectively. In the first 3 nm each ion deposits on average 20 eV/nm in to the Ge lattice and produces, on average, 5 vacancies/nm. This implies that defects larger than the single vacancy, e.g. divacancy and vacancy or interstitial clusters, can be formed. Whereas vacancy clusters, such as the divacancy, are stable at room temperature [2], interstitial clusters, by nature, are not very stable. It is therefore conceivable that when they break up, interstitials are injected into the Ge during sputter deposition. Based on this we speculate that the defects we observe after sputter deposition are related to interstitial–impurity complexes (e.g. I–Sb) or vacancy or interstitial clusters, or complexes of these clusters with impurities. The signature of $E_{0.31}$ is close to that reported for the divacancy ($E_{0.29}$) [2], whereas the signatures of $E_{0.14}$, $E_{0.20}$ and $E_{0.21}$ are close to that of the $E_{0.13}$, $E_{0.19}$ and $E_{0.23}$ proposed to be related to Sb and the Ge interstitial [2].

3.4. Annealing of the metallization-induced defects

We have previously investigated the thermal stability of the defects introduced by EBD of Pt contacts by isochronal annealing in argon (Fig. 5) [7]. Only after annealing at 225 °C could the $E_{0.38}$ and $H_{0.30}$ levels no longer be detected. This is slightly higher than the 175–200 °C reported in Ref. [3] for removing the E-centre. However, it should be borne in mind that the annealing in Ref. [3] was under zero bias where most of the E-centres are filled with electrons. In our case, although we annealed at zero bias, the E-centres are very close to the surface and hence the levels of most of them are above the Fermi level. It has been reported that reverse bias annealing (E-centre level above the Fermi level) impedes the annealing of E-centres [2]. During annealing the concentration of $H_{0.26}$ increased up to 200–225 °C, rendering it the most prominent defect, and then it annealed out at 350 °C. At this temperature all the defects introduced during EBD were removed.

We have also previously investigated the thermal stability of the defects introduced by sputter deposition of Au contacts by isochronal annealing in argon [9]. After annealing at 150 °C the $E_{0.14}$, $E_{0.20}$ and $E_{0.24}$ levels could no longer be detected but the concentration of $E_{0.31}$ increased by about a factor of two. Annealing at 200 °C reduced the

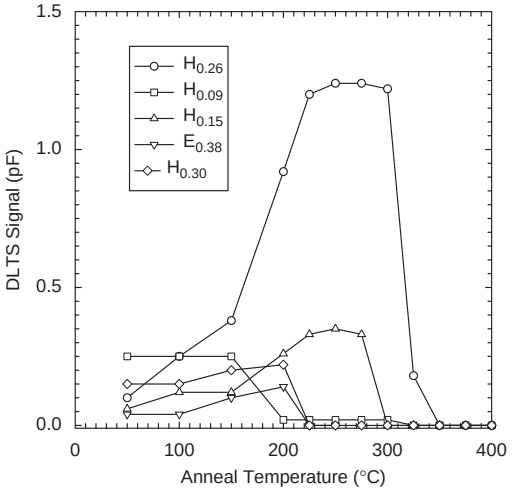

Fig. 5. Isochronal annealing (20 min periods) of the most prominent defects introduced by EBD in n-Ge [8].

concentrations of $E_{0.21}$ and $E_{0.31}$ by 10% and 30%, respectively, and annealing at 250 °C removed these defects completely, and no sputter deposition-induced defects could be detected any more. After annealing at 300 °C, no additional defects, i.e. no "second generation" defects could be observed, indicating that the sputter-deposition-induced defects did not reconstruct during annealing to form larger defects or different defect complexes.

4. Summary and conclusions

The *I–V* measurements demonstrated that both EBD and sputter deposition resulted in degraded *I–V* characteristics, but that sputter deposition yields the poorest diodes of the two metallization methods. The higher forward and reverse currents of Au Schottky contacts formed by sputter deposition and EBD as compared to resistively deposited Au contacts is most probably the result of process-induced defects that act as generation centres. Also, the sputter-deposited diode shows a significant increase in series resistance compared to the other diodes. This may be due to surface disorder introduced during the sputter deposition process.

Our DLTS results revealed that the main defect introduced during EBD has the same electronic properties as that of the V–Sb complex, or E-centre, introduced during high-energy electron irradiation of Ge. EBD also introduced several defects that are not introduced by electron irradiation, speculated to be higher-order vacancy clusters and complexes thereof with impurities. We show that the concentrations of the most prominent EBD-induced defect, the V–Sb centre, depended on the metal deposited by EBD via the melting point of the metal and the influence thereof on the vacuum during metallization: in general, low melting point metals resulted in less EBD damage. All the defects introduced by sputter deposition have also been observed after high-energy electron irradiation, but the V–Sb complex was not observed after sputter deposition. Annealing at 350 and 250 °C in Ar removed the defects introduced during EBD and sputter deposition, respectively, and annealing at higher temperatures did not introduce any new defects.

The role of these electron beam deposition and radiation-induced defects in optimising device performance for specific applications of Ge diodes will have to be carefully examined in order to ensure optimum device performance.

Acknowledgements

The authors gratefully acknowledge financial support of the South African National Research Foundation. The Laplace DLTS software and hardware used in the research was kindly provided by A.R. Peaker (Centre for Electronic Materials Devices and Nanostructures, University of Manchester) and L. Dobaczewski (Institute of Physics, Polish Academy of Sciences).

References

[1] Germanium silicon: physics and materials. In: Hull R, Bean JC, editors. Semiconductors and semimetals, vol. 56. San Diego: Academic Press; 1999.
[2] Fage-Pedersen J, Nylandsted Larsen A, Mesli A. Phys Rev B 2000;62(10):116.
[3] Markevich VP, Peaker AR, Litvinov VV, Emstev VV, Murin LI. J Appl Phys 2004;95:4078.
[4] Markevich VP, Hawkins ID, Peaker AR, Emstev KV, Emstev VV, Litvinov VV, et al. Phys Rev B 2004;70:235213–21.
[5] Markevich VP, Hawkins ID, Peaker AR, Litvinov VV, Dobaczewski L, Lindström JL. Appl Phys Lett 2002;81:1821.
[6] Auret FD, Meyer WE, Coelho SMM, Hayes M. Appl Phys Lettt 2006;88:242110.
[7] Auret FD, Meyer WE, Coelho SMM, Hayes M, Nel JM. Mater Sci Semiconductor Process 2006;9:576–9.
[8] Auret FD, Coelho SMM, Hayes M, Meyer WE, Nel JM. Phys Status Solidi (a) 2008;205(1):159–61.
[9] Auret FD, Coelho S, Meyer WE, Nyamhere C, Hayes M, Nel JM. J Electron Mater 2007;36(12):1604.
[10] Simoen E, Opsomer K, Claeys C, Maex K, Detavernier C, Van Meirhaegh RL, et al. Appl Phys Lett 2006;89:202114.
[11] Myburg G, Auret FD. J Appl Phys 1992;71:6172.
[12] Sawko DC, Bartko J. IEEE Nucl Sci 1983;30:1756.
[13] Dobaczewski L, Kaczor P, Hawkins ID, Peaker AR. J Appl Phys 1994;76:194.
[14] Dobaczewski L, Peaker AR, Bonde Nielsen K. J Appl Phys 2004;96:4689.
[15] Christensen C, Petersen JW, Nylandsted Larsen A. Appl Phys Lett 1992;61:1426.

Physica B 404 (2009) 4376–4378

Contents lists available at ScienceDirect

Physica B

journal homepage: www.elsevier.com/locate/physb

Electronic and annealing properties of the $E_{0.31}$ defect introduced during Ar plasma etching of germanium

F.D. Auret *, S.M.M. Coelho, G. Myburg, P.J. Janse van Rensburg, W.E. Meyer

Department of Physics, University of Pretoria, Pretoria, South Africa

ARTICLE INFO

PACS:
61.72.J–
61.72.uf
61.82.–d
66.30.Lw

Keywords:
Germanium
Ar plasma etching
Defects
DLTS
Annealing

ABSTRACT

Low energy (±80 eV) Ar plasma etching has been successfully used to etch several semiconductors, including GaAs, GaP, and InP. We have studied the only prominent defect, $E_{0.31}$, introduced in n-type Sb-doped Ge during this process by deep level transient spectroscopy (DLTS). The $E_{0.31}$ defect has an energy level at 0.31 eV below the conduction band and an apparent capture cross-section of 1.4×10^{-14} cm^2. The fact that no V–Sb defects and no interstitial-related defects were observed implies that the etch process did not introduce single vacancies or single interstitials. Instead it appears that higher order vacancy or interstitial clusters are introduced due to the large amount of energy deposited per unit length along the path of the Ar ions in the Ge. The $E_{0.31}$ defect may therefore be related to one of these defects. DLTS depth profiling revealed the $E_{0.31}$ concentration had a maximum (6×10^{13} cm^{-3}) close to the Ge surface and then it decreased more or less exponentially into the Ge. Finally, annealing at 250 °C reduced the $E_{0.31}$ concentration to below the DLTS detection limit.

1. Introduction

The low effective mass of holes in Ge has opened up the possibility of using Ge in ultrafast complimentary metal-oxide-semiconductor devices [1]. This, in turn, has sparked renewed interest in the properties of defects in Ge because defects ultimately determine the performance of devices. In recent studies the properties of the defects introduced during high energy gamma-, electron- and proton irradiation of Ge were reported [2–5]. We have reported the properties of defects introduced in Ge during electron beam deposition of various metals [6–8] and sputter deposition of Au [9]. However, no investigations regarding the defects introduced in Ge during surface cleaning processes, e.g. sputter and plasma etching, have been reported yet. These investigations are important because it is well known that the low energy ions utilized in these processes introduces defects at and close to the metal-semiconductor junction [10]. These defects influence device performance and alter the barrier heights of the contacts [6–9]. The defects responsible for these barrier adjustments are formed when energetic particles strike the semiconductor surface and interact with the semiconductor.

In this study we report the electronic properties of defects introduced in n-type Ge during low energy (±80 eV) inductively coupled plasma (ICP) Ar etching. We show that this process introduces only one prominent electron trap with an energy level at $E_C-0.31$ eV. It is noteworthy that no defects involving single vacancies and interstitials were introduced by ICP etching.

2. Experimental procedure

We have used bulk-grown (111) n-type material doped with Sb to a level of 2.5×10^{15} cm^{-3} for this experiment. The samples were first degreased and then etched in a mixture of H_2O_2:H_2O (1:5, 30% H_2O_2) for 1 min. Directly after cleaning they were inserted into a vacuum chamber where AuSb (0.6% Sb) was resistively deposited on their back surfaces. The samples were then annealed at 350 °C in Ar for 10 min to obtain low resistivity ohmic contacts. Next, four samples were etched in an inductively coupled plasma (ICP) for times as indicated in Table 1. On three of the samples Pd contacts, 0.60 mm in diameter and 100 nm thick, were deposited (without breaking vacuum) using electron beam deposition (EBD) in the same vacuum chamber containing the ICP etcher. On the fourth, sample Pd Schottky contacts were deposited by resistive evaporation after ICP etching. It is well known that resistive evaporation does not introduce any defects in semiconductors. "Control" Pd Schottky contacts (no etching) were deposited on identical samples by resistive evaporation. Conventional deep level transient spectroscopy (DLTS) was used to study the defects introduced in the Ge during the ICP etch process.

* Corresponding author.
E-mail address: danie.auret@up.ac.za (F.D. Auret).

0921-4526/$ - see front matter © 2009 Elsevier B.V. All rights reserved.
doi:10.1016/j.physb.2009.09.028

Table 1
Sample preparation.

Sample	Plasma etching (10 min)	Electron beam deposition	Resistive evaporation
a	No	No	Yes
b	No	Yes	No
c	Yes	No	Yes
d	Yes	Yes	No

3. Results and discussion

In Fig. 1 we depict the DLTS spectra for the control sample (curve (a)), for a sample with Pd contacts deposited by EBD without ICP etching (curve (b)), a sample that received a 10 min. ICP etch followed by resistive deposition of Pd contacts (curve (c)) and a sample that received a 10 min. ICP etch followed by EBD Pd contacts (curve (d)). Curve (a) clearly indicates that this material does not contain electron traps in measurable concentrations. The traps introduced in the Ge during EBD of Pd contacts (no ICP etching) are shown by curve (b). The two main traps are an electron trap, $E_{0.38}$, and a hole trap, $H_{0.30}$. In the nomenclature used here "E" and "H" mean electron and hole trap, respectively, and the subscripts are the activation energies determined from the Arrhenius plots in Fig. 2. These two levels have been shown to be related to the (–/-) and (-/0) charge states, respectively, of the E-center (V–Sb) in Sb-doped Ge [2,3] and have also previously been observed after EBD of Schottky contacts to Ge [6–8]. Evidently, the EBD process introduces vacancies in the Ge, at and close to the interface, that migrate and combine with, among others, Sb atoms to form Sb–V pairs. These vacancies have been proposed to be the result of energetic particles that originate in the region of the filament and then impinge on the semiconductor [11]. For comparison, we have also shown (in Fig. 2) the Arrhenius plots of the electron trap, $E_{0.38}$, and hole trap, $H_{0.30}$, associated with the E-center, as observed in a Ge sample that was irradiated with MeV electrons from a Sr^{90} radio-nuclide source. Whereas the plots for the $E_{0.38}$ align almost perfectly, there is a slight shift between the plots for the $H_{0.30}$ levels, that corresponds to about 1 K temperature difference for a given emission rate.

From curve (c) we note that ICP etching introduced only one prominent defect, $E_{0.31}$. Its properties are included in Table 2. DLTS spectra recorded under hole injection conditions revealed that no hole traps were present in this sample. It is instructive to note that no V–Sb centers or interstitial related defects [2,3] are introduced during the plasma etching of Ge. This implies that no single vacancies or interstitials were created at and below the Ge surface that could diffuse into the Ge to form the E-center. Alternatively, they were introduced at and near the surface but their migration into the Ge was impeded. This latter scenario is perhaps the most plausible because curve (d) shows that, although the contacts were deposited by EBD after ICP etching, the sample still only contains the $E_{0.31}$ defect. In this case no vacancies were injected into the Ge to form the E-center. From Fig. 2 it is also clear that the DLTS "signature" of the $E_{0.31}$ introduced by ICP etching is very different from the $E_{0.31}$ defect introduced by high-energy electron irradiation, indicating that they may be physically different defects.

We have used the fixed-bias variable pulse DLTS method to obtain the spatial distribution of the EBD and ICP etched induced defects into the Ge. From Fig. 3 we see that the $E_{0.31}$ defect is distributed much deeper (up to beyond one μm) into the Ge than the $E_{0.38}$ introduced by EBD. Furthermore, $E_{0.31}$ is significantly deeper into the Ge when the Schottky contact is deposited

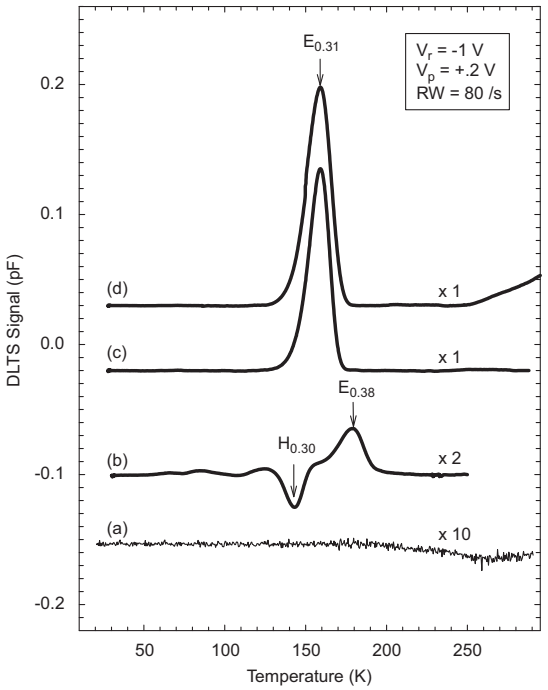

Fig. 1. DLTS spectra of resistively deposited (control) Pd Schottky contacts to n-Ge (curve (a)), of Pd Schottky contacts deposited by EBD (curve (b)), plasma etched Ge with resistively deposited Pd contacts (curve (c)) and plasma etched Ge with electron beam deposited Pd contacts (curve (d)). All spectra were recorded using a rate window of $80\,s^{-1}$ at a quiescent reverse bias of -1 V. For the electron-trap spectra the pulse, V_p, was 0.15 V into forward bias. Hole-trap spectra were obtained by applying an injection pulse of V_p=3 V into forward bias.

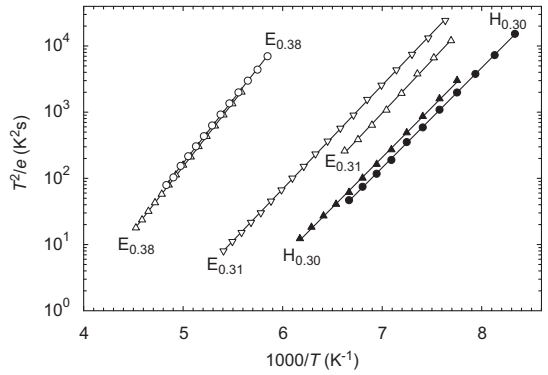

Fig. 2. Arrhenius plots traps introduced in n-type Ge by electron beam deposition (circles), high energy electron irradiation from a Sr^{90} radio-nuclide source (up triangles) and plasma etching (down triangles). Electron traps are indicated with empty symbols and hole traps by solid symbols. All data was acquired using the bias and pulsing conditions defined in the caption of Fig. 1.

afterwards by EBD. This may be defect annealing due to sample heating during the EBD process.

Finally, we have performed isochronal annealing (10 min periods, 25 °C intervals) to establish the thermal stability of

Table 2
Electronic properties of some prominent defects introduced in n-type Ge during plasma etching, Pd electron beam deposition and MeV electron irradiation.

Process	Defect	E_T (eV)	σ_a (cm^2)	T_{peak}[a] (K)	Similar defects/defect ID
Plasma etching	$E_{0.31}$	$E_C-0.31$	1.4×10^{-14}	156	–
EBD	$E_{0.38}$	$E_C-0.38$	1.0×10^{-14}	191	$E_{0.377}$[b], $E_{0.37}$[c], V–Sb (–/-)[b,c]
MeV	$H_{0.30}$	$E_V+0.30$	6.2×10^{-13}	141	$H_{0.307}$[b], $H_{0.30}$[c], V–Sb (-/0)[b]
Electron	$E_{0.38}$	$E_C-0.38$	1.1×10^{-14}	191	$E_{0.377}$[b], $E_{0.37}$[c], V–Sb (–/-)[b,c]
Irradiation	$H_{0.30}$	$E_V+0.30$	3.66×10^{-13}	142	$H_{0.307}$[b], $H_{0.30}$[c], V–Sb (-/0)[b]

[a] Peak temperature at a rate window of 80 s^{-1}.
[b] See Ref. [3].
[c] See Ref. [2].

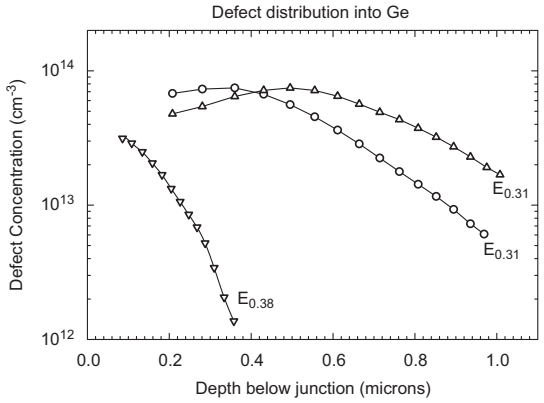

Fig. 3. DLTS depth profiles for the E-center ($E_{0.38}$) introduced by electron beam deposition (down triangles), the $E_{0.31}$ defects by plasma etching followed by resistive deposition of Pd (circles) and the $E_{0.31}$ defect introduced by plasma etching followed by electron beam deposition of Pd contacts (up triangles).

$E_{0.31}$. The DLTS measurements showed that the $E_{0.31}$ concentration remained constant up to 100 °C. Upon annealing at higher temperatures its concentration gradually decreased with increasing annealing temperature until it annealed out at 250 °C. By comparison, we have found that the E-center introduced by EBD in the same material annealed out at 225 °C.

4. Conclusions

Our results revealed that ICP Ar etching introduced only one detectable electron trap defect, $E_{0.31}$, in n-type Ge. This defect has not been observed in high energy electron irradiated Ge or after typical processing steps such as electron beam deposition, sputter deposition and ion implantation. DLTS depth profiling indicated that this defect could be detected even beyond one μm below the Pd–Ge interface. This is significantly deeper than the E-center introduced during electron beam deposition that could be detected only up to 0.4 μm below the interface in same material. The fact that no vacancy- or interstitial-related defects was detected after plasma etching (e.g. the V–Sb center) implies either that no single vacancies or interstitials are introduced, or that their migration into the Ge is impeded during the plasma etching.

EBD also introduced several defects that are not introduced by electron irradiation. Since EBD defects are introduced by heavy metal or gas ions, these defects could possibly be higher order vacancy clusters and complexes thereof with impurities. Annealing at 325 °C removed all the defects introduced during EBD of Pt Schottky contacts.

Acknowledgement

The authors gratefully acknowledge financial support of the South African National Research Foundation.

References

[1] Germanium Silicon: Physics and Materials, Semiconductors and Semimetals Vol. 56, R. Hull, J.C. Bean (Eds.), Academic Press, San Diego, 1999.
[2] J. Fage-Pedersen, A. Nylandsted Larsen, A. Mesli, Phys. Rev. B 62 (2000) 10.
[3] V.P. Markevich, A.R. Peaker, V.V. Litvinov, V.V. Emstev, L.I. Murin, J. Appl. Phys. 95 (2004) 4078.
[4] V.P. Markevich, I.D. Hawkins, A.R. Peaker, K.V. Emstev, V.V. Emstev, V.V. Litvinov, L. Dobaczewski, Phys. Rev. B 70 (2004) 235213.
[5] V.P. Markevich, I.D. Hawkins, A.R. Peaker, V.V. Litvinov, L. Dobaczewski, J.L. Lindström, Appl. Phys. Lett. 81 (2002) 1821.
[6] F.D. Auret, W.E. Meyer, S. Coelho, M. Hayes, Appl. Phys. Lett. 88 (2006) 242110.
[7] F.D. Auret, W.E. Meyer, S. Coelho, M. Hayes, J.M. Nel, Mater. Sci. Semicond. Process. 9 (2006) 576.
[8] F.D. Auret, S.M.M. Coelho, M. Hayes, W.E. Meyer, J.M. Nel, Phys. Status Solidi (a) 205 (2008) 159.
[9] F.D. Auret, S. Coelho, W.E. Meyer, C. Nyamhere, M. Hayes, J.M. Nel, J. Electron. Mater. 36 (2007) 1604.
[10] P.N.K. Deenapanray, F.D. Auret, G. Myburg, J. Vac. Sci. Technol. B 16 (1998) 1873.
[11] C. Christensen, J.W. Petersen, A. Nylandsted, Larsen, Appl. Phys. Lett. 61 (1992) 1426.

Journal of Alloys and Compounds 513 (2012) 44–49

Contents lists available at SciVerse ScienceDirect

Journal of Alloys and Compounds

journal homepage: www.elsevier.com/locate/jallcom

Effect of thermal treatment on the characteristics of iridium Schottky barrier diodes on n-Ge (1 0 0)

A. Chawanda[a,b,*], S.M.M. Coelho[a], F.D. Auret[a], W. Mtangi[a], C. Nyamhere[c], J.M. Nel[a], M. Diale[a]

[a] Department of Physics, University of Pretoria, 0002, South Africa
[b] Department of Physics, Midlands State University, Bag 9055, Gweru, Zimbabwe
[c] Department of Physics, Nelson Mandela Metropolitan University, Box 77000, Port Elizabeth 6031, South Africa

ARTICLE INFO

Article history:
Received 22 November 2010
Received in revised form
16 September 2011
Accepted 19 September 2011
Available online 6 October 2011

Keywords:
Schottky contact
Germanium
Annealing
Ideality factor
Agglomeration

ABSTRACT

Iridium (Ir) Schottky barrier diodes were deposited on bulk grown (1 0 0) Sb-doped *n*-type germanium by using the electron beam deposition system. Electrical characterization of these contacts using current–voltage (*I–V*) and capacitance–voltage (*C–V*) measurements was performed under various annealing conditions. The variation of the electrical properties of these Schottky diodes can be attributed to combined effects of interfacial reaction and phase transformation during the annealing process. Thermal stability of the Ir/n-Ge (1 0 0) was observed up to annealing temperature of 500 °C. Furthermore, structural characterization of these samples was performed by using a scanning electron microscopy (SEM) at different annealing temperatures. Results have also revealed that the onset temperature for agglomeration in a 20 nm Ir/n-Ge (1 0 0) system occurs between 600 and 700 °C.

1. Introduction

Schottky barrier diodes (SBDs) have already been studied for more than 50 years and they have been used in many applications such as gates for metal-semiconductor field-effect transistors, solar cells, and detectors [1–4]. Schottky contacts play an important role in controlling the electrical performances of semiconductor devices and Schottky barrier height (SBH) which is highly sensitive to thermal treatment [5]. Microelectronics has primarily been a Si-based technology because of the stability and high quality of SiO_2 [6], as stability and reproducibility of contact properties are essential prerequisites for device development [2,7,8]. As the scaling of silicon complementary metal-oxide semiconductor (CMOS) devices becomes more and more challenging, both innovative structures and new materials with high carrier mobility are needed to continue improving the device performance [9]. Germanium (Ge) has been regarded as a possible replacement for Si as the channel material in future high-speed CMOS technology, because it offers two times higher intrinsic electron mobility and four times higher intrinsic hole mobility than Si [10]. The lack of a stable native Ge oxide has been the obstacle in the use of Ge in CMOS devices [11]. However, recent developments of the next generation deposited high-*k* gate dielectrics allow for the fabrication of high performance Ge-based metal-oxide semiconductor field effect transistors (MOSFETs) [11,12]. Low reactivity with oxygen in the high-*k* dielectric is expected in the germanide/high-k gate stack structure [13].

Although in previous studies focus has been on the reactions of germanium with Pd [6,14–23], Pt [6,13,22,24–29], and Ni [6,9,11,13–16,22,28–38], so far there is very little literature on reactions of germanium with Ir [39]. Gaudet et al. [6] carried out a systematic study of thermally induced reaction of 20 transition metals with Ge substrates. They monitored metal-Ge reactions in situ during ramp anneals at 3 °C s^{-1} using time-resolved X-ray diffraction, diffuse light scattering, and resistance measurements. Their results show that Fe, Co, Ni, Pd, Pt, and Cu were the most promising candidates for microelectronic applications. A reduction of the PtGe/Ge electron SBH by rapid thermal diffusion of phosphorous was reported by Henkel et al. [24]. Their results show that rapid thermal diffusion from a solid diffusion doping source is effective in reducing SBHs of platinum germanide SBDs on Ge. Saedi et al. [25] reported a scanning tunneling microscopy and spectroscopy study of the formation of platinum–germanide phases on Ge (1 1 1). Chawanda et al. [28] investigated the change in the (*I–V*) electrical properties of Pt-, Ni- and Ti Schottky diodes on n-Ge (1 0 0) at different annealing temperatures. Their results reveal that the as-deposited barrier heights have values that are near the bandgap of Ge for Pt/-, Ni/- and Ti/n-Ge (1 0 0) Schottky

* Corresponding author at: Department of Physics, University of Pretoria, 0002, South Africa. Tel.: +27 12 420 3508; fax: +27 12 362 5288.
E-mail address: albert.chawanda@up.ac.za (A. Chawanda).

0925-8388/$ – see front matter © 2011 Elsevier B.V. All rights reserved.
doi:10.1016/j.jallcom.2011.09.053

diodes resulting in good Schottky source/drain contact materials in p-channel Ge-MOSFETS, for the hole injection from source into inverted p-channel [40]. Peng et al. [36] reported on the *I–V* characteristics of Ni/n-Ge (1 0 0) Schottky diodes and the nickel germanide induced strain after subjecting the Schottky contacts to rapid thermal anneal in the temperature range of 300–600 °C. Their results also show that the orthorhombic structure of NiGe induces epitaxial tensile strain on Ge substrate due to the difference in lattice constants. They also suggested that the increase in barrier height with increasing annealing temperature may be due to the conduction band edge shift by the strain after germanidation process. Peng et al. [37] have also reported micro-Raman studies on nickel germanides formed on (1 1 0) crystalline Ge. Their results reveal that Ni_5Ge_3, NiGe and Ni_2Ge phases are formed sequentially with increasing annealing temperatures from 300 °C to 600 °C on n-Ge (1 1 0) substrate. Perrin et al. [38] investigated the phase formation and growth kinetics for both Ni–Si and Ni–Ge systems. They have shown that the Ni–Si system has three major phases (Ni_2Si, NiSi and $NiSi_2$) that grow sequentially while Ni–Ge system showed only two phases (Ni_5Ge and NiGe) that grow simultaneously. Habanyama and Comrie [39] used ion beam analysis employing micro-Rutherford backscattering spectrometry to investigate the interaction between germanium and iridium in a lateral diffusion couple. Their results indicate that the germanide phase Ir_3Ge_7 stretches across the original island interface at all annealing temperatures, with a phase Ir_4Ge_5 forming in the reaction region with unreacted iridium. The phase $IrGe_4$ was observed to nucleate in the middle of the island at annealing temperatures above 800 °C.

In this work we investigate the change in the electrical properties of Ir Schottky barrier diode on n-Ge (1 0 0) at different annealing temperatures in the temperature range 25–500 °C. Results presented here reveal the effects of thermal treatment, particularly the combined effects of interfacial reaction and phase transition [41] of Ir/n-Ge (1 0 0) Schottky barrier diodes using the *I–V* and *C–V* characteristics. Furthermore, morphological evolution of Ir films on n-Ge (1 0 0) is studied using the scanning electron microscopy (SEM) characterization method.

2. Experimental procedures

To study the thermal annealing effects on the Schottky barrier diode, we have used bulk-grown (1 0 0) oriented n-type Ge doped with antimony (Sb) to a density of $(1.5–2.0) \times 10^{15}$ cm^{-3} and supplied by Umicore. Before metallization, the samples were first degreased and subsequently etched in a mixture of H_2O_2 (30%): H_2O (1:5) for 1 min. Immediately after cleaning they were inserted into a vacuum chamber where AuSb (0.6% Sb), 120 nm thick, was deposited by resistive evaporation on their back surfaces as ohmic contacts. The samples were then annealed at 350 °C in Ar ambient for 10 min to minimize the contact resistivity of the ohmic contacts [42]. Before Schottky barrier diodes deposition, the samples were again chemically cleaned as described above. Ir Schottky barrier diodes were deposited onto Ge wafers using electron beam evaporation through a mechanical mask. The contacts were (0.60 ± 0.05) mm in diameter and 20 nm thick. The metal thickness layer and deposition rates were monitored by using an INFICON XTC 751-001-G1 quartz crystal thickness monitor. After Schottky barrier diode fabrication, the samples were characterized by *I–V* measurements at room temperature to determine the quality of the diodes. The Schottky barrier diodes were then isochronally annealed in an oven under Ar ambient in the temperature range 25 °C to 500 °C in steps of 25 °C for 30 min. *I–V* and *C–V* characteristic measurements followed each additive annealing cycle. Characterization of the Ir films at different annealing temperatures was accomplished using a ZEISS ULTRA PLUS Scanning electron microscopy (SEM) system operating at 1 kV.

3. Results and discussion

The Schottky barrier heights of the diodes were deduced from *I–V* characteristics, which were analyzed by using the thermionic emission model [7,43]:

$$I(V) = I_o \exp\left(\frac{qV}{nkT}\right)\left[1 - \exp\left(-\frac{qV}{kT}\right)\right] \quad (1)$$

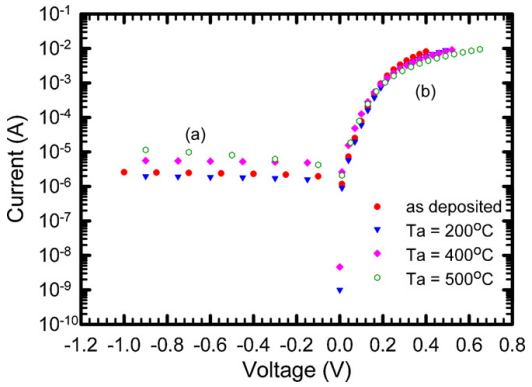

Fig. 1. Experimental (a) reverse and (b) *I–V* characteristics of one of the Ir/n-Ge (1 0 0) Schottky barrier diodes after isochronal thermal treatment for 30 min at different annealing temperatures: as-deposited, 200 °C, 400 °C and 500 °C.

where I_o is the reverse saturation current given by the following relation [44,45]:

$$I_o = AA^*T^2 \exp\left(-\frac{q\Phi_B}{kT}\right), \quad (2)$$

obtained from the straight line intercept of $\ln I$ at $V = 0$, A^* is the effective Richardson constant, A is the diode area, T the measurement temperature, k the Boltzmann constant, Φ_B is the zero bias effective Schottky barrier height (SBH), q is the electronic charge and n the ideality factor which can be determined accurately from the slope of the linear part of a $\ln I$ versus V plot, assuming pure thermionic emission can be obtained from Eq. (1) as

$$n = \frac{q}{kT}\frac{dV}{d(\ln(I))} \quad (3)$$

The value on n is equal to 1.0 for an ideal diode and usually has a value greater than unit.

We fabricated eight Ir/n-Ge (1 0 0) Schottky barrier diodes (SBDs). Fig. 1 shows the semilog forward and reverse bias *I–V* characteristics of these SBDs for as-deposited samples and after annealing the samples in the temperature range of 25–525 °C. Since the annealing temperature range is wide, we have assumed that the change in thermal properties of Ir/n-Ge (1 0 0) SBDs (e.g. thermal expansion) have negligible effects on our results. Using Eq. (2) and intercept of the straight line fit of the semilog-forward bias *I–V* graph the value of effective SBH is determined.

Fig. 2 presents the variation of the Schottky barrier height and reverse current at −1 V with annealing temperature for the Ir Schottky diodes. The SBH and reverse current at a bias voltage of −1 V for as-deposited Ir Schottky diodes were found to be (0.574 ± 0.005) eV and (2.57 ± 0.02) μA, respectively. After annealing at temperatures higher than 200 °C, the Schottky barrier height (SBH) drops significantly, reaching (0.542 ± 0.005) eV after a 400 °C anneal. We suggest that there is a significant reaction between Ir and Ge. The change coincides with the initial phase formation of the germanides IrGe and Ir_4Ge_5, which have been reported by Habanyama and Comrie [39] to coexist and form at annealing temperatures around 350 °C. Bhan and Schubert [46] also reported the phases IrGe and Ir_4Ge_5 to coexist in bulk diffusion couples. The change in the barrier height after the 400 °C anneal coincides with the temperature of formation of Iridium germanide Ir_3Ge_7, reported by Habanyama and Comrie [39] to form after 400 °C anneal. Fig. 2 also depicts that, throughout the annealing process the reverse current at −1 V remains in the same order of magnitude, 10^{-6} A. Annealing at temperatures higher than 500 °C resulted in near ohmic contacts and

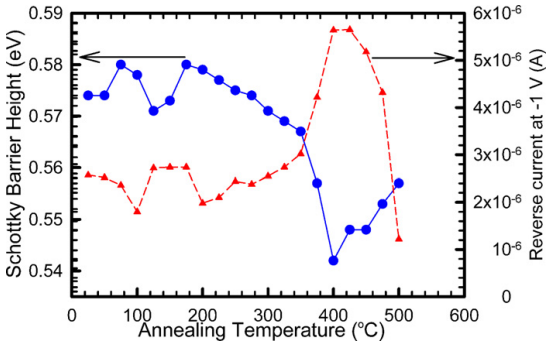

Fig. 2. Plot of the Schottky barrier height and reverse current at −1 V as a function of annealing temperature for Ir/n-Ge (1 0 0) Schottky barrier diode.

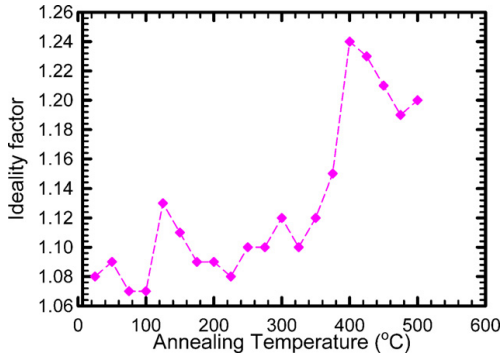

Fig. 3. Plot of ideality factor as a function of annealing temperature for Ir/n-Ge (1 0 0) Schottky barrier diode

further analysis of the *I–V* and *C–V* characteristics of the Ir Schottky barrier diodes was not possible. These results show that Ir/n-Ge (1 0 0) Schottky diodes are thermally stable over a wide range of temperature, 25–500 °C. Similar results have been reported by [6,23,28]. Pd/n-Ge Schottky diodes have been observed to be stable over a wide temperature range 25–525 °C [6,23]. Pt/n-Ge Schottky diodes have been reported to be thermally stable in the temperature range of 25–600 °C [28].

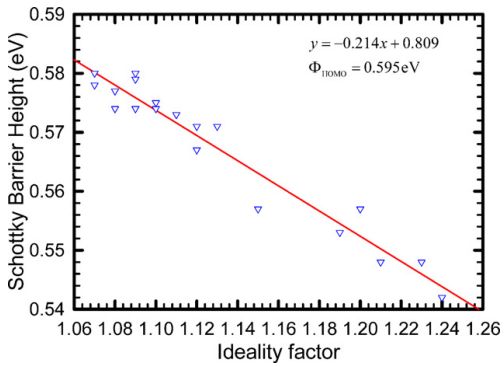

Fig. 4. The plot of Schottky barrier heights as a function of their respective ideality factors of Ir/n-Ge (1 0 0) Schottky barrier diode at various annealing temperatures.

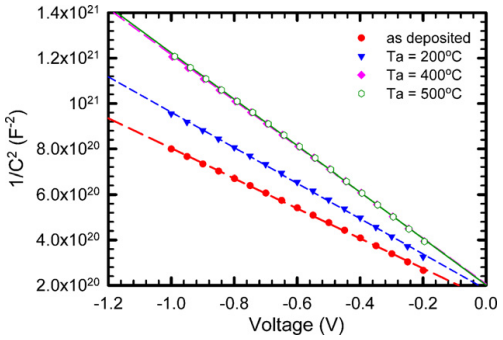

Fig. 5. Reverse bias C^{-2}–V characteristics of one of the Ir/n-Ge (1 0 0) Schottky barrier diodes frequency of 1 MHz after isochronal treatment for 30 min at different annealing temperatures: as-deposited, 200 °C, 400 °C and 500 °C.

The SBH is likely to be a function of the interface atomic structure, and atomic inhomogeneities at MS interface which are caused by grain boundaries, multiple phases, facets, defects, a mixture of different phases, etc. [47,48]. It is well known that the chemical reactions between metals and semiconductors at interfaces can play an important role in the electrical properties of devices. Boyarby et al. [49] suggested that the recent motivation for studying Schottky barrier formation is due to the recognition that both electronic and chemical equilibrium have to be considered together across a reactive interface between metal and semiconductor, as surface states and metal-induced gap states failed to take into consideration the chemical equilibrium at interface. The chemical equilibrium after a heat treatment results in interfacial atomic rearrangement, interdiffusion, and compound formation, which should have a profound effect on the electronic equilibrium producing the Schottky barrier [50]. Hence, the change in Schottky barrier heights may be attributed to combined effects of interfacial reaction and phase transformation [51].

The ideality factor was calculated from the gradient of the linear region of the experimental ln *I–V* characteristics in forward bias [7]. The variation of the Ir Schottky diodes ideality factor as a function of annealing temperature is shown in Fig. 3. The as-deposited value of the ideality factor was found to be 1.08. At annealing temperatures between 275 and 500 °C, ideality factors significantly greater than 1.1 indicate that the transport properties are not well modeled by thermionic emission alone although their contacts remain rectifying [52]. The non-idealities are mostly

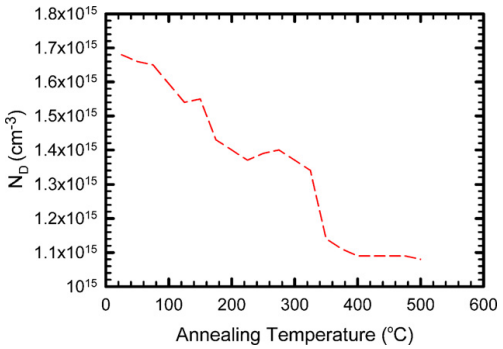

Fig. 6. The variation of non-compensated ionized donors (N_D) concentration with annealing temperature.

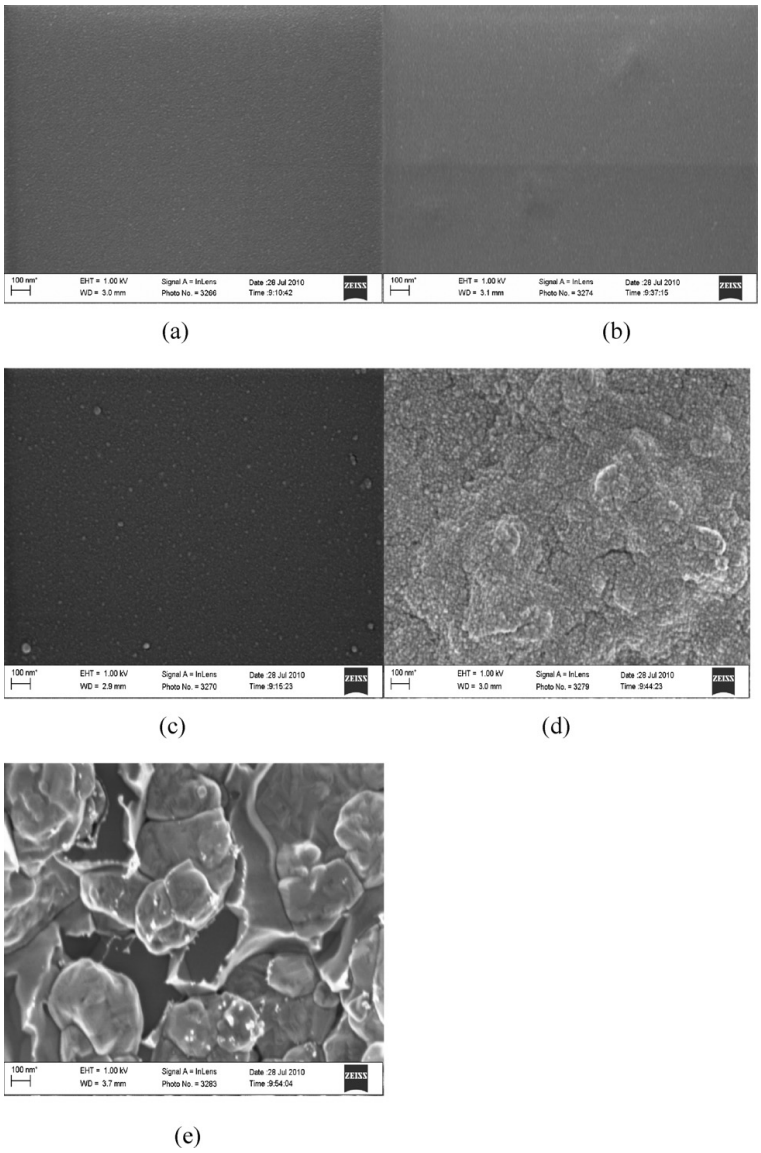

Fig. 7. SEM observations for Ir films on germanium after isochronal thermal treatment for 30 min at different annealing temperatures: (a) as-deposited, (b) 400 °C, (c) 500 °C, (d) 600 °C and (e) 700 °C.

due to the states associated with the defects near the surface of the semiconductor [7]. In a Schottky contact, even with a good surface treatment, there is an interfacial oxide layer of thickness about 1 nm with considerable amount of surface states [7]. These interface states, and inter-diffusion, chemical reaction, compound formation, defects generation, etc. can all be derived from thermodynamics due to thermal annealing [8,53,54]. These may result in the formation of recombination centres [52] and SBH inhomogeneities [55], which cause an excess current leading to a deviation from the ideal thermionic emission behaviour. Additionally, there are other sources of SBH inhomogeneity. For instance, there may be a mixture of different metallic phases with different SBHs due to incomplete interfacial reaction, and doping inhomogeneity at a MS interface [56]. Thus, the current across the MS contact may be mainly due to the presence of SBH inhomogeneity and this inhomogeneity leads to large ideality factors.

Fig. 4 shows a plot of the SBHs as a function of their respective ideality factors, obtained from the annealing process in the temperature range 25–500 °C. The straight line in Fig. 4 is the least-squares fit to experimental data. Since the results show a linear correlation between SBHs and ideality factors, we extrapolated the plot to $n = 1.0$, and obtained a laterally homogeneous SBH of 0.595 eV

for Ir/n-Ge (1 0 0) Schottky barrier diodes. The homogeneous SBHs rather than effective SBHs of Schottky diodes or their mean values should be used to discuss theories on the physical mechanisms that determine the SBHs of MS contacts [57,58].

Fig. 5 shows the plots of Ir/n-Ge (1 0 0) Schottky barrier diodes reverse bias C^{-2}–V characteristics at 1.0 MHz at different annealing temperatures. The plots of C^{-2} as a function of reverse bias voltage are linear, indicating the formation of Schottky diodes [59], and a constant non-compensated ionized donor concentration. In Schottky diodes, the depletion layer capacitance (C), can be expressed as [2,7]:

$$\frac{1}{C^2} = \frac{2(V_0 - V)}{q\varepsilon_s A^2 N_D} \quad (4)$$

where A is the area of the diode, ε_s is the permittivity of semiconductor, N_D is the concentration of non-compensated ionized donors, that can be temperature dependent, V is the magnitude of the reverse bias and V_0 is the diffusion potential at zero bias. From Eq. (4), the values of V_0 and N_D can be determined from the intercept and slope of the C^{-2}–V plot. The C–V SBH for as-deposited Ir/n-Ge (1 0 0) Schottky barrier diode was found to be (0.473 ± 0.005) eV. Due to the different nature of the measurement techniques, SBHs obtained from I–V and C^{-2}–V are not always the same [60]. Although, in general, SBHs from C–V measurements are higher than SBHs from I–V measurements, in our study, we obtained I–V SBHs that were higher than C–V SBHs. Similar results have been reported [35]. Therefore, further studies are needed to clarify these results. Fig. 6 depicts the variation of non-compensated ionized donor concentration with annealing temperature. The non-compensated ionized donor concentration decreases with annealing temperature. Similar results have been reported by Serin [61], Nuhoglu and Gulen [62] and Opsomer et al. [63]. This may be due to either presence of high density of compensating deep acceptor levels [61], possibly related to in-diffused Ir or the decrease in the dangling bonds due to annealing [62] and formation of Iridium germanide [39].

SEM observations were conducted for Ir/n-Ge (1 0 0) samples, as-deposited and after annealing at different temperatures. The morphological evolution is shown in Fig. 7. As seen in Fig. 7(a) and (b), metal surfaces show little change when samples were annealed below 400 °C. Grain growth at the surface (see Fig. 7(c)) were evident after a 500 °C anneal, indicating inception of agglomeration. Agglomeration starts with grain boundary grooving and progresses to island formation [64]. We observed development of severe grain grooving after a 600 °C anneal (see Fig. 7(d)). We also observed that after 700 °C anneal (see Fig. 7(e)), film continuity was severely interrupted as revealed by dark spots caused by exposed Ge regions. From these observations we conclude that the onset of the agglomeration process for 20 nm Ir/n-Ge (1 0 0) system occurs between 600 and 700 °C. The morphological degradation for Ni–Ge, Pd–Ge and Pt–Ge begins at 580, 550, and 600 °C, respectively [6,28]. We suggest a good morphological stability for Ir germanide films up to 500 °C.

4. Conclusions

Ir Schottky barrier diodes were fabricated by using an electron beam deposition system. The Schottky barrier diodes behaviour was investigated under various annealing conditions. The variation of Schottky barrier heights and ideality factors with annealing may be attributed to interfacial reactions of Ir with germanium and phase transformation of Ir germanides during the annealing process. The electrical properties reveal that Ir Schottky barrier diodes are of high quality with low reverse currents at −1 V of the order 10^{-6} A and as-deposited ideality factors as low as 1.08. The homogeneous SBH value of 0.595 eV for the Schottky barrier diodes was obtained from the linear relationship between SBHs and their respective ideality factors. The homogeneous SBH near the bandgap of Ge in Ir/n-Ge (1 0 0) Schottky barrier diodes imply good Schottky source/drain contact material in p-channel Ge-MOSFETS, for the hole injection from source into inverted p-channel [40]. Thermal stability of the Ir/n-Ge (1 0 0) Schottky barrier diodes is maintained up to annealing temperature of 500 °C. Furthermore, SEM observations were conducted for samples annealed at different temperatures, and the results depict that the onset temperature for agglomeration in 20 nm Ir/n-Ge (1 0 0) system occurs between 600 and 700 °C. From these results we conclude that Ir is a promising candidate for its use as first level interconnections in Ge-based microelectronic circuits.

Acknowledgements

This work has been made possible by financial assistance from the South African National Research Foundation. The authors gratefully acknowledge SEM observation measurements by Helena Steyn.

References

[1] E. Hökelek, G.Y. Robinson, Solid State Electron. 99 (1981) 24.
[2] E.H. Rhoderick, R.H. Williams, Metal-semiconductor Contacts, Clarendon Press, Oxford, 1988.
[3] G.A. Barti, M. Schlilter, Phys. Rev. B 33 (1986) 7346.
[4] A. Asubay, Ö. Güllü, A. Türüt, Appl. Surf. Sci. 254 (2008) 3558.
[5] A.R. Saha, S. Chattopadhyay, C.K. Maiti, Mater. Sci. Eng. B 114–115 (2004) 218.
[6] S. Gaudet, C. Detavernier, A.J. Kellock, P. Desjardins, C. Lavoie, J. Vac. Sci. Technol. A 24 (2006) 474.
[7] S.M. Sze, Physics of Semiconductor Devices, 2nd ed., Wiley, New York, 1981.
[8] T. Sands, Appl. Phys. Lett. 52 (1988) 197.
[9] H. De-Dong, L. Xiao-Yan, K. Jin-Feng, X. Zhi-Liang, D. Gang, H. Ru-Qi, Chin. Phys. 14 (2005) 1041.
[10] R. Li, H.B. Yao, S.J. Lee, D.Z. Chi, M.B. Yu, G.Q. Lo, D.L. Kwong, Thin Solid Films 504 (2006) 28.
[11] D.Z. Chi, H.B. Yao, S.L. Liew, C.C. Tan, C.T. Chua, K.C. Chua, R. Li, S.J. Lee, 7th International Workshop on Junction Technology Proceeding, 2007.
[12] C.O. Chui, S. Ramanathan, B.B. Triplett, P.C. McIntyre, K.C. Saraswat, IEEE Electron Dev. Lett. 23 (2002) 473.
[13] D. Ikeno, Y. Kaneko, H. Kondo, M. Sakashita, A. Sakai, M. Ogawa, S. Zaima, Jpn. J. Appl. Phys. 46 (2007) 1865.
[14] A. Thanailakis, D.C. Northrop, Solid State Electron. 16 (1973) 1383.
[15] M. Wittmer, M.-A. Nicolet, J.W. Mayer, Thin Solid Films 42 (1977) 51.
[16] I. Abbati, G. Rossi, L. Braicovich, I. Lindau, W.E. Spicer, Appl. Surf. Sci. 9 (1981) 243.
[17] G. Majni, G. Ferrari, C. Canali, F. Catellani, G. Ottaviani, G. Della Mea, Thin Solid Films 47 (1977) 193.
[18] G. Ottaviani, G. Majni, G. Ferrari, R. Ferrari, M. Prudenziati, S.S. Lau, Thin Solid Films 47 (1977) 187.
[19] G. Ottaviani, G. Majni, C. Canali, Appl. Phys. 18 (1979) 285.
[20] Y.F. Hsieh, L.J. Chen, Thin Solid Films 162 (1988) 295.
[21] C.L. Churms, C.M. Corie, R.S. Nemtudi, Nucl. Instr. Methods B 158 (1999) 713.
[22] E. Simoen, K. Opsomer, C. Claeys, K. Maex, C. Detavernier, R.L. Van Meirhaeghe, P. Clauws, J. Electrochem. Soc. 154 (2007) H857.
[23] A. Chawanda, C. Nyamhere, F.D. Auret, W. Mtangi, T.T. Hlatshwayo, M. Diale, J. Nel, Physica B 404 (2009) 4482.
[24] C. Henkel, S. Abermann, O. Bethege, G. Pozzovivo, S. Puchner, H. Hutter, E. Bertagnolli, J. Electrochem. Soc. 157 (2010) H815.
[25] A. Saedi, B. Poelsema, H.J.W. Zandvliet, Surf. Sci. 605 (2011) 507.
[26] V. Janardhanam, J.-S. Kim, K.-W. Moon, K.-S. Ahn, C.-J. Choi, Microelectron. Eng. (2011), doi:10.1016/j.meee.2011.04010.
[27] R.S. Nemutudi, C.M. Comrie, C.L. Churns, Thin Solid Films 358 (2000) 270.
[28] A. Chawanda, C. Nyamhere, F.D. Auret, W. Mtangi, M. Diale, J.M. Nel, J. Alloys Compd. 492 (2009) 649.
[29] C. Nyamhere, A. Chawanda, A.G.M. Das, F.D. Auret, M. Hayes, Physica B 401–402 (2007) 226.
[30] T. Nishimura, O. Nakatsuka, Y. Shimura, S. Takeuchi, B. Vincent, A. Vantome, J. Dekoster, M. Caymax, R. Loo, S. Zaima, Solid-State Electron. 60 (2011) 46.
[31] H.-X. Liu, X.-F. Wu, S.-G. Hu, L.-C. Shi, Chin. Phys. B 19 (2010) 057303.
[32] J.K. Patterson, B.J. Park, K. Ritly, H.Z. Xiao, L.H. Allen, A. Rockett, Thin Solid Films 253 (1994) 456.
[33] K.Y. Lee, S.L. Liew, S.J. Chua, D.Z. Chi, H.P. Sun, X.Q. Pan, Mater. Res. Soc. Symp. Proc. 810 (2004), C.2.4.1.
[34] D. Han, Y. Wang, D. Tian, W. Wang, X. Liu, J. Kang, R. Han, Microelectron. Eng. 82 (2005) 93.
[35] A. Chawanda, J. Nel, F.D. Auret, W. Mtangi, C. Nyamhere, M. Diale, L. Leach, J. Kor. Phys. Soc. 57 (2010) 1970.

[36] C.-Y. Peng, Y.-H. Yang, C.-M. Lin, Y.-J. Yang, C.-F. Huang, C.W. Liuv, International Conference on Solid-state and Integrated Circuits Technology Proceedings (ICSICT), 2008, p. 681, art. no. 4734645.
[37] C.-Y. Peng, C.-F. Huang, Y.-H. Yang, C.W. Liu, ECS Trans. 16 (2008) 249.
[38] C. Perrin, D. Mangelinck, F. Nemouchi, J. Labar, C. Lavoie, C. Bergman, P. Gas, Mater. Sci. Eng. B 154–155 (2008) 163.
[39] A. Habanyama, C.M. Comrie, Thin Solid Films 516 (2008) 5137.
[40] H.B. Yao, C.C. Tan, S.L. Liew, C.T. Chua, C.K. Chua, R. Li, R.T.P. Lee, S.J. Lee, D.Z. Chi, International Workshop on Junction Technology Proceeding, 2006, p. 64.
[41] Y. Sun, X.M. Shen, J. Wang, D.G. Zhao, G. Feng, Y. Fu, Y. Fu, S.M. Zhang, Z.H. Zhang, Z.H. Feng, Y.X. Bai, H. Yang, J. Phys. D: Appl. Phys. 35 (2002) 2648.
[42] F.D. Auret, P.J. Janse van Rensburg, M. Hayes, J.M. Nel, S. Coelho, W.E. Meyer, S. Decoster, V. Matias, A. Vantomme, D. Smeets, Nucl. Instr. Methods B 257 (2007) 169.
[43] I.S. Yahia, M. Fadel, G.B. Sark, F. Yakuphanoglu, S.S. Shenouda, W.A. Farooq, J. Alloys Compd. 509 (2011) 4414.
[44] H. Uslu, S. Altindal, U. Aydemir, I. Dokme, I.M. Afandiyeva, J. Alloys Compd. 503 (2010) 96.
[45] F. Yakuphanoglu, J. Alloys Compd. 494 (2010) 451.
[46] S. Bhan, K. Schubert, Z. Metallkd. 51 (1960) 327.
[47] J.P. Sullivan, R.T. Tung, M.R. Pinto, W.R. Graham, J. Appl. Phys. 70 (1991) 7403.
[48] R.T. Tung, Mater. Sci. Eng. Rep. 35 (2001) 1.
[49] B. Boyarby, H. Çetin, M. Kaya, E. Ayyildiz, Microelectron. Eng. 85 (2008) 721.
[50] R.D. Thomson, K.N. Tu, J. Appl. Phys. 53 (1982) 4285.
[51] Y. Sun, X.M. Shen, J. Wang, D.G. Zhao, G. Feng, Y. Fu, S.M. Zhang, Z.H. Zhang, Z.H. Feng, Y.X. Bai, H. Yang, J. Phys. D: Appl. Phys. 35 (2002) 2648.
[52] H. Doğan, N. Yildirim, A. Turut, Microelectron. Eng. 85 (2008) 655.
[53] S.K. Cheung, N.W. Cheung, Appl. Phys. Lett. 49 (1986) 85.
[54] J.L. Everaet, R.L. Van Meirhaeghe, W.H. Laflere, F. Cardon, Semicond. Sci.Technol. 5 (1990) 60.
[55] R.T. Tung, J.P. Sullivan, F. Schrey, Mater. Sci. Eng. B 14 (1992) 266.
[56] M. Soylu, F. Yakuphanoglu, J. Alloys Compd. 506 (2010) 418.
[57] R.F. Schmitsdorf, T.U. Kampen, W. Mönch, J. Vac. Sci. Technol. B 15 (1997) 1221.
[58] H. Çetin, B. Şahin, E. Ayyilidiz, A. Turut, Semicon. Sci. Technol. 19 (2004) 1113.
[59] V. Saxen, R. Prakash, Polym. Bull. 45 (2000) 267.
[60] G. Güler, Ş. Karataş, Ö. Güllü, Ö.F. Bakkaloğlu, J. Alloys Compd. 486 (2009) 343.
[61] T. Serin, Turk. J. Phys. 22 (1998) 423.
[62] C. Nuhoglu, Y. Gulen, Vacuum 84 (2010) 812.
[63] K. Opsomer, E. Simoen, C. Clayes, K. Maex, C. Detaernier, R.L. Van Meirhaeghe, S. Forment, P. Clauws, Mater. Sci. Semicond. Process. 9 (2006).
[64] K.Y. Lee, S.L. Liew, S.J. Chua, D.Z. Chi, H.P. Sun, X.Q. Pan, Mater. Res. Symp. 810 (2004) 55.

4.8 Summary

Results obtained have already appeared in the articles that were included in this chapter. However, it is useful to repeat a few important results:

- From early on good SBDs were produced with an ideality of 1.07 (section 4.2) that were later improved further (section 4.3.2).
- EBD was found to introduce a number of electron and hole traps near the germanium surface, the V-Sb complex or E-center being one of them (section 4.3). Two additional electron traps were observed when EBD was performed with the vacuum chamber backfilled with forming gas up to a pressure of 10^{-4} mbar.
- A number of new defects, both electron and hole traps, were observed when germanium was exposed to the condition of EBD without metal deposition (EBE). At least eight of these defects have not been reported on before (section 4.3.2).
- SD of Au introduced a number of defects that were also observed after MeV electron irradiation. RE produced superior diodes to SD, especially when compared at operating temperatures below 300 K (section 4.4).
- ICP treatment of the germanium surface prior to SBD evaporation resulted in diodes being produced with excellent rectifying qualities when measured at low temperatures (section 4.5).
- ICP etching of germanium was found to introduce only one defect, $E_{0.31}$, with a distribution that was measured up to a micrometre into the germanium sample. EBD on ICP etched germanium failed to introduce the defects that were previously seen after EBD. $E_{0.31}$ had not been reported on previously, but subsequently was also found after low energy (300 eV) argon RF sputtering, hydrogen plasma exposure and helium plasma exposure (section 4.5 and the abstracts therein).
- Thermal annealing kinetics studies of $E_{0.31}$ suggest that it anneals out by diffusion, however, once it had been removed could then not be reintroduced by further ICP treatment (section 4.5).

- Defects introduced by MeV electron and alpha-particle irradiations were characterized. Their energy levels, apparent capture cross-sections and DLTS peak temperatures for an 80 s^{-1} rate window have been listed in section 4.7.
- Annealing of the prominent defects introduced by EBD revealed that they were all annealed out after a 350 °C treatment (section 4.7).

Conclusions drawn from these results will be presented in the following chapter.

Chapter 5

Conclusions

This chapter summarises the conclusions from the articles that are included in chapter 4. Most of the conclusions listed in Section 5.1 have already been discussed in the aforementioned articles in great detail but in some instances insight gained from follow-up investigations has lead to the results being viewed with greater clarity. This is especially true of the inductively coupled plasma (ICP) induced defect in germanium as the first experiments yielded anomalous results that were impossible to interpret without additional information. This plasma treatment bestows interesting properties on germanium that opens an area for future research that will be discussed in more detail in section 5.2.

5.1 Summary of Conclusions

Throughout this study exceptional Schottky barrier diodes (SBDs) were produced with ideality values close to one. With thorough sample degreasing and subsequent etching with dilute H_2O_2 followed by resistive evaporation (RE) of palladium, SBDs were measured with an ideality of 1.06 as RE did not damage the semiconductor. Conventional electron beam deposition (EBD) produced Au, Pd, Pt and Ru diodes that had an ideality that was only slightly higher than 1.06 with reverse bias currents at 300 K that were slightly higher than the lowest values recorded except for Au diodes, with almost 10×

higher current being drawn at 1 V reverse bias. Modifying the EBD system by introducing shields resulted in platinum SBDs with an ideality of 1.02 and a current density of 2.48×10^{-4} A· cm^{-2} at 1 V reverse bias being produced. The high work function of Pt in combination with the defect concentration in the Ge substrate being negligibly low was responsible for these near ideal diodes being produced, establishing the importance of controlling defect introduction during processing. Ion etching of the Ge surface prior to diode deposition is a damaging process that introduces defects at the surface and deeper in the material as measured after sputter deposition (SD) of Au or RF sputtering with Ar ions. In spite of this damage diodes evaporated onto ICP cleaned Ge were only slightly inferior compared to the best diodes when measured at room temperature, and proved to have superior rectifying qualities when measured at lower temperatures. In conclusion, careful application of plasma etching resulted in exceptional diodes being produced.

A number of novel defects, both electron and hole traps, were discovered and characterized during this study, the details of which are listed in Table I of Coelho, Auret, Janse van Rensburg et al. 2013. These were discovered after EBD, electron beam exposure (EBE), MeV electron irradiation, alpha particle irradiation and ICP etching. A trend is evident that certain defects are only observed after one subjects the crystal to subthreshold processes whereas other defects are found after irradiations of above threshold energetic particles, with the E-center being common to both processes. The accepted theory is that above threshold damage may result in point defects and this is not possible when the incident particle energy is too low. Subthreshold irradiation is not able to induce Frenkel pair production, a condition of vacancy formation, but is capable of displacing substitutional hydrogen in the Ge crystal lattice, resulting in some distortion that may occasionally be observed as an electrically active defect. The defects found in the bulk after EBD were created at the site where they were measured with the exception of vacancy related defects as the vacancy is mobile at room temperature. Ion-solid interactions cannot account for the creation of subthreshold defects found in the first µm below the junction, thus another mechanism is at play. Moving intrinsic localised modes as an energy transfer mechanism is considered the best fit to the observations but has not been reported on before in this context. While most of the observations of EBD induced

defects were from devices prepared on germanium, similar results obtained from silicon investigations established that conclusions drawn with regards to defect creation in this deposition process should be valid for other semiconductors as well, i.e. the conclusions are valid for the process.

EBE introduced a number of novel defects in germanium in a treatment that subjected the samples to irradiation from low energy particles, transferring at most 1.4 eV to individual germanium atoms in the crystal lattice. These defects, mostly different to those observed after EBD, were measured in very low concentrations and in some instances may be due to impurity residual atoms that were present in the vacuum chamber being accelerated into the germanium. With the exception of the E-center, none of these defects has been observed before and thus, without further investigation any additional conclusions drawn will be speculative.

5.2 Future Work

The study of defects in germanium, while very advanced in some regards, is still in its infancy when we consider how few defects have been identified. There is no simple way to identify the defects that have been observed and characterized, but in the case of the ICP induced defect a concerted effort should be made to identify its physical form.

ICP treatment of semiconductor surfaces, especially with ultra low energy ions, opens the way for detailed studies into the effect of these unique plasma conditions on defects, not only in germanium but in other semiconductors too. The electronic properties of germanium were substantially modified by this plasma treatment and a thorough understanding of the implications may yield new processing techniques for future devices.

The study of defects in ultra-low concentrations can be undertaken with Laplace-DLTS (L-DLTS) as measurements can be repeated hundreds or even thousands of times, if necessary, and the results averaged to obtain acceptable signal to noise ratios. Samples that were previously analysed using conventional deep level transient spectroscopy (DLTS) should be looked at again to see if additional defects are present.

Intrinsic localized modes or discrete breathers travelling through a solid are able to modify the medium that they travel in and semiconductor defect studies offer us an ideal opportunity to observe the changes that these excitations bring about. Defect generation and modification by this mechanism has far-reaching implications for the manufacture of electronic devices of the future.

Bibliography

[1] F.D. Auret, S. Coelho, W.E. Meyer, C. Nyamhere, M. Hayes and J.M. Nel. 'Electrical Characterization of Defects Introduced During Sputter Deposition of Schottky Contacts on n-type Ge'. *Journal of Electronic Materials* **36**.12 (2007), pp. 1604–1607. DOI: 10.1007/s11664-007-0245-y (cit. on pp. 31, 81, 102, 143).

[2] F.D. Auret, S.M.M. Coelho, M. Hayes, W.E. Meyer and J.M. Nel. 'Electrical characterization of defects introduced in Ge during electron beam deposition of different metals'. *Physica Status Solidi (a)* **205**.1 (2008), pp. 159–161. DOI: 10.1002/pssa.200776814 (cit. on pp. 54, 64).

[3] F.D. Auret, S.M.M. Coelho, P.J. Janse van Rensburg, C. Nyamhere and W.E. Meyer. 'Electrical characterization of defects introduced during metallization processes in n-type germanium'. *Materials Science in Semiconductor Processing* **11**.5-6 (2008), pp. 348–353. DOI: 10.1016/j.mssp.2008.09.001 (cit. on pp. 54, 64, 81, 102).

[4] F.D. Auret, S.M.M. Coelho, G. Myburg, P.J. Janse van Rensburg and W.E. Meyer. 'Electronic and annealing properties of the E0.31 defect introduced during Ar plasma etching of germanium'. *Physica B: Condensed Matter* **404**.22 (2009), pp. 4376–4378. DOI: 10.1016/j.physb.2009.09.028 (cit. on pp. 86, 102, 143).

[5] F.D. Auret, S.M.M. Coelho, G. Myburg, P.J. Janse van Rensburg and W.E. Meyer. 'Defect introduction in Ge during inductively coupled plasma etching and Schottky barrier diode fabrication processes'. *Thin Solid Films* **518**.9 (2010). Proceedings of the EMRS 2009 Spring Meeting Symposium I: Silicon and germanium

issues for future CMOS devices, pp. 2485–2488. DOI: 10.1016/j.tsf.2009.09.130 (cit. on pp. 64, 86, 101).

[6] F.D. Auret, S.M.M. Coelho, J.M. Nel and W.E. Meyer. 'Electrical characterization of defects introduced in n-Si during electron beam deposition of Pt'. *Physica Status Solidi (a)* **209**.10 (2012), pp. 1926–1933. DOI: 10.1002/pssa.201200578 (cit. on p. 72).

[7] F.D. Auret, S.A. Goodman, G. Myburg and W.E. Meyer. 'Electrical characterization of defects introduced in n-GaAs by alpha and beta irradiation from radionuclides'. English. *Applied Physics A* **56**.6 (1993), pp. 547–553. DOI: 10.1007/BF00331403 (cit. on p. 48).

[8] F.D. Auret, P.J. Janse van Rensburg, M. Hayes, J.M. Nel, S. Coelho, W.E. Meyer, S. Decoster, V. Matias, A. Vantomme and D. Smeets. 'Electrical characterization of defects in heavy-ion implanted n-type Ge'. *Nuclear Instruments and Methods in Physics Research Section B: Beam Interactions with Materials and Atoms* **257**.1-2 (2007), pp. 169–171. DOI: 10.1016/j.nimb.2007.01.107 (cit. on p. 101).

[9] F.D. Auret, P.J. Janse van Rensburg, W.E. Meyer, S.M.M. Coelho, Vl. Kolkovsky, J.R. Botha, C. Nyamhere and A. Venter. 'Inductively coupled plasma induced deep levels in epitaxial n-GaAs'. *Physica B: Condensed Matter* **407**.10 (2012), pp. 1497–1500. DOI: 10.1016/j.physb.2011.09.070 (cit. on p. 87).

[10] F.D. Auret, W.E. Meyer, S. Coelho and M. Hayes. 'Electrical characterization of defects introduced during electron beam deposition of Pd Schottky contacts on n-type Ge'. *Applied Physics Letters* **88**.24 (2006), pp. 242110–4. DOI: 10.1063/1.2213203 (cit. on pp. 26, 64, 102, 143).

[11] F.D. Auret, W.E. Meyer, S. Coelho, M. Hayes and J.M. Nel. 'Electrical characterization of defects introduced during electron beam deposition of Schottky contacts on n-type Ge'. *Materials Science in Semiconductor Processing* **9**.4-5 (2006), pp. 576–579. DOI: 10.1016/j.mssp.2006.08.008 (cit. on p. 64).

[12] F.D. Auret and P.M. Mooney. 'Deep levels introduced during electron-beam deposition of metals on n-type silicon'. *Journal of Applied Physics* **55**.4 (1984), pp. 988–993. DOI: 10.1063/1.333155 (cit. on p. 15).

[13] W. Bauer and A. Sosin. 'Threshold Displacement Energies and Subthreshold Displacements in Copper and Gold Near 10°K'. *Journal of Applied Physics* **35**.3 (1964), pp. 703–709. DOI: 10.1063/1.1713440 (cit. on p. 16).

[14] M.I. Boulos. 'The inductively coupled R.F. (radio frequency) plasma'. *Pure and Applied Chemistry* **57**.9 (1985), pp. 1321–1352. DOI: 10.1351/pac198557091321 (cit. on p. 24).

[15] M. Budde, B. Bech Nielsen, J.C. Keay and L.C. Feldman. 'Vacancy hydrogen complexes in group-IV semiconductors'. *Physica B: Condensed Matter* **273-274** (1999), pp. 208–211. DOI: 10.1016/S0921-4526(99)00448-2 (cit. on p. 29).

[16] M. Budde, B. Bech Nielsen, P. Leary, J. Goss, R. Jones, P. Briddon, S. Öberg and S. Breuer. 'Identification of the hydrogen-saturated self-interstitials in silicon and germanium'. *Physical Review B* **57**.8 (1998), pp. 4397–4412. DOI: 10.1103/PhysRevB.57.4397 (cit. on p. 27).

[17] R.F. Bunshah. *Handbook of Deposition Technologies for Films and Coatings - Science, Technology and Applications*. Second. William Andrew Publishing/Noyes, 1994, pp. 812–821 (cit. on p. 49).

[18] Paul R. Camp. 'A Study of the Etching Rate of Single-Crystal Germanium'. *Journal of The Electrochemical Society* **102**.10 (1955), pp. 586–593 (cit. on p. 43).

[19] I. Capan, B. Pivac, I.D. Hawkins, V.P. Markevich, A.R. Peaker, L. Dobaczewski and R. Jačimović. 'Neutron-irradiation-induced defects in germanium: A Laplace deep level transient spectroscopy study'. *Vacuum* **84**.1 (2010), pp. 32–36. DOI: 10.1016/j.vacuum.2009.04.003 (cit. on p. 41).

[20] M. Cardona. 'Foreword'. *Theory of Defects in Semiconductors*. Ed. by David A. Drabold and Stefan K. Estreicher. Vol. 104. Topics in Applied Physics. Springer Berlin Heidelberg, 2007, pp. 1–10. DOI: 10.1007/11690320_1 (cit. on p. 26).

[21] A. Carvalho, R. Jones, C. Janke, J.P. Goss, P.R. Briddon, J. Coutinho and S. Öberg. 'Self-Interstitial in Germanium'. *Physical Review Letters* **99**.17 (2007), p. 175502. DOI: 10.1103/PhysRevLett.99.175502 (cit. on p. 26).

[22] H. Cerva, M. Engelhardt, M. Hierlemann, M. Pölzl and T. Thenikl. 'Misfortune , challenge , and success : defects in processed semiconductor devices'. *Phys. Rev. B* **308-310** (2001), pp. 13–17 (cit. on p. 30).

[23] A. Chawanda, S.M.M. Coelho, F.D. Auret, W. Mtangi, C. Nyamhere, J.M. Nel and M. Diale. 'Effect of thermal treatment on the characteristics of iridium Schottky barrier diodes on n-Ge (100)'. *Journal of Alloys and Compounds* **513** (2012), pp. 44–49. DOI: 10.1016/j.jallcom.2011.09.053 (cit. on pp. 54, 65, 102).

[24] Y. Chen and J.W. MacKay. 'Subthreshold Electron Damage in n-Type Germanium'. *Physical Review* **167**.3 (1968), pp. 745–753. DOI: 10.1103/PhysRev.167.745 (cit. on pp. 16, 17).

[25] T. Chevolleau and W. Fukarek. 'Ion flux , ion energy distribution and neutral density in an inductively ccoupled argon discharge'. *Plasma Sources Science and Technology* **9**.4 (2000), pp. 568–573. DOI: 10.1088/0963-0252/9/4/312 (cit. on p. 25).

[26] Gregory Choppin, Jan-Olov Liljenzin, Jan Rydberg and Christian Ekberg. *Radiochemistry and Nuclear Chemistry*. Fourth. Elsevier, 2013, pp. 497–499 (cit. on p. 49).

[27] C. Claeys and J. Vanhellemont. 'Recent progress in the understanding of crystallographic defects in silicon'. *Journal of Crystal Growth* **126** (1993), pp. 41–62 (cit. on p. 30).

[28] Cor L. Claeys and E. Simoen. *Extended Defects in Germanium : Fundamental and Technological Aspects*. Berlin: Springer-Verlag, 2009, pp. 241–292 (cit. on pp. 30, 32, 41).

[29] Cor Claeys and Eddy Simoen, eds. *Germanium-Based Technologies From Materials to Devices*. 1st. Oxford: Elsevier, 2007, p. 480 (cit. on pp. 1, 3).

[30] P. Clauws. 'Chapter 4 - Oxygen in Germanium'. *Germanium-Based Technologies*. Ed. by Cor Claeys and Eddy Simoen. Oxford: Elsevier, 2007, pp. 97–130. DOI: 10.1016/B978-008044953-1/50006-5 (cit. on p. 28).

[31] S.M.M. Coelho, F.D. Auret, P.J. Janse Van Rensberg, C. Nyamhere, J.M. Nel and M. Hayes. 'IV and CV measurements of Schottky diodes deposited on Ge by electron beam and sputter deposition'. *Physica Status Solidi C* **5**.2 (2008), pp. 626–629. DOI: 10.1002/pssc.200776815 (cit. on p. 53).

[32] S.M.M. Coelho, F.D. Auret, P.J. Janse van Rensburg and J.M. Nel. 'Electrical characterization of defects introduced in n-Ge during electron beam deposition or exposure'. *Journal of Applied Physics* **114**.17 (2013), p. 173708. DOI: 10.1063/1.4828999 (cit. on pp. 26, 54, 65, 72, 125, 149).

[33] S.M.M. Coelho, F.D. Auret, G. Myburg, P.J. Janse van Rensburg and W.E. Meyer. 'Current-temperature measurements of a SBD evaporated onto inductively coupled plasma cleaned germanium'. *Physica B: Condensed Matter* **404**.22 (2009), pp. 4389–4392. DOI: 10.1016/j.physb.2009.09.026 (cit. on pp. 37, 54, 86).

[34] S.M.M. Coelho, Auret F.D., P.J. Janse van Rensburg and J.M. Nel. 'Unexpected properties of the inductively coupled plasma induced defect in germanium'. *Physica B: Condensed Matter* **439** (2014), pp. 97–100. DOI: 10.1016/j.physb.2013.10.061 (cit. on p. 86).

[35] B.J. Coomer, P. Leary, M. Budde, B. Bech Nielsen, R. Jones and P.R. Briddon. 'Vacancy-hydrogen complexes in germanium'. *Materials Science and Engineering: B* **58**.1-2 (1999), pp. 36–38. DOI: 10.1016/S0921-5107(98)00271-2 (cit. on pp. 27, 29).

[36] D. Depla, S. Mahieu and J.E. Greene. 'Chapter 5 - Sputter Deposition Processes'. *Handbook of Deposition Technologies for Films and Coatings (Third Edition)*. Ed. by Peter M. Martin. Third Edition. Boston: William Andrew Publishing, 2010, pp. 253–296. DOI: 10.1016/B978-0-8155-2031-3.00005-3 (cit. on p. 20).

[37] C.V. Deshpandey and R.F. Bunshah. 'Evaporation Processes'. *Thin Film Processes II*. Ed. by J.L. Vossen and W. Kern. Boston: Academic Press, 1991. Chap. II-2, pp. 79–130 (cit. on p. 12).

[38] L Dobaczewski, P Kaczor, I.D. Hawkins and A.R. Peaker. 'Laplace transform deep-level transient spectroscopic studies of defects in semiconductors'. *Journal of Applied Physics* **76**.1 (1994), pp. 194–198. DOI: 10.1063/1.357126 (cit. on pp. 3, 40).

[39] J. Fage-Pedersen, A. Nylandsted Larsen and A. Mesli. 'Irradiation-induced defects in Ge studied by transient spectroscopies'. *Physical Review B* **62**.15 (2000), pp. 10116–10125. DOI: 10.1103/PhysRevB.62.10116 (cit. on pp. 3, 26, 33, 143).

[40] D.M. Fleetwood and R.D. Schrimpf. *Defects in Microelectronic Materials and Devices*. Taylor & Francis, 2008 (cit. on pp. 41, 42).

[41] N. Fukuoka and H. Saito. 'The Defects Produced by Electron Irradiation and Annealed at 360K in n-Germanium'. *Japanese Journal of Applied Physics* **13**.10 (1974), pp. 1524–1532. DOI: 10.1143/JJAP.13.1524 (cit. on p. 32).

[42] E.B. Graper. 'Electron Beam Evaporation'. *Handbook of Thin Film Process Technology*. Ed. by D. Glocker and S. Shah. Bristol, UK and Philadelphia, USA: Taylor & Francis, 1996. Chap. A1.2 (cit. on pp. 14, 15).

[43] E.B. Graper. 'Resistance Evaporation'. *Handbook of Thin Film Process Technology*. Ed. by D. Glocker and S. Shah. Bristol, UK and Philadelphia, USA: Taylor & Francis, 1996 (cit. on pp. 12, 13).

[44] E.B. Graper. 'Thermal Evaporation - Introduction and General Discussion'. *Handbook of Thin Film Process Technology*. Ed. by David A Glocker and S Ismat Shah. Bristol, UK and Philadelphia, USA: Taylor & Francis, 1996. Chap. A1.0, pp. 1–26 (cit. on pp. 9, 10).

[45] M. Grundmann. *The Physics of Semiconductors: An Introduction Including Nanophysics and Applications*. Second. Graduate Texts in Physics. Springer, 2010 (cit. on p. 34).

[46] E. Grusell, S. Berg and L.P. Andersson. 'Electrical Defects in Silicon Introduced by Sputtering and Sputter-Etching'. *Journal of The Electrochemical Society* **127**.7 (1980), pp. 1573–1576. DOI: 10.1149/1.2129953 (cit. on p. 11).

[47] E.E. Haller. 'Germanium: From its discovery to SiGe devices'. *Materials Science in Semiconductor Processing* **9**.4-5 (2006), pp. 408–422. DOI: 10.1016/j.mssp.2006.08.063 (cit. on p. 2).

[48] Nigel S. Harris. *Modern Vacuum Practice*. McGraw-Hill Book Company, 1989, p. 315 (cit. on p. 52).

[49] M. Hayes, F. Schrempel, S.M.M. Coelho, F.D. Auret, J.M. Nel and W. Wesch. 'RBS investigation of annealed thin gold layers on crystalline germanium'. *Journal of Physics: Conference Series* **100**.4 (2008), p. 042005. DOI: 10.1088/1742-6596/100/4/042005 (cit. on pp. 49, 54).

[50] N. Hershkowitz. 'Plasma Probes - Langmuir Probe Diagnostics'. *Handbook of Thin Film Process Technology*. Ed. by S Ismat Glocker, David A and Shah. Bristol, UK and Philadelphia, USA: Taylor & Francis, 1996. Chap. D3.0, pp. 1–10 (cit. on p. 21).

[51] R.E. Honig. 'Vapor pressure data for the solid and liquid elements'. *RCA Review* **23**.4 (1962), pp. 567–586 (cit. on p. 10).

[52] R.E. Honig and D.A. Kramer. 'Vapor Pressure Data for the Solid and Liquid Elements'. *RCA Review* **30** (1969), pp. 285–305 (cit. on p. 10).

[53] G. Impellizzeri, S. Mirabella and M.G. Grimaldi. 'Ion implantation damage and crystalline-amorphous transition in Ge'. *Applied Physics A* **103**.2 (2010), pp. 323–328. DOI: 10.1007/s00339-010-6123-0 (cit. on p. 30).

[54] W. Kern and K.K. Schuegraf. 'Deposition Technologies and Applications: Introduction and Overview'. *Handbook of Thin Film Deposition Processes and Techniques (Second Edition)*. Ed. by Krishna Seshan. Second Edition. Norwich, NY: William Andrew Publishing, 2001, pp. 11–43. DOI: 10.1016/B978-081551442-8.50005-5 (cit. on p. 9).

[55] R. Kleinhenz, P.M. Mooney, C.P. Schneider and O. Paz. 'Defects produced in silicon and GaAs during E-beam evaporation of metals'. *Journal of Electronic Materials* **14a** (1985), pp. 627–633 (cit. on p. 15).

[56] H.A. Klose, P. Thiele and S. Zinnow. 'Modification of near-surface regions in Si by low energy particles'. *Surface and Coatings Technology* **59**.1-3 (1993), pp. 221–225. DOI: 10.1016/0257-8972(93)90087-5 (cit. on p. 15).

[57] Vl. Kolkovsky, M. Christian Petersen, A. Nylandsted Larsen and A. Mesli. 'Low-temperature irradiation-induced defects in p-type germanium'. *Physical Review B* **81**.3 (2010), p. 035208. DOI: 10.1103/PhysRevB.81.035208 (cit. on pp. 26, 27).

[58] Vl. Kolkovsky, M. Christian Petersen, A. Nylandsted Larsen and Vl. Kolkovsky. 'Alpha-particle irradiation-induced defects in n-type germanium'. *Applied Physics Letters* **90**.11 (2007), p. 112110. DOI: 10.1063/1.2713864 (cit. on p. 33).

[59] L. Lajaunie, M.L. David and J.F. Barbot. 'Physical properties of Co/n-Ge Schottky contacts'. *Journal of Physics D: Applied Physics* **44**.12 (2011), p. 125103. DOI: 10.1088/0022-3727/44/12/125103 (cit. on pp. 26, 65).

[60] D.V. Lang. 'Deep-level transient spectroscopy: A new method to characterize traps in semiconductors'. *Journal of Applied Physics* **45**.7 (1974), pp. 3023–3032. DOI: 10.1063/1.1663719 (cit. on pp. 3, 38).

[61] A.N. Larsen and A. Mesli. 'The hidden secrets of the E-center in Si and Ge'. *Physica B: Condensed Matter* **401-402** (2007), pp. 85–90. DOI: 10.1016/j.physb.2007.08.119 (cit. on p. 41).

[62] J. Lauwaert and P. Clauws. 'Majority carrier capture rates for transition metal impurities in germanium'. *Thin Solid Films* **518**.9 (2010), pp. 2330–2333. DOI: 10.1016/j.tsf.2009.09.125 (cit. on p. 26).

[63] J. Lauwaert, J. Van Gheluwe and P. Clauws. 'Electrical passivation by hydrogen plasma treatment of transition metal impurities in germanium'. *Materials Science in Semiconductor Processing* **11**.5-6 (2008), pp. 360–363. DOI: 10.1016/j.mssp.2008.09.010 (cit. on p. 33).

[64] M.E. Law, R. Camillo-Castillo, L. Robertson and K.S. Jones. 'Defects in Ultra-Shallow Junctions'. *Defects in Microelectronic Materials and Devices*. Ed. by Daniel M . Fleetwood, Sokrates T . Pantelides and Ronald D . Schrimpf. CRC Press, 2008, pp. 1–25. DOI: 10.1201/9781420043778.ch1 (cit. on p. 2).

[65] Y. Leclerc, F.D. Auret, S.A. Goodman, G. Myburg and C. Schutte. 'Electronic properties of defects introduced during sputter deposition of Cr Schottky contacts on GaAs'. *Ion Beam Modification of Materials*. Ed. by J.S. WILLIAMS, R.G. ELLIMAN and M.C. RIDGWAY. Amsterdam: Elsevier, 1996, pp. 870–873. DOI: 10.1016/B978-0-444-82334-2.50170-2 (cit. on p. 11).

[66] V. Markevich, A.R. Peaker and A.N. Larsen. 'Chapter 7 - Radiation Performance of Ge Technologies'. *Germanium-Based Technologies*. Ed. by Cor Claeys and Eddy Simoen. Oxford: Elsevier, 2007, pp. 211–232. DOI: 10.1016/B978-008044953-1/50006-5 (cit. on p. 31).

[67] V.P. Markevich. 'A comparative study of ion implantation and irradiation-induced defects in Ge crystals'. *Materials Science in Semiconductor Processing* **9**.4-5 (2006), pp. 589–596. DOI: 10.1016/j.mssp.2006.08.062 (cit. on p. 30).

[68] V.P. Markevich. 'A comparative study of ion implantation and irradiation-induced defects in Ge crystals'. *Materials Science in Semiconductor Processing* **9**.4-5 (2006), pp. 589–596. DOI: 10.1016/j.mssp.2006.08.062 (cit. on pp. 41, 143).

[69] V.P. Markevich, I.D. Hawkins, A.R. Peaker, V.V. Litvinov, L.I. Murin and L. Dobaczewski. 'Vacancy-group-V-impurity atom pairs in Ge crystals doped with P, As, Sb, and Bi'. *Physical Review B* **70**.23 (2004), p. 235213. DOI: 10.1103/PhysRevB.70.235213 (cit. on p. 26).

[70] V.P. Markevich, I.D. Hawkins, A.R. Peaker, V.V. Litvinov, L.I. Murin, L. Dobaczewski and J.L. Lindström. 'Electronic properties of vacancy-oxygen complex in Ge crystals'. *Applied Physics Letters* **81**.10 (2002), pp. 1821–1823. DOI: 10.1063/1.1504871 (cit. on pp. 26, 28).

[71] V.P. Markevich, A.R. Peaker, V.V. Litvinov, V.V. Emtsev and L.I. Murin. 'Electronic properties of antimony-vacancy complex in Ge crystals'. *Journal of Applied Physics* **95**.8 (2004), p. 4078. DOI: 10.1063/1.1669059 (cit. on p. 143).

[72] V.P. Markevich, A.R. Peaker, A.V. Markevich, V.V. Litvinov, L.I. Murin and V.V. Emtsev. 'Interaction of self-interstitials with oxygen-related defects in electron-irradiated Ge crystals'. *Materials Science in Semiconductor Processing* **9**.4-5 (2006), pp. 613–618. DOI: 10.1016/j.mssp.2006.08.068 (cit. on p. 33).

[73] Peter M. Martin, ed. *Handbook of Deposition Technologies for Films and Coatings (Third Edition)*. William Andrew Publishing, 2010, p. 936 (cit. on pp. 9, 19).

[74] Donald Mattox. 'Processes for Substrate Cleaning'. *Handbook of Thin Film Process Technology*. Ed. by David A Glocker and S Ismat Shah. Bristol, UK and Philadelphia, USA: Taylor & Francis, 1996. Chap. E1.0, pp. 1–26 (cit. on p. 43).

[75] G.E. McGuire. *Semiconductor Materials and Process Technology Handbook*. Ed. by Gary E. McGuire. William Andrew Publishing/Noyes, 1988, pp. 635–640 (cit. on p. 49).

[76] A. Mesli, L. Dobaczewski, K. Bonde Nielsen, Vl. Kolkovsky, M. Christian Petersen and A. Nylandsted Larsen. 'Low-temperature irradiation-induced defects in germanium: In situ analysis'. *Physical Review B* **78**.16 (2008), p. 165202. DOI: 10.1103/PhysRevB.78.165202 (cit. on pp. 26, 27).

[77] T. Meziani, P. Colpo and F. Rossi. 'Design of a magnetic-pole enhanced inductively coupled plasma source'. *Plasma Sources Science and Technology* **10**.2 (2001), pp. 276–282. DOI: 10.1088/0963-0252/10/2/317 (cit. on p. 25).

[78] P.M. Mooney, F. Poulin and J.C. Bourgoin. 'Annealing of electron-induced defects in n-type germanium'. *Phys. Rev. B* **28** (1983), pp. 3372–3377. DOI: 10.1103/PhysRevB.28.3372 (cit. on p. 32).

[79] J.A. Naber and H.M. James. *Bulletin of the American Physical Society* **3** (1958), p. 142 (cit. on p. 16).

[80] J.M Nel, A. Chawanda, F.D Auret, W. Jordaan, R.Q. Odendaal, M. Hayes and S. Coelho. 'Microstructural and surface characterization of thin gold films on n-Ge (1 1 1)'. *Physica B: Condensed Matter* **404**.22 (2009), pp. 4493–4495. DOI: 10.1016/j.physb.2009.09.035 (cit. on pp. 49, 55, 64).

[81] C. Nyamhere, A.G.M. Das, F.D. Auret, A. Chawanda, W. Mtangi, Q. Odendaal and A. Carr. 'Characterization of defects introduced in Sb doped Ge by 3keV Ar sputtering using deep level transient spectroscopy (DLTS) and Laplace-DLTS (LDLTS)'. *Physica B: Condensed Matter* **404**.22 (2009), pp. 4379–4381. DOI: 10.1016/j.physb.2009.09.037 (cit. on p. 31).

[82] C. Nyamhere, M. Das, F.D. Auret and A. Chawanda. 'A study of electron induced defects in n-type germanium by deep level transient spectroscopy (DLTS)'. *Physica Status Solidi (C)* **5**.2 (2008), pp. 623–625. DOI: 10.1002/pssc.200776812 (cit. on p. 143).

[83] C. Nyamhere, A. Venter, F.D. Auret, S.M.M. Coelho and D.M. Murape. 'Characterization of the E(0.31) defect introduced in bulk *n*-Ge by H or He plasma exposure'. *Journal of Applied Physics* **111**.4 (2012), p. 044511. DOI: 10.1063/1.3687426 (cit. on pp. 86, 100, 143).

[84] C. Nyamhere, A. Venter, D.M. Murape, F.D. Auret, S.M.M. Coelho and J.R. Botha. 'dc-Hydrogen plasma induced defects in bulk *n*-Ge'. *Physica B: Condensed Matter* **407**.15 (2012), pp. 2935–2938. DOI: 10.1016/j.physb.2011.08.047 (cit. on pp. 86, 100).

[85] A.R. Peaker, V.P. Markevich, I.D. Hawkins, B. Hamilton, K. Bonde Nielsen and K. Gościński. 'Laplace deep level transient spectroscopy: Embodiment and evolution'. *Physica B: Condensed Matter* **407**.15 (2012), pp. 3026–3030. DOI: 10.1016/j.physb.2011.08.107 (cit. on p. 4).

[86] A.R. Peaker, V.P. Markevich, L.I. Murin, N.V. Abrosimov and V.V. Litvinov. 'Ion implantation and electron irradiation damage in unstrained germanium and silicon-germanium alloys'. *Materials Science and Engineering: B* **124-125** (2005), pp. 166–169. DOI: 10.1016/j.mseb.2005.08.102 (cit. on pp. 30, 33).

[87] S.J. Pearton and A.J. Tavendale. 'Hydrogen passivation of laserinduced defects in germanium'. *Journal of Applied Physics* **54**.1 (1983), pp. 440–441. DOI: 10.1063/1.331678 (cit. on p. 33).

[88] A.S. Penfold. 'Sputtering - Magnetron Sputtering'. *Handbook of Thin Film Process Technology*. Ed. by David A. Glocker and S. Ismat Shah. Bristol, UK and Philadelphia, USA: Taylor & Francis, 1996. Chap. A3.2, pp. 1–27 (cit. on p. 22).

[89] F. Poulin and J.C. Bourgoin. 'Threshold energy for atomic displacement in electron irradiated germanium (*)'. *Rev. Phys. Appl. (Paris)* **15**.1 (1980), pp. 15–19. DOI: http://dx.doi.org/10.1051/rphysap:0198000150101500 (cit. on p. 32).

[90] H.J. Queisser and E.E. Haller. 'Defects in Semiconductors: Some Fatal, Some Vital'. *Science* **281**.5379 (1998), pp. 945–950. DOI: 10.1126/science.281.5379.945 (cit. on p. 30).

[91] E. Reinhold and J. Faber. 'Large area electron beam physical vapor deposition (EB-PVD) and plasma activated electron beam (EB) evaporation - Status and prospects'. *Surface and Coatings Technology* **206**.7 (2011), pp. 1653–1659. DOI: 10.1016/j.surfcoat.2011.09.022 (cit. on pp. 14, 17, 18).

[92] E.H. Rhoderick and Williams R.H. *Metal-Semiconductor Contacts*. Second. Monographs in Electrical and Electronic Engineering. Clarendon Press, 1988, p. 251 (cit. on p. 36).

[93] K.T. Roro, P.J. Janse van Rensburg, F.D. Auret and S. Coelho. 'Effect of alpha-particle irradiation on the electrical properties of n-type Ge'. *Physica B: Condensed Matter* **404**.22 (2009), pp. 4496–4498. DOI: 10.1016/j.physb.2009.09.033 (cit. on pp. 33, 101, 143).

[94] Stephen M. Rossnagel, Jerome J. Cuomo and William D. Westwood, eds. *Handbook of Plasma Processing Technology: Fundamentals, Etching, Deposition and Surface Interactions*. William Andrew Publishing/Noyes, 1990, p. 546 (cit. on pp. 19, 21, 25).

[95] C.T. Sah, L. Forbes, L.L. Rosier and A.F. Tasch Jr. 'Thermal and optical emission and capture rates and cross sections of electrons and holes at imperfection centers in semiconductors from photo and dark junction current and capacitance experiments'. *Solid-State Electronics* **13**.6 (1970), pp. 759–788. DOI: http://dx.doi.org/10.1016/0038-1101(70)90064-X (cit. on p. 38).

[96] D.K. Schroder. *Semiconductor Material and Device Characterization*. Third. Wiley, 2006, p. 800 (cit. on pp. 34, 35, 38).

[97] A. Schwabedissen, E.C. Benck and J.R. Roberts. 'Langmuir probe measurements in an inductively coupled plasma source'. *Physical Review E* **55**.3 (1997), pp. 3450–3459. DOI: 10.1103/PhysRevE.55.3450 (cit. on pp. 21, 23, 24).

[98] K. Seshan. 'Recent Changes in the Semiconductor Industry'. *Handbook of Thin Film Deposition Processes and Techniques (Second Edition)*. Ed. by Krishna Seshan. Norwich, NY: William Andrew Publishing, 2001, pp. 1–9. DOI: 10.1016/B978-081551442-8.50005-5 (cit. on pp. 9, 19).

[99] S. Ismat Shah. 'Sputtering : Introduction and General Discussion'. *Handbook of Thin Film Process Technology*. Ed. by David A. Glocker and S. Ismat Shah. Bristol, UK and Philadelphia, USA: Taylor & Francis, 1996. Chap. A3.0, pp. 1–18 (cit. on pp. 20, 23).

[100] E. Simoen and C. Claeys. 'Chapter 13 - Trends and outlook'. *Germanium-Based Technologies*. Ed. by Cor Claeys and Eddy Simoen. Oxford: Elsevier, 2007. Chap. 13, pp. 417–432. DOI: 10.1016/B978-008044953-1/50017-X (cit. on p. 3).

[101] E. Simoen, C. Claeys, S. Sioncke, J. Steenbergen, M. Meuris, S. Forment, J. Vanhellemont, P. Clauws and A. Theuwis. 'Lifetime and leakage current considerations in metal-doped germanium'. *Journal of Materials Science: Materials in Electronics* **18**.7 (2007), pp. 799–804. DOI: 10.1007/s10854-006-9110-7 (cit. on p. 2).

[102] E. Simoen, K. Opsomer, C. Claeys, K. Maex, C. Detavernier, R.L. Van Meirhaeghe and P. Clauws. 'Study of metal-related deep-level defects in germanide Schottky barriers on n-type germanium'. *Journal of Applied Physics* **104**.2 (2008), p. 023705. DOI: 10.1063/1.2956708 (cit. on p. 26).

[103] T. Sinno, E. Dornberger, W. von Ammon, R.A. Brown and F. Dupret. 'Defect engineering of Czochralski single-crystal silicon'. *Materials Science and Engineering: R: Reports* **28**.5-6 (2000), pp. 149–198. DOI: 10.1016/S0927-796X(00)00015-2 (cit. on p. 28).

[104] S.M. Sze and K.K. Ng. *Physics of Semiconductor Devices*. Second. Wiley, 1981 (cit. on p. 49).

[105] J. Vanhellemont, S. Hens, J. Lauwaert, O. De Gryse, P. Vanmeerbeek, D. Poelman, P. Śpiewak, I. Romandic, A. Theuwis and P. Clauws. 'Recent progress in understanding of lattice defects in Czochralski-grown germanium: catching-up

with silicon'. *Solid State Phenomena* **108-109** (2005), pp. 683–690. DOI: 10.4028/www.scientific.net/SSP.108-109.683 (cit. on p. 27).

[106] J. Vanhellemont, J. Lauwaert, A. Witecka, P. Śpiewak, I. Romandic and P. Clauws. 'Experimental and theoretical study of the thermal solubility of the vacancy in germanium'. *Physica B: Condensed Matter* **404**.23-24 (2009), pp. 4529–4532. DOI: 10.1016/j.physb.2009.08.121 (cit. on p. 26).

[107] J. Vanhellemont, E. Simoen, I. Romandic and A. Theuwis. 'Chapter 2 - Grown-in Defects in Germanium'. *Germanium-Based Technologies*. Ed. by Cor Claeys and Eddy Simoen. Oxford: Elsevier, 2007, pp. 41–66. DOI: 10.1016/B978-008044953-1/50006-5 (cit. on pp. 4, 26–28).

[108] A. Venter, C. Nyamhere, J.R. Botha, F.D. Auret, S.M.M. Coelho and W.E. Meyer. 'Field dependence of the E1' and M3' electron traps in inductively coupled Ar plasma treated n-Gallium Arsenide'. *Journal of Applied Physics* **111**.9 (2012), p. 093703. DOI: 10.1063/1.4709390 (cit. on p. 87).

[109] A. Venter, C. Nyamhere, J.R. Botha, F.D. Auret, P.J. Janse van Rensburg, W.E. Meyer, S.M.M. Coelho and V.I. Kolkovsky. 'Ar plasma induced deep levels in epitaxial n-GaAs'. *Journal of Applied Physics* **111**.1 (2012), p. 013703. DOI: 10.1063/1.3673322 (cit. on p. 87).

[110] J.L. Vossen and W. Kern, eds. *Thin Film Processes II*. Boston: Academic Press, 1991, p. 888 (cit. on pp. 19, 22).

[111] S.G. Walton and J.E. Greene. 'Chapter 2 - Plasmas in Deposition Processes'. *Handbook of Deposition Technologies for Films and Coatings (Third Edition)*. Ed. by Peter M. Martin. Third Edition. Boston: William Andrew Publishing, 2010. Chap. 2, pp. 32–92. DOI: 10.1016/B978-0-8155-2031-3.00002-8 (cit. on pp. 20, 21).

[112] J. Weber, M. Hiller and E.V. Lavrov. 'Hydrogen in germanium'. *Materials Science in Semiconductor Processing* **9**.4-5 (2006), pp. 564–570. DOI: 10.1016/j.mssp.2006.08.007 (cit. on p. 27).

[113] J.R. Weber, A. Janotti, P. Rinke and C.G. Van de Walle. 'Dangling-bond defects and hydrogen passivation in germanium'. *Applied Physics Letters* **91**.14 (2007), p. 142101. DOI: 10.1063/1.2793184 (cit. on pp. 29, 33).

Appendix A

Ge defects analysed

Defects with deep levels that were measured have been included in Table A.1. Publications appearing before 2000 where these defects were first reported have not been included as the energy levels vary greatly with the latest findings and in most cases these are referenced in the cited articles. A prominent defect that has been omitted is the A-centre (oxygen-antimony) as research into the introduction of this defect during processing is on-going.

Key for Table A.1:

a	Auret, Meyer, Coelho and Hayes 2006
b	Fage-Pedersen et al. 2000
c	Markevich, Peaker, Litvinov et al. 2004
d	Auret, Meyer, Coelho and Hayes 2006
e	Markevich 2006b
f	Auret et al. 2009
g	Nyamhere, Venter, Auret et al. 2012
h	Auret, Coelho, Meyer et al. 2007
i	Roro et al. 2009
j	Nyamhere, Das, Auret and Chawanda 2008
*	Experimental data first observed during this study.
†	Peak temperature at a rate window of 80 s^{-1}.

Table A.1: Defects observed in Ge after various processing or irradiation techniques.

Process	Defect label	E_T (eV)	σ_a ($\times 10^{-15}$ cm^2)	$T^{\dagger}_{80}$ (K)	Similar defects / defect ID / Ref.
EBD	$E_{0.10}$	E_c - 0.10	0.37	65	$E_{0.10}$ [a]
	$E_{0.13}$	E_c - 0.13	0.19	85	$E_{0.13}$ [a]
	$E_{0.23}$	E_c - 0.23	34	116	$E_{0.23}$ [a]
	$E_{0.38}$	E_c - 0.38	10	191	$E_{0.38}$ [a,d], $E_{0.37}$, E_{377}, V-Sb (--/-) [b,c]
	$H_{0.09}$	E_v + 0.09	210	47	$H_{0.09}$ [a], V-Sb (0/+) [e]
	$H_{0.15}$	E_v + 0.15	71	82	$H_{0.15}$ [a]
	$H_{0.18}$	E_v + 0.18	35	97	$H_{0.18}$ [a]
	$H_{0.27}$	E_v + 0.27	240	133	$H_{0.27}$ [a], H_{270} [c]
	$H_{0.30}$	E_v + 0.30	620	141	$H_{0.30}$ [b], H_{307}, V-Sb (-/0) [c]
	$H_{0.29}$	E_v + 0.29	1.3	176	$H_{0.29}$ [d]
EBD (f/gas)	$E_{0.28}$	E_c - 0.28	11	153	*
	$E_{0.31}$	E_c - 0.31	9.0	163	*
EBE	$E_{0.16}$	E_c - 0.16	320	77	*
	$E_{0.22}$	E_c - 0.22	515	101	*
	$E'_{0.22}$	E_c - 0.22	69	108	*
	$E_{0.33}$	E_c - 0.33	246	152	*
	$E_{0.37}$	E_c - 0.37	35.4	182	*, $E_{0.37}$ [a]
	$E_{0.38}$	E_c - 0.38	13.8	192	*, $E_{0.38}$ [a,d], E_{377}, V-Sb (--/-) [c]
	$H'_{0.15}$	E_v + 0.15	65	86	*
	$H_{0.22}$	E_v + 0.22	1960	106	*
	$H_{0.26}$	E_v + 0.26	89	139	*
	$H_{0.34}$	E_v + 0.34	172	171	*
ICP	$E_{0.31}$	E_c - 0.31	10	157	$E_{0.31}$ [f], $E(0.30)$ [g]
Sputter etch	$E_{0.31}$	E_c - 0.31	10	157	* (300 eV Ar), $E_{0.31}$ [f,g]
Sputter	$ES_{0.14}$	E_c - 0.14	5.5	78	$ES_{0.14}$ [h], $E_{0.13}$, Sb and I related [b]
deposition	$ES_{0.20}$	E_c - 0.20	37	100	$ES_{0.20}$ [h], $E_{0.19}$, Sb and I related [b]
	$ES_{0.21}$	E_c - 0.21	20	109	$ES_{0.21}$ [h], $E_{0.21}$ [b]
	$ES_{0.24}$	E_c - 0.24	3.3	131	$ES_{0.24}$ [h], $E_{0.23}$ [b]
	$ES_{0.31}$	E_c - 0.31	15	151	$ES_{0.31}$ [h], $E_{0.29}$, Divacancy? [b]
MeV electron	$E_{0.15}$	E_c - 0.15	50	77	$E_{0.15}$ [a]
irradiation	$E_{0.20}$	E_c - 0.20	14	100	$E_{0.20}$ [a], $E_{0.19}$, Sb and I related [b]
	$E_{0.21}$	E_c - 0.21	36	109	$E_{0.21}$ [a], $E_{0.21}$, Sb related? [b]
	$E_{0.24}$	E_c - 0.24	2.5	131	$E_{0.24}$ [a], E(0.23) [j]
	$E_{0.31}$	E_c - 0.31	50	151	$E_{0.31}$ [a]
	$E_{0.37}$	E_c - 0.37	29	181	$E_{0.37}$ [a]
	$E_{0.38}$	E_c - 0.38	11	191	$E_{0.37}$ [b], E_{377}, V-Sb (--/-) [c]
	$H_{030.}$	E_v + 0.30	366	142	$H_{0.30}$ [b], H_{307}, V-Sb (-/0) [c]
Alpha	$E_{0.09}$	E_c - 0.09	0.66	63	*, $E_{0.10}$? [a]
irradiation	$E_{0.10}$	E_c - 0.10	9.2	59	$E_{0.10}$ [i]
	$E_{0.15}$	E_c - 0.15	62	76	$E_{0.15}$ [i]
	$E_{0.20}$	E_c - 0.20	78	99	$E_{0.20}$ [i], $E_{0.19}$, Sb and I related [b]
	$E_{0.21}$	E_c - 0.21	29	109	$E_{0.21}$ [i], $E_{0.21}$, Sb related? [b]
	$E_{0.24}$	E_c - 0.24	14.5	130	*, $E_{0.23}$ [b]
	$E_{0.25}$	E_c - 0.25	0.37	149	*
	$E_{0.31}$	E_c - 0.31	98	151	*, $E_{0.30}$ [b]
	$E_{0.38}$	E_c - 0.38	13	190	$E_{0.38}$ [i], V-Sb (--/-) [c]
	$H_{0.31}$	E_v + 0.31	1000	142	*, $H_{0.30}$ [b], $H_{0.31}$ [i], H_{307}, V-Sb (-/0) [c]

Appendix B

Derived Publications

Research undertaken for this thesis contributed towards the following publications:

References

[1] F.D. Auret, S. Coelho, W.E. Meyer, C. Nyamhere, M. Hayes and J.M. Nel. 'Electrical Characterization of Defects Introduced During Sputter Deposition of Schottky Contacts on n-type Ge'. *Journal of Electronic Materials* **36**.12 (2007), pp. 1604–1607. DOI: 10.1007/s11664-007-0245-y.

[2] F.D. Auret, S.M.M. Coelho, M. Hayes, W.E. Meyer and J.M. Nel. 'Electrical characterization of defects introduced in Ge during electron beam deposition of different metals'. *Physica Status Solidi (a)* **205**.1 (2008), pp. 159–161. DOI: 10.1002/pssa.200776814.

[3] F.D. Auret, S.M.M. Coelho, P.J. Janse van Rensburg, C. Nyamhere and W.E. Meyer. 'Electrical characterization of defects introduced during metallization processes in n-type germanium'. *Materials Science in Semiconductor Processing* **11**.5-6 (2008), pp. 348–353. DOI: 10.1016/j.mssp.2008.09.001.

[4] F.D. Auret, S.M.M. Coelho, G. Myburg, P.J. Janse van Rensburg and W.E. Meyer. 'Electronic and annealing properties of the E0.31 defect introduced during Ar plasma etching of germanium'. *Physica B: Condensed Matter* **404**.22 (2009), pp. 4376–4378. DOI: 10.1016/j.physb.2009.09.028.

[5] F.D. Auret, S.M.M. Coelho, G. Myburg, P.J. Janse van Rensburg and W.E. Meyer. 'Defect introduction in Ge during inductively coupled plasma etching and Schottky barrier diode fabrication processes'. *Thin Solid Films* **518**.9 (2010). Proceedings of the EMRS 2009 Spring Meeting Symposium I: Silicon and germanium issues for future CMOS devices, pp. 2485–2488. DOI: 10.1016/j.tsf.2009.09.130.

[6] F.D. Auret, S.M.M. Coelho, J.M. Nel and W.E. Meyer. 'Electrical characterization of defects introduced in n-Si during electron beam deposition of Pt'. *Physica Status Solidi (a)* **209**.10 (2012), pp. 1926–1933. DOI: 10.1002/pssa.201200578.

[7] F.D. Auret, P.J. Janse van Rensburg, M. Hayes, J.M. Nel, S. Coelho, W.E. Meyer, S. Decoster, V. Matias, A. Vantomme and D. Smeets. 'Electrical characterization of defects in heavy-ion implanted n-type Ge'. *Nuclear Instruments and Methods in Physics Research Section B: Beam Interactions with Materials and Atoms* **257**.1-2 (2007), pp. 169–171. DOI: 10.1016/j.nimb.2007.01.107.

[8] F.D. Auret, P.J. Janse van Rensburg, W.E. Meyer, S.M.M. Coelho, Vl. Kolkovsky, J.R. Botha, C. Nyamhere and A. Venter. 'Inductively coupled plasma induced deep levels in epitaxial n-GaAs'. *Physica B: Condensed Matter* **407**.10 (2012), pp. 1497–1500. DOI: 10.1016/j.physb.2011.09.070.

[9] F.D. Auret, W.E. Meyer, S. Coelho and M. Hayes. 'Electrical characterization of defects introduced during electron beam deposition of Pd Schottky contacts on n-type Ge'. *Applied Physics Letters* **88**.24 (2006), pp. 242110–4. DOI: 10.1063/1.2213203.

[10] F.D. Auret, W.E. Meyer, S. Coelho, M. Hayes and J.M. Nel. 'Electrical characterization of defects introduced during electron beam deposition of Schottky contacts on n-type Ge'. *Materials Science in Semiconductor Processing* **9**.4-5 (2006), pp. 576–579. DOI: 10.1016/j.mssp.2006.08.008.

[11] A. Chawanda, S.M.M. Coelho, F.D. Auret, W. Mtangi, C. Nyamhere, J.M. Nel and M. Diale. 'Effect of thermal treatment on the characteristics of iridium Schottky barrier diodes on n-Ge (100)'. *Journal of Alloys and Compounds* **513** (2012), pp. 44–49. DOI: 10.1016/j.jallcom.2011.09.053.

[12] S.M.M. Coelho, F.D. Auret, P.J. Janse Van Rensberg, C. Nyamhere, J.M. Nel and M. Hayes. 'IV and CV measurements of Schottky diodes deposited on Ge by electron beam and sputter deposition'. *Physica Status Solidi C* **5**.2 (2008), pp. 626–629. DOI: 10.1002/pssc.200776815.

[13] S.M.M. Coelho, F.D. Auret, P.J. Janse van Rensburg and J.M. Nel. 'Electrical characterization of defects introduced in n-Ge during electron beam deposition or exposure'. *Journal of Applied Physics* **114**.17 (2013), p. 173708. DOI: 10.1063/1.4828999.

[14] S.M.M. Coelho, F.D. Auret, G. Myburg, P.J. Janse van Rensburg and W.E. Meyer. 'Current-temperature measurements of a SBD evaporated onto inductively coupled plasma cleaned germanium'. *Physica B: Condensed Matter* **404**.22 (2009), pp. 4389–4392. DOI: 10.1016/j.physb.2009.09.026.

[15] S.M.M. Coelho, Auret F.D., P.J. Janse van Rensburg and J.M. Nel. 'Unexpected properties of the inductively coupled plasma induced defect in germanium'. *Physica B: Condensed Matter* **439** (2014), pp. 97–100. DOI: 10.1016/j.physb.2013.10.061.

[16] S.M.M. Coelho, C. Zander and H.G. Miller. 'Gross features of finite nuclei at finite temperatures'. *The European Physical Journal A - Hadrons and Nuclei* **44** (2010), pp. 257–260. DOI: 10.1140/epja/i2010-10941-y.

[17] M. Hayes, F. Schrempel, S.M.M. Coelho, F.D. Auret, J.M. Nel and W. Wesch. 'RBS investigation of annealed thin gold layers on crystalline germanium'. *Journal of Physics: Conference Series* **100**.4 (2008), p. 042005. DOI: 10.1088/1742-6596/100/4/042005.

[18] J.M Nel, A. Chawanda, F.D Auret, W. Jordaan, R.Q. Odendaal, M. Hayes and S. Coelho. 'Microstructural and surface characterization of thin gold films on n-

Ge (1 1 1)'. *Physica B: Condensed Matter* **404**.22 (2009), pp. 4493–4495. DOI: 10.1016/j.physb.2009.09.035.

[19] C. Nyamhere, A. Venter, F.D. Auret, S.M.M. Coelho and D.M. Murape. 'Characterization of the E(0.31) defect introduced in bulk *n*-Ge by H or He plasma exposure'. *Journal of Applied Physics* **111**.4 (2012), p. 044511. DOI: 10.1063/1.3687426.

[20] C. Nyamhere, A. Venter, D.M. Murape, F.D. Auret, S.M.M. Coelho and J.R. Botha. 'dc-Hydrogen plasma induced defects in bulk *n*-Ge'. *Physica B: Condensed Matter* **407**.15 (2012), pp. 2935–2938. DOI: 10.1016/j.physb.2011.08.047.

[21] J. Pienaar, W.E. Meyer, F.D. Auret and S.M.M. Coelho. 'Comparison of two models for phonon assisted tunneling field enhanced emission from defects in Ge measured by DLTS'. *Physica B: Condensed Matter* **407**.10 (2012), pp. 1641–1644. DOI: 10.1016/j.physb.2011.09.106.

[22] K.T. Roro, P.J. Janse van Rensburg, F.D. Auret and S. Coelho. 'Effect of alpha-particle irradiation on the electrical properties of n-type Ge'. *Physica B: Condensed Matter* **404**.22 (2009), pp. 4496–4498. DOI: 10.1016/j.physb.2009.09.033.

[23] A. Venter, C. Nyamhere, J.R. Botha, F.D. Auret, S.M.M. Coelho and W.E. Meyer. 'Field dependence of the E1' and M3' electron traps in inductively coupled Ar plasma treated n-Gallium Arsenide'. *Journal of Applied Physics* **111**.9 (2012), p. 093703. DOI: 10.1063/1.4709390.

[24] A. Venter, C. Nyamhere, J.R. Botha, F.D. Auret, P.J. Janse van Rensburg, W.E. Meyer, S.M.M. Coelho and V.I. Kolkovsky. 'Ar plasma induced deep levels in epitaxial n-GaAs'. *Journal of Applied Physics* **111**.1 (2012), p. 013703. DOI: 10.1063/1.3673322.

Appendix C

EBD introduced defects in n-Si

The investigation of the effect of shielding on Ge SBDs fabricated by EBD (Coelho, Auret, Janse van Rensburg et al. 2013) was repeated on Si. For the first time EBE of Si was carried out, where the semiconductor was exposed to the conditions of EBD without metal deposition. This study produced diodes with exceptionally good rectifying characteristics and applying shielding during deposition in a superior vacuum lowered the defect concentration dramatically. A number of defects were also observed after EBE of Si that have not been reported on before.

C.1 Conclusions

The defect concentration was lowered by the introduction of static shields and by the lowering of the pressure in the deposition chamber during the fabrication of Si and Ge SBDs. As for Ge, EBE of Si also introduced additional defects that had not been reported on before. The origin of these defects in both materials is not certain but may be due to particles that are accelerated by collisions with the electron beam (EB) being implanted in the samples. That all these defects are implantation related is unlikely as the concentrations of all EBE defects were similarly lowered when the sample temperature was allowed to rise during defect introduction.

Phys. Status Solidi A **209,** No. 10, 1926–1933 (2012) / **DOI** 10.1002/pssa.201200578

Part of Topical Section on
Advanced Silicon Materials for Electronics and Photovoltaics

physica status solidi a
www.pss-a.com
applications and materials science

Electrical characterization of defects introduced in n-Si during electron beam deposition of Pt

F. D. Auret*, S. M. M. Coelho, J. M. Nel, and W. E. Meyer

Physics Department, University of Pretoria, Pretoria, South Africa

Received 15 August 2012, accepted 13 September 2012
Published online 4 October 2012

Keywords deep level transient spectroscopy, defects, electron beam deposition, silicon

* Corresponding author: e-mail danie.auret@up.ac.za, Phone: +2712 4202684, Fax: +2712 3625288

We have used deep level transient spectroscopy (DLTS) and high resolution DLTS to characterize the defects introduced in epitaxially grown n-type, P-doped, Si during electron beam deposition (EBD) of Pt for Schottky contact formation. The identity of some of these defects could be established by comparing their properties to those of well-known defects introduced by high energy electron irradiation of the same material. The most prominent EBD-induced defects thus identified were the E-center (VP center), the A-center (VO center), interstitial carbon (C_i), and the interstitial carbon–substitutional carbon (C_iC_s) pair. EBD also introduced some defects that were not observed after high energy electron irradiation. DLTS depth profiling revealed that the main defects, VO and VP, could be detected up to 0.5 μm below the metal–Si interface. Shielding the sample from particles originating in the region of the electron beam significantly reduced defect introduction and resulted in Schottky contacts with improved rectification properties. Finally, we have found that exposing the sample to EBD conditions, without actually depositing metal, introduced a different set of electron traps, not introduced by the EBD process.

1 Introduction Metallization is a critically important processing step in the microelectronic and photovoltaic industries. Electron beam deposition (EBD) is a popular method for depositing metals because of its ability to deposit at a highly controllable rate (both low and high rates) and because of its ability to deposit high melting point metals. The investigation of metallization-induced defects is important because it is well known that metallization procedures, including EBD, introduce defects at and close to the metal–semiconductor junction [1, 2]. These defects influence device performance and alter the barrier heights of the contacts [3].

The defects responsible for these barrier adjustments are formed when energetic particles reach the semiconductor surface and interact with it, resulting in lattice damage. Depending on the application, these defects may either be beneficial or detrimental for optimum device functioning. For Si, as an example, defect introduction during high energy electron and proton irradiation increases the switching speed of devices [4]. On the other hand, in the case of high open circuit voltage solar cells, degraded device properties have been reported after EBD of contacts [5].

The defects introduced during EBD of metals on Si grown by the Czochralski (CZ) process [1] and float zone method [2] have previously been reported. It was shown that the main defects appeared to be similar to the E-center (VP) [1, 2] and the A-center (VO) [1]. A defect similar to the divacancy was also observed [1, 2]. The differences between the observed defects in Refs. [1, 2] may be attributed to different electron beam systems, different vacuum conditions as well as the use of Si with different concentrations of impurities, such as C and O.

In this paper we report the defects introduced in epitaxially grown, phosphorous-doped, n-type Si. We show that in addition to the A- and E-centers, EBD also introduced the interstitial carbon, C_i, and interstitial carbon–substitutional carbon pair, C_iC_s, defects, as well as several other unidentified defects. We also show the effect of shielding and vacuum quality on defect introduction. Finally, we demonstrate that when exposing the sample to EBD conditions,

Phys. Status Solidi A 209, No. 10 (2012) 1927

without depositing any metal, a different set of defects are introduced.

2 Experimental procedure We have used epitaxially grown Si (12 μm thick, doped with P to a level of $3.5 \times 10^{15}\,cm^{-3}$), grown on an n^{++} Si substrate, for the investigation. Before metallization the samples were first degreased and then dipped in HF for 1 min. Directly after cleaning the samples were inserted into the vacuum system that was pumped down overnight to a vacuum better than 10^{-6} mbar. Pt Schottky contacts, 0.6 mm in diameter and of various thicknesses, were deposited in an EBD system through a mechanical mask. Typically, eight Schottky contacts were fabricated on a 3 mm × 5 mm piece of Si. A MDC 10 kW electron gun (Model e-Vap CVS-10) vacuum evaporation system was used for this process. In this system the samples are positioned about 50 cm above the crucible containing the metal. The vacuum before deposition was typically 10^{-6} mbar and this would increase to about 10^{-5} mbar during EBD. "Control" Pd Schottky contacts were deposited on identical samples by resistive evaporation – a process known not to introduce defects in semiconductors. After the Schottky deposition, InGa was rubbed onto the back n^{++} surface of the Si to serve as an ohmic contact.

Following contact fabrication, current–voltage (*I*–*V*) and capacitance–voltage (*C*–*V*) measurements were performed to assess the quality of the diodes and to determine the free carrier density of the EPI Si, measured as $3.5 \times 10^{15}\,cm^{-3}$. Thereafter conventional deep level transient spectroscopy (DLTS) was used to study the defects introduced in the Si during the EBD process. High-resolution Laplace DLTS [6, 7] was used to separate the DLTS signals of defects with closely spaced energy levels. It should be pointed out that in this study Schottky diodes to n-Si were used for DLTS, without optical excitation. Therefore, only electron traps were detected and studied. In the case of Ge hole traps can be studied in n-type material because hole injection is achieved by simply applying a large forward bias [8]. Minority carrier injection in Si is also possible but then a very low carrier density ($10^{14}\,cm^{-3}$) is required [9].

In order to identify the defects introduced by EBD, they were compared to defects introduced in identical samples exposed to high energy (MeV) electron irradiation from a Sr-90 source [10]. For this source the effective electron fluence rate of electrons with energies above 200 keV is 10^{9} electrons$^{-}\,cm^{-2}\,s^{-1}$.

3 Results and discussion

3.1 High energy electron irradiation Since we will be comparing the defects introduced during EBD with those introduced by high energy (MeV) electrons, we first discuss the latter defects in n-type Si. High energy electron irradiation of Si introduces single vacancies and self-interstitials that are mobile at room temperature [11]. These defects are created when the atoms are displaced by elastic scattering of the high-energy electrons. Due to the low mass of the electron relative to the nucleus, only point defects are formed since the recoiling nucleus does not have enough kinetic energy to cause further displacements [11]. For Si the energy required to displace an atom is about 12.9 eV, which would be imparted by a head on collision with an electron at about 160 keV [12].

If a mobile interstitial moves next to a substitutional carbon (C_s) in the Si lattice, it may replace C_s to create C_i, which is also mobile at room temperature [13–15]. The DLTS spectrum that we record after room temperature irradiation will therefore contain the products that form when vacancies, interstitials and C_i form when reacting with each other (V_2, C_iC_s), and with impurities (VP, VO, C_iP_s) in the lattice [16, 17].

In Fig. 1 we illustrate the dependence of the concentrations of the two main defects (A-center: E0.17 and the E-center E0.46) on the method by which the Si was grown. In the nomenclature used below to label the traps, "E" means electron trap and the number that follows after the "E," for example, 0.17, is the activation enthalpy of the defect with respect to the conduction band. Clearly, in CZ-grown Si the concentration of the A-center is much higher than in the EPI material. The reason for this is that the oxygen concentration in CZ grown Si is typically much higher than in epitaxially grown Si. Therefore, more of the

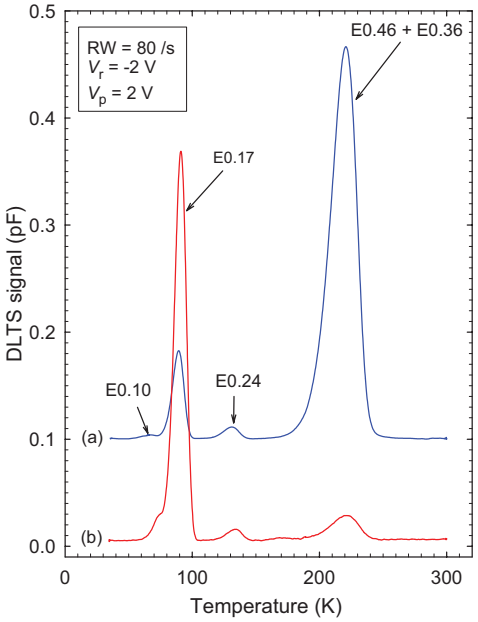

Figure 1 (online color at: www.pss-a.com) DLTS spectra of n-Si irradiated by MeV electrons from a Sr-90 radio-nuclide at a fluence of $1 \times 10^{15}\,cm^{-2}$: curve (a) is for epitaxially (EPI) grown n-Si and curve (b) is for Czochralski (CZ) grown n-Si with the same free carrier density of $3.5 \times 10^{15}\,cm^{-3}$. These spectra were recorded 7 days after irradiation.

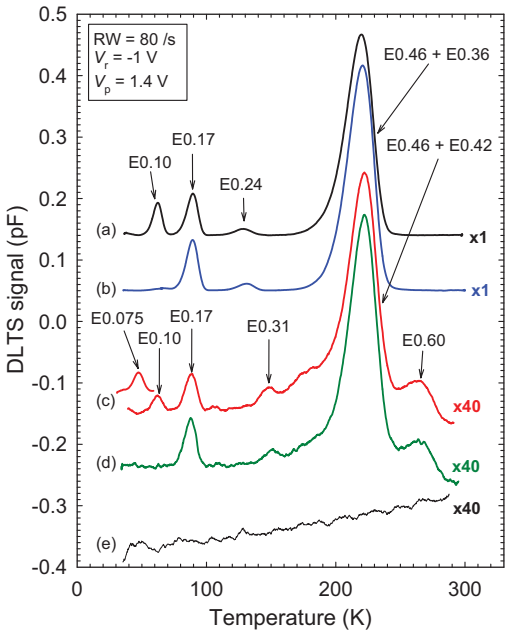

Figure 2 (online color at: www.pss-a.com) DLTS spectra of EPI n-Si: (a) irradiated with MeV electrons; (b) as (a), but storing for 1 week at room temperature; (c) Pt Schottky diode deposited by EBD; (d) as (c), but 1 week storage at room temperature. Curve (e) is a control spectrum recorded using resistively deposited Schottky diodes.

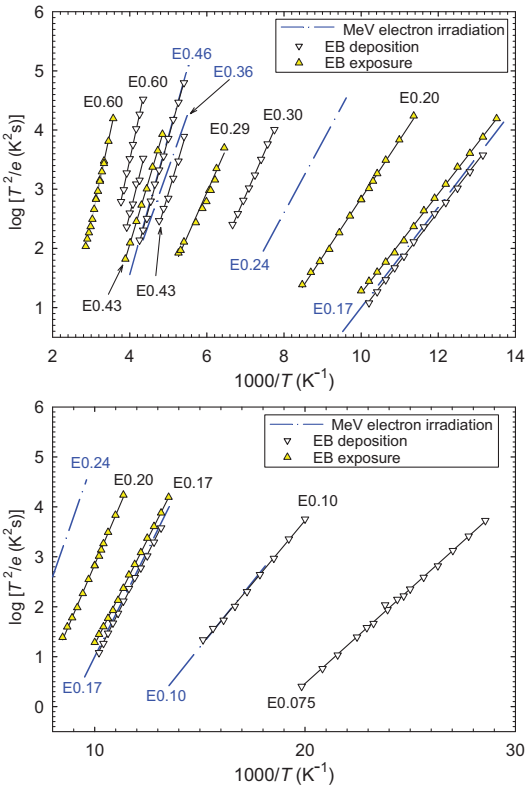

Figure 3 (online color at: www.pss-a.com) (a) and (b) Arrhenius plots for defects introduced by: MeV electron irradiated n-Si (blue dash-dotted line); electron beam deposition (down triangles); exposure to electron beam conditions, *without metal deposition* (up triangles).

mobile vacancies introduced by irradiation bonded with O than with the P to form a higher A-center concentration than an E-center concentration. It can be expected that the relative concentrations of defects introduced by EBD will also depend on the growth method. For the current investigation we confined our study to EBD defects introduced in epitaxially grown (EPI) Si.

Curve (a) in Fig. 2 is the DLTS spectrum of MeV electron irradiated EPI n-Si recorded directly after irradiation with a fluence of 10^{15} electrons^{-} cm^{-2}. It contains at least four DLTS peaks. From the Arrhenius plots where the signatures of these defects were determined (Fig. 3a and b), these peaks are identified as E0.10 (C_i), E0.17 (A-center (VO) and C_iC_s), E0.24 ($V_2^{=/-}$), and E0.46 + E0.36 [13–17]. Here the E0.46 and E0.36 contributions to the peak at 220 K were determined by high resolution Laplace DLTS measurements (Fig. 4). E0.46 is the VP or E-center, while E0.36 has a similar signature as one of the metastable components of the C_iP_s center [17]. The concentration ratio of VP to E0.36 is about 5:2. The VP + E0.36 peak also contains a small contribution due to the $V^{-/0}$ but this is too small to be distinguished from the two main peaks (VP and E0.36). The properties of these defects are summarized in Table 1.

Note that the contributions of VO and C_iC_s to the E0.17 peak cannot be separated by Laplace DLTS and can only be distinguished by monitoring their filling kinetics [18]. The VO has a larger capture cross-section and at 80 K pulses as short as 100–200 ns completely fill the defect. The contribution of C_iC_s to the E0.17 peak only becomes noticeable for filling pulses with duration, $t_p > 100$ µs.

Curve (b) in Fig. 2 was recorded after storing the irradiated sample at room temperature (300 K) for 1 week. It is clear that the E0.10 (C_i) peak has decreased to below the detection limit, indicating that all the C_i has reacted with other impurities to form, among others, C_iC_s and C_iP_s. Increases in the peaks of E0.17 and E0.46 + E0.36 (Fig. 2) demonstrate this.

3.2 Electron beam deposition The DLTS spectra recorded from Pt Schottky contacts that were fabricated by EBD, without any intentional shielding, are shown in curves (c) and (d) in Fig. 2. Curve (c) was recorded directly after device fabrication, while curve (d) was recorded after 1 week. The similarities between some of the defects

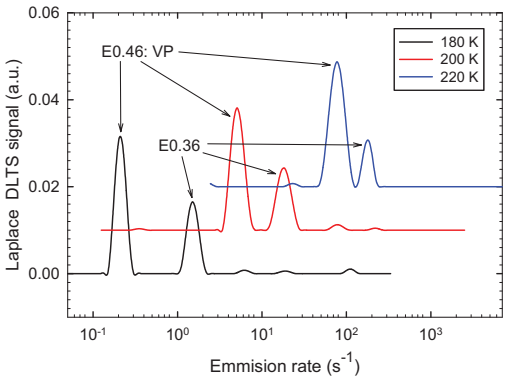

Figure 4 (online color at: www.pss-a.com) Laplace DLTS spectra of VP and E0.36 in MeV electron irradiated EPI Si measured at 180, 200, and 220 K.

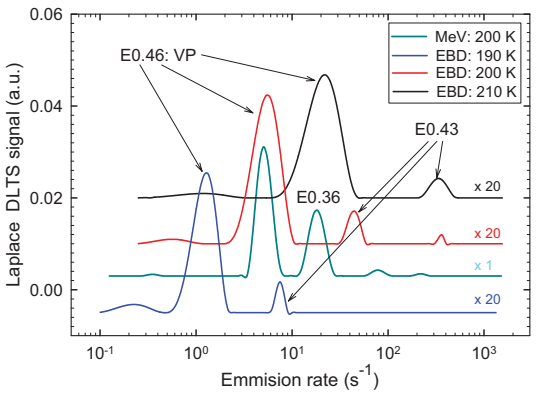

Figure 5 (online color at: www.pss-a.com) Laplace DLTS spectra of VP and E0.43 in Si with Schottky contacts deposited by EBD at 190, 200, and 210 K. For comparison the spectrum for MeV irradiated Si, measured at 200 K, is also included.

introduced by EBD and by MeV electron irradiation are evident. Both processes introduce E0.10 (C_i), E0.17 ($VO + C_iC_s$), and E0.46 (VP) [13–17]. This correspondence is confirmed by the Arrhenius plots in Fig. 3a and b.

From the Laplace DLTS spectra in Fig. 5, it is seen that EBD does not introduce the E0.36 defect, but instead a defect peak E0.43 of which the DLTS peak also overlaps with that of the E0.46 (VP) peak. From the spectra in Fig. 2 it is also evident that EBD introduces at least three other defects not seen after MeV electron irradiation: E0.075 could be seen only in some samples with EBD contacts; E0.30 (similar, but not the same, signature as VOH [19]) and a defect E0.60. This latter defect consists of two closely spaced levels (see the Arrhenius plots in Fig. 3). This defect was also not observed in all EBD samples. The properties of the EBD defects are summarized in Table 1. It is also noteworthy that no divacancies ($V_2^{=/-}$) in measurable concentrations could be detected in samples prepared by EBD. Previously, a

Table 1 Electronic properties of defects introduced in EPI n-Si by MeV electrons, electron beam deposition (EBD), and exposure to EBD conditions, *without depositing metal*. T_{80} is the peak temperature at a rate window of 80 s^{-1}.

process	defect label	E_C–E_T (eV)	σ_a (10^{-15} cm^2)	T_{80} (K)	defect ID	Refs.
MeV electrons						
	E0.10	0.10	1.7	62	C_i	[13–15]
	E0.17	0.17	8.2	89	VO	[16]
	E0.17	0.17	8.2	89	C_iC_s	[13–15]
	E0.24	0.24	2.8	129	$V_2^{=/-}$	[16]
	E0.36	0.36	0.2	214	CP?	[17]
	E0.46	0.46	15	220	VP	[16]
EBD						
	E0.075	0.075	3.7	45	–	
	E0.10	0.10	1.2	62	C_i	[13–15]
	E0.17	0.17	8.4	89	VO	[16]
	E0.17	0.17	8.4	89	C_iC_s	[13–15]
	E0.30	0.30	10	150	VOH?	[19]
	E0.43	0.43	31	204	–	
	E0.46	0.46	20	220	VP	[16]
	E0.60	0.60	130	261	–	
EB exposure						
	E0.17	0.17	2–5	91	not VO	
	E0.20	0.20	3.0	107	–	
	E0.29	0.29	0.2	172	–	
	E0.43	0.43	0.8	229	–	
	E0.60	0.60	1.1	312	–	

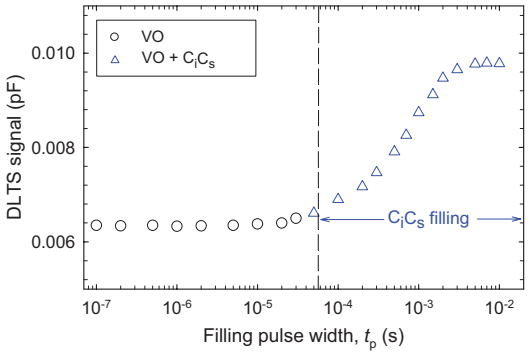

Figure 6 (online color at: www.pss-a.com) DLTS peak height of the combined VO + C_iC_s peak as a function of filling pulse duration, t_p.

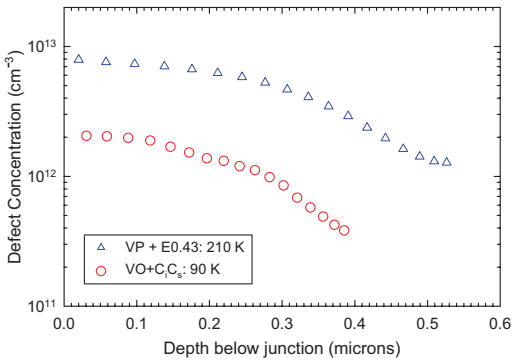

Figure 7 (online color at: www.pss-a.com) Concentration profiles of the two main defect combinations (VO + C_iC_s and VP + E0.43) below a Schottky contact deposited by EBD.

defect with very similar properties to $V_2^{=/-}$ was reported to be introduced after EBD of metal contacts on CZ Si [1].

We have assessed the composition of the E0.17 DLTS peak in samples deposited by EBD, by recording the DLTS peak height as a function of filling pulse duration at 80 K. As shown in Fig. 6, the peak height is practically constant for filling pulses of 100 ns to about 50 μs. For longer filling pulses the peak height increases until a maximum is reached at about 9–10 ms. This filling behaviour is identical to that of the contributions of VO and C_iC_s to the E0.17 DLTS peak in high energy ion implanted Si [18]. It is therefore evident that mobile vacancies and C_i are introduced during EBD and that these diffuse and combine to form, among others, VO and C_iC_s, respectively. C_i also combines with O_i to form C_iO_i but this gives rise to a hole trap that could not be detected in the present study.

It is also important to point out that EBD introduced some defects that were not observed after MeV electron irradiation, for example, E0.075, E0.30, and E0.60. These defects are most likely not simple point defects and are probably introduced during the collisions of heavier ions with the Si surface.

Fixed bias – variable pulse DLTS depth profiling [20] was used to assess the depth distribution of the main defects (VP + E0.43) and (VO + C_iC_s). During this method the quiescent reverse bias, V_r, is kept constant at, for example, −2 V and then the DLTS peak height is recorded as the amplitude of the filling pulse, V_p, is increased in small steps, typically 0.05 V, at a time. It is evident from Fig. 7 that the concentration of (VP + E0.43) drops from almost $10^{13}\,cm^{-3}$ at the interface to about $10^{12}\,cm^{-3}$ at 0.5 μm below the interface. The concentration of (VO + C_iC_s) decreases from $2 \times 10^{12}\,cm^{-3}$ at the interface, to about $3 \times 10^{11}\,cm^{-3}$ at 0.4 μm below the surface. The shapes of these curves resemble diffusion profiles. This suggests that mobile impurities are introduced at and close to the interface, which then diffuse into the Si where they combine to form VO, C_iC_s, VP, and E0.43. Note that we have not attempted to separate the profiles of VO and C_iC_s as was done in Ref. [18] but efforts to achieve this are in progress.

In a previous study of EBD induced defects in Si, only the E-center could be clearly identified and it was reported that the defect that appeared where the A-center normally appears on a DLTS spectrum, was indeed not the A-center because the two defects did not have matching DLTS signatures [2]. The reason why we clearly detect the A-center as well as C_iC_s may be that the geometries and vacuum conditions of the two EBD systems (the one used here and that of Ref. [2]) are different, as well as the fact that Si grown by different methods (containing different impurity levels) were used. Therefore different particles with different energies may have impinged on the samples in the two systems.

We have previously shown that for EBD of different metals on Ge, the defect concentrations are functions of the metal deposited (specifically its melting point), the deposition rate, as well as the vacuum conditions [21]. Of these three factors, only the deposition rate can readily be changed, but only in a limited range for high melting point metals like Ru. We have found that the defect concentrations decrease as the deposition rate increases. This is understood by noting that for higher deposition rates, that is, shorter exposure times, the sample is sooner covered with the critical metal layer thickness that significantly reduces defect introduction. For Ge we have found the EBD of Ru with a melting point of 2250 °C at a rate of $0.02\,nm\,s^{-1}$, introduces about three to four times more defects than when depositing Au with a melting point of 1552 °C at a rate of $0.5\,nm\,s^{-1}$ [21]. The melting points of metals and the vacuum are interrelated: the deposition of a high melting point metal requires a higher electron beam current, which in turn means that the environment of the molten metal becomes hotter and therefore more outgassing occurs. This leads to an increase of the pressure in the vacuum chamber and hence more particles can impinge on the sample, which in turn leads to an increase in the defect concentration.

3.3 The effect of shielding It has been proposed that the defects introduced during EBD are caused by ionized particles that originate in the region of the EB filament and that are then accelerated towards the sample where they collide and cause defects [2]. In Ref. [2] the electron beam evaporator was a 4 keV system, which meant that the maximum energy that a singly ionized ion could acquire would be 4 keV. Our electron beam system has an accelerating voltage of 10 kV, so that ions could have an energy of up to 10 keV, however, as our system's filament is remotely positioned from the sample, it is improbable that such ions will reach the sample. The energetic products of collisions in the electron beam path, however, be they particles or stray electrons, are able to follow a direct path to the sample. The long mean free path at high vacuum pressures makes further collisions unlikely. Placing a mechanical shield between the electron beam path and the sample should prevent these energetic particles from reaching the sample directly but will not shield the sample from light ions that can follow a curved trajectory around the shield due to the EB system magnetic field. Stray electrons that have been reflected off the molten metal and the energetic products of collisions between these electrons and residual vacuum gases may also reach the sample.

This shield should therefore eliminate, or at least reduce, the defects introduced by EBD. Such a process is depicted diagrammatically in Fig. 8. Here, two possible paths, P_1 and P_2, of particles are shown. Firstly, particles may follow a direct path (P_1) to the sample from the electron beam region. They would be blocked by shield S_1. Secondly, particles may be elastically reflected from the side of the vacuum chamber (P_2) and these particles would be blocked by shield S_2.

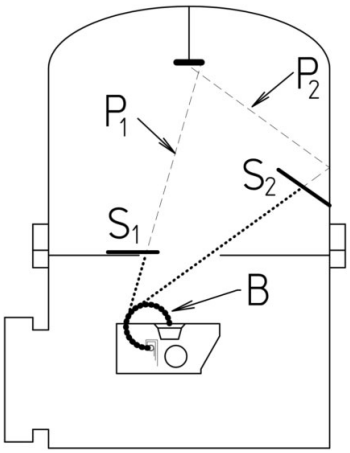

Figure 8 Diagram of an electron beam evaporator showing the path of the 10 keV electrons and possible paths of heavier particles, directly (path P_1) to the sample or reflected (path P_2) off the chamber wall. The particles will be blocked if the shields S_1 and S_2 are in place. Of course, the shield S_1 should not be blocking metal from the crucible on route to the sample.

The spectra in Fig. 2 were all recorded from Schottky contacts fabricated without any deliberate shielding. In Fig. 9 we show DLTS spectra, recorded with and without shielding the sample from particles originating in the region of the filament. Curve (a) was recorded from Schottky contacts deposited without shielding and is the same as curve (c) in Fig. 2, for comparison. Curve (b) in Fig. 9 was recorded using a Schottky contact deposited with shield S_1 in place. A comparison between curves (a) and (b) shows a sharp reduction in the VP + E0.43 peak, caused by shielding with shield S_1. Laplace DLTS revealed that the VP peak in curve (b) contains almost no E0.43. This also explains the slight temperature shift of this peak in curve (b) to higher temperatures. In addition, no E0.10 and E0.17 defects could be detected with certainty. It is not clear at the moment why VP is still introduced during shielding and not VO, because both are vacancy related.

Curve (c) in Fig. 9 was recorded with both shields (S_1 and S_2) in position. There is no noticeable difference between the spectra in curves (b) and (c). This implies that, from a defect detection point of view, the second shield that is supposed to block reflected particles is not necessary since, according to curves (b) and (c), particles reflected as indicated in Fig. 8 are too low in concentration to cause any defects. However, the fact that defects are still observed after shielding implies that the particle paths indicated in Fig. 8 clearly are not the only ones present.

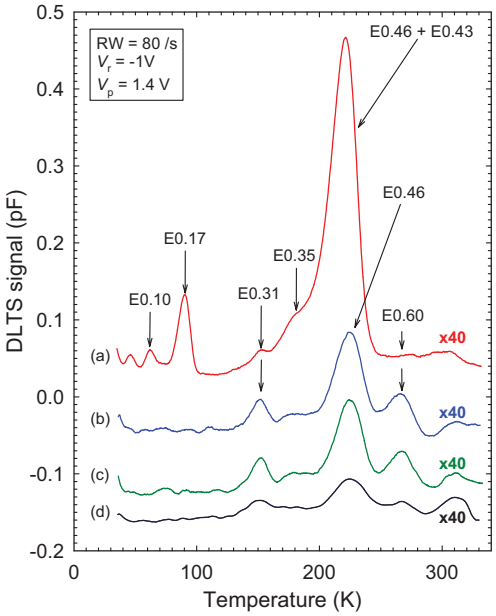

Figure 9 (online color at: www.pss-a.com) DLTS spectra of Pt Schottky contacts deposited at a rate of 0.02 nm s^{-1}: (a) without any shielding; (b) with shield S_1 in place (see Fig. 8); (c) with both shields (S_1 and S_2) in place; (d) both shields and an improved vacuum.

It is also instructive to evaluate the effect of these defects with and without shielding on the *I–V* characteristics of the diodes. For an unshielded diode the best ideality factor was 1.075, the reverse leakage current at 1 V reverse bias was 1.5×10^{-8} A and the barrier height was 0.78 eV. For a diode with shield S_1 in place these values were 1.042, 7.0×10^{-10} A and 0.79 eV, respectively. Clearly the reduction in defect introduction by shielding the diodes improved their rectification characteristics. For metallization with two shields in place we have found that the best ideality factor was 1.031, the reverse leakage current at 1 V reverse bias was 5.6×10^{-10} A and the barrier height was 0.79 eV. From the *I–V* measurements it seems that the diodes fabricated with two shields in place are slightly better than those fabricated with only shield S_1 in place. A possible explanation for this is that the energy of the reflected ions (P_2) is only sufficient to cause some surface damage, not detectable with DLTS. Surface damage will, however, impact on the *I–V* characteristics of these samples.

Curves (a)–(c) in Fig. 9 were all recorded from diodes fabricated during EBD in approximately the same vacuum (5×10^{-5} mbar). During these evaporations the hydrogen (H_2) concentration, as monitored by a RGA, was of the order of 10^{-6} mbar. In curve (d) we depict a DLTS spectrum recorded from a Schottky diode formed by EBD, with shielding, in a vacuum of 2×10^{-6} mbar. In this case the H_2 concentration before metallization was 5×10^{-9} mbar and increased to 10^{-8} mbar at the end of the metallization. It is clear from curve (d) that by evaporating under a better vacuum with a reduced H_2 concentration, the defect introduction was reduced at least by a factor of 2–3 compared to curves (b) and (c). The improved vacuum was obtained by evaporating first Ti and then Pd, with the sample masked/turned away from the metals, to getter oxygen and hydrogen, respectively. Ti getters residual gasses, such as OH, H_2O, and CO_2, well, whereas Pd getters hydrogen.

3.4 Exposure to EBD conditions *without* depositing any metal In most experimental electron beam evaporators there is some form of flexibility regarding the position of the sample and sample holder during pre-metallization heating and degassing of the metal. Sometimes a shutter is used to protect the sample and in other instances the sample may be rotated to face away from the metal during this procedure. These options may not necessarily be available for larger commercial systems where metallization of large areas is required. In the next section we explore the effect of pre-metallization exposure, *without metallization*, on defect introduction in the EPI Si sample.

In Fig. 10 we compare the spectra recorded using Schottky contacts prepared by EBD without shielding (curve (a)) and exposed to EBD conditions, *without metal deposition*, followed by resistive evaporation of Pd (curves (b)–(d)). It is evident that the spectra of samples that were exposed to EBD conditions (curves (b)–(d), without metallization, are very different from that of a normal EBD

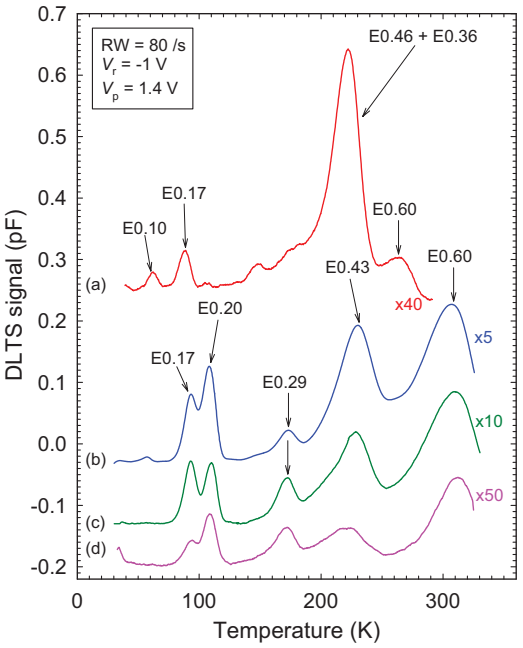

Figure 10 (online color at: www.pss-a.com) DLTS spectra recorded using Schottky contacts (a) deposited under normal EBD conditions (no shielding during evaporation); (b), (c), and (d) samples exposed to EBD conditions for 50, 10, and 2 min, respectively, *without any EBD metallization*; then Pd Schottky contacts were formed by resistive evaporation on the exposed surfaces.

metallization (curve (a)). At first glance, the only defect common to both spectra seems to be the E-center. However, closer comparison of curves (a) and (b) shows that the DLTS peak of the E-center is displaced by about 5° to a higher temperature in curve (b). Laplace DLTS revealed that this peak seems to be a defect band rather than closely spaced defect levels: if transients are recorded at different temperatures and analyzed by Laplace DLTS then in some instances the transient is deconvoluted into three closely space exponentials and in other instances into four components. When using conventional DLTS to extract the average defect enthalpy by recording scans at different rate windows, the value of 0.43 eV was obtained. We therefore label the peak E0.43. Although the activation enthalpy of this defect (0.43 eV) is the same as that of the E0.43 introduced by EBD, their apparent capture cross-sections, determined from the Arrhenius plots, differ by a factor of 40 (Table 1).

It is noteworthy that there is not a single defect that is common to normal EBD and exposure to EBD conditions followed by resistive evaporation: each procedure introduces a unique set of defects. The reason for this is probably that during EBD the surface of the sample is covered by a thin

metal layer within a few seconds after the start of the EBD process. This metal layer will shield the sample from the heavier particles and will only allow light particles, for example, H, to penetrate it and react with the surface.

4 Summary and conclusions In our investigation of defects introduced in EPI n-Si by EBD of Pt and exposure to electron beam conditions we have made several interesting observations.

Four of the point defects introduced during EBD (without shielding) are well known and are also introduced by MeV electron irradiation and ion implantation: interstitial carbon, C_i (E0.10), VO or A-center (E0.17), interstitial carbon, C_i, paired with substitutinal carbon, C_iC_s (E0.17), and the VP or E-center (E0.46). Although the VO and C_iC_s have the same DLTS signature, they could be distinguished from each other by their unique filling kinetics. Several defects were also introduced by EBD that were not observed after MeV electron irradiation. These defects are not necessarily point defects.

The use of a mechanical shield, strategically placed, significantly reduced defect introduction during EBD and led to the complete elimination of some defects (C_i, C_iC_s, and VO). Diodes fabricated with the shield in place had significantly improved rectification characteristics when compared to diodes fabricated without shielding. Placing a second shield in order to protect the surface from reflected particles did not lower the defect concentration, as measured by DLTS, but lead to a slight further improvement of the rectification properties of the diodes. Shielding in conjunction with an improved vacuum, with a lower hydrogen partial pressure, lead to a further reduction in defect introduction.

When exposing the Si surface to EBD conditions, without depositing any metal, a totally different set of defects was introduced compared to those introduced by the EBD process. None of these defects have been observed after MeV electron irradiation or EBD of identical EPI n-Si.

For optimum device properties it is therefore recommended that the sample surface not be exposed to electron beam condition, without metal deposition. In addition, proper shielding should be employed as well as the deposition of metal in the best possible vacuum. Specifically, the hydrogen partial pressure should be as low as possible. The vacuum can be improved by Ti gettering and the hydrogen can be reduced by Pd gettering.

Acknowledgements The authors gratefully acknowledge financial support of the South African National Research Foundation. The Laplace DLTS software and hardware used in the research was kindly provided by A. R. Peaker (Centre for Electronic Materials Devices and Nanostructures, University of Manchester) and L. Dobaczewski (Institute of Physics, Polish Academy of Sciences). We also thank Mr. H de Meyer for his technical drawing.

References

[1] F. D. Auret and P. M. Mooney, J. Appl. Phys. **55**, 988 (1984).
[2] C. Christensen, J. W. Petersen, and A. Nylandsted Larsen, Appl. Phys. Lett. **61**, 1426 (1992).
[3] G. Myburg and F. D. Auret, J. Appl. Phys. **71**, 6172 (1992).
[4] D. C. Sawko and J. Bartko, IEEE Nucl. Sci. **30**, 1756 (1983).
[5] A. W. Blakers and M. A. Green, IEEE Electron Device Lett. **EDL-5**, 246 (1984).
[6] L. Dobaczewski, P. Kaczor, I. D. Hawkins, and A. R. Peaker, J. Appl. Phys. **76**, 194 (1994).
[7] L. Dobaczewski, A. R. Peaker, and K. Bonde Nielsen, J. Appl. Phys. **96**, 4689 (2004).
[8] V. P. Markevich, I. D. Hawkins, A. R. Peaker, V. V. Litvinov, L. Dobaczewski, and J. L. Lindström, Appl. Phys. Lett. **81**, 1821 (2002).
[9] F. D. Auret and M. Nel, J. Appl. Phys. **61**, 2546 (1987).
[10] F. D. Auret, S. A. Goodman, G. Myburg, and W. E. Meyer, Appl. Phys. A **56**, 547 (1993).
[11] G. D. Watkins, Mater. Sci. Semicond. Process. **3**, 227 (2000).
[12] J. Loferski and P. Rappaport, Phys. Rev. **111**, 432 (1958).
[13] M. T. Asom, J. L. Benton, R. Sauer, and L. C. Kimerling, Appl. Phys. Lett. **51**, 256 (1987).
[14] G. D. Watkins and K. L. Brower, Phys. Rev. Lett. **36**, 1329 (1976).
[15] G. E. Jellison, Jr., J. Appl. Phys. **53**, 5715 (1982).
[16] G. D. Watkins, in: Properties of Crystalline Silicon, edited by R. Hull (INSPEC, London, 1999), chap. 11.1.
[17] E. Gurer, B. W. Benson, and G. D. Watkins, Mater. Sci. Forum **83–87**, 339 (1992).
[18] P. Lévêque, H. Kortegaard Nielsen, P. Pellegrino, A. Hallén, B. G. Svensson, A. Yu. Kuznetsov, J. Wong-Leung, C. Jagadish, and V. Privitera, J. Appl. Phys. **93**, 871 (2003).
[19] K. Bonde Nielsen, L. Dobaczewski, K. Goscinski, R. Bendesen, O. Andersen, and B. Bech Nielsen, Physica B **273/274**, 167 (1999).
[20] Y. Zohta and M. O. Watanabe, J. Appl. Phys. **53**, 1890 (1982).
[21] F. D. Auret, S. M. M. Coelho, M. Hayes, W. E. Meyer, and J. M. Nel, Phys. Status Solidi A **205**, 159 (2008).